Mechanisms of Nanoparticle Toxicity in Cancer and Normal Cells

Thesis

Mechanisms of Nanoparticle Toxicity in Normal and Cancer Cells

Konstantina Tzelepi

A thesis submission to The Open University in fulfilment for the degree of Doctor of Philosophy

November 2018

Faculty of Science, Technology, Engineering and Mathematics; School of Life, Health and Chemical Sciences; Walton Hall, MK7 6AA, Milton Keynes, United Kingdom

Declaration

I hereby declare that this thesis is a result of my own work and contributions to this study are fully acknowledged accordingly in the acknowledgments section. This thesis does not include material submitted for the award of any other degree.

Konstantina Tzelepi

Abstract

Nanotechnology offers vital tools for cancer diagnosis, early detection and novel treatments. Gold nanoparticles (AuNPs) are at the forefront of biological and biomedical research and show an increased promise in targeted cancer therapy due to their unique physicochemical properties. They offer the advantage of biomolecular interaction both at the cell surface level and inside the cell.

In this thesis, 2nm AuNPs surface functionalised with a 50:50 ratio of a thiolated α-Galactose derivative and a thiol-PEGamine were examined for their toxicity and uptake in normal and cancer cell lines *in vitro*. Using this simple ligand structure, a selective cancer toxicity was observed, which was highly dependent upon the nanoparticles' synthesis duration. This observation was correlated to ligand density, which decreased with shorter synthesis time, making particles less toxic. Detailed insight into the mechanism of toxicity and uptake was gained by energy-dependent experiments and cell death assays, revealing a significant adhesion of these particles to filopodia. The proposed mechanism of cell death in HSC oral squamous carcinoma cells exposed to AuNPs was identified to be the extrinsic apoptotic pathway, as toxicity was abrogated by inhibition of either caspase 3/7 or caspase 8, but not by inhibition of caspase 9.

Future directions include batch standardisation of the optimum nanoparticle synthesis conditions and elucidation of the mechanisms of cell uptake and toxicity in a variety of cancer and normal cell lines.

Keywords: *gold nanoparticles, toxicity, cancer therapy, mechanism, extrinsic apoptosis*

Acknowledgements

I am very grateful to my supervisor Jon Golding. He was always there for me supporting me and giving me valuable advice. I thank him for the long scientific discussions and experimental plans we were making from the start to finish of this journey and the persuasion he was providing me so I could keep going. To my second supervisor, Katja Rietdorf, I am thankful for her advice and valuable feedback particularly during the writing process. Also, I am very appreciative to David Male for always making me think from a different perspective about my research and make me question even more the science behind it! My former supervisor from Midatech Pharma, Meike Roskamp, whom I was glad to work with on my first year before her resigning, I am thankful for her patience and help to answer every question I had when I first joined the world of a pharmaceutical company. I owe a big thank you to people from Midatech UK and Spain: Phil, Cristina, Tom, Alejandro, Valentin, Africa and Dan for their significant insight into my project during our regular progress meetings.

All this hard work wouldn't have been completed without the valuable help from people both at The Open University and Midatech Pharma. Specifically, Cristina Espinosa Garcia and Phil Williams were responsible for the synthesis and characterization (DLS, UV-Vis, FPLC, zeta) of all the AuNPs formulations supplied. SEM machine was run by Gordon Imlach and contributed to the ligand density characterization of the AuNPs. TEM sectioning and processing was conducted by Radka Gromnicova. Lastly, I would like to thank Brett, Igor and George, for the great laboratory support they provide to all students. From the students, a big thanks to Said, Sophie, Sarah, Chrysanthi and Conor for making my time at OU a better experience.

I could not thank enough my family for their constant support and belief in me that I can manage this hard journey of a PhD. I am and will always be grateful to my mum for being there for me when I needed her. This thesis is dedicated to her. Thank you for believing in me and even though I am far from you for so many years so I can complete my studies and pursue the career I want, I feel like you are here with me. Last but not least, no words could describe the support I felt from my other half, Veer, who always made me laugh and travelled to amazing places around the world with me on our little gateways during these 3 years. Thank you for putting up with me for so long and waiting hours at the university on weekends so I run my experiments.

Preface

The choice of nanoparticles in this thesis was based on previous work conducted in the group's laboratory which showed that 2nm AuNPs surface functionalised with a 50:50 ratio of a thiolated α-Galactose derivative and a thiol-PEGamine resulted in selective uptake and toxicity towards skin cancer cells at low nanomolar concentrations (Grellet et al., 2017). Previous published data by Lund and colleagues also correlated with the above findings and additionally revealed that ligand organization around the Au core was of crucial importance to the internalization rate of AuNPs by colorectal cancer cells (Lund et al., 2011). Both of these studies were funded by Midatech Pharma Plc and was a core motivation of this thesis.

List of publications

Tzelepi K., Garcia C.E., Williams P., Golding J. (2019) Galactose:PEGamine coated gold nanoparticles adhere to filopodia and cause extrinsic apoptosis. Nanoscale Adv., 1: 807-816, doi: 10.1039/C8NA00270C

Grellet S., Tzelepi K., Roskamp M., Williams P., Sharif A., et al. (2017) Cancer-selective, single agent chemoradiosensitising gold nanoparticles. PLOS ONE 12(7): e0181103, doi.org/10.1371/journal.pone.0181103

Conference items:

Tzelepi K., Garcia C.E., Williams P., Golding J. (2018) Galactose:PEGamine coated gold nanoparticles adhere to filopodia: Effects of nanoparticle synthesis time on cellular uptake and toxicity, 2nd International Conference and Exhibition on Nanomedicine and Drug Delivery, Tokyo, Japan, Volume 7, doi:10.4172/2325-9604-C2-030

Tzelepi K., Garcia C.E., Roskamp M., Golding J. (2016) Cancer-selective toxicity of gold nanoparticles: effects of synthesis time and charge, CLINAM, Basel, Switzerland, doi: 10.13140/RG.2.1.1260.1845

Tzelepi K. (2016) Gold Nanoparticles. Magic bullets killing cancer? Student Conference, The Open University, doi: 10.13140/RG.2.1.2404.6966

Online articles:

Tzelepi K. (2017) Good things come in small packages, Open Learning http://www.open.edu/openlearn/science-maths-technology/across-the-sciences/nanotechnology-good-things-come-small-packages

Abbreviations

A498	Kidney cancer
AMA	Antimycin-A
Au	Gold
AuNPs	Gold nanoparticles
Bcl-2	B-cell lymphoma 2
Caco2	Caucasian colon adenocarcinoma
CNS	Central Nervous System
CTAB	Cetyl Trimethylammonium Bromide
DLS	Dynamic light scattering
DMEM	Dulbecco's Modified Eagle Medium
DNA	Deoxyribonucleic acid
EDX	Energy-dispersive X-ray spectroscopy
EGF	Epidermal Growth Factor
EPR	Enhanced Permeability and Retention
ER	Endoplasmic Reticulum
FADD	Fas-associated protein with death domain
FBS	Fetal bovine serum
FCCP	Carbonyl cyanide-p-trifluoromethoxyphenylhydrazone
FDA	Food and Drug Administration
FPLC	Fast Protein Liquid Chromatography
GTP	Guanosine triphosphate
HaCaT	Human keratinocytes
HAuCl4	Hydrogen tetrachloroaurate
HBSS	Hank's Balanced Salt Solution
HEK293	Human Embryonic Kidney
HeLa	Henrietta Lacks (cervical cancer)
HMEC	Human mammary epithelial cells
HSC	Human skin cancer
IC50	Half maximal inhibitory concentration
KOH	Potassium hydroxide
LDH	Lactate dehydrogenase
LDL	Low Density Lipoprotein
MCF-7	Michigan Cancer Foundation-7 (breast cancer)
MeOH	Methanol
miRNA	Micro RNA
MTT	3-(4,5-Dimethylthiazol-2-yl)-2,5- diphenyltetrazolium bromide
NaBH4	Sodium borohydride
NMR	Nuclear magnetic resonance
NP	Nanoparticle (s)
PAMAM	Poly(amidoamine)
PBS	Phosphate-buffered saline
PCL	Polycaprolactone
PCR	Polymerase chain reaction

PDGFR	Platelet-derived growth factor receptor
PEG	Polyethylene glycol
PFA	Paraformaldehyde
PI	Propidium iodide
PLGA	Poly Lactic-co-Glycolic Acid
QD	Quantum Dots
RFU	Relative Fluorescence Unit
ROS	Reactive oxygen species
SEM	Scanning electron microscope
siRNA	Small interfering RNA
TBE	Tris Borate ethylenediaminetetraacetic acid
TBHP	Tert-butyl hydroperoxide
TEM	Transmission electron microscope
TRAIL	Tumour necrosis factor Related Apoptosis Inducing Ligand
TUNEL	Terminal deoxynucleotidyl transferase dUTP nick end labeling
Tx-100	Triton-x
U-373	Uppsala cell line (glioblastoma)
UV-Vis	Ultraviolet–Visible spectroscopy
XPS	X-Ray Photoelectron Spectroscopy
αGal	Alpha-galactose

Table of Contents

List of Figures

List of Tables

Chapter 1: Introduction

Cancer is a highly complex heterogeneous disease characterized by abnormal continuous cellular growth affecting many physiological functions, such as cell signalling and apoptosis (Feinberg et al., 2006). Despite important breakthroughs in cancer biology, cancer still remains a challenge and a leading cause of death worldwide. So far, more than 200 different types of cancer have been reported demonstrating the variability and complexity of this disease (Madani et al., 2011, Blackadar, 2016).

The widespread occurrence, recurrence after treatment and high death rates indicate an unmet need for early diagnosis and improved therapies (Ferlay et al., 2010, Jaffee et al., 2017). Most of the cancer treatments include combinations of surgery, radiotherapy and chemotherapy. Chemotherapeutic agents confer limited disease-free state. Limitations also exist regarding drug resistance and non-specific tissue toxicity (Chidabaram et al., 2011, Sinha et al., 2006). Challenges in radiotherapy are associated with development of resistance and damage to healthy surrounding cells and tissues, while surgery can only be used for discrete solid tumours and risks incomplete excision at tumour margins (Misra et al., 2010, Wang et al., 2008, Choi et al., 2010).

Some of the biological processes underlying cancer are summarized into disturbances in cell-cycle checkpoints and signal transduction pathways which lead to triggering of angiogenesis and apoptosis (Nebbioso et al., 2018, Sasahira and Kirita, 2018). Extensive ongoing research in cancer biology revealed processes vital for the disease initiation and progression and led to identification of novel targets and compounds for cancer management (Sikora, 2002, Singh

and Nehru, 2008). This chapter is a brief introduction of the basic topics presented in this thesis, followed by a more extensive review in each chapter.

1.1 Nanotechnology in cancer

The goal in every cancer therapy is to specifically target the tumour site with minimal destruction to normal healthy surrounding tissues and cells. Nanotechnology offers this advantage and constitutes one of the most promising emerging fields in cancer management (Chen et al., 2018). This research field is based on the utilization and creation of materials that range from 1-100 nm in size and spans across various disciplines from chemistry and biology to engineering and material sciences (Bharali et al., 2009). Nanotechnology has remarkable potential in cancer diagnosis, early detection and therapy (Rosenblum et al., 2018, Cai et al., 2008, Sengupta et al., 2005).

Also, nanotechnology research shows promise of overcoming obstacles of resistance and targeted toxicity by encapsulating chemotherapeutic agents into site-specific drug delivery systems which provide enhanced efficacy of treatment (Bharali et al., 2009). This enhanced efficacy of treatment can be achieved by designing nanomaterials that consist of high-affinity specific ligands for target cells, carry high concentrations of a drug, as well as multiple drug molecules for a combined therapeutic outcome (Misra et al., 2010). Therefore, nanotechnology-based systems confer many advantages over conventional therapies, which are: stability, high carrier capacity, long shelf-life, improved bio-distribution of drugs and administration by various routes (intraocular, nasal, parenteral, oral) (Chidabaram et al., 2011). These advantages are attributed to their unique physicochemical properties, such as small size, surface nature and pharmacokinetics (Chen et al., 2018, Ferrari, 2005).

1.1.1 Types of nanotechnology-based tools in cancer management

The types of nanotechnology-based drug tools that are used in cancer detection and therapy are summarized into: liposomes, nanoparticles, polymeric micelles, dendrimers, quantum dots and carbon nanotubes (Figure 1.1).

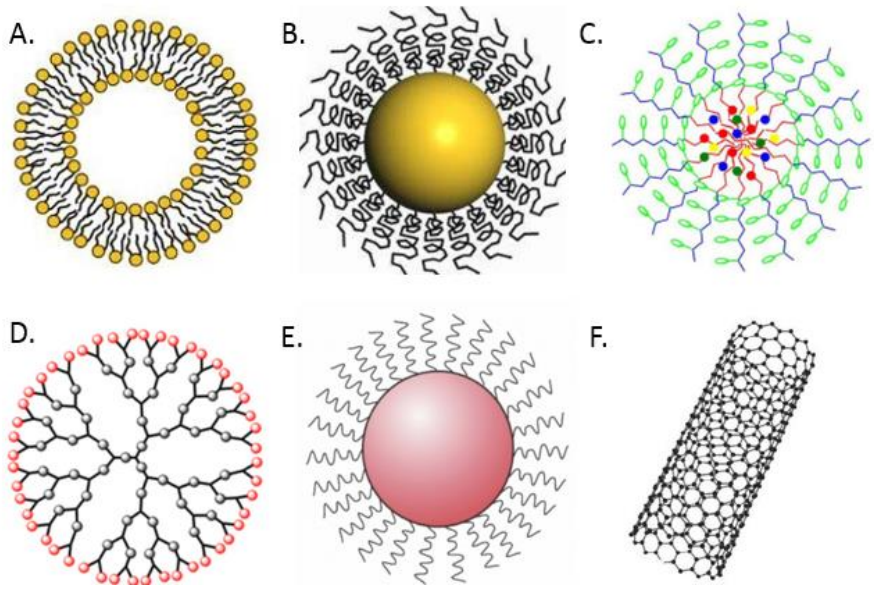

Figure 1.1: Nanotechnology-based systems used in cancer therapy and detection. A. Liposomes, **B.** Nanoparticle, **C.** Polymeric micelles, **D.** Dendrimers, **E.** Quantum dots and **F.** Carbon nanotube.

1.1.1.1 Liposomes

Liposomes are one of the most versatile tools in cancer management due to their wide range of structures and compositions as drug delivery agents. They are artificial small spherical vesicles comprised of a phospholipid bilayer membrane that encapsulate drug molecules or genetic material for their delivery into cells or tissues (Cevc, 1993, Torchillin, 2006). Their lipid bilayer is a highly chemically reactive component and provides a platform for coupling agents and tags such as antigens, antibodies, cell receptors and more (De Serrano and Burkhart, 2017). There are various ways by which liposome contents are efficiently delivered. These include fusion of their bilayer with the plasma

membrane and diffusion of the drug payload into the cell, or targeting of the endocytic pathway (Barani and Montazer, 2008, Park, 2002). Liposomes can also be designed in a way that have high or low pH and can deliver their soluble contents by diffusion through the plasma membrane (Bertrand et al., 2010). Another method of liposome content delivery is to design their size in a way to activate phagocytic uptake by macrophages (Wang et al., 2008). Uptake and digestion by macrophages leads to dissolving of the liposome contents and thus effective release of the drug. Uptake of liposomes by other cell types can be mediated by the use of ligands such as opsonins on their surface (Qureshi et al., 2011).

Targeting of cancer is achieved by designing liposomes at sizes <400 nm and their internalization due to the enhanced permeability and retention effect (EPR), a phenomenon which is characterized by enhanced accumulation of certain sized particles in tumour rather than in healthy tissues (Qureshi et al., 2011). Examples of liposomes that are approved by FDA, as drug delivery systems and are currently on the market, include doxorubicin and daunorubicin for the treatment of ovarian cancer and Kaposi's sarcoma (James et al., 1994, Gibbs et al., 2002, Fassas and Anagnostopoulos, 2005). A study by Immortino et al., showed the effective delivery of doxorubicin *in vivo* by folate receptor targeted liposomes (Immordino et al., 2006).

1.1.1.2 Nanoparticles

Nanoparticles are the most widely used nanomaterials in cancer therapy and detection. Their unique properties render them at the forefront of nanotechnology research for use as drug delivery or imaging agents (Singh et al., 2018). The control of their size and shape during synthesis allows for fine

tuning of their physico-chemical properties such as light emission/absorption properties, stability and chemical reactivity (Portney and Ozkan, 2006, Mohanty and Sahoo, 2010). Nanoparticles are sub-micron sized materials which either encapsulate a therapeutic agent in their core or are covalently or ionically conjugated to an agent via their surface (Sahoo and Labhasetwar, 2003).

Depending on the targeting molecule used during their synthesis, nanoparticles are engineered in a way that can bind specifically to receptors expressed by cancer cells and deliver the encapsulated contents (Portney and Ozkan, 2006). Also, depending on their coating or surface properties, they confer the advantage of crossing biological barriers such as the blood-brain barrier. Kreuter et al., demonstrated drug delivery to CNS by polysorbate-80-coated butylcyanoacrylate nanoparticles (Kreuter et al., 2003). Misra et al., increased the therapeutic capacity of the anticancer drug doxorubicin by specifically targeting the drug to the nucleus via conjugation of a nuclear localisation sequence on the surface of nanoparticles (Misra and Sahoo, 2010).

1.1.1.3 Polymeric micelles

Polymeric micelles are composed of amphiphilic surfactant molecules. They are mainly used for the delivery of compounds to the tumour site (Croy and Kwon, 2016). Torchillin et al., found that an antibody conjugated polymeric micelle encapsulating the drug Taxol efficiently recognized cancer cells *in vitro* (Torchillin et al., 2003). Some of the advantages of this type of nanomaterial include the solubilisation of poorly solubilized substances, protection of encapsulated drugs from degradation and sustained release (Bae et al., 2005). Numerous PEG-micelle molecules have undergone phase I clinical trials as cancer therapeutics delivery systems (Portney and Ozkan, 2006).

1.1.1.4 Dendrimers

Dendrimers are star-shaped, highly branched macromolecular compounds whose shape and size can be altered accordingly to confer desired properties (Svenson and Tomalia, 2005). Their unique architecture enables the attachment of targeting moieties or imaging probes, critical for the efficient diagnosis or treatment of cancer (Menjoge et al., 2010). For example, Choi et al., prepared DNA-assembled polyamidoamine dendrimers for targeting of tumours (Choi et al., 2005).

1.1.1.5 Carbon nanotubes

Carbon nanotubes are carbon cylinders made of graphene sheets that are rolled into a cylinder shape. They are engineered in a way that specific groups functionalized in their surface provide desirable physico-chemical properties for use as carriers for gene, proteins and drug delivery (Abdelbary et al., 2012). Also, their high optical absorbance properties render them a valuable tool in cancer irradiation, leading to destruction of cancer cells with internalized nanotubes (Ferrari et al., 2005). Their mechanism of uptake by cancer cells is still not well understood but it is being considered that their cylinder shape facilitates membrane passage (Clump et al., 2006). It has been shown *in vitro* that drugs carried by carbon nanotubes are internalized more efficiently into cells as opposed to the free drug alone (Abdelbary et al., 2012).

1.1.1.6 Quantum dots

Quantum dots represent a class of nanometre sized semiconductor particles with distinct optical and electronic properties (Misra et al., 2010). They are mainly used as fluorescent labels for imaging and therapeutic purposes (Gao et al., 2005). Their resistance to photo-bleaching along with the intense fluorescent signals they produce makes this type of nanomaterials of great significance as fluorescent tags for *in vivo* imaging (Pinaud et al., 2006). They also provide a scaffold of various agents that can modify their specificity, solubility and sensitivity. For instance, the use of PEG-silica makes them biocompatible, eliminating toxicological concerns *in vitro* (Misra et al., 2010). Nie et al., demonstrated the imaging and targeting ability of prostate membrane antigen labelled quantum dots in animal models (Nie et al., 2007).

1.1.2 Targeting of nanomaterials to tumour site

There are various factors determining the effectiveness of any of the above discussed nanotechnology-based systems in cancer management, such as their toxicity, degradation/elimination and their capacity of carrying an active agent (Muller and Keck, 2004). Important factors also include the ability of these systems to penetrate biological barriers and selectively bind to cancer cells without affecting the normal cells and tissues (Rosenblum et al., 2018). There are two strategies that can be utilized in the design of nanomaterials for their delivery inside the cancers cells. These include the design in a way to either undergo passive or active targeting (Figure 1.2).

1.1.2.1 Passive targeting

The accumulation of a drug in the tumour site due to its physico-chemical properties is called passive targeting. Apart from the properties of a nanomaterial, the properties of cancer cells, including the tumour microenvironment, facilitate this type of targeting (Sagnella et al., 2012). In the tumour vasculature, angiogenic blood vessels have large gaps of up to 800 nm between the adjacent endothelial cells, leading to a defective and leaky vasculature and poor lymphatic drainage, whilst the gaps in normal vasculature are much smaller and the vessels are not leaky (Maeda et al., 2000, Nakamura et al., 2016). This feature is described as the EPR effect which enables the transport of nanomaterials through the gaps and their subsequent accumulation to the tumour site (Matsumura and Maeda, 1986).

Accumulation of nanoparticles in cancer cells is also affected by cellular properties. These properties are defined by a hyper-proliferative ability, high metabolic rates and an acidic microenvironment (Misra et al., 2010). This environment allows for example, the design of pH sensitive liposomes to target cancer cells and release their drug contents at tumour sites with a lower than normal pH value, whilst they are stable at the normal cell/tissue pH of 7.4 (Misra et al., 2010).

1.1.2.2 Active targeting

Active targeting includes the attachment of a targeting moiety on the surface of a nanomaterial such as a ligand or an antibody, for the delivery of the therapeutic drug to cancer cells via a molecular recognition process (Nakamura et al., 2016). This process involves mainly internalization via receptor mediated endocytosis, which will be described in detail in chapter 4. In order for this

strategy to be efficient, the targeted receptors should be expressed only by cancer cells. Using ligands such as growth or folate factors, provides advantages over antibodies in terms of lower immunogenicity (Fenart et al., 1999, Muller and Keck, 2004). An example of the delivery of a chemotherapeutic drug, paclitaxel® by active targeting involves the delivery of artificially engineered antibodies coupled as a conjugate to affisomes (thermosensitive liposomes) and polyethylene glycol maleimide copolymer (Alexis et al., 2008, Puri et al., 2008).

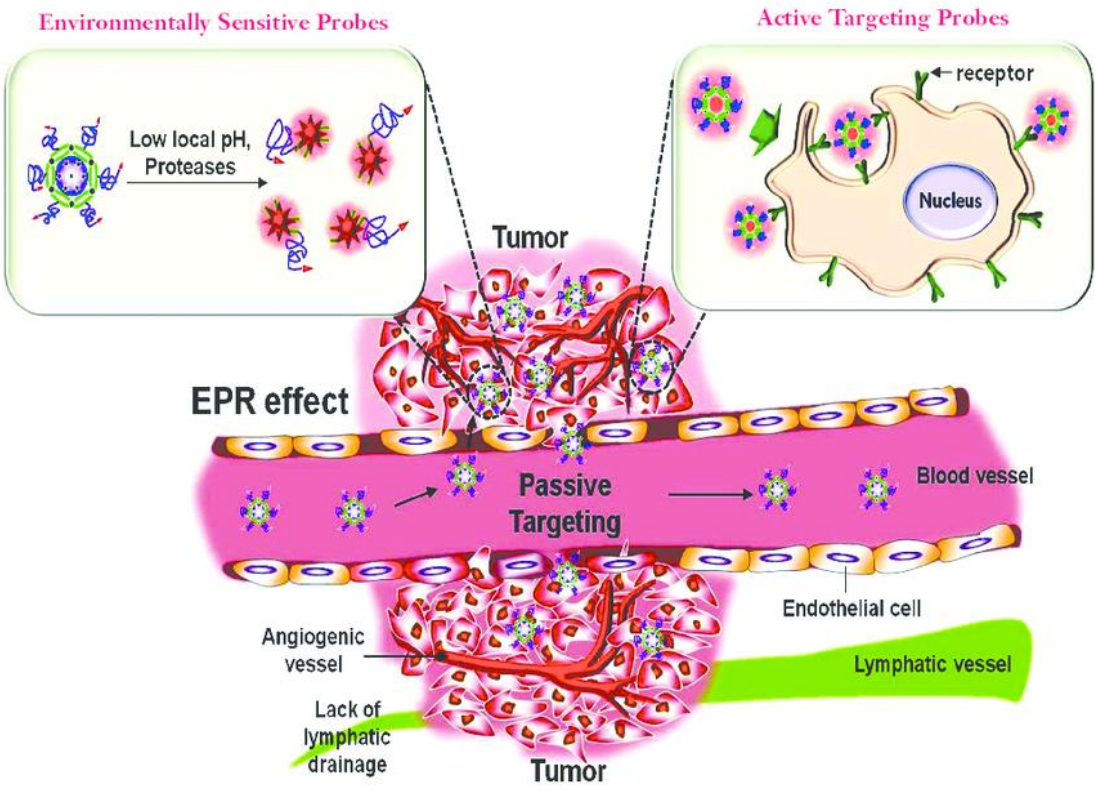

Figure 1.2: Passive and active targeting strategies utilized by nanomaterials for the delivery of therapeutic drugs in cancer management. Passive targeting is characterized by transport of nanomaterials to the tumour site due to EPR effect, leaky vasculature and cancer cells microenvironment. Active targeting is achieved via targeting moieties attached to a cell surface receptor leading to receptor mediated endocytosis and internalization. From Park, 2012.

1.2 AuNPs in cancer

Amongst all the nanomaterials presented above, gold nanoparticles (AuNPs) are at the forefront of the nanomedicine research due to their unique physico-chemical properties (Singh et al., 2018). Their use ranges from targeted delivery of drugs to contrast agents for imaging and detection of cancer (Ghosh et al., 2008, Eck et al., 2010, Bhattacharya et al., 2008). Gold in its elemental form is considered as an inert, bio-compatible, non-toxic noble metal. However, when the size of gold is significantly small, at nanoscale level, it behaves very differently from its elemental form and can be considerably toxic (Connor et al., 2005). This feature, along with its strong optical properties, ease of surface chemistry modifications and control of its size and shape, contribute to the strong preference of using gold instead of other types of nanoparticles in a range of *in vitro* and *in vivo* applications (Cobley et al., 2011, Kim et al., 2009, DeLong et al., 2010).

1.2.1 Toxicity of AuNPs

The term ‘toxicity’, refers to the adverse reactions that a substance has on living subjects and its principle was introduced almost five centuries ago by Paracelsus, when he expressed that “most drugs are beneficial at low doses, but toxic at high doses” (Timbrell, 1998, Schmid et al., 2009, Grass et al., 2010). There is a variety of conflicting studies showing both the toxicity (Dobrovolskaia, 2007, Patra et al., 2007, Peng et al., 2009) and non-toxicity (Pan et al., 2007, Zhang et al., 2009, Sung et al., 2011) of AuNPs. The nature of such conflicts relies on the fact that gold is toxic both *in vitro* and *in vivo* but various factors can affect the level of toxicity. These factors are mainly summarized into coating materials, size, shape and surface chemistry. More specifically, the various

physicochemical characteristics of NPs, such as surface charge, surface area and stabilizing coating agents could affect the biological readout of NPs toxicity along with their concentration, incubation time, types of assays and cells used (Soenen et al., 2011). It is frequently found that the toxicity of AuNPs depends on the specific cell type examined in toxicity assays. For instance, citrate-capped AuNPs (13 nm in diameter) were found to be toxic to a human carcinoma lung cell line but not to a human liver carcinoma at the same dose (Patra et al., 2007).

1.2.2 Synthesis of AuNPs

AuNPs are synthesized by the chemical reduction of $HAuCl_4$. This process results in neutral gold atoms via reduction of Au^{3+}, which are subsequently precipitated and supersaturated into atomic clusters of gold particles (Sardar et al., 2009, Low et al., 2010). Most of the synthesis methods for AuNPs involve $HAuCl_4$ as the main source of gold atoms with different modifications to control the rate of AuNP growth and the type of capping agent to preserve AuNP integrity.

One of the modifications is the Turkevich method by which citrate ions act as capping and reducing agents to produce spherical mono-dispersed AuNPs suspended in water (Kimling et al., 2006). AuNPs in water-immiscible organic liquids can be produced by the Brust method (Brust et al., 1994). AuNP seeds are made by the Perrault method, which utilizes hydroquinone as reduction agent for $HAuCl_4$ in an aqueous solution (Perrault et al., 2009). Reduction of $HAuCl_4$ by $NaBH_4$ results in monodisperse AuNPs coated with borate ions in water by the Martin method (Martin et al., 2010). Lastly, the Sonolysis process generates AuNPs based on ultrasound and the use of sugar and hydroxyl pyrolysis as reducing agents in an aqueous solution of $HAuCl_4$ in glucose (Vinodgopal et al., 2010). There are numerous alternatives to these methodologies for AuNPs

production, as their main disadvantage is lack of process reproducibility. These alternatives rely on biological agents such as microorganisms (yeast and bacteria), microbial enzymes and plant phytochemicals. For example, chickpea leaves have been shown to induce the reduction of 0.1mM $HAuCl_4$ solution to AuNPs at room temperature (Chauhan et al., 2011).

1.2.3 Characterization of AuNPs

Various techniques are used to characterize AuNPs. The size and the shape of the nanoparticles is characterized by electron microscopy and dynamic light scattering (DLS) (Fratoddi et al., 2015). EM is a technique that allows visualization of a small number of particles and subsequent size analysis, whereas DLS analyses the entire population in solution. However, some limitations exist with these methods. Artefacts may arise from EM as it operates for highly polydisperse systems under vacuum conditions. High scattering intensity of large objects could lead to difficult data interpretation of DLS analysis because of false estimates of mean particle size.

Laser Doppler electrophoresis is the technique by which surface charge of the nanoparticles is obtained by measuring their ζ-potential (Fratoddi et al., 2015). The ζ-potential can be affected by various parameters that should be taken into consideration for its accurate measurement. These parameters include the concentration of the particles present in the solution, their aggregation state, pH of the solution and the electrical conductivity. The gold concentration of a solution can be measured by inductively coupled plasma atomic emission spectrometry (ICP-AES), atomic absorption spectroscopy (AAS) and inductively coupled plasma mass spectrometry (ICP-MS) (Fratoddi et al., 2015).

Accurate AuNP characterization is vital for correlating it to toxicity. Trace impurities within the nanoparticle formulation, coating modifications and aggregation state can interfere with the cellular environment and the toxic effects observed. Such interference is unrelated to nanoparticles themselves. For example, a study showed that nano-rod formulations included impurities of free cetyltrimethylammonium bromide (CTAB) in solution and caused toxic effects in human colon carcinoma cells (Alkilany et al., 2009).

1.2.4 Applications of AuNPs

1.2.4.1 Cancer detection and imaging

AuNPs are a vital tool in cancer diagnosis due to their unique optical scattering properties which make them appropriate probes for cancer imaging *in vitro* and *in vivo* (Kumar et al., 2007). AuNPs have the ability to scatter and absorb visible light. This phenomenon is termed as surface plasmon resonance, which represents a quantum mechanical feature that occurs when the size of the nanoparticle is smaller than the wavelength of the incident light (Kumar et al., 2007). Numerous techniques are used for the detection of AuNPs at a site of interest, such as dark field microscopy, phase contrast optical microscopy and photothermal imaging (Roth et al., 1996, Sperling et al., 2008). Also, a study of antibody-conjugated gold nanospheres has shown the use of surface enhanced Raman spectroscopy (SERS) in the imaging of HER-2 markers overexpressed in MCF-7 cells (Less et al., 2009).

1.2.4.2 Delivery agents

AuNPs are promising carriers in drug delivery for cancer therapy due to their small size, shape, biocompatibility, ease of synthesis and functionalization (Zhang et al., 2009). However, limitations exist with regard to their use and the effective delivery of drugs and molecules inside the cells. Some of these limitations relate to the penetration rate being affected by biological barriers, their specificity and selectivity on the tumour site and their retention in the blood circulation (Kim et al., 2009, De Jong et al., 2008). Phase I clinical trial on PEGylated colloidal gold-TNF construct showed promising results in patients with advanced solid cancers (Libutti et al., 2010).

1.2.4.3 Photo-thermal therapy

Traditionally, hyperthermia, induced via external electromagnetic radiation, has been used to trigger cell death. Sources of heat include laser, radiowaves or ultrasound waves (Liu et al., 2009). For instance, it has been shown before that either cancer or normal cells when exposed to temperatures ranging from 41^{o}C-47^{o}C show signs of apoptosis, whereas at temperatures above 50^{o}C, cell death via necrosis has been observed (Cherukuri et al., 2010). The issue that exists with this approach is the damage to healthy surrounding cells and tissues. AuNPs provide the advantage of minimum damage to non-cancerous cells due to their specific uptake into cancer cells and strong absorbance of the light. Thus, the hyperthermic effect is greater in cancer cells than in surrounding healthy tissues (Huang et al., 2008). Cherukuri et al. illustrated that AuNPs heated with radio-frequency fields, applied to cells after NPs internalization, resulted in cancer cell death by a localized heat effect (Cherukuri et al., 2010).

1.2.4.4 Radiation therapy

Several studies have revealed the application of AuNP as radiosensitizers. The effectiveness of AuNPs as radiosensitizers is attributed to their surface functionality and the nature of their coating (Hebert et al., 2010, De Long et al., 2008). However, conflicting studies exist about the size and the tumour cell type being responsible for the radiosensitizing properties of AuNPs (De Long et al., 2008). For instance, 1.9 nm AuNPs enhanced the X-Ray effect on mice with EMT-6 mammary carcinoma leading to 86% cell death as opposed to 20% or 0% with X-Rays and NPs alone, respectively (Hainfeld et al., 2004). On the other hand, another study on 1.9 nm AuNPs provided evidence of cytotoxic effects of AuNPs by causing DNA damage and oxidative stress leading to apoptosis (Butterworth et al., 2010). Therefore, an understanding into the properties of AuNPs that confer desired abilities is crucial in order to improve their therapeutic potential as tools for cancer management.

1.3 AuNPs challenges and limitations

There is a great promise for the use of AuNPs in cancer therapy and this is evident by the numerous publications on the topic. Currently, most of the scientific community focusses on improvements of AuNPs treatments by changing AuNP functionalization and surface characteristics. However, little or no evidence exist on the exact mechanism of toxicity and induction of cell death caused by the AuNPs. Cell-type dependent differences in toxicity and uptake complicate the optimization of AuNPs for cancer therapy. If such differences are clearly understood, more selective and efficient AuNPs can be designed to target only the tumour microenvironment without affecting the normal cells and tissues.

1.4 Aims of the thesis

As discussed above, AuNPs represent a class of nanomaterials with promising advantages in cancer management. AuNPs are developed as drug vectors due to being biocompatible, easy to manufacture and inert. However, there is evidence that AuNPs can be toxic. The main aim of the thesis was to characterize the mechanism by which AuNPs cause toxicity in cancer and normal cells *in vitro*. Midatech Pharma's AuNP technology was used for the production of 50:50 αGal:PEGamine AuNPs utilized throughout the majority of the project. The key advantages of this technology were their ease of synthesis and penetration into the cells. Also, their production and scalability could be performed and controlled in the company's cGMP facility and R&D departments. In detail, the objectives listed below were addressed in this thesis and were analysed within each chapter:

- **Chapter 3:** Assessment of different physico-chemical and cellular factors affecting AuNP toxicity.
- **Chapter 4:** Role of the synthesis time and ligand density in AuNP toxicity and their effect on the transport of AuNPs.
- **Chapter 5:** Analysis of the mechanisms of cell death caused by AuNPs.
- **Chapter 6:** Evaluation of AuNP toxicity in a range of cancer and normal cell lines.

A list of appendices is also included in this thesis along with copyright permission evidence attached at the back, for each figure used.

Chapter 2: Materials and Methods

2.1 Gold Nanoparticle Based Methods

2.1.1 Chemical synthesis

All AuNPs were supplied and synthesized by Midatech Pharma PLC (Oxford, UK). They consist of a gold core (~1.2 nm in diameter) to which an organic layer of HS-C2-α-galactose (Sigma Aldrich®, 134031) and 1-amino-6-mercapto-hexaethyleneglycol (PEG-amine) were attached via gold-sulphur bonds, as described previously (Lund et al. 2011). In detail, the AuNPs were synthesized by the reduction of 100 g/L $HAuCl_4$ (Sigma-Aldrich®, 254169) with 90 mM $NaBH_4$ in the presence of disulfide-containing ligands with Milli-Q water as a solvent (ELGA purification system). The synthesis process was carried out for 1h, 2h and 5h. After the end of the synthesis incubation times, the samples were purified either by spin washing with excess Milli-Q water using an Amicon 10kDa ultrafiltration device. AuNPs were resuspended in Milli-Q water to 2 mg/ml [Au] and stored in amber vials at 4ºC.

Throughout the project, various nanoparticle formulations with different characteristics were tested. These different characteristics ranged from differences in the nanoparticle synthesis time, scale of synthesis, method of purification, Au stock concentration and ligand ratios. A list of all the nanoparticle formulations' code and description is presented in the table below (Table 2.1).

Table 2.1: A list of all the AuNPs formulations supplied by Midatech.

Category	Midatech's Identification Code	Description
AuNPs with different ligand ratios	M175-042-01	0:100 GalC2
	M175-042-02	11:89 PEG:GalC2
	M175-065-03	30:70 PEG:GalC2
	M175-065-04	45:55 PEG:GalC2
	M175-042-05	51:49 PEG:GalC2
AuNPs with different synthesis time	M218-024-01	50:50 1h reaction
	M218-024-02	50:50 2h reaction
	M218-024-05	50:50 5h reaction
AuNPs with different purification method	M218-095-01	50:50 no purification MeOH/H_2O
	M218-095-02	50:50 MeOH/H_2O purified
	M218-104-01	50:50 alkaline purified
AuNPs with different scale of synthesis	M218-086-01	50:50 Small scale
	M182-073-1	50:50 Large scale
Identical AuNPs with different synthesis day	M229-062-01	50:50 2h reaction
	M229-062-02	50:50 2h reaction
	M229-062-03	50:50 2h reaction
AuNPs from previous work in the lab	NP146-49	50:50
	NP 118-40-1	50:50

Note: 50:50 ratio refers to αGal:Pegamine AuNPs.

2.1.2 Nanoparticle physico-chemical characterization

2.1.2.1 Transmission Electron Microscopy (TEM)

The core size of the nanoparticles was determined by TEM. Samples were prepared by drying drop-coating films of the nanoparticle solutions on electrostatically discharged carbon-coated copper TEM grids and visualized on a JEM-1400 model EM (JEOL, USA) operated at an accelerating voltage of 80 kV and 100,000x magnification. Core sizes were calculated from TEM images using the automated particle analysis feature based on the threshold approach on ImageJ 1.49 software, as described in detail below.

Specifically, 5 images were taken for each nanoparticle sample and loaded into the software for subsequent analysis. The brightness of the images was adjusted in order to visualize dark (black) nanoparticles in a bright (white) background. A threshold was applied to the adjusted images and the nanoparticle area was measured by the function “Measure particles”. Pixel dimensions were converted into nanometres based on the magnification factor. The dimensions for size estimates calculations were set between 1 nm-infinity. All the measurements from each individual image were transferred and combined into an excel spreadsheet and the diameter of the nanoparticles was calculated by the formula: $d = 2 * \sqrt{A}/\pi$, where A=measured area, d=diameter and π=3.14.

2.1.2.2 Dynamic Light Scattering (DLS)/Zeta potential

The hydrodynamic diameter and zeta potential of the AuNPs (500 μg/ml) were calculated using a Nano ZSP zetasizer (Malvern instruments). Zeta potential measurements were made in 20% PBS at pH 7 in a DTS1070 cell, whereas DLS was measured in pH 7.4 PBS in a ZEN0040 cell.

2.1.2.3 ^{1}H-Nuclear Magnetic Resonance (^{1}H-NMR)

The ligand shell of the nanoparticles was analysed by ^{1}H-NMR. For each sample, 5 mg of gold was transferred into D_2O using ultrafiltration (Amicon Ultra-4, MWCO 10kDa). Three centrifugation steps were performed in 2 ml D_2O (4,000 rpm, 12 min). After the last centrifugation step, the particles were transferred into Eppendorf tubes and treated with 0.3M KCN/0.1 M KOH. The samples were kept at 37^{o}C overnight before transfer to NMR tubes. Samples were then centrifuged (4,000 rpm, 1 min) and analysed by ^{1}H-NMR at 500 MHz (Avance III HD, Bruker) and MestReNova software. The protons for the αGal and PEGamine ligands were identified to resonate at 4.95 ppm and 2.75 ppm, respectively. These correspond to the single anomeric proton of αGal (NMR doublet) and the two CH_2 protons proximal to the terminal NH_2 group in the PEGamine linker (NMR triplet), thus their integrals were used to quantify the abundance of the two ligands.

2.1.2.4 Au concentration assay

In order to determine the Au concentration of the samples, a spectrophotometric assay was used. Three gold standards were prepared at 0, 5 and 10 mg/ml concentrations (Gold standard for AAS, 1000 mg/L Au in hydrochloric acid, Sigma-Aldrich®, 08269). 10 µl of AuNPs were mixed with 30 µl of 30% fresh cold aqua regia in H_2O and 150 µl of 2 M NaBr and run against the prepared gold standards in a 96-well plate. The absorbance was read immediately in a microplate reader (OPTIMA FluoSTAR) at a wavelength of 382 nm.

2.1.2.5 UV-Vis Absorbance spectrum

The surface plasmon resonance of the AuNPs was checked by their absorbance at 520 nm. 200 µl of 100-400 µg/ml AuNPs were measured against a water blank in 96-well plates in a Labtech Spectrostar Nano spectrophotometer.

2.1.2.6 X-ray Photoelectron Spectroscopy (XPS)

The ligand density for each nanoparticle was estimated by XPS in Midatech's external collaborators facilities, CIC BioMagune, Spain. XPS experiments were performed in a SPECS Sage HR 100 spectrometer with a non-monochromatic X-ray source at 1253.6 eV energy and 250 W. The selected resolution for the spectra was 15 eV of pass energy and 0.15 eV/step. All measurements were conducted in an ultra-high vacuum (UHV) chamber at a pressure around $5x10^{-8}$ mbar. The calculation of the ligand density was obtained via Au:S ratio and is based on the fact that each ligand on the AuNPs surface carries a single S atom, while Au atoms constitute the AuNP core. For simplicity of calculation, the geometry of AuNPs is assumed to be spherical as verified by TEM images.

2.1.2.7 Scanning Electron Microscopy (SEM)

The ligand density of the AuNPs was also confirmed by SEM. 3 µl of 2 mg/ml AuNPs were dried onto aluminium stubs and analysed with a Zeiss Supra 55VP Field Emission Gun Scanning Electron Microscope (FEGSEM) at 20 kV. Analysis was performed with AZtec Energy software (Oxford Instruments) for measurements of the % Wt of Au and S atoms.

2.1.2.8 FPLC

Any possible aggregation of the AuNPs was tested by FPLC. Aggregated and individual nanoparticles were separated by ÄKTA™ pure chromatography FPLC system (GE Healthcare, UK). The particles were incubated with PBS or DMEM+10% FBS for 30min at 37^{o}C at a concentration of 200 μg/ml. Samples were run on a Superdex 200 10/300 GL FPLC column at 0.5 ml/min, using a 100 μl injection loop. The absorbance was monitored at 400 nm.

2.1.2.9 Agarose gel electrophoresis

The AuNPs were also run in an agarose gel in order to separate and visualize mixed charged/sized particles within a single population. 20 μl of a 2 mg/ml nanoparticle solution was diluted 1:1 in H_2O, PBS or 10% FBS and left for 3h at room temperature and 37^{o}C in order to examine any aggregate formation. Particles have a positive net charge and therefore run towards the negative electrode. 1% agarose gel was prepared in 0.5% TBE buffer and left to set into the gel tray of the electrophoresis apparatus (Thermo Scientific, Owl™ EasyCast™) for approximately 30 minutes. Samples were loaded with 5 μl of 30% glycerol diluted in H_2O and run for 45 min at 100 mV and 0.5X TBE buffer. A DNA ladder was used as a marker (Quick-Load® Purple 1 kb Plus DNA Ladder, BioLabs, N05525). Gel was visualized using the ImageJ software.

2.2 Cell Culture Based Methods

2.2.1 Cell Culture

A list of all the cell lines used throughout the project is presented in the table below (Table 2.2). The origin of the cell lines was: *Homo sapiens*, human.

Table 2.2: **A list of all the cell lines used throughout the project.** Alternated shading corresponds to pair of cell lines indicating normal and cancer cell type.

Abbreviation	Tissue/Disease
HSC-3	Oral squamous/carcinoma
HaCaT	Keratinocyte
MCF-7	Mammary gland, breast; derived from metastatic site: pleural effusion/adenocarcinoma
HMEC	Mammary Epithelial Cells
hA	Primary astrocytes
U-373	Glioblastoma/astrocytoma
A-498	Kidney/carcinoma
HEK-293	Embryonic kidney
Caco-2	Colon colorectal/adenocarcinoma
HeLa	Cervix/adenocarcinoma

HSC cells were purchased from the American Type Culture Collection. HaCaT cells were obtained from Erik Walbeehm, Erasmus Medical Centre (Rotterdam, Netherlands) and hA cells were supplied by ScienCell Research Laboratories (Carlsbad, California, USA). For all other cell lines, vials were taken from the archived liquid nitrogen facility at The Open University.

All cell lines apart from hA, HMEC and Caco-2 were cultured in low glucose (1 g/L) DMEM media (Gibco®, 21885-108) supplemented with 10% FBS (Sigma-Aldrich®, F9885) and 1% penicillin/streptomycin (ThermoFisher Scientific, 15140122) in a humidified incubator at 37°C with 5% CO_2. Cells were grown in T-75 culture flasks to about 80% confluency before passage. hA cells were cultured in Astrocyte Medium (ScienCell™,1801) supplemented with 2% FBS and 1% astrocyte growth supplement (ScienCell™,1852). HMEC cells were cultured in HuMEC Ready Medium (Gibco®, 12752-010), containing 1% HuMEC supplement (Gibco®, 12754-016) and 25 mg bovine pituitary extract (Gibco®, 13028-014). Caco-2 cell culture conditions and medium were the same as for all the cell lines apart from being supplemented with 20% FBS instead of 10%. To plate cells at required densities for various experiments, cells were washed with Ca^{2+} free HBSS (Sigma-Aldrich®, H6648) and trypsinized with 0.05 % T/E (Invitrogen™ Life Technologies, 25200056) for less than 10 min at 37°C.

2.2.2 Cytotoxicity of AuNPs

2.2.2.1 Clonogenic assay

The toxicity of the AuNPs and their effect on cell survival and proliferation was evaluated using clonogenic assays on HSC, HaCaT, A-498 and HEK-293. The rest of the cell lines listed above (Table 2.2) did not grow in colonies. HSC and HaCaT cells were seeded at 300 cells/well in a 24-well plate, HEK-293 at 1,000 cells/well and A-498 at 800 cells/well and allowed to adhere overnight. The next day, cells were acutely exposed for 3h to 0, 1, 3 and 10 μg/ml AuNPs. Cells were left to grow for 6 days to form colonies. At the end of day 6, cells were briefly rinsed with water, stained and fixed with 2% methylene blue in 50% ethanol solution for 3h. The staining/fixation solution was removed, plates were rinsed with distilled water and dried.

Images of stained plates were captured using a G:Box Chemi XX6 gel documentation system with GeneSys v1.4.6 software (Syngene). Colonies containing >50 cells were quantified using GeneTools v.4.03 software (Syngene). Automated counts were verified by eye. IC50 values were estimated from logarithmic plots of AuNP concentration versus percent of control colonies. IC50 is the concentration at which the AuNPs cause 50% cell colony reduction compared to the untreated controls.

2.2.2.2 CyQUANT cell proliferation assay

The proliferation and cell number of all the cell lines listed in Table 2.2 were assessed by CyQUANT cell proliferation assay (ThermoFisher Scientific, C35006). This assay is based on a DNA-intercalating fluorescent dye, which determines the amount of DNA present in a sample. Cells were seeded in a 96-

well plate at a density of 2,000 cells/well and incubated at 37^{o}C and 5% CO_2 for 6 days after an acute 3h AuNP exposure at 0, 5, 10 µg/ml. At day 0, 1, 2, 3, 4, 5, and 6 cells were washed with HBSS and frozen at -80^{o}C for at least 24h for subsequent analysis. A mixture of CyQUANT dye and cell lysis buffer in distilled water was prepared as follows. The cell lysis buffer stock solution was diluted 20-fold in distilled water and the CyQUANT stock solution was diluted 400-fold into the 1X cell lysis buffer. For up to 100,000 cells detection, 200 µl of the mixture was added to the 96-well plates and incubated for 5 min at room temperature in the dark. Readings of DNA content/well were obtained by fluorescent microplate reader at Ex480/Em520 nm. Background fluorescence was subtracted when plotting the data.

2.2.3 Silver staining

Detection of AuNPs using a standard light microscope was achieved by silver staining. Cells were seeded at 30,000 cells/well and exposed to AuNPs for 3h. After the end of the exposure time, media was removed, cells were washed with PBS and fixed by 4% PFA (Merck, 100496) for 15 min. The cell membrane was permeabilized by 0.05% Triton™ X-100 (Sigma-Aldrich®, X100) in PBS for 2 min. The silver staining developer and enhancer solutions (R-Gent, Aurion, 500.011) were allowed to reach room temperature equilibrium and mixed at 50:50 ratio. The complete silver staining solution was applied to cells for 5-10 min in the dark. Cells were then washed twice with PBS and samples were stored at 4^{o}C for subsequent imaging. Samples were imaged by bright-field and phase contrast microscopy at 20x and 40x objective.

2.2.4 TEM

2.2.4.1 TEM for cellular uptake quantification of AuNPs

Cellular uptake was quantified by TEM. Cells were seeded onto 12 trans-well inserts at a density of 100,000 cells/insert and left to adhere overnight. The next day, cells were incubated with AuNPs for 3h at a concentration of 10 µg/ml at 37^{o}C or 4^{o}C. In the latter case, cells were kept at 4^{o}C for at least 30 min prior to AuNPs exposure. At the end of the incubation period, cells were washed 3x with HBSS, fixed and the AuNPs were silver enhanced (R-Gent, Aurion, 500.011) for 45 min at room temperature and processed for TEM imaging according to Gromnicova (Gromnicova et al., 2013). Ultrathin sections of cells were visualized on a JEOL 1010 TEM operated at an accelerating voltage of 80 kV at 15,000x and 50,000x magnifications.

2.2.4.2 Nanoparticle TEM counts on cells

A systematic sampling method was used to evaluate nanoparticle counts in cells. This method was based on acquiring 25 TEM images at the same magnification and same settings across the samples at regular intervals which included every fifth field of view with a cell. Each picture was loaded into ImageJ software, where the area of the nucleus, cytoplasm and the length of the cell surface was measured. Nanoparticles in each region were manually counted and their number was assigned to one of the three different categories (nucleus, cytoplasm and cell surface). Data were expressed as nanoparticles per micron for cell surface nanoparticle counts or nanoparticles per micron^{2} for nuclear/cytoplasmic nanoparticle counts. Three independent experiments were performed for AuNPs quantification with two technical replicates per condition. Images shown are from a representative experiment.

2.2.4.3 Fascin inhibition

Fascin-G2, a fascin Inhibitor (Xcessbio, M60269-2s) was used to inhibit filopodia formation. Cells were exposed to the inhibitor at 50 μM for 2h at 37ºC prior to AuNP exposure. Cells were then incubated with 10 μg/ml AuNPs in 50 μM Fascin-G2 for a further 3h, either at 37ºC or at 4ºC. At the end of the incubation times, cells were washed, fixed and prepared for TEM analysis.

2.3 Mechanism of Cell Death Related Assays

2.3.1 Apoptosis/Necrosis

In order to discriminate between apoptotic, necrotic and live cells within a cell population after an acute 3h exposure to AuNPs, a cytometry based assay kit, Annexin V-FITC Apoptosis Detection (Sigma-Aldrich®, APOAF-20TST) was used. Quantification was obtained via the Tali® Image-Based Cytometer (ThermoFisher Scientific, T10796). HSC cells were seeded at 25,000 cells/well in a 24-well plate and left to adhere overnight. The next day, cells were exposed to 10 μg/ml of AuNPs for 3h and a time-course of 3h, 24h, 48h and 72h was followed to establish a cell death time-course of events. Staurosporine (Abcam, ab120056) was used at 1 μM for 3h as a positive control for apoptosis induction. For quantification after each time-point, the supernatant was kept in a 1.5 ml Eppendorf tube and cells were washed with HBSS and trypsinized with 0.05% T/E for 7 min. The trypsinized samples with their supernatant were centrifuged at 1,000 rpm for 5 min and the pellet was washed twice in PBS.

Each pellet was re-suspended in 1x Binding Buffer (Sigma-Aldrich®, B9796) at a concentration of ~1 x 10^6 cells/ml and 5 μl of Annexin V FITC Conjugate (Sigma-Aldrich®, A9210) plus 10 μl of Propidium Iodide Solution (Sigma-Aldrich®, P2667) was added to each tube. The samples were incubated at room temperature for exactly 10 minutes, protected from light. Red (Ex535/Em617 nm) and green (Ex494/Em518 nm) fluorescence of the cells was immediately quantified by Tali cytometer. Cells that were early in the apoptotic process were stained positive only for the Annexin V FITC Conjugate. Live cells showed no staining and necrotic/late apoptotic cells were stained by both Propidium Iodide and Annexin V FITC Conjugate.

2.3.2 Caspases

2.3.2.1 Caspase 3/7 Activation

Further insight into the apoptotic cell death mechanism involved quantification of the caspase 3/7 activity via a fluorescence assay. CellEvent™ Caspase-3/7 Green Detection Reagent (ThermoFisher Scientific, C10723) was used to determine the caspase 3/7 activation in HSC cells. HSC cells were seeded at 25,000 cells/well in a 24-well plate and left to adhere overnight. The next day, cells were exposed to 10 μg/ml of AuNPs for 3h and a time-course of 3h, 24h, 48h and 72h was followed to establish a cell death time-course of events. Staurosporine was used at 1 μM for 3h as a positive control for apoptosis. Cells were prepared as described above for subsequent analysis. The CellEvent™ Caspase-3/7 reagent was diluted into PBS+5% FBS and added to cells at an optimized concentration of 6 μM for 30 min at 37^{o}C. The fluorescence was recorded by Tali cytometer at Ex502/Em530 nm.

2.3.2.2 Caspase 3/7 inhibition

Caspase 3/7 mediated apoptosis in HSC cells after an acute 3h exposure was also validated by using a caspase 3/7 inhibitor, Z-VAD-FMK (Abcam, ab120382). HSC cells were seeded at 300 cells/ well at a 24-well plate for clonogenic assay. Cells were left to grow overnight and the next day, they were pre-loaded with 50 μM of the caspase inhibitor for 1h at 37^{o}C before exposure to AuNPs. After 1h, 10 μg/ml of AuNPs was added to the cells for 3h at 37^{o}C. Antimycin-A (Abcam, ab141904) was used at 10 μM as a positive control. At the end of the incubation period, cells were washed with media and left to grow for 6 days for clonogenic assay. Data were expressed as percentage of control colonies.

2.3.2.3 Caspase 8/9 inhibition

To effectively distinguish between extrinsic and intrinsic apoptotic pathways, caspase 8 and caspase 9 inhibition was evaluated. HSC cells were seeded at 300 cells/ well at a 24-well plate for clonogenic assay. Cells were left to grow overnight and the next day they were pre-incubated with either 70 nM caspase 8 inhibitor I (Merck, 218773) or 50 nM caspase 9 inhibitor II (Merck, 218776) for 1h prior to addition of 10 μg/ml AuNPs and incubation for 3h. Antimycin-A (Abcam, ab141904) at 10 μM was used as a positive control for apoptosis and 50 ng/ml Apo2 ligand/TRAIL as a positive control for inducing extrinsic apoptosis. Clonogenic assays were analysed after 6 days, as previously described.

2.3.3 Mitochondrial membrane potential

2.3.3.1 JC-10

Alterations in the mitochondrial membrane potential were assessed by using the JC-10 fluorescent dye. The JC-10 Mitochondrial Membrane Potential Assay Kit (Abcam, ab112133) is based on the principle that JC-10 dye diffuses out of mitochondria in apoptotic/necrotic cells, staining cells in green fluorescence as opposed to red staining in live cells. An orange colour is observed when the mitochondrial membrane becomes more polarized. A ratio of green to red fluorescence was plotted for analysis and FCCP was used at 20 μM as a positive control. In detail, HSC cells were seeded at 25,000 cells/well in a 24-well plate and left to adhere overnight. The next day, cells were exposed to 10 μg/ml of AuNPs for 3h and a time-course of 3h, 24h, 48h and 72h was followed.

For quantification after each time-point, the supernatant was kept in a 1.5 ml Eppendorf tube and cells were washed with HBSS and trypsinized with 0.05% T/E for 7 min. The trypsinized samples and their supernatants were centrifuged at 1,000 rpm for 5 min and the pellet was washed twice in PBS. 1X JC-10 dye solution (component A) was prepared in assay buffer (component B) and 100 µl was added to each cell suspension ranging from 2-5 × 10^5 cells/sample. The samples were incubated for 30 minutes at 37ºC and 5%CO_2, protected from light. The fluorescence of each sample was monitored by Tali cytometer in red (Ex535/Em617 nm) and green channels (Ex494/Em518 nm).

2.3.4 ROS oxidative measurements

2.3.4.1 ROSBrite

Oxidative damage caused by AuNPs to HSC cells was determined by measuring the ROS increase on a Tali cytometer. Cells were seeded and prepared as described previously. A 10 mM stock solution of ROS Brite™ 570 (AAT Bioquest, 16000) was prepared in DMSO. TBHP at 150 µM was used as positive control to induce ROS production. Trypsinized cells were incubated with 10 µM ROSBrite solution diluted into HBSS with 20 mM HEPES buffer at pH 7.4 and left to incubate for 15 minutes at 37ºC and 5%CO_2. The dye loading solution was replaced by HBSS and fluorescence was read at Ex556/Em566 nm.

2.3.5 Cell cycle

In order to evaluate whether the AuNPs cause cell cycle arrest at a specific checkpoint, Tali™ Cell Cycle Kit (ThermoFisher Scientific, A10798) was used. HSC cells were prepared as described above and exposed to 10 µg/ml of AuNPS for 3h and 24h. At the end of the exposure times, cells were washed twice with

PBS by centrifugation at 1,000 rpm for 5 minutes and fixed with 70% ice-cold ethanol. Samples were placed at -20^{o}C overnight and analysed the next day. For analysis, cells were centrifuged for 5 minutes at 4^{o}C and re-suspended in PBS. PBS was removed and cells were stained with 200 µL of Tali solution to a final concentration of 1×10^5 –5×10^6 cells/ml for 30 minutes at room temperature protected from light. Samples were imaged using the Tali cytometer at Ex535/Em617 nm. Nocodazole at a concentration of 50 nM for 24h was used as a positive control for causing G_2 arrest.

2.4 Statistical analysis

Data were analysed using GraphPad 6.0 Prism® software. One-way or two-way ANOVA with Tukey's post-tests were performed to determine significant differences at a critical value of α=0.05. An unpaired two-tailed t-test was used for comparison of the mean value between two groups. All the experiments were performed in triplicate and on three independent times, unless otherwise stated. Asterisks indicate significant differences of *P<0.05, **P<0.01, ***P<0.001, ****P<0.0001. Non-significant differences were not plotted. Mean±SEM was plotted on all graphs.

Chapter 3: Assessment of Different Physico-chemical and Cellular Factors Affecting AuNP Toxicity

3.1 Introduction

The toxicity of the AuNPs is a topic, on which contradictory evidence is frequently published. Few studies propose that AuNPs are non-toxic, whereas others describe them as toxic. Specifically, a study using 3.5 nm AuNPs on immune system cell lines showed that particles were internalized by endocytosis and did not cause toxicity as measured by MTT assays (Shukla et al., 2005). Similarly, Villiers et al. found that 10 nm citrate capped AuNPs were not toxic in dendritic cells and did not alter the phenotypic profile of the cells (Villiers et al., 2009). In contrast to these results, Goodman et al., explained the toxicity of cationic gold nanospheres by their ability to interact with the cellular membrane, leading to membrane depolarization (Goodman et al., 2004). Data from Pan et al. also showed that 1.4 nm gold nanospheres were cytotoxic in a range of cell lines by triggering mitochondrial damage and ROS production (Pan et al., 2009).

There are numerous potential reasons for this controversy. It is difficult to compare published data because of the cytotoxicity assays used which often differ between the studies. Other differences might include the cell type used or the nanoparticle properties themselves. For instance, Patra et al., showed that 15 nm citrate-capped AuNPs were toxic to cancer lung cell type but not to a liver carcinoma cell line when using the same concentration of particles (Patra et al., 2007). In addition, the dose and exposure time of the particles make it difficult to compare results. This chapter will explain the factors that need to be considered for toxicity evaluation and how nanoparticle physicochemical parameters affect toxicity *in vitro*.

3.1.1 Experimental considerations in the design of cytotoxicity assays

The majority of published research is based on examination of the cytotoxicity of AuNPs *in vitro* due to the ease in the design and execution of the experimental set up and the overall control. Careful design of cytotoxicity assays *in vitro* could mimic *in vivo* conditions and therefore, certain considerations need to be taken into account. Some of these considerations that will be discussed in detail below include finding the appropriate cell type to be used, the choice of the toxicity assay, the dose of the AuNPs along with exposure time and the effects of the physicochemical properties of the AuNPs.

3.1.1.1 Cell types

In general, the choice of cell types to be used when evaluating the cytotoxicity of AuNPs is dependent on the target organ and the administration route (Oberdörster et al., 2005). Cell types are characterized by differences in their proliferation rate, membrane and cell physiology, therefore it is important to understand the effects of the nanoparticles in a range of cell lines. Regarding the administration route of nanoparticles for biomedical applications, the most common routes include subcutaneous, intramuscular, intraocular or intravenous pathways (Oberdörster et al., 2005). Therefore, the cell lines to be used in evaluation of the cytotoxic potential of a nanoparticle should represent the exposure route or organs to be targeted such as nervous system, kidney, liver or endothelial cells.

It is important for the cytotoxicity assays to go beyond a single cell type study as AuNPs elicit different systemic responses. Depending on the route of exposure, particles can accumulate in various parts of the body and trigger an immune response, inflammation or stress (Dobrovolskaia and McNeil, 2007, Nel

et al., 2006). For instance, macrophages, a type of a white blood cell, are responsible for identifying and eliminating any foreign particles from the body (Jepson and Clark, 1998). Thus, it is important to study the effects of any nanoparticle on immune cells, which will provide further information into the effective design of nanomaterials (Rothen-Rutishauser et al., 2005).

In addition to studying uptake and toxicity in macrophages and other immune cells, the use of endothelial and epithelial cells could provide an insight into nanoparticles cytotoxicity in an *in vivo* situation. Optimization of cell density and culture conditions are of crucial significance in cytotoxicity assays as there are cell type dependent differences in proliferation rates and cell death mechanisms (Frattodi et al., 2015). Also, cells at the logarithmic growth phase are more susceptible to nanoparticle toxicity than cells at the stationary phase (Pan et al., 2007). All these factors affect the sensitivity of cells to nanoparticles and could translate into inconsistencies in toxicity.

3.1.1.2 Dose of AuNPs in cytotoxicity assays

Many studies have presented the concentration dependent toxicities of AuNPs (Nan et al., 2008, Lewinski et al., 2010). The chosen concentrations to be tested in toxicity assays *in vitro* should be representative of the indicative dose to be administered in patients. However, it is a very complicated process to determine this dose in cell culture, as many parameters influence the actual value of the dose. Nanoparticle parameters itself, such as their aggregation state in media, affect the number of particles internalized into the cells (Teeguarden et al., 2007). Also, the fact that different studies do not express the nanoparticle dose in the same unit, makes it harder to compare and distinguish the most effective dosage. Most studies express the toxicity of a particle as µg/ml volume,

μg/cm^2 surface area of a culture dish or μg/10^6 cells. For example, a report on the cytotoxicity of silica nanotubes converted the mass per unit volume to number of particles inside the cells when comparing 200 nm and 500 nm nanotubes. They found double the number of 200 nm nanotubes inside the cells as opposed to 500 nm nanotubes, correlating the increased number of particles to increased toxicity due to smaller size of the nanotubes (Nan et al., 2008).

Apart from the actual administered concentration described above, there are specific methods that accurately determine the concentration of particles inside the cells. Some of these methods include the analytical techniques of LC-MS, ICP-MS, MS and electron microscopy (Moss et al., 2007, Gulson and Wong, 2016). Depending on the dosimetry computational method used, different information is acquired. For instance, microscopy provides a qualitative and visual analysis of the localization of particles inside the cells, but is hard to quantify at larger scale, whereas MS provides a quantitative analysis of a large number of cells with no information on localization. These limitations need to be considered before performing a cytotoxicity assay and attempting a comparison of uptake between nanoparticles.

3.1.1.3 Choice of cytotoxicity assay

The dose-dependent toxicity of nanomaterials in cells is mainly examined by assays of metabolic activity, proliferation/cell viability and apoptosis. The most common assays include PI or trypan blue tests, LDH leakage, MTT or MTS assays, calcein AM, measurement of caspase substrates or Annexin V (Marquis et al., 2009, Soenen and Cuyper, 2009). PI and trypan blue assays are indicative of the cell membrane permeability and allow entry of the dye into cells with a disrupted cell membrane. The LDH method also determines the level of cell

membrane disruption (Frattodi et al., 2015). The most common method in *in vitro* toxicological studies is the MTT assay, which measures the metabolic activity of mitochondria in cells and quantifies the number of metabolically active, proliferating cells. Calcein AM is non-fluorescent after being taken up into the cells and is becoming fluorescent only after cleavage by esterases, showing cell viability. In contrast, caspases 3/7 and Annexin V are indicative of apoptosis (Frattodi et al., 2015).

Depending on the assay and the type of the nanomaterial being examined for toxicity, there is a possibility of the nanoparticle to interfere with the assay. For instance, in the case of aluminium nanoparticles, a strong interference occurred with the MTT dye leading to misinterpretation of data (Monteiro-Riviere et al., 2010). Also, subcellular changes could take place with nanoparticles affecting specific cell functions, such as mitochondrial respiration without leading to cell death. Effect on cell viability by AuNPs exposure might not be visible, but transcription alterations and genetic damage might occur which are not phenotypically expressed.

3.1.1.4 Chemical properties

In addition to the parameters explained above, the physico-chemical properties of the nanoparticles affect cytotoxicity. These properties include the size and shape of the particles, agglomeration state and the surface ligands. Besides the effects on the cytotoxicity, these properties also affect cellular uptake, bio-distribution and protein adsorption. A table of the effects of AuNPs toxicity on various cell lines depending on their properties is presented below (Table 3.1).

Size and shape

AuNPs are synthesized in numerous shapes, for instance spheres, tubes, wires and rods and sizes ranging from 1-500 nm. There are conflicting studies of whether toxicity is dependent on nanoparticle size or not (Lewinksi et al., 2010, Pan et al., 2007). Some studies showed that the smaller the size of a nanoparticle, the easier the penetration into biological systems (Frattodi et al., 2015). It is suggested that this size-dependent toxicity arises either because of the presence of specific coated surface ligands or because of the large surface area to volume ratio that increases the nanoparticle activity. For example, it is reported that 1.4 nm triphenylphosphine stabilised AuNPs tested on four cell lines were more toxic and induced cell death by necrosis than 15 nm AuNPs that found to be non-toxic *in vitro* (Pan et al., 2007). For various types of nanoparticles including silica nanotubes and quantum dots, it is proposed that as particle size decreases, toxicity increases (Lewinksi et al., 2010, Pan et al., 2007).

Apart from the size, nanoparticle shape also plays an important role in cytotoxicity. For instance, gold nanorods were more toxic than spherical gold nanomaterials on HaCaT cells (Lasagna-Reeves et al., 2010). The exact mechanism of this observation is not understood, but surface properties, such as the ligand shell might be a key reason. Table 3.1 summarizes the findings of various studies conducted so far on the effects of size, type of cell line and shape of AuNPs and their biological effects *in vitro*.

Table 3.1: **Summary of some in vitro AuNPs cytotoxicity studies.**

Type of cell line	Size of AuNP	Dose	Shape, Surface group	Type of test	Biological effect	Ref.
Human leukemia cells (K562)	4, 12, 18 nm	25mM-250mM	Citrate coated	MTT assay	Non-toxic to these cells	Murphy, 2010
Mytilus edulis	1, ~13 nm	1mM	Citrate coated	Oxidative stress, catalase activity	AuNPs induced oxidative stress in digestive gland	Van Doren et al., 2011
Human dermal fibroblast	10-50 nm	10, 50, 100, 200, 300 µM	Spherically citrate coating	MTT	20nm were not toxic even at 300 µM	Patra et al., 2010
Healthy volunteer blood specimens	30-50 nm	0.450 & 0.420 mg/ml	Colloids citrate-stabilized	2D PAGE, AFM, DLS & TEM	69 different proteins bound to AuNPs surface.Change in plasma coagulation time	Renault et al., 2008
Human umbilical vein endothelia (ECV-304) cells	100 nm	20 µl	Spherically bare and PCL-coated Au NPs	Microtubule staining	AuNPs found in endosomes or lysosomes, cytoplasm, nucleic envelope and nucleus. Bare were slightly toxic while PCL had no effect	Ghosh et al., 2008
Human hepatocellular carcinoma (HepG2) cells	25±35 nm	1.0 nmol/L AuNP, 1.2 mol/L Paclitaxel (T)	Spherical particles	MTT, quartz crystal microbalance (QCM) and flow cytometer assay	AuNPs: low cytotocxicity but disrupt adhesion and enhance apoptosis	Yum et al., 2010
Human skin cell line (HaCaT) Keratinocytes	1.5 nm	10 µl	Spherically and nanorods CTAB coated	MTT	Spherical AuNPs were non- toxic. AuNP nanorods were highly toxic due to presence of CTAB coat layer	Connor et al., 2005
Human prostate carcinoma PC-3 cells	30-90 nm	1.5 nM	Spherical AuNPs	MTT and LDH assay	No LDH leakage observed up to 34 nM.	Tsoli et al., 2005

Pancreatic carcinoma & Cama-1	20 nm	100 nM	Cetuximab conjugated AuNPs	Flow cytometry	Panc-1 had viability of 46% ± 12%, Cama-1 cell had a viability of 92% ± 2%	Bar-Ilan et al., 2009
Optical cells	20 nm	2 mM	protein-coated	Optical images	AuNP were found to disrupt the mixed phospholipid/cholesterol monolayer	Chithrani et al., 2006
MRC-5 human lung Fibroblasts	20 nm	1nM	FBS coated AuNPs	Oxidative stress PCR array, Lipid hydro-peroxide assay	Oxidative damage, induced up-regulation of antioxidants, stress response genes and protein expression	Khan et al., 2007
Mammary adenocarcinoma (SKBR3), Human leukemia cells (HL60)	L= 44.8±2.8 & 41.8± 3.3 W= 18.5 ±1.6 and 11.7 ±1.4 nm	20 µl	PEG coated nanorod and PSS-coated nanorods	MTS assay	PEGylated particles did not induce toxicity to any cells tested. PEGylated gold nanorods exhibited better dispersion stability, PSS coated rods tended to flocculate or cluster with induced toxicity	Hauck et al., 2007
A549 cells, human alveolar epithelial-like cell	15 nm	200-2000 µg	AuNPs	Real-time PCR, ELISA	No adverse effects from AuNPs were observed. No induction of oxidative stress markers and inflammatory cytokines	Fanord et al., 2011
Human Sperm	9 nm	500 µL	AuNPs	Media	AuNPs penetrated the sperm cells head and tails. 25% of the sperm became non-motile compared to 95% control	Donaldson et al., 2009

Agglomeration state and surface coating

Agglomeration of nanoparticles greatly influences particle-cell interactions and leads to changes in their shape and size. Especially in *in vitro* studies, particle aggregation is affected by the cell culture media due to the presence of proteins, fixed pH and ionic strength (Auffan et al., 2010). Therefore, it is important to assess whether the surface chemistry, size and shape of the nanoparticles is altered by the surrounding environment before any toxicity evaluation. Surface modifications of the nanoparticles such as the introduction of a PEG molecule, enable the particles to remain well dispersed in solution (Bagwe et al., 2006). PEG is the most common functional group used as a modifying agent due to its solubility and amphiphilic characteristics (Dong et al., 2010).

Although there are various ways to maintain a well dispersed solution of nanoparticles via addition of specific ligands and the use of surfactants there are two main issues that need to be considered. Firstly, the correct characterization of the actual size of the particles via methods such as DLS and TEM, which provide an accurate estimate and visualization of any aggregates. Secondly, the consideration of any sample impurities left after synthesis of nanoparticles and purification. Any impurity of the sample can lead to additional false positive toxic effects. For instance, it has been shown that cetrimonium bromide in solution after synthesis of gold nanorods, has led to toxicity in HeLa cells (Alkilany et al., 2008). Similarly, an inflammatory response was produced via cytokine secretion due to un-purified AuNPs and iron oxide particles (Shvedova et al., 2005).

In the next section of this chapter, the cytotoxicity of 2 nm αGal:PEGamine AuNPs is presented. The toxic dose was established using various concentrations of the AuNPs to obtain an IC50 value. Prevention of particle growth and aggregation were achieved through the choice of the PEG ligand. The cytotoxicity was measured using clonogenic assays. This method is a cell proliferation and survival assay, enabling the determination of the long term AuNPs effects on cells as opposed to fast and real time readouts. It is a cost-effective, straight forward assay that limits the risks of particles interaction with the reporter dye. However, this approach is limited to cell types which grow in discrete colonies.

3.2 Results

Previous work in the lab identified 50:50 aGal:PEGamine AuNPs as the most selectively toxic particles towards HSC cells as compared with HaCaT cells (Grellet et al., 2017). The same cell lines and the same AuNP ligand ratio were used in this project in order to further characterize the mechanism by which these AuNPs cause toxicity and cell death. However, it was discovered early on that different batches of the 50:50 αGal:PEGamine AuNPs showed a variability in their toxicity. A range of parameters was investigated to identify what was the component of these AuNPs responsible for the batch variability observed. The relevant factors were separated into two categories: nanoparticle-related factors and cellular-related changes. Other factors such as pH, cell density and presence of proteins that could affect nanoparticle behaviour are not taken into account in this chapter as were kept consistent throughout all experiments.

One major issue that was initially identified was that some of these formulations were made with different synthesis times and different scales of synthesis. Moreover, not every batch was characterised to the same extent, making it difficult to isolate those variables that were causing differences in cellular toxicity. This chapter will show that following the same synthesis protocol does not always produce identical particles with same features. The structure of this chapter is based on first identifying the batch variability issue, followed by an investigation of whether cellular maturation changes were involved. Lastly, unravelling of how the batch variability issue was solved will be discussed based on a table below of the various factors tested (Table 3.2).

Table 3.2: Parameters that could account for batch variability observed on the toxicity of the AuNPs.

Parameters changing:
1. Ligand ratio 2. Surface charge 3. Synthesis method 4. Scale of synthesis 5. Synthesis time 6. Ligand density

3.2.1 Batch variability was observed between AuNPs samples

Three batches of AuNPs were initially tested for toxicity evaluation by clonogenic assays in HSC and HaCaT cells. Each of these AuNPs had an input ligand ratio of 50:50 αGal:PEGamine and it was therefore assumed that they would maintain this ratio on the fully-formed AuNPs. Two of them, the NP118-40-1 and M175-042-05, were made in the R&D facility in Oxford, whereas the NP146-149 was made in the manufacturing facility in Bilbao. The toxicity of these particles was highly variable in HSC cells, with IC50 values ranging from 0.9 to >10 μg/ml (Figure 3.1A). A more consistent toxicity was observed in HaCaT cells, with IC50 values >10 μg/ml (Figure 3.1B). A selective toxicity was evident with all three particles, correlating with previously published data in the lab (Grellet et al., 2017). However, the variation in IC50 values led to questioning of the batches reproducibility, and the underlying reason had to be solved by testing various chemical parameters and their effects on the toxicity of AuNPs.

A.

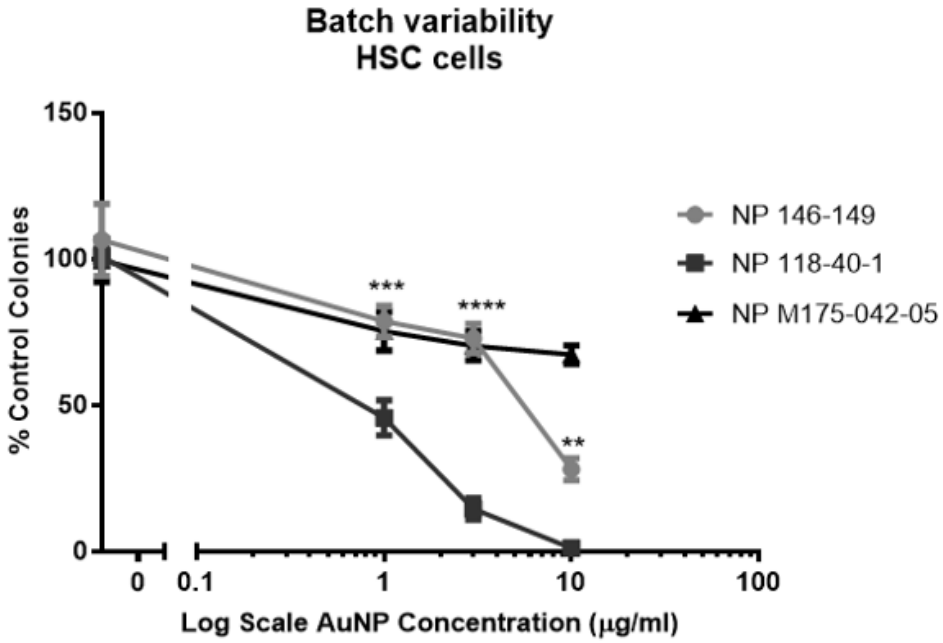

B.

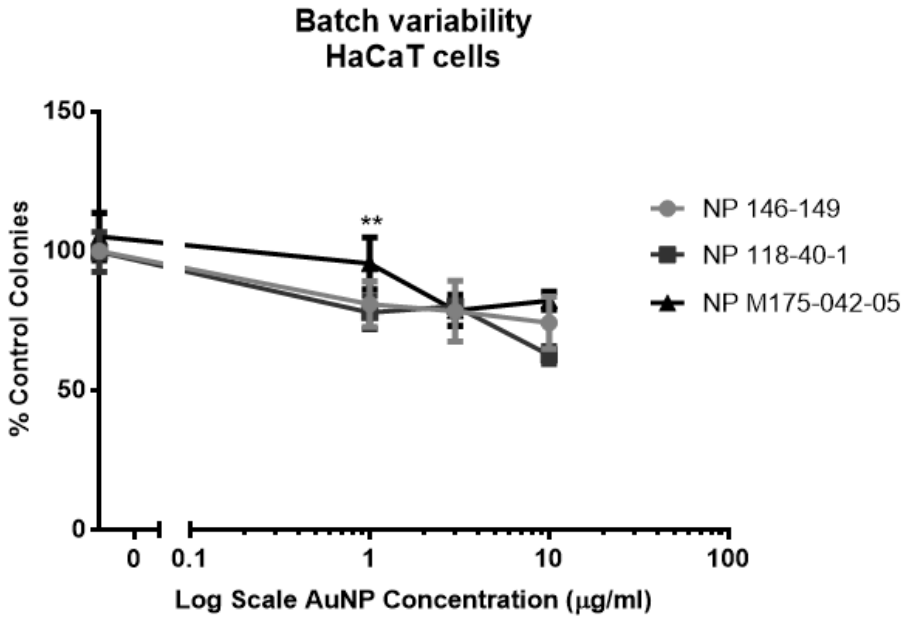

Figure 3.1: Toxicity evaluation of three batches of 50:50 αGal:PEGamine AuNPs as tested by clonogenic assays in A. HSC and B. HaCaT cells. The NP118-40-1 and M175-042-05 AuNPs were made in the R&D facility in Oxford, whereas the NP146-149 was made in the manufacturing facility in Bilbao. Data were expressed as % of control colonies and plotted as mean±SEM, n=3 independent experiments. One-way ANOVA, **P<0.01, ***P<0.001, ****P<0.0001.

3.2.2 Cellular changes evaluation

Before evaluating any chemical parameters related to the batch variability issue, the effect of any possible cellular maturation was addressed. Such effect was questioned as all of these experiments were performed in triplicate and on three independent days. The assessment was performed by taking one of the particles tested above, the NP146-149 and conducting the same clonogenic assay experiment on early (Passage number 4) and late passage cells (Passage number 30) (Figure 3.2). The passage number did not affect the toxicity in HSC cells (Figure 3.2A). In contrast, HaCaT cells of a high passage number were less sensitive to AuNP exposure at high concentrations with almost 2-fold differences to be observed in the AuNP IC50 value between high and low passage (Figure 3.2B). This observation suggested a possible connection between cellular maturation and toxicity that had to be carefully taken into consideration in performing subsequent experiments.

Cellular maturation could account for differences between experimental outcomes in HaCaT cells, but the batch variability observed in HSC cells could not be explained by the non-significant differences noted between high and low passage number of cells. Surprisingly, little variability was observed between the AuNPs tested for this cell type. Therefore, one or more other factors accounted for the variation in HSC cells. Throughout the following experiments and the cell culture of the cell lines, precautions were taken to maintain the cell cultures up to a specific passage. Reproducibility was ensured by always splitting the cells between 70-80% confluency in order to minimize the cell maturation element as much as possible between the experiments.

A.

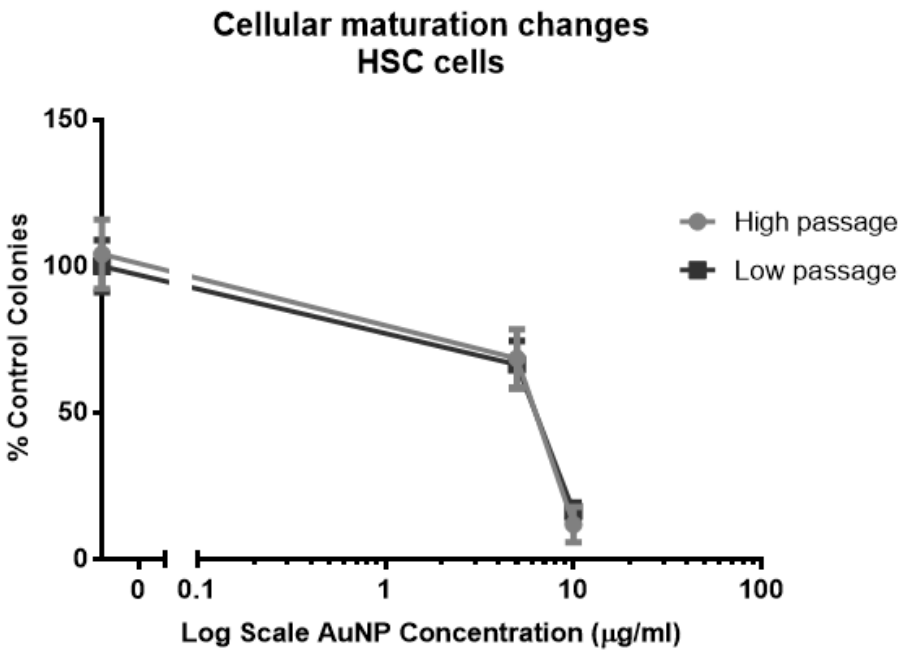

B.

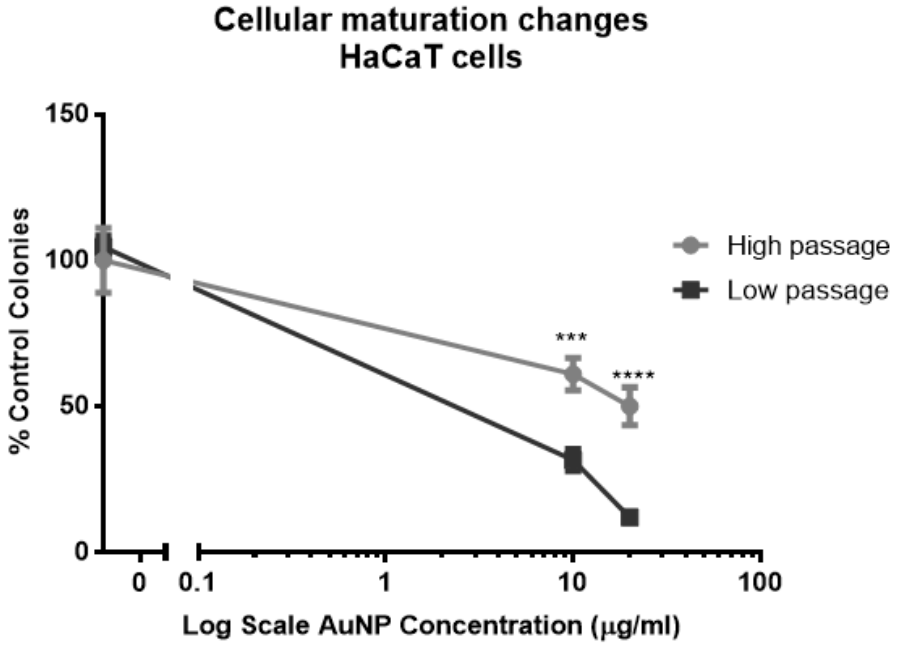

Figure 3.2: Evaluation of cellular maturation changes from comparison of the IC50 values of the 50:50 αGal:PEGamine AuNP NP146-149 obtained by clonogenic assays in A. HSC and B. HaCaT cells. The effect on toxicity was compared in high (30) and low passage number (4) of both cell lines. Data were expressed as % of control colonies and plotted as mean±SEM, n=3 independent experiments. One-way ANOVA, ***P<0.001, ****P<0.0001.

3.2.3 Stability of AuNPs

Another issue that had to be tested was the stability of the AuNPs over time. To study the long term stability, the same 50:50 AuNP was tested for toxicity early in the project and then repeated after a period of 1.5 years. The IC50 value increased by approximately 3-fold, from ~5 µg/ml to ~12 µg/ml, with the particles to be less toxic upon aging (Figure 3.3). Therefore, when comparing any data of various tests performed on AuNPs and how they translate into toxicity, cellular maturation and batch age over time needed to be considered.

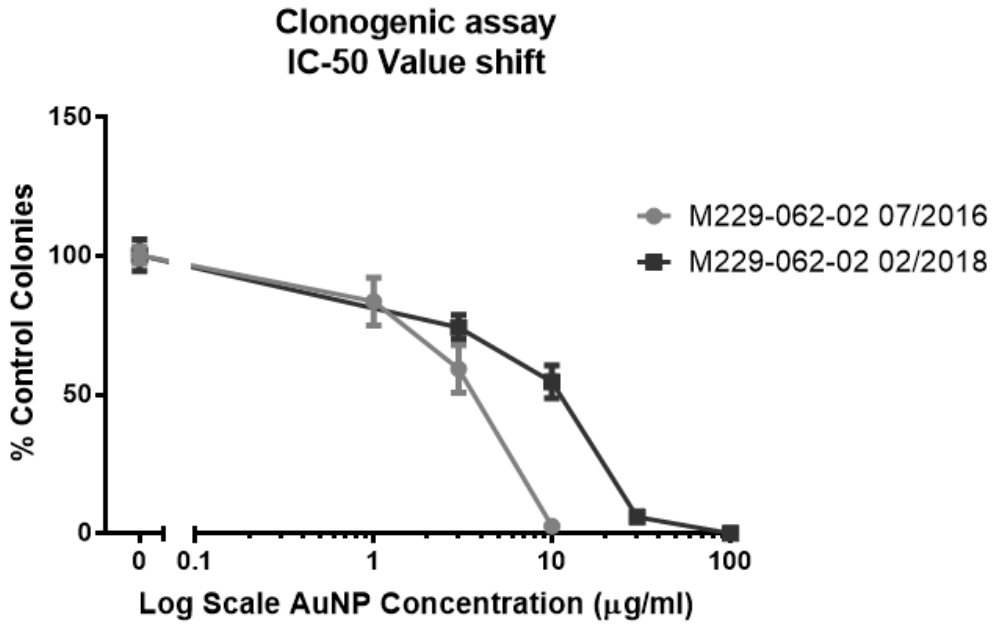

Figure 3.3: IC50 value shift of the same 50:50 αGal:PEGamine AuNP M229-062-02 over 1.5 years in HSC cells. The age of the AuNPs was examined for possible changes in their toxicity profile within 1.5 years apart since their synthesis. Data were expressed as % of control colonies and plotted as mean ±SEM, n=3 independent experiments.

The agglomeration status of the AuNPs in DMEM cell culture media supplemented with 10% FBS was also evaluated. TEM was chosen as the best method to determine the agglomeration status, as it allows visualisation of large numbers of individual AuNPs. The presence or absence of FBS did not affect the agglomeration state of the NPs used in this study (Figure 3.4), a phenomenon that was also confirmed by FPLC studies as presented in chapter 4. A grey blob appearance under the TEM was attributed to serum componenets present in FBS.

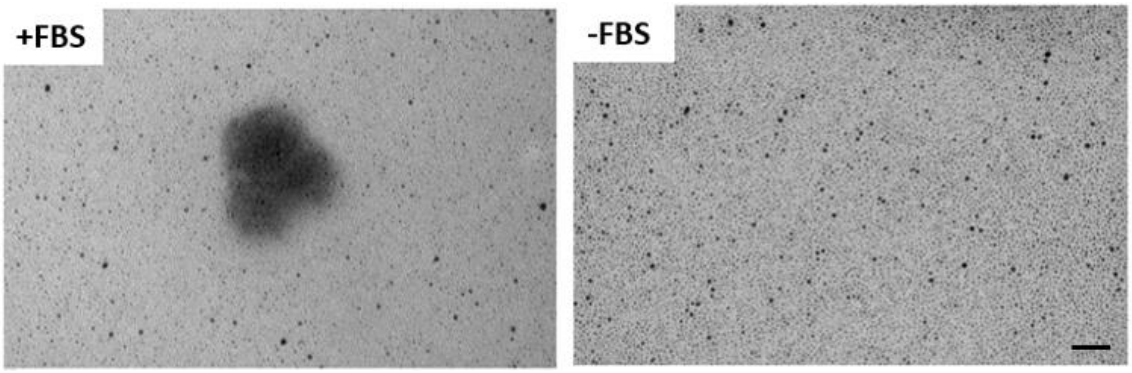

Figure 3.4: TEM images of the aggregation state of the AuNPs (M218-024-05, 5h synthesis time) in 10% +/- FBS. Small dark dots represent the AuNPs, whereas the grey cloud appearing in the +FBS image was attributed to serum components. Images were taken at 100x magnification, Scale bar=5 nm.

3.2.4 Uptake and toxicity of AuNPs in +/- FBS cell culture conditions

AuNPs agglomeration state was not affected by the presence of FBS in solution. The next step was to test whether the uptake and toxicity of the AuNPs into the cells was different between +/-FBS cell culture conditions during their exposure on HSC and HaCaT cells. Silver staining of AuNPs exposed to HSC cells in +/- FBS conditions showed better uptake of the AuNPs in presence of FBS (Figure 3.5). Uptake data at varied FBS conditions are not presented for HaCaT cells as previous published data in the lab showed no AuNP internalization into this type of cell (Grellet et al., 2017).

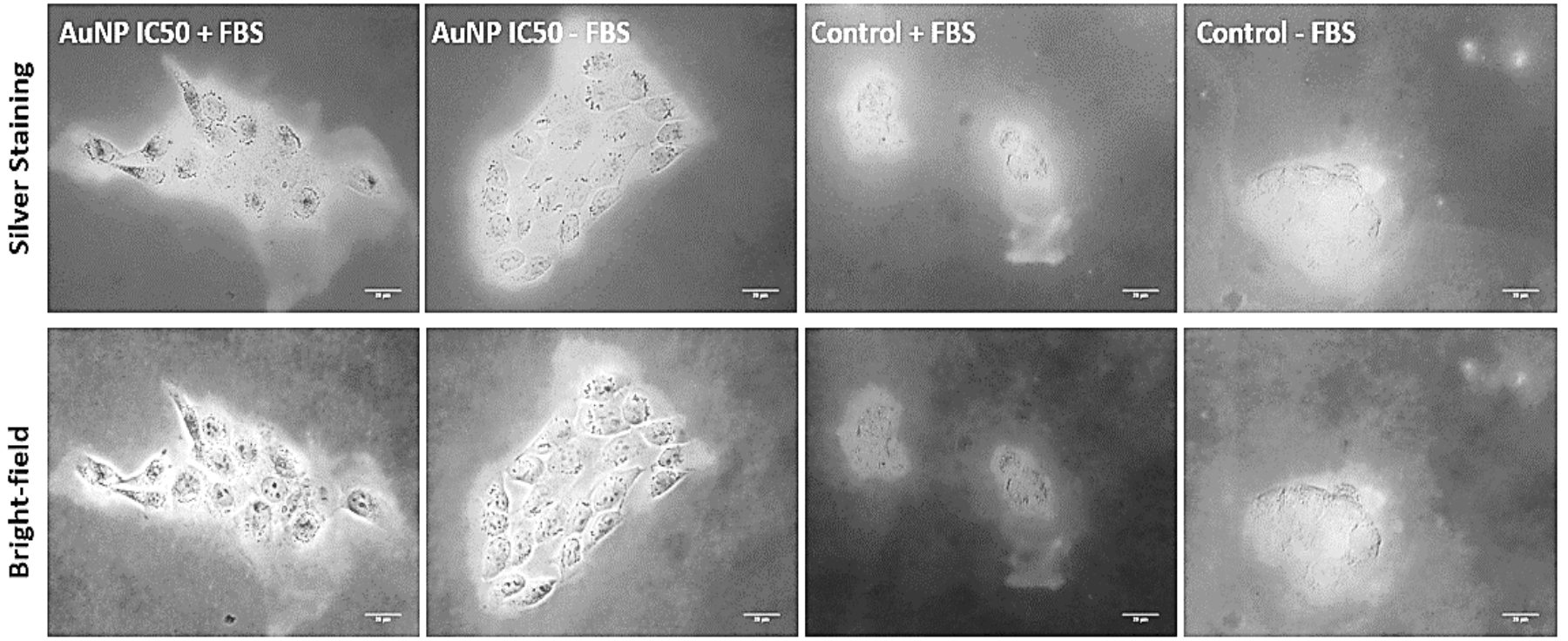

Figure 3.5: Uptake of 50:50 αGal:PEGamine AuNPs in HSC cells after 3h acute exposure at +/- FBS. Phase contrast=20x, silver staining=20x objective. Scale bar=50 μm.

In order to have a quantitative measure for the effects of the presence or absence of FBS on AuNP toxicity, clonogenic assays were performed using the 50:50 αGal:PEGamine AuNPs (Figure 3.6). No significant differences in the toxicity of AuNPs were detected for either cell line, despite a trend for a reduced toxicity in the presence of FBS.

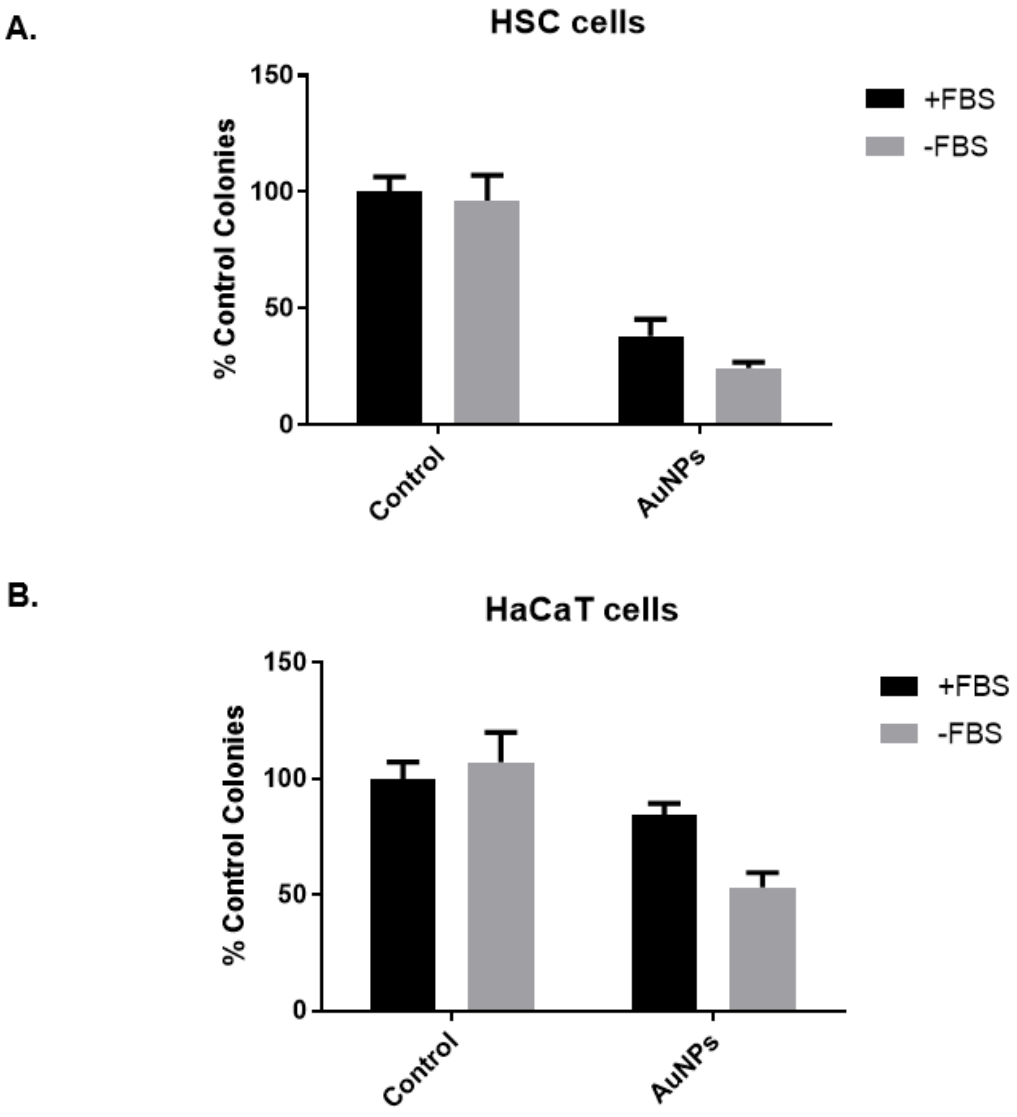

Figure 3.6: Differences in the cytotoxicity of 50:50 αGal:PEGamine AuNPs when cells are grown in the presence or absence of FBS to A. HSC and B. HaCaT cells. Data were expressed as % of control colonies. Data were plotted as mean±SEM, n=3 independent experiments.

3.2.5 Ligand ratio effects

A list of parameters that potentially affected the toxicity was given in Table 3.2. To elucidate which is the critical factor responsible for batch variability, they were tested one by one. This allowed not only to specify the causes of batch to batch variability but also the main effector of the particle's toxicity. The first factor to be tested was the ligand ratio of the AuNPs. Many studies have shown that the ligand organization affects the particle interactions with the cell membrane and the way they are internalized by cells (Beddoes et al., 2015, Chithrani et al., 2009). According to the study by Grellet and previous work in the lab, the toxicity and the uptake of the AuNPs was influenced by the ratio of αGal:PEGamine ligands (Grellet et al., 2017).

Therefore, AuNPs bearing different ratios of ligands were tested by clonogenic assays on HSC and HaCaT cells after an acute 3h exposure at 0, 3, 10 and 30 μg/ml. The most selectively toxic formulations were the 51:49 ratio and the 0:100 ratio with IC50 values of 5.5 and 11.7 μg/ml, respectively for HSC cells (Figure 3.7A). This correlates with data from previous work in the lab that has shown a 50:50 ratio of AuNPs to be the most selectively toxic in HSC cells (Grellet et al., 2017). IC50 values of more than 10 μg/ml were noted for HaCaT cells for all the ratios (Figure 3.7B). Nonetheless, the ratio 45:55, is very close to the 50:50 ratio of αGal:PEGamine, which represents the most selectively toxic AuNP in HSC cells, did not behave similarly to the 51:49 ratio. More than 2-fold differences were noted in their IC50 values. The fact that there were big differences in their toxicity despite small changes in the ligand ratio makes it very likely that toxicity is attributed to a factor other the ligand ratio.

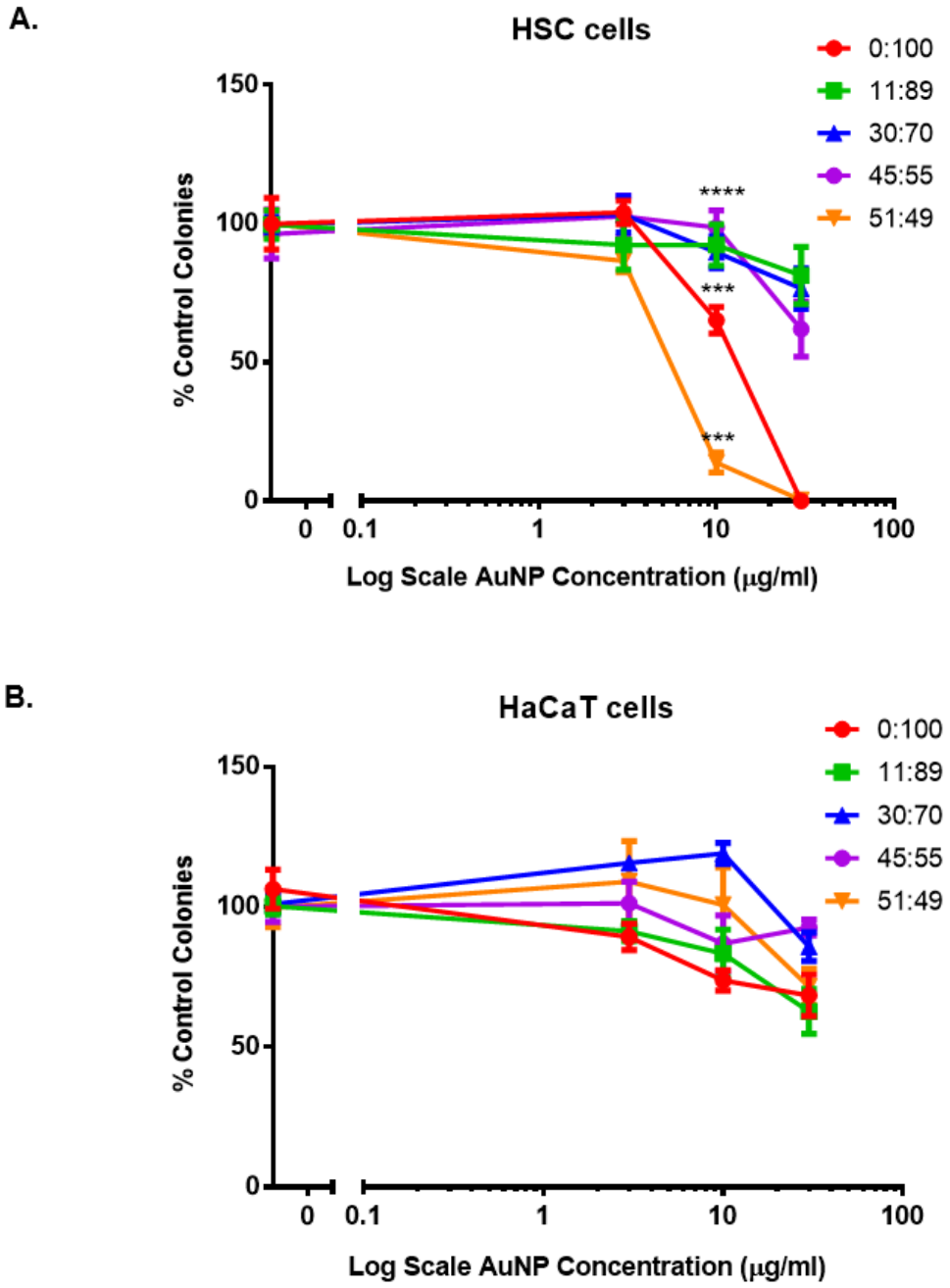

Figure 3.7: Ligand ratio effects on the toxicity of the AuNPs in A. HSC and B. HaCaT cells as examined by clonogenic assays after an acute 3h exposure of all the AuNPs at 0, 3, 10 and 30 µg/ml. The ratios included: 0:100 (M175-042-01), 11:89 (M175-042-02), 30:70 (M175-065-03), 45:55 (M175-065-04), 51:49 (M175-042-05) αGal:PEGamine as measured by NMR. Data were expressed as % of control colonies and plotted as mean±SEM, n=3 independent experiments. One-way ANOVA, ***P<0.001, ****P<0.0001.

3.2.6 Surface charge

The differences in ligand ratio around the Au core can have an impact on the surface charge of the AuNPs (Feng et al., 2015). To investigate whether the AuNPs with different ligand ratios varied in their surface charge, measurements of their zeta potential were conducted and are presented in the table below (Table 3.3). Despite showing different toxicities in HSC cells, small variations in zeta potential were found between 45:55 and 51:49 ratio AuNPs. Therefore, the ζ potential could not explain the variation observed in the toxicities between these particles.

Table 3.3: Zeta potential measurements of the different αGal:PEGamine ratios of AuNPs.

αGal:PEGamine ratio	ζ potential (mV) ± SD
0:100 (M175-042-01)	+43.0±5.7
11:89 (M175-042-02)	+4.27±10.8
30:70 (M175-065-03)	+11.6±7.16
45:55 (M175-065-04)	+16.6±5.56
51:49 (M175-042-05)	+17.2±4.95

After ruling out the ligand ratio and the ζ potential as factors that affect the AuNP toxicity, differences in the surface charge of similarly sized particles were evaluated for their effects on the toxicity using clonogenic assays. A negatively charged AuNP containing only αGal (ζ=-16.0±6.3 mV) as a surface coating was compared to a positively charged 50:50 ratio αGal:PEGamine AuNP (ζ=+17.2±4.95 mV) and a positively charged PAMAM dendrimer G4 (ζ=+37.2±1.95 mV) (Figure 3.8). All of the three nanoparticles had a hydrodynamic diameter of ~4 nm and their toxicity was tested on HSC and HaCaT cells at five different concentrations (0, 1, 3, 10, 30 μg/ml).

An estimated IC50 value of ~6 µg/ml for HSC and an IC50 of >10 µg/ml for HaCaT cells was calculated for the 50:50 AuNP (Figure 3.8A&B). The other two nanoparticles that were tested had much higher IC50 values and showed less selective toxicities between the cell lines. This result indicated that surface charge was not the only factor responsible for selective toxicity, as particles with positive charge and similar size did not show the same toxicity.

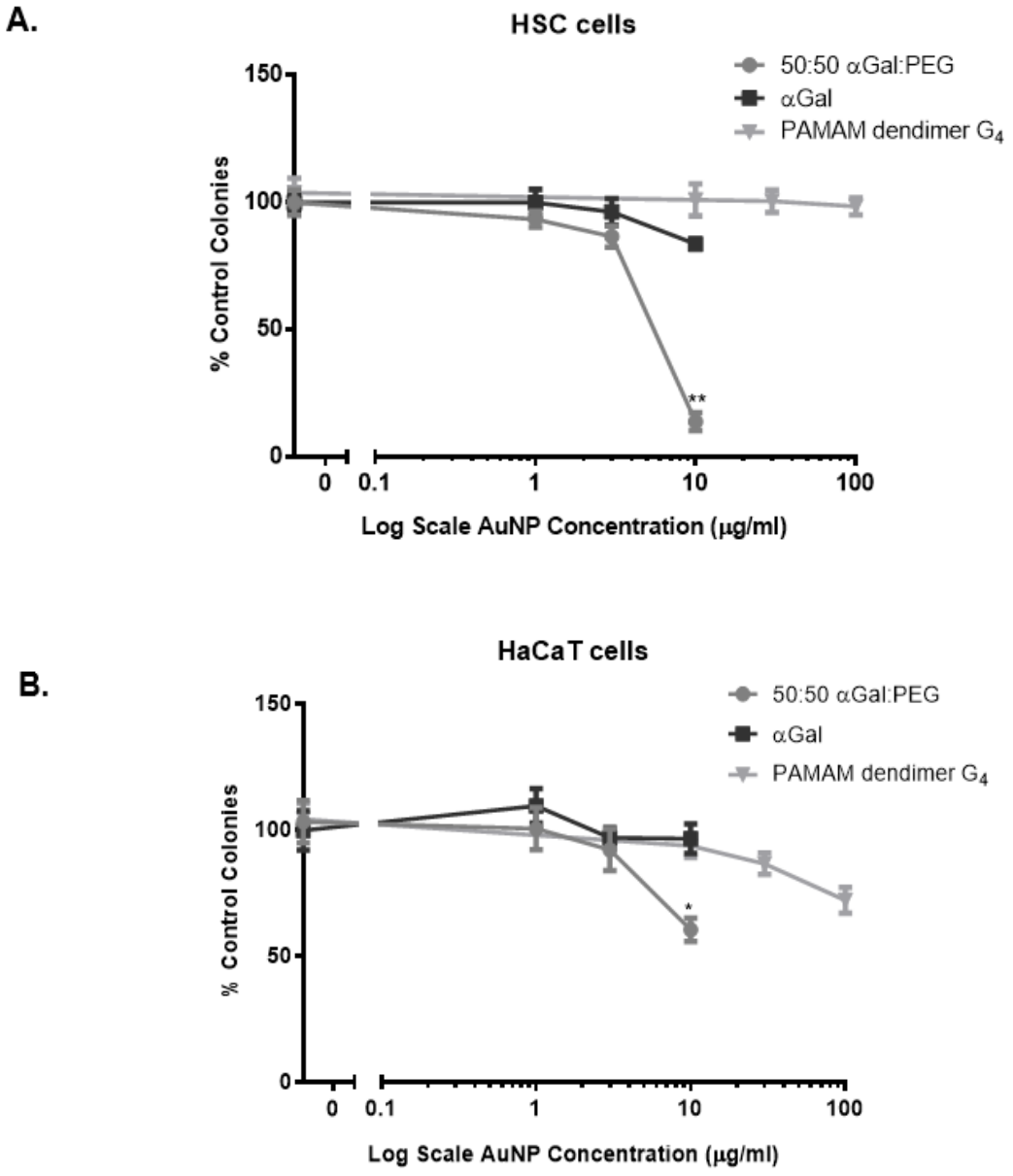

Figure 3.8: Effect of surface charge and size as determined by clonogenic assays of three different nanoparticles on A. HSC and B. HaCaT cells. 50:50 αGal:PEGamine, 4nm, +ve charge, αGal only AuNP, 4nm, -ve charge and PAMAM dendrimer G4, 4nm, +ve charge. Data were plotted as mean±SEM, n=3 independent experiments. One-way ANOVA, *P<0.05, **P<0.01.

3.2.7 Synthesis method

One of the parameters changing between the R&D and manufacturing facilities was the synthesis method of the AuNPs. The effect of the purification method after synthesis had to be assessed for differences in toxicity in both HSC and HaCaT cell lines. When comparing the toxicity of the particles purified with the different methods on HSC cells (Figure 3.9A), particles prepared with methanol without being purified were more toxic, with an IC50 of <1 μg/ml than the other two synthesis types. A similar pattern was found in HaCaT cells with less selective differences to occur (Figure 3.9B).

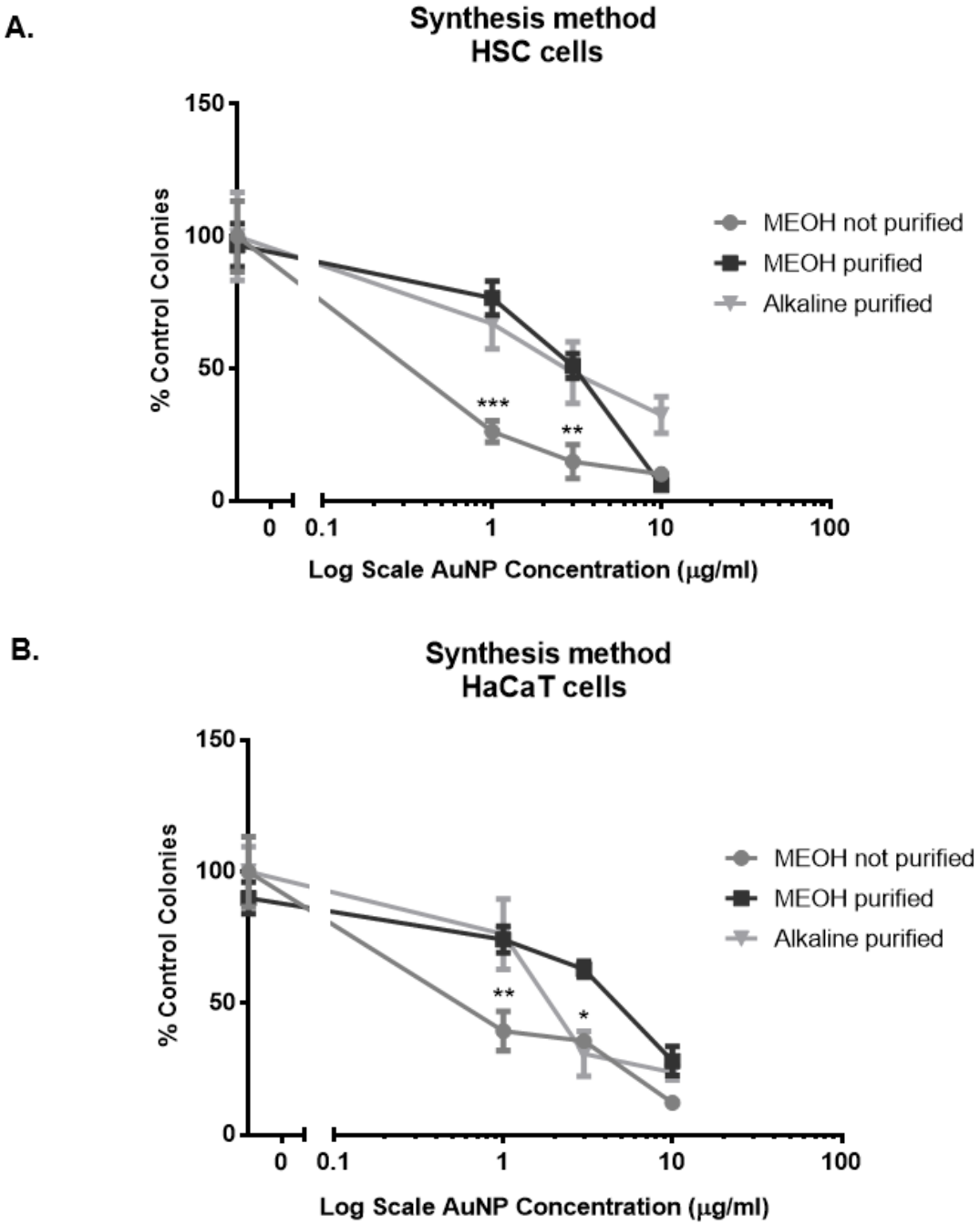

Figure 3.9: Cell survival (expressed as % control colonies) determined by clonogenic assays of 50:50 αGal:PEGamine AuNPs prepared with either alkaline (M218-104-01) or methanol (M218-095-01, -02) method in A. HSC and B. HaCaT cells. Data were plotted as mean±SEM, n=3 independent experiments. One-way ANOVA, *P<0.05, **P<0.01, ***P<0.001.

3.2.8 Scale of synthesis

Apart from the synthesis method changing between the two facilities, the scale of synthesis also varied. Particles prepared for research purposes were made at a small scale (2 ml) as opposed to the large scale (10 ml) of the manufacturing facility. Therefore, the toxicity of batches synthesized at small and large scale was compared in order to assess whether the scale of synthesis affect toxicity. To obtain comparable results, only the synthesis scale was changed. Clonogenic assays showed that there were no differences between the different synthesis scales for both HSC and HaCaT cells (Figure 3.10A&B).

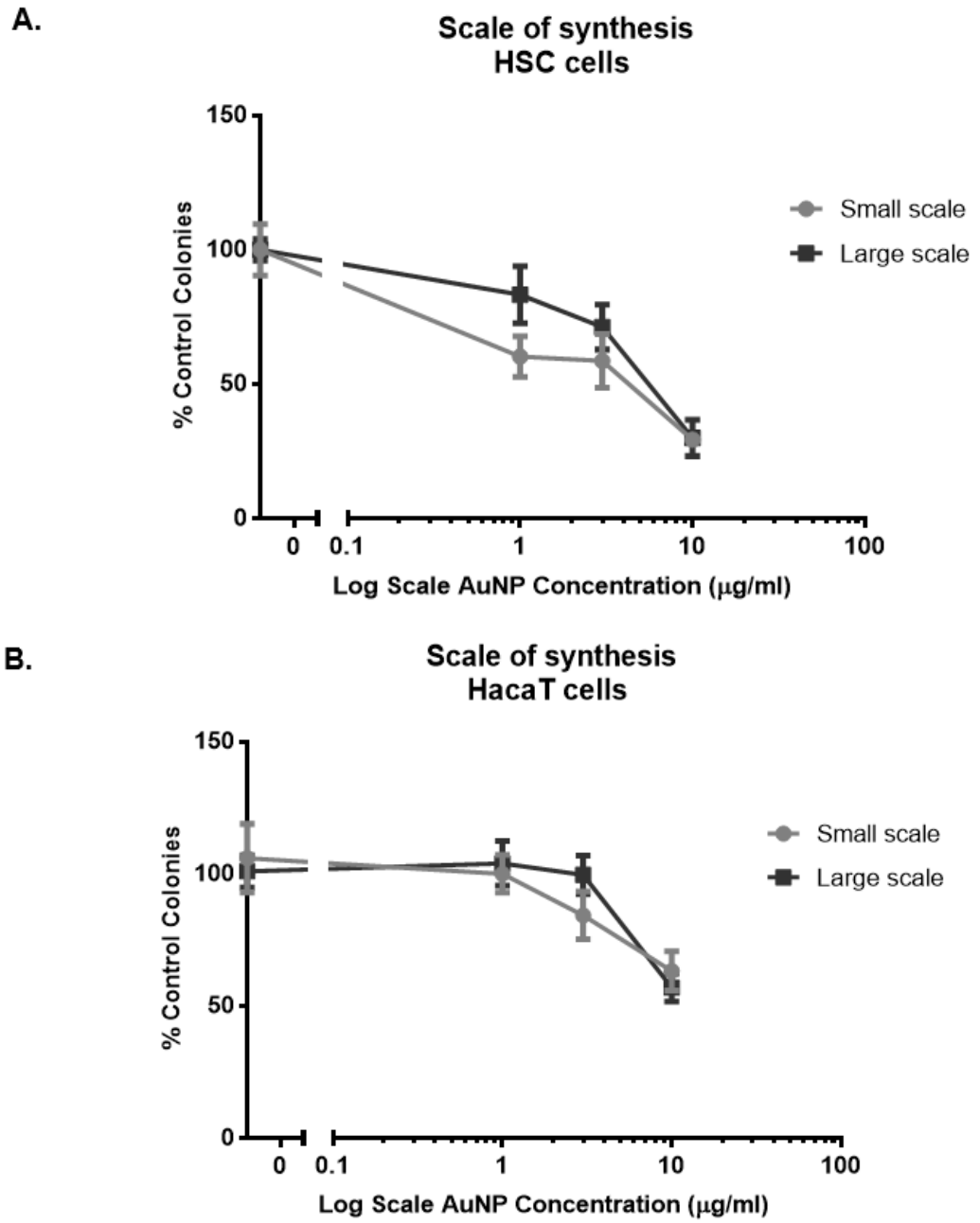

Figure 3.10: Clonogenic assays of AuNPs acute exposure to A. HSC and B. HaCaT cells of AuNPs prepared at small and large scale. Particles prepared for research materials were made at small scale (2 ml, M218-086-01) in R&D as opposed to the large scale (10 ml, M182-073-1) of the manufacturing facility in Bilbao. Data were plotted as mean±SEM.

3.2.9 Synthesis time

During the large scale synthesis it takes more time to purify the particles, increasing their actual synthesis time, and thus the contact time between ligands, gold and reducing agent. Therefore, the effect of the synthesis time of AuNPs on their toxicity was tested by comparing the toxicities of the same batch of the 50:50 AuNP aliquoted at 1h, 2h and 5h.

The results showed that with increasing synthesis time, the toxicity increased and the selectivity decreased. Concentration-dependent significant differences occurred with 10 µg/ml to be very toxic for all synthesis time for HSC cells and less toxic for HaCaT (Figure 3.11A&B). Details of how changes in synthesis time of AuNPs leads to differences in ligand density and affects the mechanism of toxicity are presented in the next chapters.

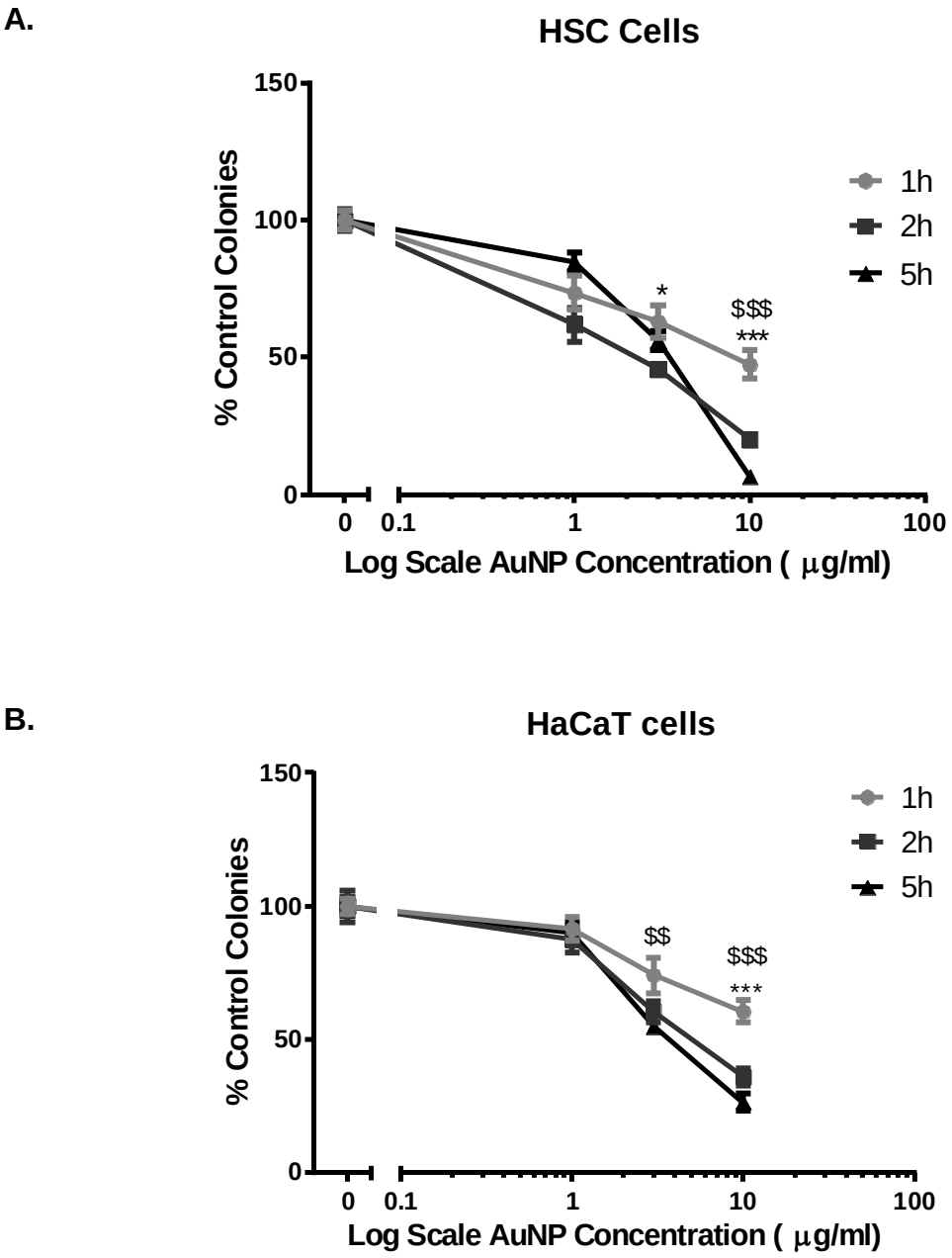

Figure 3.11: Clonogenic assays of 1h (M218-024-01), 2h (M218-024-02) and 5h (M218-024-05) synthesis time AuNPs on A. HSC and B. HaCaT cells. Significant differences between 1h and 2h synthesis AuNPs are marked by * symbols, while significant differences between 1h and 5h synthesis AuNPs are marked by § symbols. Data were expressed as % of the number of control colonies and plotted as mean±SEM, n=3 independent experiments. One-way ANOVA, *P<0.05, **P<0.01, ***P<0.001.

3.3 Discussion

3.3.1 Batch variability

A problem that often exists in pharmaceutical industries with the production of nanoparticles is the batch to batch variability. This can have a significant impact on the toxicity and behaviour of these particles in biological applications and therefore sufficient effort has to be made to ensure reproducibility (Roebben et al., 2013, Yu et al., 2012). Control over synthesis method, optimization and validation along with a better understanding of the physico-chemical parameters that produce batch to batch variability is of great importance. Such control was possible from Midatech after identification of the batch variability issues, which efficiently provided 3 identical batches (M229-062-01, -02,-03) under controlled conditions. These batches were tested for their toxicity towards HSC and HaCaT cells by clonogenic assay, resulting in similar IC50 values of around ~5 and 8 µg/ml, respectively to these cells lines.

The Organization for Economic Co-operation and Development (OECD) has set up three main categories as an area of focus for method validation during the development of nanomaterials. These categories include characterization of the physico-chemical properties of the particles such as size, shape, composition and surface features, biological and environmental fate of the nanoparticles regarding toxicity, bio-distribution and solubility and lastly, reactivity in biological conditions, photo-reactivity and physical hazards (OECD 2016, Rasmussen et al., 2018). These categories describe most of the parameters that need to be evaluated in every batch and ensure reproducibility. In this chapter, physicochemical parameters of the different batches were not examined in detail as limited amount of material was provided for full chemical characterization.

3.3.2 Cellular maturation

The batch to batch variability can not only be attributed to the nanoparticle themselves, but in an *in vitro* situation cellular maturation could also be the reason of batches variations observed. When performing studies using cultured cells, long term cell culture can affect the biological readout of the toxicity of the AuNPs used in this project. The two cell lines used in this study, HSC and HaCaT cells, differed on the effect their passage number had on the AuNP toxicity. Whilst the passage number did not affect the toxicity of the particles in HSC cells, a decreased toxicity was found in HaCaT cells of high passage number (Figure 3.2).

HSCs are an immortalized skin cancer cell line that in theory can be cultured indefinitely without differentiating and without changing their morphology and phenotype. HaCaT cells on the other hand are an immortalized keratinocyte cell line that its differentiation ability has been previously examined by Colombo and colleagues (Colombo et al., 2017). Colombo et al., has shown in his study that the differentiation of HaCaT cells was affected by both the cell seeding density and the level of extracellular Ca^{2+} in the medium of long-term *in vitro* cultures. In order for HaCaT cells to be maintained in their basal non-differentiated level, which is characterized by high levels of the expression marker K14, the cells need to be cultured up to 80% confluency and kept in low Ca^{2+} conditions (Boukamp et al., 1988, Micallef et al., 2009). Although these conditions have been maintained throughout the cell culture of this project, it should be taken into account from the above studies, that HaCaT differentiation is a very likely event to occur, therefore any data interpretation regarding this cell line should be made with caution.

3.3.3 PEG stability

The IC50 values of the same batch of particles after long term storage (Figure 3.3) clearly showed that the AuNPs used throughout the project were changing and thus these data reinforced the idea that the ability to produce batches in a reproducible manner were of critical importance. The exact timing of when and how the particles changed was not studied as the main question of this thesis was not to identify how and why particles changed but try to understand why fresh batches varied.

According to literature, aging of PEG compounds lead to the reduction of pH, increased ionic strength and increased metal binding (Jurnak, 1986, Ray and Puvathingal, 1985). These effects can result from the presence of oxygen, light and elevated temperature (Jurnak, 1986). The aging of the PEG molecules can be minimized by storage at -20^{o}C or 4^{o}C in a sealed vial protected from light. Midatech's AuNPs were stored at 4^{o}C and it was ensured that a set of experiments was completed with one batch in a short period of time (within 6 months) in order for the results to be comparable. A study published on 8 different polyethylene glycols stored in typical laboratory storage conditions proved that the molecules were stable up to 18 months as measured by their conductivity and pH (Jurnak, 1986). Therefore, with correct storage conditions PEG stability can be ensured.

3.3.4 Aggregation

A factor that had also to be addressed before examining the physico-chemical properties of the AuNPs and how they interfere with toxicity, was the aggregation state of the particles. Before performing the toxicity experiments, particles dispersity in solution was visualized under TEM to ensure homogeneous distribution in the storage solution and in culture media used for application of AuNPs in the cells. Particles did not aggregate in either solutions. However, many studies showed that any type of nanoparticle is prone to aggregation in culture media due to being exposed to proteins and ions that cause van der Waals attractive forces being greater than the repulsive forces on the surface of the particles (Rausch et al., 2010, Derjaguin et al., 1993, Qiu et al., 2010, Cingolani and Pompa, 2010).

Thus, the 50:50 AuNPs were tested for their toxicity and uptake in absence and presence of FBS as serum proteins can lead to a thermodynamically more favourable replacement of surface molecules with serum. Another reason for testing the AuNPs in presence and absence of serum was that increased concentration of ions in culture media after FBS addition could interfere with the charge on the nanoparticle surface and alter its properties. Although no significant differences were observed regarding the toxicity (Figure 3.6), AuNP uptake was influenced by the presence of serum (Figure 3.5), making the particles either to internalize more or stick more at the cell surface of HSC cells. The silver staining method performed did not provide the ability to distinguish between internalized particles and particles at the cell surface. Therefore, it was not possible to conclude whether serum facilitates nanoparticle uptake. Since no differences

were observed in terms of toxicity, particle aggregation was ruled out as a factor responsible for the batch variation.

3.3.5 Physico-chemical Properties

The different physicochemical properties of AuNPs that likely influence biological activity and toxicity are the nanoparticle size, shape, charge and surface characteristics (Auffan et al., 2010). For example, AuNPs 1.4 nm in diameter capped with triphenylphosphine monosulfonate caused mitochondrial damage and necrosis via oxidative stress, while 3.7 nm AuNPs modified with PEG were non-toxic when internalized into the nucleus of HeLa cells (Goodman et al., 2004). With Midatech's AuNPs, the size and shape remained constant in every batch tested, therefore the variability was not based on these properties. However, surface characteristics were questioned. Specifically, ligands attached to the AuNPs modify their surface characteristics. Grellet et al., showed that the ligand ratio around the Au core influenced the toxicity of the AuNPs (Grellet et al., 2017). However, in the data presented in this thesis the differences in toxicity observed between similar ratios batches did not explain the variation (Figure 3.7).

Depending on the nature of the charge, cationic or anionic, differences in reactivity with other protein complexes or molecules occurs (Goodman et al., 2004). In the case of the AuNPs presented in this study no difference in the zeta potential was observed (Table 3.3) and thus, no conclusions could be made of whether charge influenced the particle toxicity and uptake by HSC and HaCaT cells. Other studies found that the more positive the charge of a particle, the higher the toxicity, whereas Schaeublin et al., have demonstrated that both positively and negatively charged particles were toxic to lymphoid cells by

generation of reactive oxygen species and changes in mitochondrial membrane potential (Schaeublin et al., 2011).

After investigating the basic parameters that could be different between the AuNPs received from Midatech, it was concluded that neither the size, shape, aggregation state or charge and ligand ratio were responsible for the variation observed in toxicities and varied IC50 values between batches. As a result, the synthesis protocol was questioned. It was found that manufacturing and R&D facilities differed in their AuNPs synthesis procedure and hence, after eliminating the parameters mentioned above, only this parameter of the synthesis process, could possibly account for the batch to batch variability. The synthesis method was changing between facilities and within the facility. Regarding the purification method, only the alkaline process was of interest as methanol preparation of AuNPs could lead to particle precipitation. Although the alkaline method was consistent between the batches, a variation in the toxicity was observed. The scale of synthesis did not cause significant differences between AuNPs made at small or large scale.

The most important factor that appeared to play a major role affecting the toxicity of these αGal:PEGamine AuNPs was the synthesis time. Synthesis time is a factor vital in the synthesis and production of any nanoparticle, however no published data exist as to its relevance to toxicity. A novel finding of this work was that the longer the synthesis time of the AuNPs, the greater the toxicity. Someone might argue that as synthesis time increases, changes in size and surface area to volume ratio is altered thus the toxicity. The effect was investigated in greater detail in the next chapter showing that size remained constant and the only parameter changing with particles made at different time points was their ligand density surrounding the Au core.

To conclude, this chapter presented a series of parameters and factors that were taken into account in order to address the batch variability issue observed in the beginning of this project. By eliminating and narrowing down factors that are the only ones changing between the particles, a novel feature was identified that played a significant role in the toxicity of these AuNPs (Figure 3.12). Once an awareness was raised that batch variability was a problem and specific parameters led to it, particles made under identical conditions and at same synthesis time were synthesized and were fully characterized for next experiments.

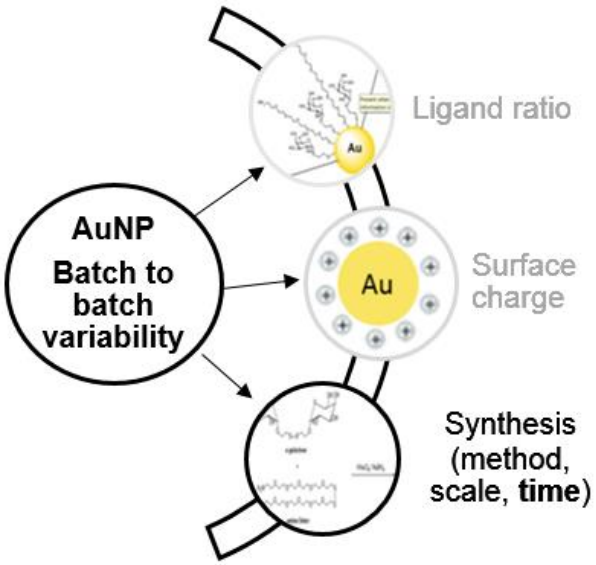

Figure 3.12: Schematic representation of the possible factors affecting AuNP toxicity, responsible for the batch to batch variability observed. Synthesis was one of the most significant parameters identified responsible for batch variability and most importantly synthesis time.

Chapter 4: Role of Synthesis Time and Ligand Density in AuNP Toxicity and Their Effect on The Transport of AuNP's

4.1 Introduction

The surface chemistry of nanoparticles plays an important role as to how they interact with the cellular machinery. An understanding of the dynamics of the coating of AuNPs and its structure is crucial in order to examine the particles' biological interactions. Such understanding is also vital in the design and synthesis of nanomaterials. A part of the nanoparticles surface coating are the ligands, a component that is used for providing stability and functionality to the particle (Boles et al., 2016, Albanese, 2012). The choice of ligands can control the size and charge of the particles (Lee et al., 2010). Many studies showed that the organization and the choice of ligands are key for targeting cells via the nanoparticle interaction with biological membranes (Chou et al., 2011, Verma et al., 2008). Other studies suggested that ligands can determine cytotoxicity and *in vivo* distribution of the nanoparticles (Kievit et al., 2011, Smith et al., 2008).

4.1.1 Mechanisms of transport pathways utilized by AuNPs in cells

Many research groups are focusing on identifying routes of uptake of various types of nanoparticles but often discrepancies are observed in the published data due to nanoparticle internalization being highly dependent on multiple factors. Some of these factors are the properties of the nanoparticles such as size, charge and ligand design. In addition to the nanoparticle's properties, cell dependent factors like the cell type and cell cycle phase can play an important part on the particle uptake. Due to the state of the cell also possibly

affecting the particle uptake, it is very difficult to conclude whether optimal cellular uptake can be achieved with one specific nanoparticle property configuration.

With regard to the features of the nanoparticle itself, different studies show that both the charge and the size are important for enhanced uptake. However, a controversy exists regarding the type of charge and the actual size of the nanoparticles. In theory, a positively charged nanoparticle will more efficiently bind to the negatively charged cell surface. This was supported by a study that compared the uptake of both positively and negatively charged mPEG-PLA nanoparticles of similar size by HeLa cells. The study found that the positively charged nanoparticles were taken up two times more than the negatively charged ones (Harush-Frenkel et al., 2007). In contrast, in HEK cells, higher uptake of negatively charged QDs nanoparticles was observed (Zhang and Monteiro-Riviere, 2009). Also, reports revealed that nanoparticles of around 20-50 nm are internalized in a higher rate than smaller or larger particles (Shang et al., 2014). Nanoparticles have been shown to get internalized via the energy-dependent pathways of endocytosis and energy-independent mechanisms. There are two main categories of endocytosis: the pinocytosis and phagocytosis (Figure 4.1).

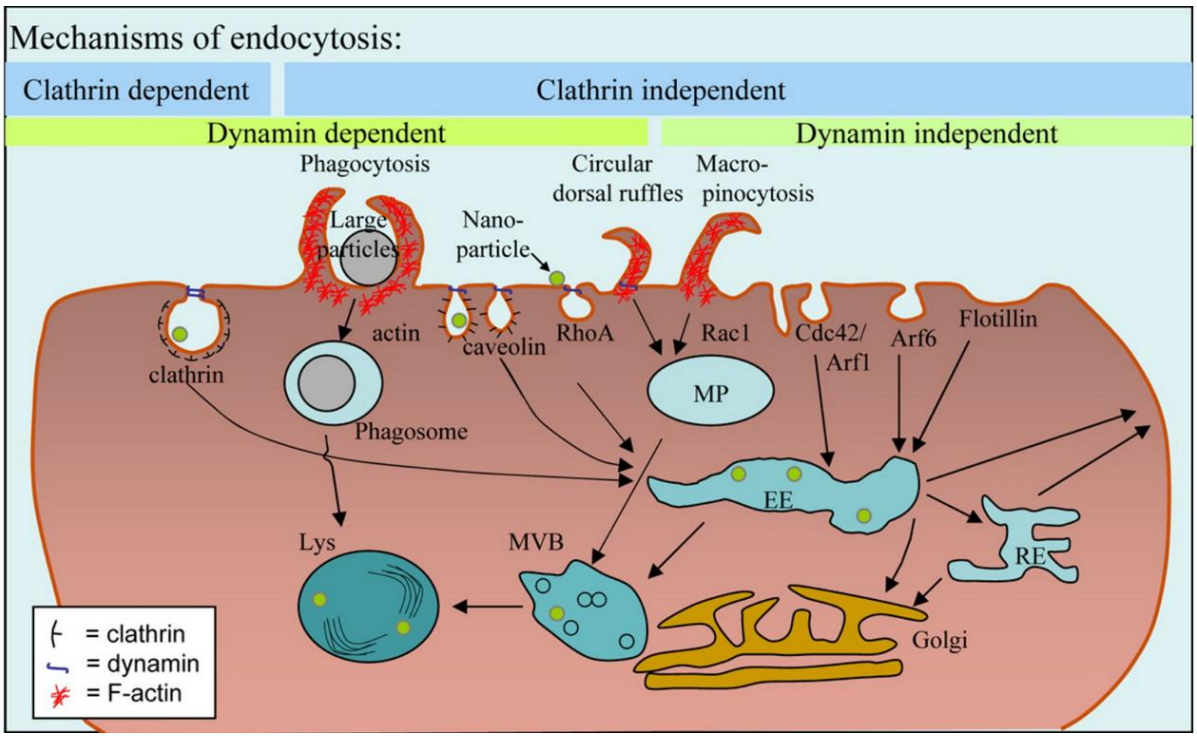

Figure 4.1: Mechanisms of internalization pathways utilized by nanoparticles. Nanoparticles (green dots) and other substances are internalized via endocytosis in a clathrin dependent and clathrin independent manner. They are taken up by either early endosomes (EE), phagosomes or macropinosomes (MP). Maturation of these vesicles lead to formation of late endosomes, multivesicular bodies (MVB) which fuse with lysosomes (Lys) down the degradative pathway. The pH of this compartment is acidic and around 4.0-5.5, which enables particle degradation via proteases and other enzymes. Particles can alternatively be recycled back to the cell surface through the EE or recycling endosomes (RE). From Iversen et al., 2011.

4.1.1.1 Phagocytosis

Phagocytosis is the main route of internalization of particles larger than 500 nm in diameter. The process is initiated by the immune's system specialized cells, the phagocytes such as dendritic cells, monocytes and macrophages, which are responsible for the elimination of bacteria, viruses and infected or dead cells. Phagocytosis of nanoparticles occurs in 3 stages. The first one is the opsonisation process in which opsonin proteins like blood proteins and immunoglobulins are adsorbed into the nanoparticle's surface and recognized by

phagocytes (Hillaireau and Couvreur, 2009, Sahay et al., 2010). This recognition triggers a cascade of signalling events leading to actin polymerization and development of cell surface protrusions called phagosome that cause nanoparticle uptake by an engulfing like mechanism. Phagosomes then fuse with lysosomes, leading to the degradation of the nanoparticles by the enzymes and acidic environment supplied by the lysosomes (May and Machesky et al., 2001).

4.1.1.2 Pinocytosis

Internalization of smaller sized nanoparticles occurs via pinocytosis. This route of uptake is classified into clathrin-dependent and clathrin-independent pathways. The clathrin-independent pathways are categorized into micropinocytosis and caveolae or dynamin-mediated endocytosis (Iversen et al., 2011).

Clathrin-mediated endocytosis

The design of many ligands is directed on the recognition of EGF, LDL or Tf receptors on the cell surface. A non-receptor mediated uptake can also happen via electrostatic or hydrophobic interactions that will lead to internalization (Conner and Schmid, 2003). Clathrin mediated endocytosis begins at the cell surface level which is rich of the protein clathrin. Adaptor proteins such as Ap-2 initiate the formation of a clathrin lattice on the cytosolic part of the plasma membrane followed by the creation of clathrin coated pits.

Clathrin coated pits represent curved invaginations of the plasma membrane which are less than 200 nm in size (Munoz and Costa, 2012, Sahay et al., 2010). The clathrin coated pit narrows by dynamin acting on the neck of the pit to promote vesicle detachment from the membrane and formation of clathrin coated vesicles. Once the clathrin coated vesicles are detached, actin

polymerization occurs to aid its movement inside the cell (McMahon and Boucrot, 2011). The clathrin coat degrades and early endosomes are formed. After maturation to the late endosome either sorting to Golgi apparatus or lysosomes occurs leading to nanoparticle degradation by acidic pH and lysosomal enzymes or recycling of endosomes back to the cell surface (Tran and Webster, 2013).

Caveolae-mediated endocytosis

Caveolae mediated endocytosis is the second pathway that draws major attention in nanoparticle drug delivery. This type of pathway has also been implicated in diseases such as cancer, viral infections and diabetes (Rothberg et al., 1992, Mora et al., 1999). Caveolae are cell membrane invaginations that are responsible for signal transduction pathways and vesicle formation. They are 50-80 nm in size and they are enriched of two important proteins, caveolin 1 and caveolin 2. Caveolin 1 is the predominant protein that determines the shape of the caveolae, whereas caveolin 2 is responsible for structural stabilization (Pelkmans and Helenius, 2002). Internalization of caveolae is initiated by the binding of specific ligands such as albumin and folic acid followed by the formation of caveolar endocytic vesicles. Dynamin is releasing the vesicles from the membrane in order to move into the cytosol towards the caveosome, a pH neutral compartment. The internalized nanoparticles end up to ER or Golgi apparatus (Hillaireau and Couvreur, 2009).

Clathrin/caveolae independent endocytosis

The clathrin/caveolae independent pathways involve different cargos with specific lipid composition taken up by the cell such as Rho GTPase, Arf 6, Cdc42 and flotillin (Kafshgari et al., 2015). As in every endocytic pathway, the membrane engulfs the cargos into vesicles, which are sorted into caveosomes or endosomes. The final destination of the particles is either lysosomal degradation, delivery to the Golgi apparatus or ER, or release back to the cytoplasm.

Macropinocytosis

Macropinocytosis is a process that does not involve any receptor mediated activation. However, it requires the activation of tyrosine kinases such as PDGFR or EGFR for actin polymerization increase and the formation of large ruffles or membrane extensions by cytoskeleton rearrangement (Kafshgari et al., 2015). Internalization of bulk fluid from the cell's surroundings into cytoplasmic vacuoles called macropinosomes occurs via this pathway. The fusion of macropinosomes with lysosomes leads to its degradation and the release of nanoparticles. Release of nanoparticles into the cytoplasm is also possible due to the leaky nature of macropinosome.

Other entry pathways

Apart from the endocytic mechanisms described above, other mechanisms of entry have been characterized, which involve passive uptake and hole formation. For instance, Wang et al., described how DPA QDs interacted with the lipid membrane bilayer leading to its reorganization and passive diffusion of the nanoparticles without affecting the membrane integrity (Wang et al., 2016). Moreover, artificial mechanisms have been utilized for entry of nanomaterials into the cells. For example, microinjection techniques have been used to directly

deliver metal oxide metallic nanoparticles and silver nanoparticles into the cytoplasm of Hela cells (Candeloro et al., 2011). The same approach was adopted for injection of compacted nanoparticles into cancer cells (Liu et al., 2003). Another artificial method, called electroporation, involves the application of high voltage electrical impulses to cells, which creates membrane pores allowing entry of nanoparticles. This method was utilized for peptide conjugated QDs and oligonucleotide conjugated gold nanoparticles (Zhao et al., 2011, Jen et al., 2004).

4.1.2 Filopodia at the cell surface

The role of this cellular structure and its mechanism of action is still not well understood. As mentioned above, for the various endocytic mechanisms, there is an important step before internalization of the nanoparticles. This step involves actin polymerization and assembly of actin filaments. Such polymerization is a precursor not only for endocytosis and phagocytosis but for cell migration as well. Cell migration is a dynamic process that depends on actin assemblies that are constantly adjusting on the cell membrane. These actin rich protrusions of the cell membrane are called filopodia. Their size ranges between 0.1 to 0.3 μm (Mallavarapu and Mitchison, 1999). There are various functions in which filopodia are involved but their main role is in cell migration, embryonic development, wound healing and cell guidance towards chemoattractants (Faix et al., 2006, Gupton et al., 2007).

4.1.2.1 Cellular functions of filopodia

The best characterized function of filopodia is cell migration and motility. In this context, filopodia act as antennae for the cells to sense their microenvironment. They contain receptors for various signalling molecules and thus, play a major role in signal transduction pathways (Vasioukhin et al., 2000). It has been found that the migration and cell adhesion abilities of filopodia are attributed to cell adhesion molecules like cadherins and integrins which are found in the filopodia's tip (Steketee and Tosnev, 2002). Also, upon pathogen invasion, filopodia will bind to pathogens and initiate their phagocytosis (Thomas et al., 2010). Another role of filopodia is on wound healing and embryonic development. In these biological processes, epithelial cells fuse into sheet like structures and filopodia assist on the formation of adherens junctions between epithelial cells (Vasioukhin et al., 2000). Filopodia also participate in the migration and guidance of neuronal growth cones at the end of neurites for guidance towards chemoattractants. Apart from their function in neurite growth, they enable the formation of cortical neurons and dendritic spines (Sekino et al., 2007).

4.1.2.2 Components of filopodia

Many proteins that are responsible for the regulation of the actin cytoskeleton are associated with filopodia formation. The major protein involved is the CDC42 that belongs to a family of Rho GTPases. The most common pathway that activates filopodia formation is via the ARP2/3-WASP complex (Ohta et al., 1999). This complex generates a branched F-actin network that leads to lamellipodial formation. Dia2 is a formin protein that initiates the development of unbranched actin filaments and along with RIF, a small GTPase, promotes

elongation of filopodia. ENA/VASP proteins localize at the tips of filopodia and on focal adhesions stimulating their elongation (Figure 4.2).

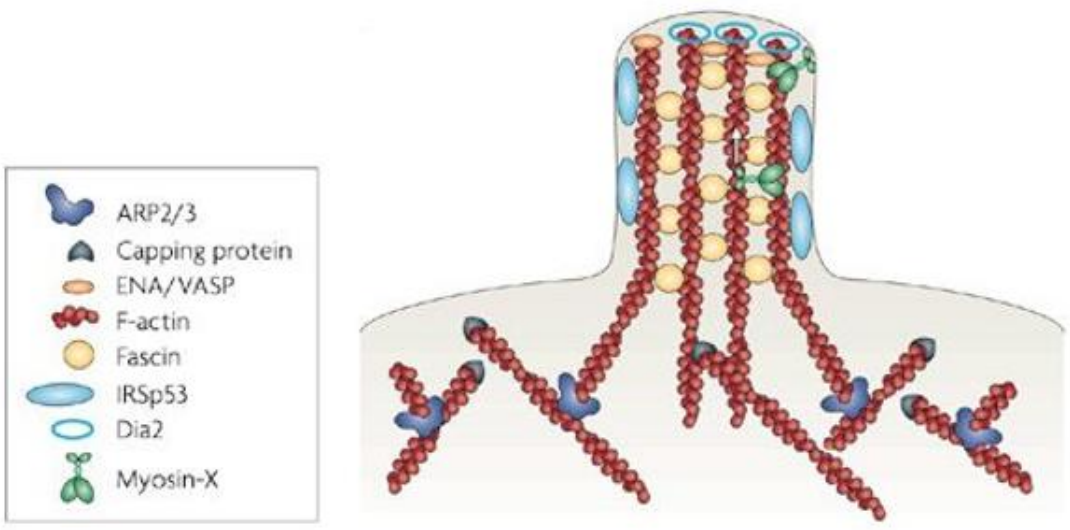

Figure 4.2: Schematic illustration of the key proteins involved in the formation of filopodia. The actin cross-linking protein fascin produces an actin filament bundle. Adhesion molecules are localized to the filopodia tip by myosin-X in order for the elongation process to begin. Dia2 controls the elongation and is localized at the tip complex. From Mattila and Lappalainen, 2008.

On the other hand, Myosin-X is a large group of motor proteins that “walk” across actin filaments to transport proteins to filopodia required for their formation (Ohta et al., 1999). A protein that maintains the F-actin bundles of filopodia is fascin. It is not directly linked to their formation, but it is associated with the production of parallel and stiff filament bundles. In addition to actin cytoskeleton reorganization, deformation of the plasma membrane has also been shown. During this deformation, an F-actin cross linking activity of IM/I-BAR domain leads to filopodia formation and plasma membrane protrusions (Scita et al., 2008). Lastly, some other proteins have been identified to be important for filopodia formation but their mechanism is not fully understood. Specifically, Sigal et al., published that a lipid phosphatase related protein, plays a role in filopodia dynamics in an independent manner of the ENA/VASP and ARP2/3 complex. It

probably resembles more the role of the I-BAR domain proteins in inducing membrane curvature but this still needs to be confirmed (Sigal et al., 2008).

4.1.3 The use of surface ligands in nanotechnology

The surface chemistry of a nanoparticle along with the choice, the design and the density of the ligands attached to it play a crucial role in the interaction of the nanoparticles with the cell membrane and cellular uptake. The use of appropriate ligands in nanotechnology provides the ability to control the nanoparticles surface properties from assembly and synthesis to biological interactions, leading to effective cellular uptake. Ligands can affect the stability, functionality, size and shape of the particles along with their agglomeration state. Advancements in characterization techniques and ligand design along with the choice of the solvent, the control of the temperature and pH during synthesis, provide the advantage to synthesize nanoparticles with various size and shapes, interacting in a desired way with a biological membrane or organ.

4.1.3.1 Ligands for nanoparticle synthesis, assembly and stability

Ligands can kinetically affect the shape and the size of the nanoparticles under thermodynamic control (Yin and Alivisatos, 2005). For instance, the introduction of a ligand that selectively binds to a metal will reduce its growth rate. However, it is very difficult to estimate the adhesion energy of a ligand when synthesizing a nanoparticle because of their various binding affinities. Core-shell nanoparticles can be generated by the approach of having a growth starting at the core of an inorganic material and via a hydrolysis step a second inorganic precursor is formed to create a core-shell structure particle (Ling et al., 2014). In biomedical applications though there is a need of controlling the hydro-dynamic radius of a nanoparticle therefore, the use of a hydrophilic or hydrophobic ligand

is more applicable depending on the purpose/proposed uptake mechanism. Hydrophobic ligands are transported though the bloodstream attached to a hydrophilic carrier whereas hydrophilic ligands are binding to a cell surface.

Nevertheless, issues of stability and agglomeration exist by using a hydrophobic ligand. The approach to overcome these issues is to replace a hydrophobic ligand with a hydrophilic one by attaching a chelating motif of amines, thiols, carboxylic acids or phosphines to the nanoparticle (Ling et al., 2014). Another approach is based on the formation of micelle like structures that include an amphiphilic ligand encapsulating nanoparticles via hydrophobic interactions (Dubertret et al., 2002, Yu et al., 2007).

4.1.3.2 Ligands for biomedical applications

PEGylated nanoparticles

Most of the time, nanoparticles are cleared too fast by the mononuclear phagocyte system, which is part of the immune system consisting of phagocytes. Therefore, the use of biocompatible ligands can enhance their effectiveness and aid the targeting of the nanoparticles to a specific place. One of the most widely used ligand attached to AuNPs for biomedical applications is the PEG molecule. PEG is a non-immunogenic and non-toxic polymer that is used in the biopharmaceuticals industry because of its advantageous pharmacokinetic properties. Some of these properties are decreased immunogenicity, enhanced nanoparticle solubility, stability and increased blood circulation time (Walkey et al., 2012, Otsuka et al., 2003, Jokerst et al., 2011).

AuNPs are often coated with PEG via PEGylation. PEGylation is an important process in the synthesis of nanomaterials as it attributes specific physico-chemical features on the nanoparticles. These include changes in their

hydrophobicity, electrostatic binding and alterations in their pharmacokinetic profile (Kim et al., 2009, Choi et al., 2007). The effectiveness of the PEG coating is affected by both the length of the PEG chain and the surface density. For example, an increased coating thickness has been linked to a reduced radiosensitization effect (Xiao et al., 2011).

The ligand density around the core of the nanoparticle interferes with the uptake of the particles by cells and with proteins present in the biological medium, forming a complex termed as protein corona. Protein corona formation is a phenomenon that depends upon both the nanoparticle and protein characteristics. The size, the type, the conformational flexibility of the protein along with the type of the nanoparticle, the charge, the shape, the size and the hydrophobicity affect the way the protein corona is formed around the nanoparticle (Cedervall et al., 2007, Yang et al., 2013). Also, medium related factors such as the ionic strength of the solution and the pH plays an important role (Monopoli et al., 2011).

Various studies have shown that there is an optimum ligand density required for particle uptake (Ling et al., 2014). Decreased PEG density can lead to activation of macrophage surface receptors and adsorption of proteins whereas, less bound proteins on a higher density PEG coated nanoparticle can affect their uptake by macrophages (You et al., 2005). There is a baseline level at which uptake is independent of protein binding, which is a density of around 0.5 molecules/ nm^2 (Figure 4.3).

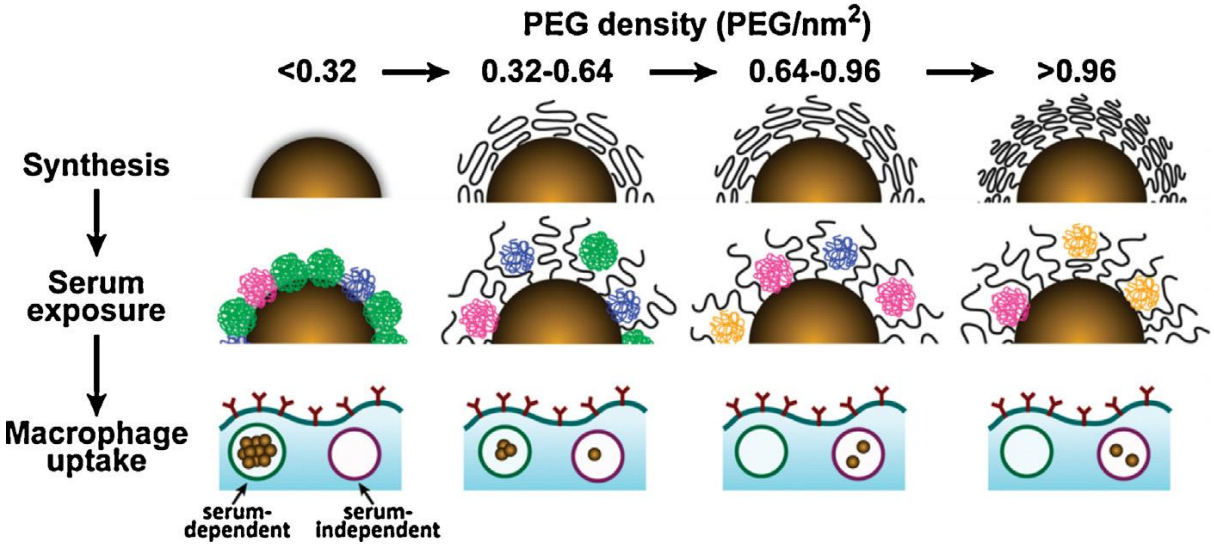

Figure 4.3: PEG density effects on the clearance of monocytes. The protein corona formation is caused by exposure to serum and is affected by the density of the PEG molecules. An opsonin-like structure is formed at low densities of PEG, whereas high densities adsorb less proteins. From Ling et al., 2014.

Zwitterionic ligands

Unlike the PEG ligands, zwitterionic ligands adsorb less protein corona, leading to a longer circulation of the particles in the bloodstream without them being taken up by monocytes. Zwitterionic ligands can either be polymeric or small molecule ligands that are both described below. A recent study showed decreased clearance and better immunotolerance with zwitterionic poly-carboxybetaine based nanomaterials (Young et al., 2014).

Small molecule ligands

This type of ligands are easy to synthesize and have different functionalities. Enhanced adsorption of proteins is attracted to the nanoparticle surface when is coated with a monolayer of small molecule ligands. This type of ligand can be used for modifying the nanoparticle assembly and the interaction with cell surface receptors. A study has previously published the use of two small molecules as ligands, the OPAP and the PDP which hydrogen bonds with the polymer PS-b-P4VP in order to direct particle assembly over large scales (Zhao et al., 2009). A study from You and colleagues demonstrated cytochrome c and α-chymotrypsin targeting via the use of a nanoparticle coated with the hydrophobic amino acids phenylalanine and leucine (You et al., 2008). Such approach yielded a high specificity and recognition capacity towards the targeted proteins with an approximately 20-fold higher affinity than nanoparticles with similar hydrophobicity (You et al., 2008).

Cell specific nanoparticle ligands

In most cases, the focus of the design of a nanomaterial is to include ligands that do not trigger an immune response. There is a bigger focus which is the targeting of the nanoparticle to a specific cell type or organ, such as in occasions of cancer targeting therapeutics. Hydrophobic particles can stick to the outer cell membrane which is of lipophilic nature leading to micropinocytic or endocytic uptake. However, hydrophobic coated nanoparticles tend to aggregate and will most likely create a protein corona around them thus ending up in agglomerated form before entering the cell (Weissleder et al., 2005). Therefore, hydrophilic ligands with small molecules, antibodies or peptides attached to them are preferred to overcome the agglomeration problem and trigger an endocytic uptake mechanism by binding to the desired receptor (McCarthy et al., 2008). A limitation arises here due to the fact that the triggering of a specific uptake mechanism is highly dependent on the expression of the receptor at the cell surface and the tissue or cell type.

Microenvironment sensitive ligands

Contrary to designing ligands for cell specific interactions, targeting of a specific tissue is also possible. One example is the use of nanoparticles to target cancerous cells and tissues not by attaching to a specific receptor but by recognising the environment. Specifically, Ling et al. used neutral pH sensitive magnetic nanogrenades that become cationic when they encounter the decreased pH of the tumour microenvironment, but remained neutral during their circulation (Ling et al., 2014).

4.1.3.3 Ligand density and organization

It is interesting how a particular type of ligand can affect both the physico-chemical properties of a nanoparticle but also the way it interacts with the cell and specific tissues. Apart from the types of ligands, ligand density and organization around the core of a nanoparticle is also vital. Lund et al. investigated how the ligand organization rather than the nanoparticles properties or charge can affect the rate of AuNPs uptake by colorectal cancer cells. AuNPs bearing 50:50 PEGamine:glucose were internalized 18 times more than AuNPs with only glucose or PEGamine, the structure of which is shown in the figure below (Figure 4.4). The mechanism by which the particles were found to be internalized was via an energy-dependent pathway through openings being created in the lipid-bilayer by the ligands of the AuNPs (Lund et al., 2011).

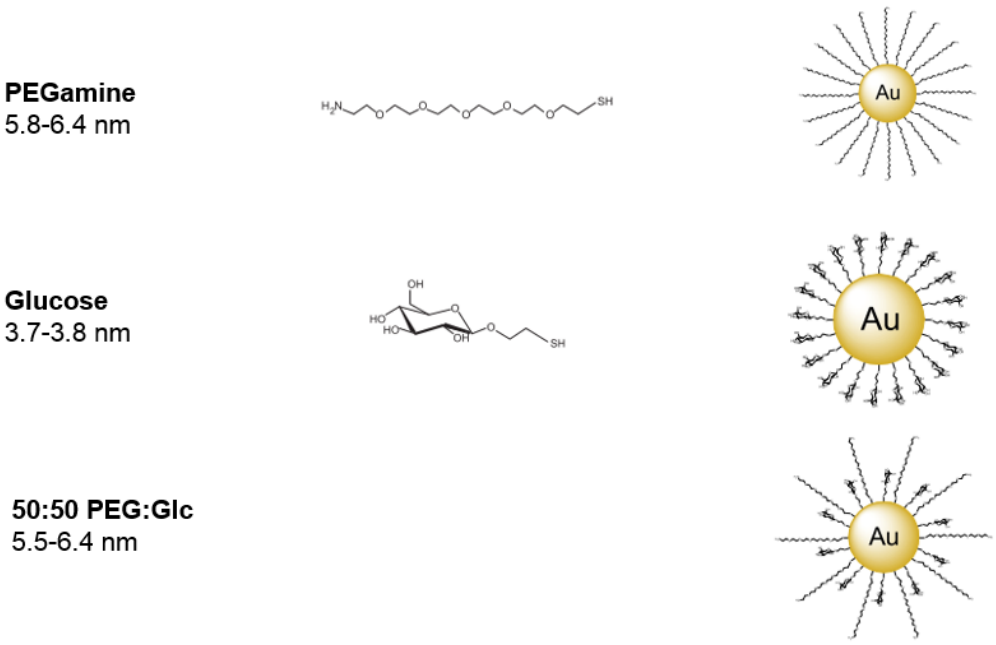

Figure 4.4: Nanoparticle representation of the ligand structures used in the study described from Lund et al. 2011. From Lund et al., 2011.

With regard to PEGylated AuNPs, the actual molecular weight of PEG and its density plays an important role to the physicochemical characteristics of the particles. The density of PEG ligands around the gold core initiates a transition from a disorganised “mushroom” like structure to a more “brush” like organisation. The total quantity of ligand molecules along with its mass, affects not only the properties of the nanoparticle but also its protein adsorption resistance. There is a contradiction on the published evidence as to what density is the correct one for uptake of nanoparticles by target cells and tissues.

One study for example, demonstrated that high density packed AuNPs with nucleic acids enhanced cellular uptake in lung and cervix human and mouse tissues (Giljohann et al., 2007). On the other hand, if the ligands are packed too tightly it can lead to reduced uptake and an increase in the antagonism between multiple ligands for a single receptor (Elias et al., 2013). The study from Elias et al., suggested that an optimal density exists with HER2/neu ligands attached to supermagnetic iron oxide nanoparticles which showed an increased cell binding with intermediate density packing. Therefore, an optimization of the correct ligand density is of great significance when designing nanoparticles.

Two main approaches exist for control of ligand density around the nanoparticle core. The first one is by modulating the shape of the nanoparticle that changes the spatial arrangement of the ligands. In this way, ligand loading will be affected by alterations in the surface area (Sajanlal et al., 2011). Another approach, involves the control of the molar ratios of the nanoparticle and ligands during the conjugation process (Gu et al., 2008). In order for this approach to be effective, adjustment of the chemical environment including the pH conditions and the salt concentrations need to be done.

To conclude, research has given an insight into how different ligands can affect and control the desired properties of a nanomaterial but still more work needs to be done to fully understand processes and mechanisms of nanoparticle assemblies and synthesis. The main area of interest in the biomedical field is to design ligands and nanoparticles which can overcome biological clearance barriers, without interfering with nanoparticle clearance once the particles have fulfilled their purpose in the body. However, lack of translational success especially in the use of nanoparticles for cancer treatment, raises questions as to whether the design of the particles or our current understanding about the disease and the use of appropriate clinical models needs to be improved. Thus, nanotechnology will progress by both engineering of successful nanoparticles and enhancing our knowledge of endocytosis mechanisms.

In the next chapter, the focus is on differences between three AuNPs with synthesis times of 1h, 2h and 5h. Results of the previous chapter revealed one of the parameters that played a vital role in toxicity of AuNPs to be their synthesis time. A full physicochemical analysis was conducted and the three AuNPs were evaluated for differences in their ligand density and uptake by HSC cells. The materials provided for these specific batches were synthesized in a small scale of 700 µl. Most of the analysis was based on 1h and 5h AuNP, unless otherwise stated, as they were the particles with significant differences observed in toxicity.

4.2 Results

Variations in the cytotoxicity of the 50:50 αGal:PEGamine AuNPs were observed when scaling up to larger volume batches. This variation was attributed to the contact time of $NaBH_4$ with the ligands during AuNP synthesis. To investigate the differences detected with the increasing synthesis time, AuNPs synthesised for 1h, 2h and 5h were tested for their physico-chemical characteristics and uptake by HSC cells.

4.2.1 Physico-chemical characterization of 3 different synthesis time AuNPs

4.2.1.1 Synthesis time effects on AuNP size

Three different AuNPs, each bearing αGalactose:PEGamine ligands (50:50 input ratio) were synthesized under identical conditions except for differences in their contact time with $NaBH_4$ during synthesis (1h, 2h and 5h). There was no surface plasmon band observed for these particles as shown by UV-Vis measurements (Figure 4.5A). This was confirmed using DLS to estimate their hydrodynamic size, which was less than 10nm (Figure 4.5B). TEM analysis revealed the AuNPs to be spherical (Figure 4.6A) with no significant differences in diameter (1h = 1.58±0.8 nm, 2h=1.58±0.9 nm, 5h = 1.52±0.7 nm) (Figure 4.6B).

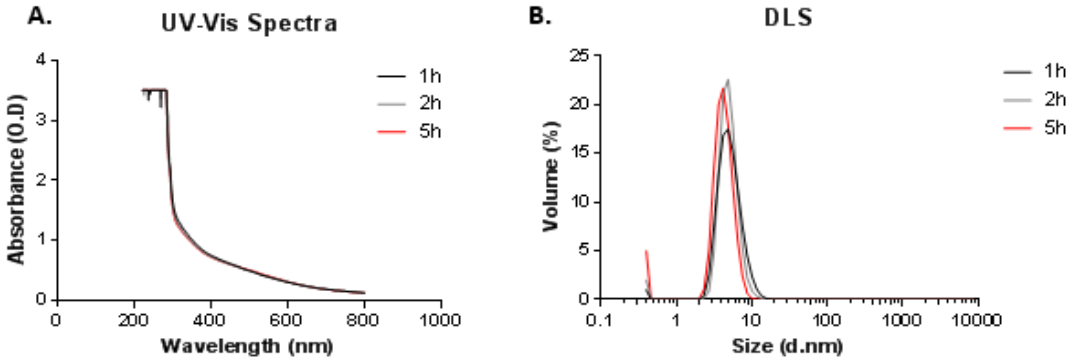

Figure 4.5: AuNPs physicochemical characterization for 1h, 2h and 5h synthesis time. A. UV-Vis spectra and **B.** Average hydrodynamic diameter measured by DLS.

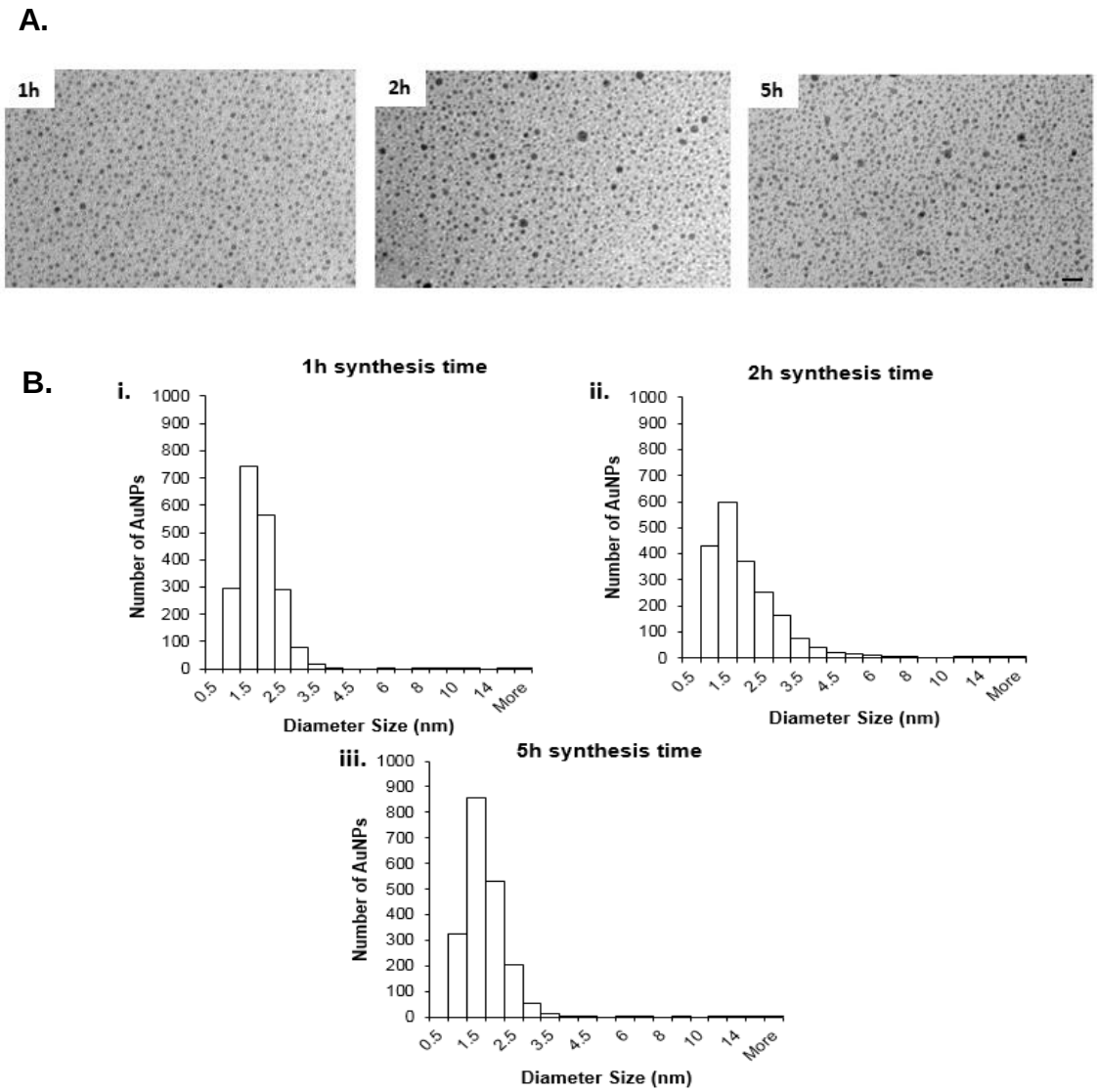

Figure 4.6: **Differences in AuNP size as calculated by TEM for 1h, 2h and 5h synthesis time. A.** TEM images of AuNPs, scale bar=5 nm. **B.** Size distribution histograms on **i.** 1h synthesis time AuNP, **ii.** 2h synthesis time AuNP and **iii.** 5h synthesis time AuNP.

TEM was selected as the best method to characterize nanoparticle size complementary to DLS and UV-Vis due to the fact that it provides the ability of visualizing individual nanoparticles in high resolution detail. This ability is crucial when quantifying any nanoparticle feature as it gives direct information about its dispersion, aggregation state and surface.

The dispersion and aggregation state of the nanoparticles is affected by their environment (Hondow et al., 2014), therefore the preparation method and the solutions used for each quantification assay needed to be taken into account when estimating their size. In this case, all three of the above assays included a step of diluting particles in water, which was their storage solution. However, in order to test the aggregation state of the particles when internalized by cells, TEM of the particles diluted in culture media with the presence and absence of FBS was conducted (Figure 4.7A). It has been previously shown that AuNPs aggregate in saline aqueous media which is explained by a power kinetics law of ionic strengths (Guillermo et al. 2014). The 50:50 αGal:PEGamine AuNPs in this study did not aggregate in culture media in presence or absence of FBS, with only the 1h synthesis time AuNP to show a tendency for aggregation in presence of FBS (Figure 4.7A, black arrow).

Another method used to evaluate the aggregation of these AuNPs in media was the FPLC (Figure 4.7B). In this method, peaks of individual or aggregated particles pass through the column at different speeds and elute at different volumes. Both the 1h and 5h synthesis time AuNPs elute at the same volume, therefore it could be concluded that there were no signs of aggregation in either of the synthesis times. The reason why only the 1h and 5h particles were analysed by FPLC was because these were the two particles which showed the greatest differences in toxicity as presented in chapter 3.

A.

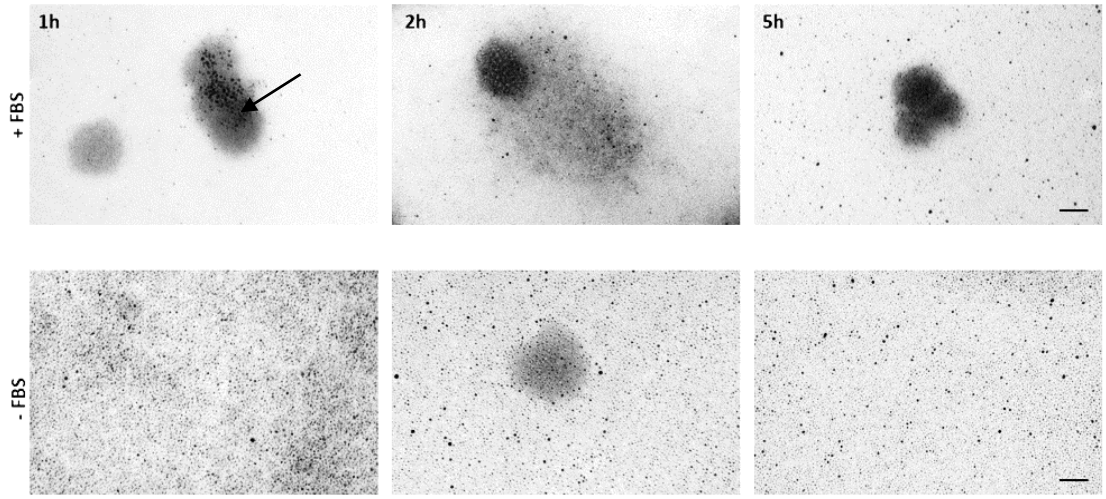

B.

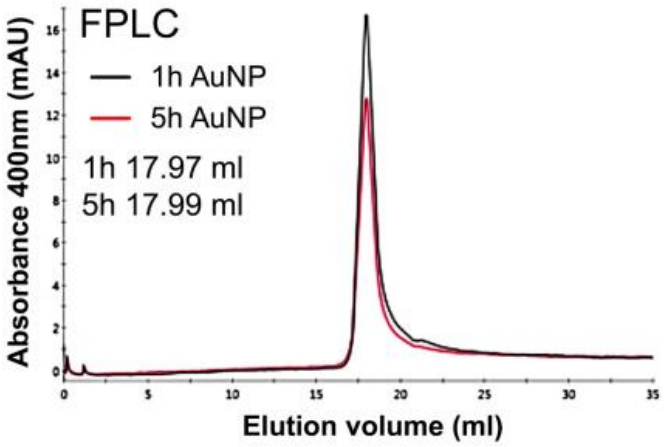

Figure 4.7: Aggregation state of the AuNPs as determined by A. TEM images for the 1h, 2h and 5h AuNPs. Small dark dots represent the AuNPs, whereas the grey clouds appearing mostly in the +FBS images were attributed to serum components. The black arrow points slightly bigger particles within the serum clouds, indicating possible aggregation. Scale bar=5nm and **B.** FPLC chromatogram for the 1h and 5h AuNPs.

4.2.1.2 Effects of AuNP synthesis time on charge

The average charge of the AuNPs was around +40 mV, although the 1h AuNP demonstrated extra peaks at 20 mV and 60 mV (Figure 4.8). Zeta potential measurements need to be carefully interpreted as values are solution and pH dependent.

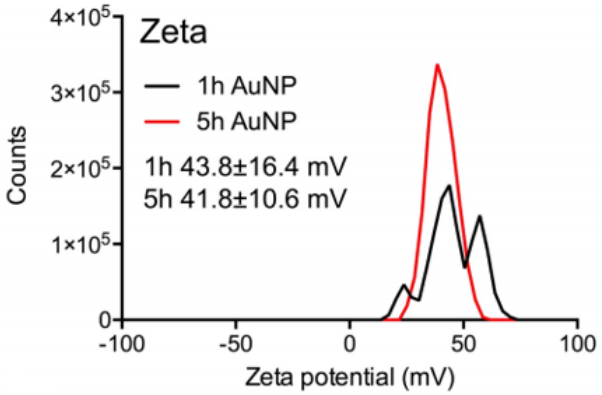

Peak	ζ potential (mV) 1h AuNP
1	41.8±5.19
2	57.0±4.37
3	24.8±3.78

Peak	ζ potential (mV) 5h AuNP
1	40.3±6.28
2	0.00±0.00
3	0.00±0.00

Figure 4.8: **Zeta potential measurements for 1h and 5h synthesis AuNPs.** Traces from a representative measurement and the calculated mean values (mV) ± SD (mV) were presented.

Considering the lack of robustness of the zeta potential measurements, the electrophoretic mobility of the particles was used as a complimentary method for charge analysis and was assessed by gel electrophoresis. 1% agarose gels provided good visualization of the particles. The AuNPs left a stain as they were migrating towards the negative electrode at 100 mV with two distinct bands to appear at the origin and at the bottom of the gel.

It was evident that only the particles from the 1h synthesis time migrated towards the negative electrode into the gel, shown by the appearance of two bands in the respective lane of the gel and indicating that they had positive charge (Figure 4.9). The most intense band was the one very close to the well, showing

that the majority of the particles did not migrate under the tested conditions. For the 5h synthesis time particle no additional bands apart from the ones close to the well were visible. The failure of AuNP to migrate into the gel could either be charge or size related. The size of the particles did not change in water as shown in the section above (Figure 4.6). However, for the gel electrophoresis, the particles were diluted in TBE buffer, which might have caused aggregation or a change in the particle's charge. Therefore, the only information drawn by this data was that the particles were positively charged. It was not possible to determine an accurate zeta potential value with either of the methods, therefore the values provided needed to be interpreted with caution, taking into account the limitations of each of the assays.

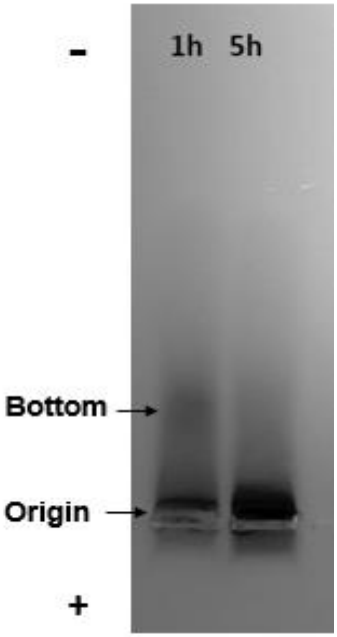

Figure 4.9: Analysis of the AuNP charge by gel electrophoresis. AuNP synthesized for 1h and 5h were run on a 1% agarose gel to measure differences in their charge.

4.2.1.3 Examination into AuNP ligand ratio and density

Ligand ratio was investigated by ^{1}H-NMR and demonstrated no change between the two AuNPs to within 2% (αGalactose:PEGamine ratios: 1h= 52.8:47.2, 5h= 51.2:48.8) (Figure 4.10A&B). The characteristic peaks from which the ratio was calculated are shown in the figure below for interpretation.

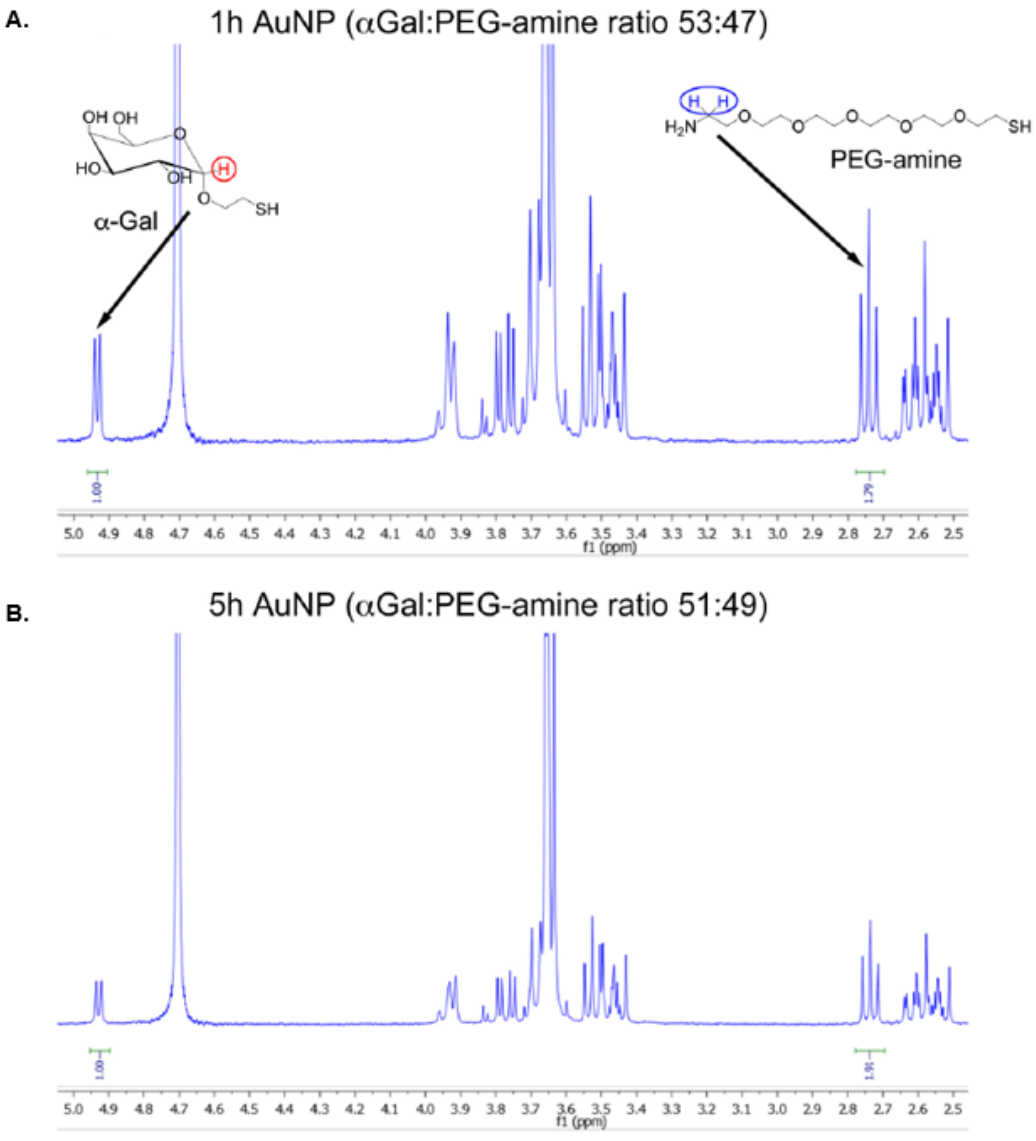

Figure 4.10: Ligand ratio determination as obtained by ^{1}H-NMR for A. 1h and B. 5h synthesis time AuNP. The input ratio of 50:50 ligands during synthesis yielded an output ratio of similar values ± 2% difference.

The S:Au ratio was used as a determination for the ligand density surrounding the Au core of the particles, as Midatech's GNP technology is based on the fact that the AuNPs comprise of a core of gold metal atoms to which an organic layer of galactose is attached via gold-sulphur bonds. The carbohydrate layer stabilises the gold core and makes the particle biocompatible and water soluble. In order to address the ligand density surrounding the Au core, the S:Au ratio was calculated based on three different techniques EDX, XPS and SEM.

Each of these analytical techniques provide elemental analysis of the AuNPs samples and characterization of the S:Au ratio, which showed decreasing ligand density in all methods. The accuracy of each technique is affected by various factors such as detection limits (signal to noise ratio), peak intensity, analysis time, degradation during the analysis and the nature of the sample itself. With regard to the sample itself, parameters like the density of the sample, the amount and the composition can affect the way the sample reaches the detector. X-Ray emission peaks will be generated by any atom that is sufficiently excited by the electron beam and some elements have overlapping peaks that make any interpretation of the chemical composition difficult.

SEM-EDX proved to be the most appropriate technique for the estimation of the ligand density as it was the most sensitive method of detecting low S levels (Figure 4.11A&B). The ligand density decreased with the longer the synthesis time (Table 4.1). S:Au calculation by EDX and XPS was difficult as the S signal detection limit was close to background level (Appendix Figure 9.1,Figure 9.2).

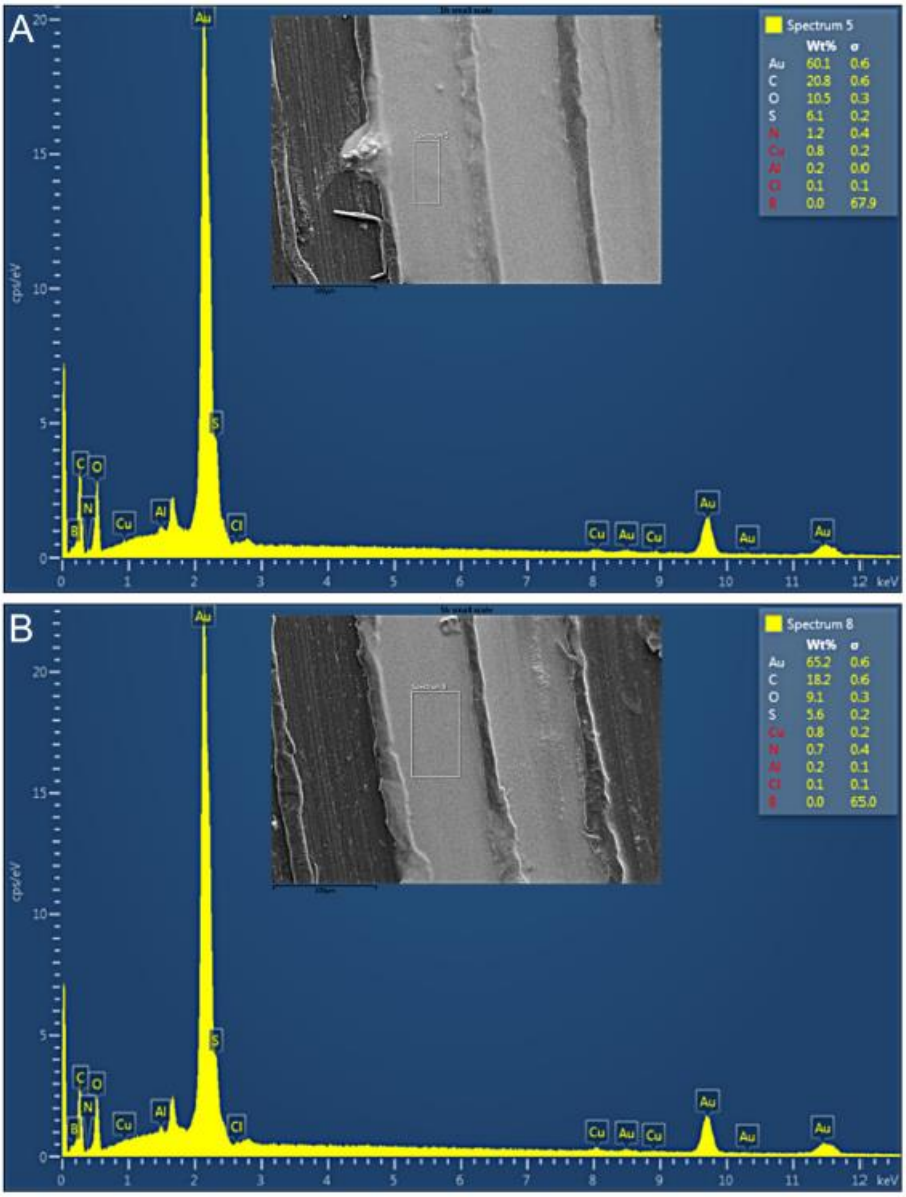

Figure 4.11: Elemental analysis of A. 1h synthesis time AuNP and B. 5h synthesis time AuNP as calculated by S:Au ratio on SEM. Representative spectra from a single run are shown with element peaks marked. Inserts represent SEM images showing the region analysed for each spectrum.

It was concluded that these two different AuNPs had similar physicochemical properties in terms of size, shape and ligand ratio (Table 4.1). As mentioned above, most of the analytical techniques focused on obtaining characterization data between 1h and 5h synthesis time as these were the AuNPs showing the biggest differences in toxicity in HSC cells. Ligand density decreased with synthesis time and the charge was positive for all the particles. No aggregation was obvious as FPLC data indicated.

Table 4.1: Summary of the physicochemical characteristics of the two different AuNPs.

AuNP Synthesis Time	**[Au]** µg/ml	**Size** (d.nm)	**Z potential** (mV)	**Plasmon band**	**aGal:PEG ratio**	**S:Au ratio**
1h	2.1	1.58±0.8	20.2±86.6	None	52.8:47.2	0.101± 0.0011
5h	2.2	1.52±0.7	40.3±6.28	None	51.2:48.8	0.08± 0.0018

4.2.2 Toxicity of AuNPs to HSC cells with increasing synthesis time

The cytotoxic potential of acute exposure to the three AuNPs was determined by clonogenic assays, using four different cell lines that represent normal or cancerous versions of human skin cells (HaCaT, HSC) and kidney cells (HEK-293, A498). For all the four cell lines, acute 3h exposure to AuNPs resulted in dose-dependent reductions in the number and size of cell colonies, with HSC cancer cells and kidney cell lines showing a greater reduction than HaCaT normal cells (Figure 4.12A&B). There were also noted AuNP synthesis time-dependent differences in colony number for HSC and HaCAT cells. In these cell lines, cell death was increased when using particles with 2h and 5h synthesis time compared to 1h synthesis time. No time-dependent differences were observed

for the kidney cell lines (Figure 4.12C&D). IC50 values for each AuNP are presented in Table 4.2 below.

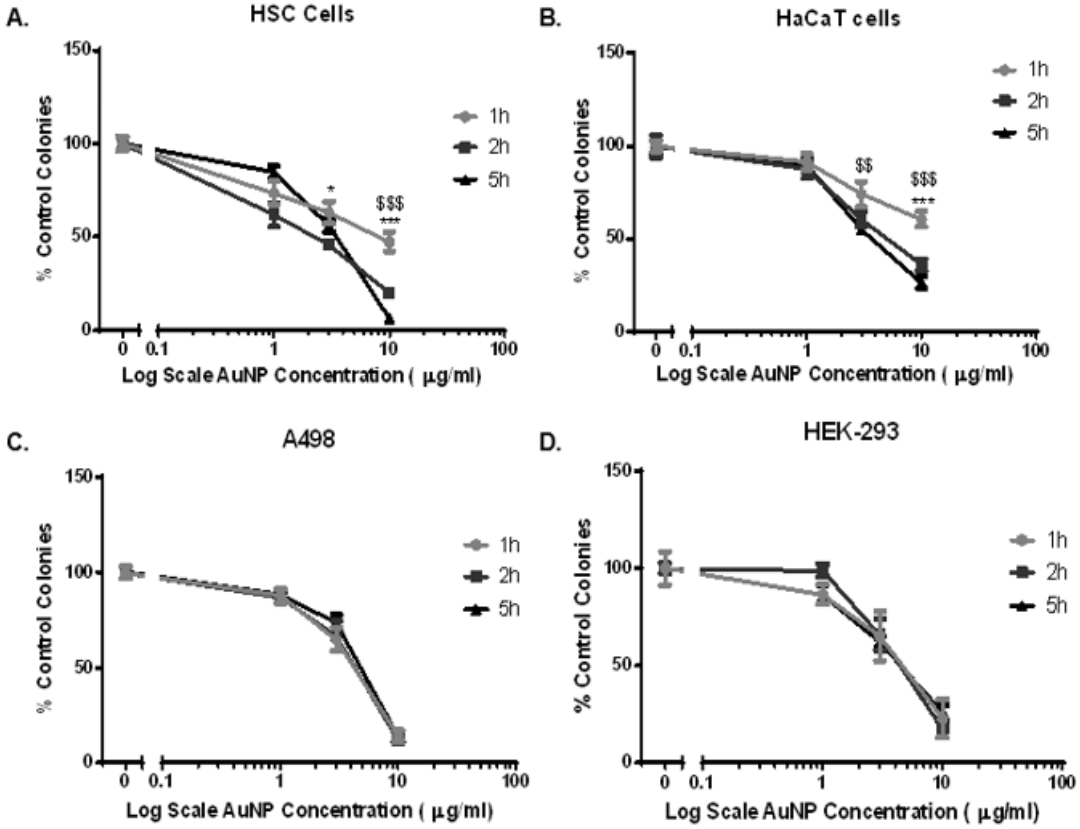

Figure 4.12: Comparison of the cytotoxicity of AuNPs with different synthesis times on A. HSC, B. HaCaT cells, C. A498 and D. HEK-293 cells. Significant differences between 1h and 2h synthesis AuNPs were marked by * symbols, while significant differences between 1h and 5h synthesis AuNPs were marked by § symbols. Data were expressed as % of control colonies and plotted as mean±SEM, n=3 independent experiments. One-way ANOVA, *P<0.05, **P<0.01, ***P<0.001.

Table 4.2: **IC50 values (µg/ml) obtained from clonogenic assays for the 3 different AuNPs on HSC, HaCaT, HEK-293 and A498 cells.**

AuNP Sample	HSC IC50 (µg/ml)	HaCaT IC50 (µg/ml)	HEK-293 IC50 (µg/ml)	A498 IC50 (µg/ml)
1h	10	>10	4	6.5
2h	2.4	6	4	6.5
5h	3.9	4	4	7

4.2.3 AuNPs adhere to filopodia in HSC cells

In order to explain the differences in cytotoxicity between 1h and 5h AuNPs on HSC cells, their cellular uptake and distribution inside the cells was examined using TEM. The number of AuNPs was quantified in three areas: the cytoplasm (including the organelles and vesicular compartments), the nucleus and the cell surface. Due to limited availability of material, TEM was only conducted in HSC and HaCaT cells as these were the cell lines that showed the biggest variation in toxicity. For HSC cells, three independent experiments were conducted to obtain robust statistical significant data but for HaCaT cells there was only n=1 with two technical replicates. Therefore, data from HaCaT cells could not be statistically analysed and only showed a trend (Appendix Figure 9.4). Any comparisons between the cell lines need to be made with caution.

To discriminate between energy-dependent and passive uptake, cell uptake studies were performed at 37^{o}C or 4^{o}C, respectively. At 37^{o}C no significant differences were observed in the distribution of 1h and 5h AuNPs on HSC cells, which were predominantly in the cytoplasm (Figure 4.13A-D). However, at 4^{o}C the distribution of both AuNPs was predominantly at the cell surface, specifically on filopodia, with significantly more 5h AuNPs sticking to filopodia than 1h AuNPs (Figure 4.14A-D). To confirm whether AuNPs were selectively binding to filopodia, HSC cells were pre-incubated with fascin G2, an inhibitor of filopodia formation that destabilizes filopodia and prevents their formation. Following fascin addition, cells incubated with AuNPs at 4^{o}C showed a significant three-fold reduction of AuNPs at the cell surface (Figure 4.15A-C,G), while cells loaded with AuNPs at 37^{o}C demonstrated significantly less AuNPs within the cytoplasm (Figure 4.15D-F,H).

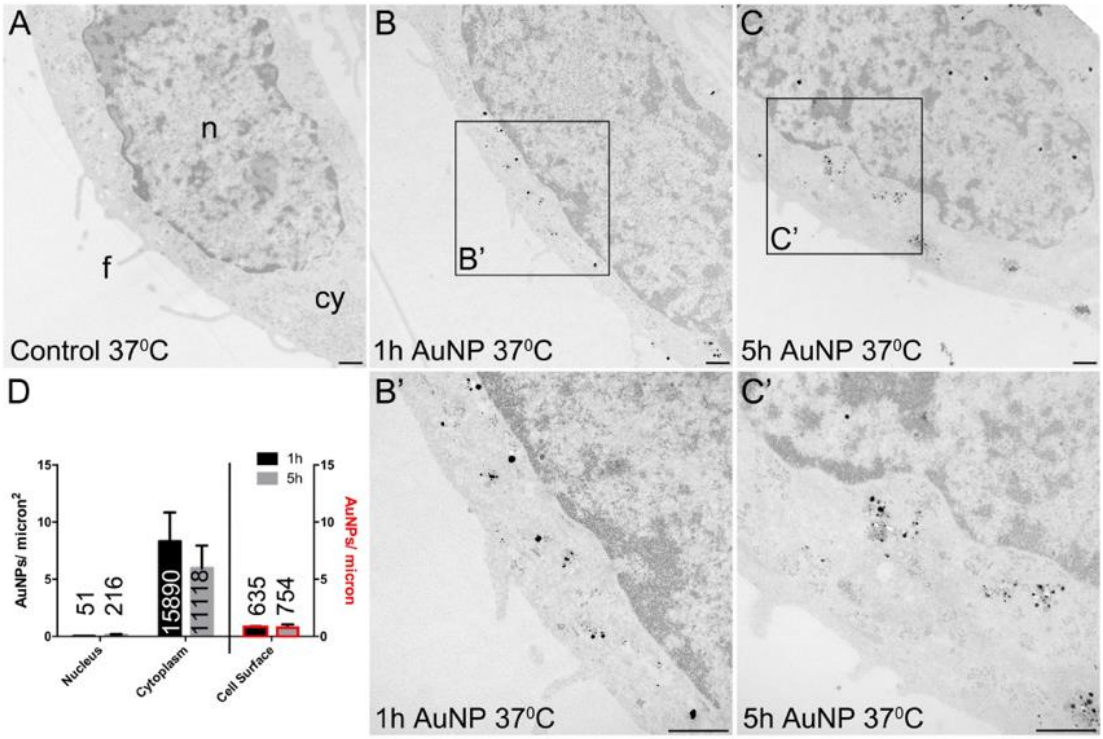

Figure 4.13: Localization of silver enhanced 1h and 5h synthesis time AuNPs in HSC cells after an acute 3h exposure at 37ºC and 10 µg/ml analysed by TEM. A. No AuNP control, **B.** 1h AuNPs, **C.** 5h AuNPs. **B'** and **C'** show magnified portions of the boxed regions of B and C, respectively. **D.** Quantitation of AuNP counts per micron^2 for nucleus and cytoplasm (left axis) and AuNP counts per micron for cell surface (right axis, bars with red border). Total numbers of AuNPs counted per category are shown on bars and data were plotted as mean±SEM, n=3 independent experiments with two technical replicates per condition. n=nucleus, cy=cytoplasm, f=filopodia. Scale bars in all images= 500nm.

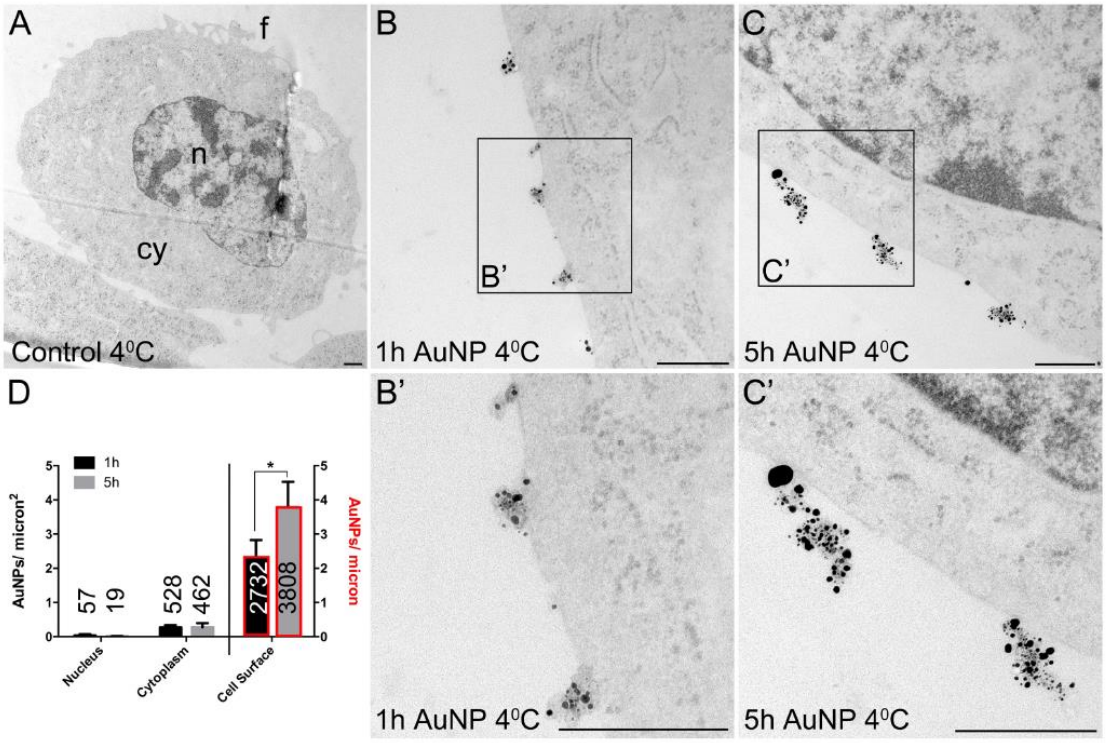

Figure 4.14: Localization of silver enhanced 1h and 5h synthesis time AuNPs in HSC cells after an acute 3h exposure at 4ºC and 10 µg/ml analysed by TEM. A. No AuNP control, **B.** 1h AuNPs, C. 5h AuNPs. **B'** and **C'** show magnified portions of the boxed regions of B and C, respectively. **D.** Quantitation of AuNP counts per micron^2 for nucleus and cytoplasm (left axis) and AuNP counts per micron for cell surface (right axis, bars with red border). Total numbers of AuNPs counted per category are shown on bars and data were plotted as mean±SEM, n=3 independent experiments with two technical replicates per condition, One-way ANOVA, *P<0.05. n=nucleus, cy=cytoplasm, f=filopodia. Scale bars in all images= 500nm.

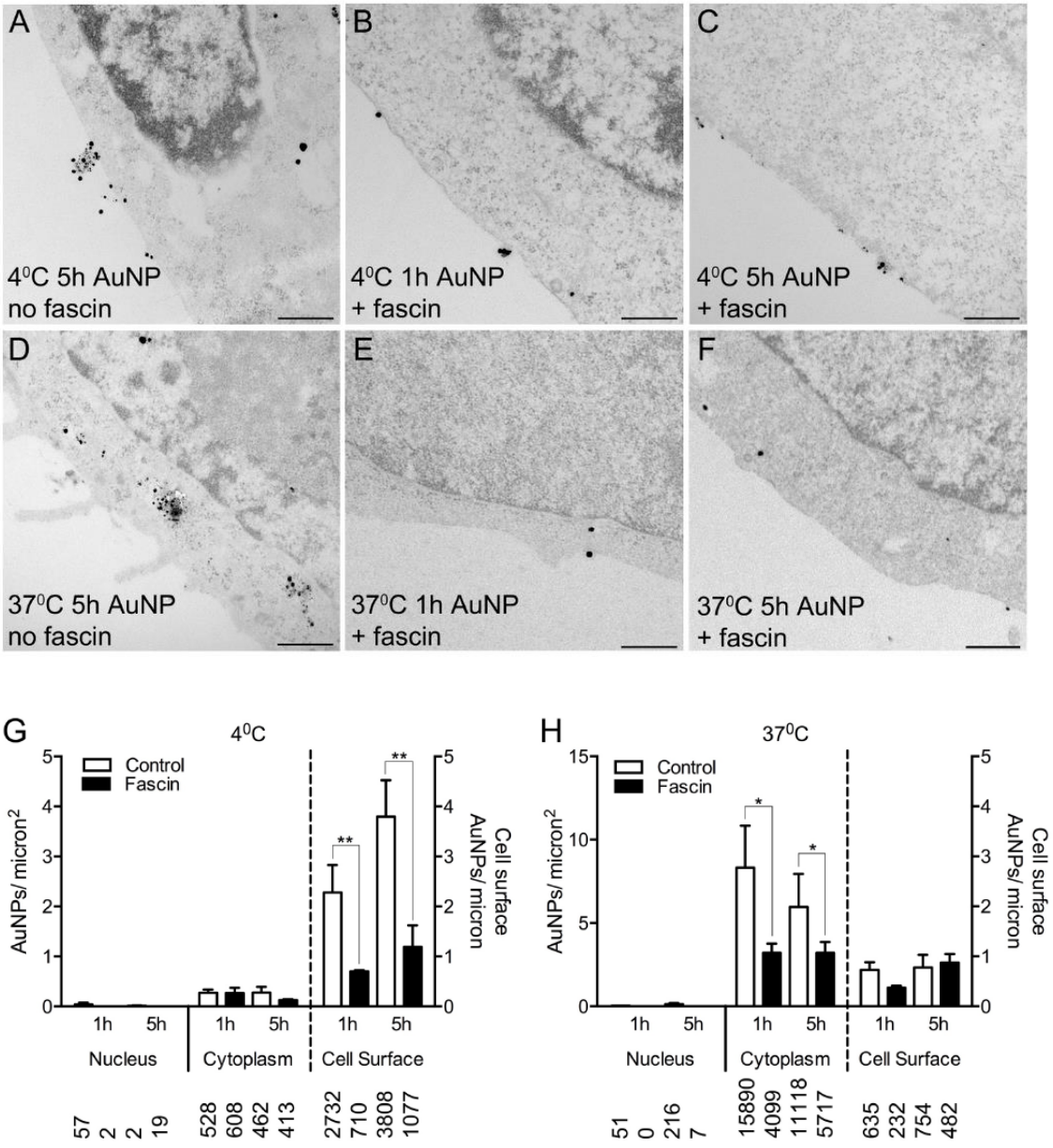

Figure 4.15: **Localization of silver enhanced 1h and 5h synthesis time AuNPs in HSC cells after an acute 3h exposure at 37ºC and 4ºC and 10 µg/ml analysed by TEM in A. the absence or B, C. the presence of fascin inhibitor, at 4ºC and in D. the absence or E, F. the presence of fascin inhibitor at 37ºC.** Quantitation of AuNP counts per micron^2 for nucleus and cytoplasm (left axis) and AuNP counts per micron for cell surface (right axis) with or without fascin inhibitor at either **G.** 4ºC or **H.** 37ºC. Total numbers of AuNPs counted per category are shown below bars and data were plotted as mean±SEM, n=3 independent experiments with two technical replicates per condition, One-way ANOVA, *P<0.05, **P<0.01. Scale bars in all images= 500nm.

4.3 Discussion

In this study, the cytotoxicity of 2nm AuNPs surface functionalised with a 50:50 ratio of a αGal:PEGamine was found to increase with $NaBH_4$ contact time during AuNP synthesis (from 1h to 5h). Ligand ratio remained unchanged, but ligand density decreased with synthesis time. Cytoplasmic uptake of AuNPs was not significantly affected by synthesis time. However, when energy-dependent transport was inhibited by lowering the temperature, a remarkable adhesion of AuNPs to filopodia was noted, mainly with the more toxic 5h synthesis time AuNPs. Inhibition of filopodial assembly prevented this AuNP binding. A possible link between increased adhesion to filopodia in HSC cells and mechanisms of cell death is presented in detail in the next chapter.

4.3.1 Factors to be considered when measuring ligand density

The SEM-EDX analysis showed that the ligand density decreased with AuNP synthesis time (Figure 4.11). However, there are multiple factors that need to be considered when addressing the ligand density measurements of the nanoparticles. These factors can be separated into two categories, ligand-related and nanoparticle-related. With regard to ligand-related factors, the actual quantity and spatial arrangement of the ligands is important in the interaction with the cell surface. These factors apart from the fact that they can affect the robustness of the ligand density quantification, they can also account for variations from sample to sample and between the batches. Thus, their control is of great significance.

Firstly, there is a possibility of ligand dissociation during washing and purification steps. Purification is a significant step after the synthesis process of nanoparticles as it ensures that any unbound or unspecific ligands are washed off. If the ligands are not strongly attached to the nanoparticle core, such as in

case of trisodium citrate on AuNPs, the ligand density on the nanoparticle core will be modified and their quantification will not be representative (Love et al., 2005). Another aspect that could account for incorrect ligand quantification measures or batch variability, is the dynamic process of ligand adsorption. Variability between samples can be observed depending on the timing that the nanoparticles are exposed to excess ligands. Therefore, in order to assess ligand loading during the synthesis process, a time-dependent ligand quantification is important. Lastly, ligand density can also be influenced by non-covalent interactions and steric effects with the solvents in which they are coming in contact with. Ligand exchange equilibria and dynamics of ligands such as their conformation might be altered (Ansar et al., 2011, Wu and Jin, 2010).

Regarding the nanoparticle-related properties, consideration of the core measurements of the nanoparticles is vital because these measurements determine the surface area of the nanoparticle. Then to calculate the ligand density surrounding the Au core, the total surface area is taken into account. For certain techniques and ligand quantification, particles need to exhibit specific size and composition to be detectable within the limits of the analytical method. For instance, localized surface plasmon resonance method need particles of specific size to be spectroscopically detectable and quantifiable (Wang et al., 2012). The surface area is influenced by both the core morphology and size of the particles thus the first part of the results shown in this chapter focused on presenting physico-chemical characterization of the different synthesis time AuNPs. In this case, size and shape related variability were excluded between the three AuNPs tested thus, differences in cytotoxicity found were attributed to changes in ligand density. ^{1}H-NMR showed no changes in ligand ratio (Figure 4.10), while SEM demonstrated a decrease in ligand density (decreasing S:Au ratio).

Sodium borohydride is widely used as a reducing agent in organic and inorganic chemistry. The reaction of $HAuCl_4$ with $NaBH_4$ produces small stable nanoparticles and the action of $NaBH_4$ can lead to the transition of metal salts to metal (0) in AuNPs synthesis (Brust et al., 2002). It has also been found by Ansar and colleagues that during AuNP synthesis, $NaBH_4$ in water can remove molecular adsorbates on AuNPs and strip the ligands off their surface (Ansar et al., 2013). This is the mechanism proposed in this chapter for ligand density reduction as shown by SEM-EDX, which is with longer the synthesis time and the presence of $NaBH_4$, this chemical leads to stripping ligands off leading to decreased ligand density around the Au core.

4.3.2 Enhanced filopodia adhesion

The longer the synthesis time the more toxic the AuNPs were for HSC and HaCaT, but not for HEK-293 and A498 cell lines. Such variability will be discussed in detail in chapter 6 when a comparison of toxicities of AuNPs is presented among a range of cell lines. As discussed in the introduction, ligand density can affect the toxicity of nanoparticles. The results presented here, showing that ligand density affected toxicity, confirms findings from previous studies. For example, Liu and co-workers showed a decreased toxicity in HeLa cells with high density PEG coated AuNPs, whereas another study from Yang et al., demonstrated that high ligand density PEG coated AuNPs were internalized by macrophages (Liu et al., 2015, Yang et al., 2014). Therefore, in this case, it could be possible that AuNPs with a synthesis time of 1h is less toxic due to its increased ligand density being associated with weaker cell surface interactions as opposed to 2h and 5h AuNPs, which they might have the required density to interact with higher affinity to the cell membrane. Other studies have also

implicated variations in ligand density with differences in cellular uptake (Elias et al., 2013, Schubertova et al., 2015).

The observation that AuNPs adhere to filopodia is novel and suggests that a better understanding of how ligand density influences this process could allow AuNPs to be engineered to exploit filopodial binding and enhance cellular uptake. Cellular morphology, polarity and controlled cell proliferation are the main characteristics of maintaining a tissue homeostasis. When this homeostasis is not maintained, cancer occurs, driving cell migration via metastasis and angiogenesis. Increased filopodial formation has been linked to support migration and cancer progression (Jacquemet et al., 2015). One of the components of filopodia associated with cancer progression is fascin (Arjonen et al., 2011). The levels of fascin expression vary between cell types (Arjonen et al., 2011) thus a possible explanation in terms of the variable toxicity observed between the cell lines.

Increased binding of AuNPs to filopodia could be linked to two events. Either the adhesion initiates a cascade of cell death events by binding and triggering to a specific receptor, or increased adhesion leads to higher internalization and phagocytosis of the AuNPs inside the cells. However, based on the observation that the uptake between AuNPs with 1h and 5h synthesis time into HSCs did not differ (Figure 4.13) whilst the particles with a 5h synthesis time had a higher toxicity (Figure 4.12) the second theory is discarded. Instead, data presented on the next chapter about caspase 8 inhibition, reinforced the idea of an involvement of the extrinsic apoptotic pathway. No evidence exists regarding the correlation between increased filopodia adhesion and extrinsic apoptosis as more work will be needed to identify such claim. Due to fascin inhibition and

reduced adhesion observed, only a proposal can be made about filopodia being an important player in the way these AuNPs interacted with the cell.

The fact that AuNPs adhesion to filopodia was only visible under the TEM when energy-dependent transport was blocked (Figure 4.14), suggests that these particles were undergoing endocytosis. By lowering the temperature to 4^{o}C during incubation of the particles, any active transport was blocked however passive transport was still possible, thus the low numbers of internalized particles noted in the graphs. Gromnicova et al., showed that the same αGal:PEGamine AuNPs were internalized via an active transport mechanism in endothelial cells (Gromnicova et al., 2016).

Chapter 5: Analysis of The Mechanisms of Cell Death Caused by AuNPs

5.1 Introduction

AuNP properties affect biological activities such as cellular uptake and toxicity, as discussed in chapter 3. A growing body of nanotechnology research is focusing on understanding the safety of these nanomaterials and the mechanism by which they cause toxicity and cell death. There are two main categories of cell death: apoptosis and necrosis. The types of cell death are defined by morphological criteria and biochemical features. The Nomenclature Committee on Cell Death (NCCD) proposes the types and definitions of cell death according to latest research published in this area (Galluzzi et al., 2018). Apoptosis is divided into two subcategories, which include the extrinsic and intrinsic pathways.

These pathways are dependent on the origin of the stimuli (surface death receptors for extrinsic or cellular stress for intrinsic apoptosis). Both act via a cascade of caspases activation and are explained in a more detail below (Fuchs et al., 2015). Necrosis is an uncontrolled and accidental cell death but evidence revealed that it can also be programmed and controlled like the apoptotic pathway (Weinlich et al., 2017). On the other hand, autophagy is interpreted as a survival mechanism instead of type of cell death, which is activated during nutrient and growth factor deprivation. Despite not being a cell death mechanism itself, an upregulation of autophagy has also been associated with cellular stress, which in turn can lead to necrotic and apoptotic cell death (Galuzzi et al., 2012).

5.1.1 Apoptosis

Apoptosis is a crucial process during development and in maintenance of tissue homeostasis. Tumour progression is attributed amongst other factors to impairment of apoptosis. Apoptosis is a type of suicidal cell death that is divided into intrinsic and extrinsic pathways, dependent on cellular stress and the activation of plasma membrane death receptors, respectively (Figure 5.1) (Conrad et al., 2016). Both pathways are caspase dependent. Caspases are cysteine and aspartate specific proteases, which are involved in inflammation, differentiation and cell death (Galluzzi et al., 2016, Ollie et al., 1998). Their classification is based on their size, function and cleavage specificity. Regulation of apoptosis is controlled by two classes of the caspases family, the initiator (-2, -8, -9 and -10) and the effector (-3, -6 and -7) caspases (Kroemer et al., 2009).

5.1.1.1 Extrinsic pathway

Extrinsic apoptosis is mediated via TNF-related transmembrane receptors. Ligands such as TNF-α, Fas ligand and TRAIL bind to death receptors at the cell surface, leading to their oligomerization, followed by a cascade of signalling events that trigger apoptotic cell death. This pathway relies on the formation of caspase 8 active dimer from caspase 8 monomers on the intracellular side of the death receptors. All death receptors share a conserved, cytoplasmic sequence termed as death domain. For instance, in case of Fas ligand, the death domain enables binding of Fas to the adaptor protein FADD, leading to the recruitment of pro-caspase 8 and pro-caspase-10 (Galluzzi et al., 2018). As a result, a multiprotein complex named DISC (death inducing signalling complex) is formed which acts as a platform for caspase activation (Fuchs et al., 2015). Depending on the cell type, extrinsic apoptosis could be either mitochondria dependent or

independent. Mitochondria independent extrinsic apoptosis occurs via activation of caspase 8 which leads to proteolysis of pro-caspase-3 into active caspase 3 (Czabotar et al., 2014). Alternatively, caspase 8 can lead to cleavage of Bid, a BH3 protein, creating a form of mitochondria targeted tBid, which is responsible for the amplification of death signal through mitochondria. Other proteins such as cFLIP and cIAPs could also be involved in extrinsic apoptosis (Kim et al., 2006, Galluzzi et al., 2018).

5.1.1.2 Intrinsic pathway

Activation of the intrinsic apoptotic pathway is a result of numerous types of cellular stress stimuli including cytosolic calcium overload, oxidative stress, DNA damage and ER stress (Roos et al., 2016). There are multiple events that can lead to intrinsic apoptotic pathway activation. Some of these events include the release of pro-apoptotic proteins into the cytosol, such as endonuclease G, cytochrome c and apoptosis inducing factor, and dissipation of mitochondrial membrane potential (Li et al., 1997, Galluzzi et al., 2018, Julien et al., 2016). Release of cytochrome c occurs via members of Bcl-2 family which regulate apoptosis. The cytosolic translocation of cytochrome c initiates the formation of a complex termed the apoptosome, which consists of pro-caspase-9, Apaf-1, dATP and cytochrome c (Riedl et al., 2007, Li et al., 1997). The apoptosome acts as a platform for the activation of signalling cascades downstream of mitochondria and activation of caspase 9 (Galluzzi et al., 2018).

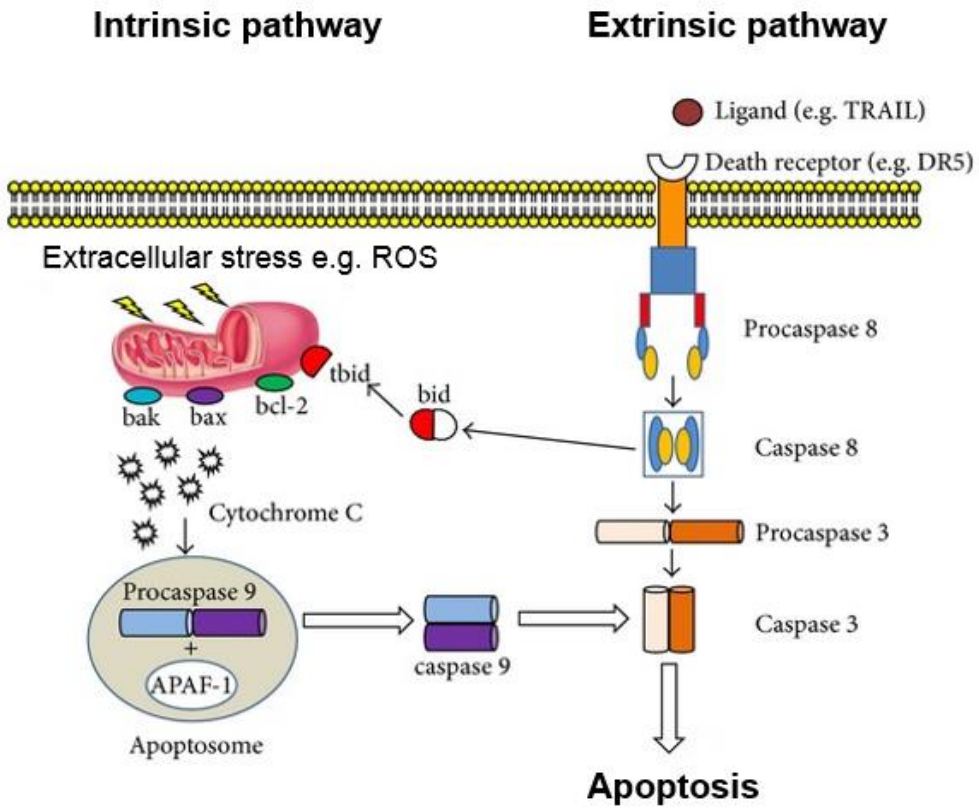

Figure 5.1: **Schematic illustration of the intrinsic and extrinsic apoptotic pathways.** Extrinsic pathway is initiated by ligation of death receptors (such as Fas, TNF, DR4 and DR5) by their specific ligands (FasL and TRAIL) leading to activation of procaspase 8 and subsequent caspase 8 activation. Apoptosis is induced by either caspase 3 activation or cleavage of bid. Cleavage of bid leads to mitochondrial dysfunction and cytochrome c release, activating caspase 9 and 3. Caspase 3 promotes the typical apoptosis features, including DNA fragmentation and cell death. The intrinsic pathway is mitochondria dependent and influenced by bcl family members bound to the mitochondrial membrane, which regulate the release of cytochrome c. A complex termed as apoptosome is formed by cytochrome c, dATP and APAF-1. The apoptosome is responsible for the recruitment of procaspase 9, caspase 9 and 3, resulting in apoptosis and cell death. From Loreto et al., 2014.

5.1.2 Necrosis

Necrosis is considered as an accidental and uncontrolled form of cell death. However, evidence accumulated from recent research showed that necrosis is regulated by a cascade of signal transduction pathways and can be controlled like the apoptotic mechanism of cell death (Conrad et al., 2016). Thus, some authors proposed the term “necroptosis”, a subset of necrosis, to specify the controlled nature of necrosis (Pasparakis et al., 2015, Weinlich et al., 2017). This term was first introduced by Yuan and colleagues who showed the inhibitory effect of necrostatin-1 on the necrosis caused by death receptor ligation (Yuan et al., 2016). Morphologically, necrosis is characterized by plasma membrane rupture, swelling of organelles and a gain in cell volume followed by loss of intracellular contents. Death domain receptors such as Fas, TNFR1 and TLR3/4, have been implicated in necrotic cell death, which in most cases is dependent on the serine/threonine kinase RIP-1 and -3 (Galluzzi et al., 2018).

The exact mechanism of necrosis is still not well understood but is accepted that several organelles, cellular processes and mediators are involved. For instance, production of ROS, mitochondrial alterations and membrane permeabilization are some of the phenomena underlying this type of cell death (Roos et al., 2016). Lysosomal and nuclear changes such as hyper-activation of PARP-1 and lipid degradation has also been addressed. Lastly, elevation of cytoplasmic Ca^{2+} levels lead to mitochondrial Ca^{2+} overload and activation of non-caspase proteases like cathepsins and calpains, which lead the activation of Jun-N terminal kinase and generation of sphingomyelinase mediated ceramide (Weinlich et al., 2017). Hitomi et al., pointed out the importance of understanding that apoptosis and necroptosis or necrosis pathways are well interconnected and

defining the signalling networks underpinning each process is difficult. More recent studies validate the interconnected nature of the different cell death pathways (Hitomi et al., 2008). For example, caspase-8, FADD and cFLIP, a regulator of caspase 8 activity, has been shown to inhibit RIPK-1 and -3, indicating the intertwined nature of both necroptosis and apoptosis (Hitomi et al., 2008). A schematic representation of the 3 main pathways described so far is presented below (Figure 5.2).

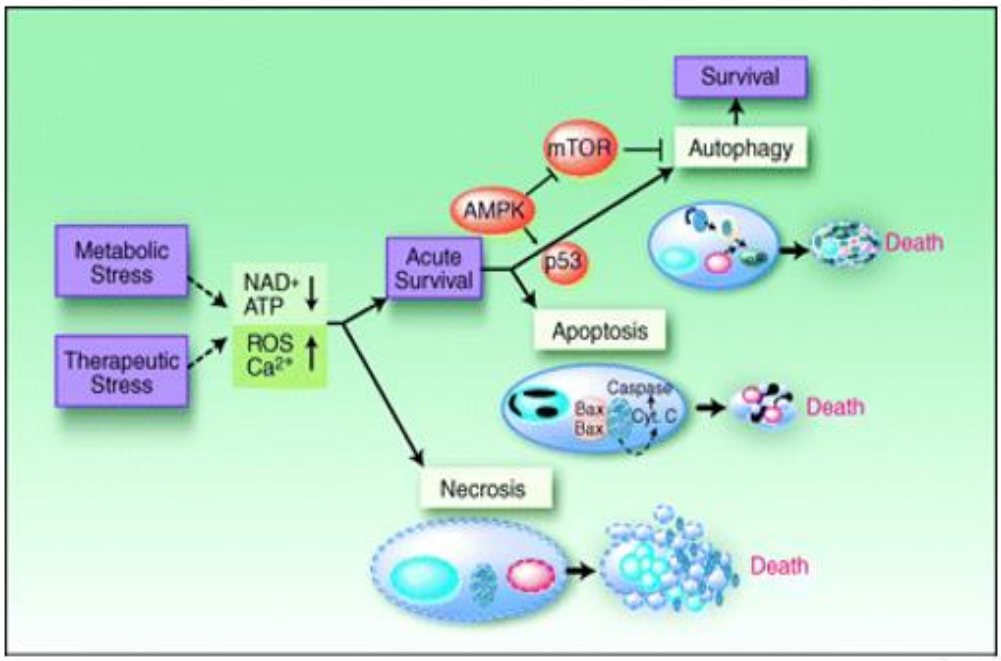

Figure 5.2: A schematic representation of the relationship between apoptosis, necrosis and autophagy. Increased intracellular Ca^{2+}, ROS generation, ATP and NAD^{+} depletion is a result of therapeutic or metabolic stress. Autophagy indicates a survival mechanism induced via a range of stress regulators such as AMPK pathway. Bak and Bax activation leads to apoptosis via the release of cytochrome c and the initiation of the caspase pathway. Necrosis is independent of the acute survival signals activation. From Amaravadi and Thompson, 2007.

5.1.3 Other types of cell death

Other types of cell death have been characterized but they all share common morphological features with either apoptosis or necrosis. For instance, “aponecrosis” has been proposed as a type of cell death by Formigli et al., who described a dynamic and molecular similarity between apoptosis and necrosis when inhibiting the mitochondrial respiratory chain with antimycin A (Formigli et al., 2000). Also, another type of cell death named as “paraptosis” has been established, referring to an alternative form of caspase-9 death independent of Apaf-1 (Dal Canto and Gurney, 1994, Turmaine et al., 2000).

A controversial debate exists with regard to whether autophagy is categorized as a mechanism of cell death or not. Autophagy plays an important role in homeostasis, leading to the recycling of cellular building blocks by mediating the removal of damaged or dysfunctional organelles. In this case, it constitutes a survival mechanism utilized by cells to cope with nutrient starvation and deprivation. On the other hand, cell death can result from unrestrained autophagy (Schwartz et al., 1993, Gozuacik and Kimchi, 2004, Debnath et al., 2005).

5.1.4 Assays to determine mechanisms of cell death

Evaluating the mechanism of cell death triggered by nanomaterials and AuNPs is highly complex. Certain cellular events, like mitochondrial dysfunction or ROS generation, are shared between both cell death pathways and thus, it is difficult to distinguish between them. Various assays can be used, each with their advantages and disadvantages to aid the identification of the type of the molecular pathway being involved in cell death. These assays are designed based on the detection of early or late apoptotic and necrotic events. The assay output is dependent upon cell type, concentration of test compounds and choice of the assay's endpoint. Some of the basic assays used to determine apoptotic cell death mechanisms and to distinguish them from the necrotic, are: cyto-morphological changes, DNA fragmentation, detection of activated caspases, membrane alterations and mitochondrial assays.

5.1.4.1 Cyto-morphological changes

Apoptotic or necrotic cells can be detected by light microscopy using methylene or toluidine blue dyes. Such approach is dependent on the cytoplasmic and nuclear condensation that occurs during these events. A more detailed method includes TEM analysis which confirms apoptotic or dead cells based on the following easily detectable morphological characteristics: nuclear fragmentation, electron dense nucleus, disorganized cytoplasmic organelles, large clear vacuoles and damaged cell membrane (White and Cinti, 2004, Weinlich et al., 2017).

5.1.4.2 DNA fragmentation

Later stages of apoptosis involve endonuclease fragmentation of the DNA. Methods to detect fragmented DNA include agarose gel electrophoresis, which shows a laddering or smear of the DNA (Wyllie, 1980). Another technique is the TUNEL assay, in which a fluorescent dye is added, binding specifically to the ends of fragmented DNA, thus staining nuclei of apoptotic cells fluorescent (Kressel and Groscurth, 1994, Otsuki, 2003).

5.1.4.3 Detection of activated caspases

Various caspase activity assays have been established for the detection of more than 13 different caspases (Galluzzi et al., 2018). Several monoclonal and polyclonal antibodies specific to the individual caspases have been designed for the detection of both active caspases and procaspases. These can be used to detect specific caspases by Western blotting, immunohistochemistry or immunofluorescence. Fluorescent substrates are also used for the detection of active caspases. Apoptosis pathway specific gene panels offer the advantages of determining the profile of the expression of at least 112 genes involved in apoptosis by PCR microarrays (Hofmann et al., 2001, Vallat et al., 2003).

5.1.4.4 Membrane alterations

Phosphatidylserine is maintained asymmetrically on the inner leaflet of the cell membrane by the action of Flippase enzymes. However, during early apoptosis, this process ceases, and phosphatidylserine randomly partitions to both sides of the cell membrane. Such externalization can be detected by the phosphatidylserine binding protein Annexin V (Bossy-Wetzel and Green, 2000). Fluorescently-tagged Annexin V labels apoptotic cells, which are visualized and

quantified by fluorescent microscopy or flow cytometry. However, loss of membrane integrity is a feature of necrotic cell death as well, therefore necrotic cells should be stained with specific membrane-impermeant dyes, for example trypan blue or propidium iodide to distinguish between apoptosis (Annexin V positive and PI negative) and necrosis (Annexin V and PI positive).

5.1.4.5 Mitochondrial assays

Changes in the early phase of the intrinsic apoptotic pathway can be detected by mitochondrial assays and cytochrome c release. Mitochondrial Ca^{2+} concentration, mitochondrial redox status, reactive oxygen species generation, membrane depolarization and permeability are some of the biological readouts used to address early apoptotic events. Fluorescent indicators are often utilized for measurement of the cellular metabolic activity, ROS levels and mitochondrial membrane or redox potential. Fluorescence microscopy can assess cytochrome c release from mitochondria and regulator proteins such as Bcl-2 and Bid (Scorrano et al., 2002, Tsien, 1998, Zhang et al., 2002).

In conclusion, understanding the mechanism of cell death is of crucial significance. Distinguishing between the types and identifying key regulators in each process can provide an important advantage in targeting a specific disease state. Apoptosis is considered a regulated, controlled energy-dependent process characterized by specific biochemical and morphological features, with caspase activation to be the most important feature. Several studies have noted the cross-talk between cell death pathways and therefore, multiple assays should be used when addressing the mechanism of cell death following nanomaterials exposure. The next section of this chapter will unravel the mechanism of cell death caused by the 50:50 αGal:PEGamine AuNPs.

5.2 Results

This chapter will focus on unravelling the mechanisms by which the 50:50 αGal:PEGamine AuNPs cause cell death and toxicity. Firstly, method development and assay validation are presented. Secondly, results obtained by these optimized assays are discussed regarding the mechanisms of cell death caused by this specific type of AuNPs.

5.2.1 Assay and method development

Unravelling the mechanism of cell death was achieved using fluorescent dyes and analysed via three main methods: fluorescence microscopy, microplate reader and Tali cytometer. Each method had its advantages and disadvantages. For instance, fluorescence microscopy provided high resolution detail of the localization of the dyes along with high sensitivity, however quantification of fluorescence intensities was time consuming. The microplate reader might represent the most effective, quick, high-throughput assessment for the evaluation of multiple dyes simultaneously along with quick data output, yet this was not the desired method in this case due to sensitivity issues (Appendix Figure 9.6). Cytometry on the other hand proved to be the best approach for obtaining qualitative and quantitative results. Two cytometry methods were available in the facilities of The Open University, a flow cytometry machine and a Tali Image-Based Cytometer. Both instruments provide analysis of individual cells within a population with the main difference between the two methods being that the Tali provides an image-based output for every field of quantification.

The same experiment was performed and analysed by both Tali and flow cytometry to compare whether the two cytometric methods produced similar results. HSC cells were treated with 10 µg/ml AuNPs for an acute 3h exposure. At 24h and 48h after exposure, cells were harvested without fixation and treated with PI to determine the percentage of dead cells. Both methods showed a base line level of ~ 6% dead cells for the control sample, slightly increasing to 10% at the 48h time-point (Figure 5.3A&B). For the sample treated with AuNP, no significant difference was observed between the 24h time-point and the control with both methods. However, after 48h, the AuNP treated cells showed 3-fold more PI staining than the control with both methods. Therefore, Tali and flow cytometry showed the same trend and similar values of percent PI positive cells.

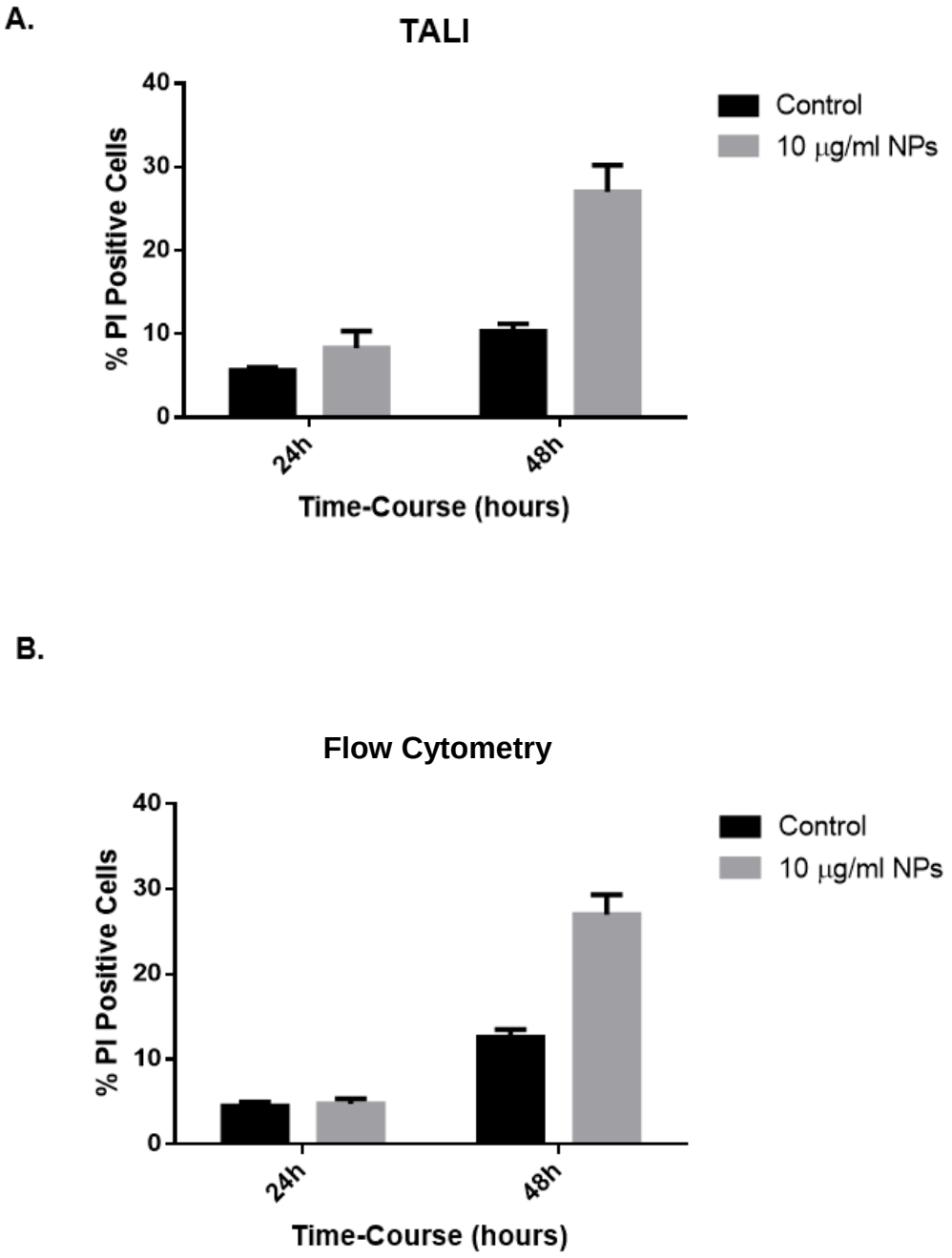

Figure 5.3: Comparison of the two cytometric assays available for the determination of cell death caused in HSC cells after an acute 3h exposure at 10 µg/ml. A. % PI positive cells as calculated by the Tali cytometer and **B.** by flow cytometry. n=1 experiment, with 3 technical replicates per condition. Data were plotted as mean±SEM.

Since Tali and Fflow cytometry did not show significant differences in the percentage of PI positive cells calculated after an exposure to AuNPs for two post-exposure time-points, the Tali method was chosen for the following reasons: 1) the visual output it produces, allowing to judge the data quality better than a flow cytometry analysis, 2) using a smaller quantity of cells and 3) less processing required for a time-efficient quantification. A method development had to be conducted regarding the procedure of harvesting the cells from the mutli-wells in which they were cultured. Specifically, every cytometry assay requires a trypsinization step before the stained cells can be analysed.

However, it was observed that prior to trypsinization there were always some cells floating in the medium. These were either dead cells, or cells that detached during division. To decide whether to include the detached cells in the data analysis, or whether to use only attached cells for the analysis, a pilot experiment was performed. The supernatant, including the detached cells, was taken off the cells prior to trypsinisation, and then the attached cells were trypsinised. Both were then stained with PI and analysed using the Tali (Figure 5.4). This was performed for control cells and using two concentrations of AuNPs to evaluate the detachment profile of cells. The percent of detached cells was calculated as less than <1% for both AuNPs concentrations used at 48h time point. The protocol for the Tali cytometry assay was established to include any detached and attached trypsinized cells since the apparent loss of cells could be attributed to detachment. Also, harvesting all cells allowed analysis within the entire population.

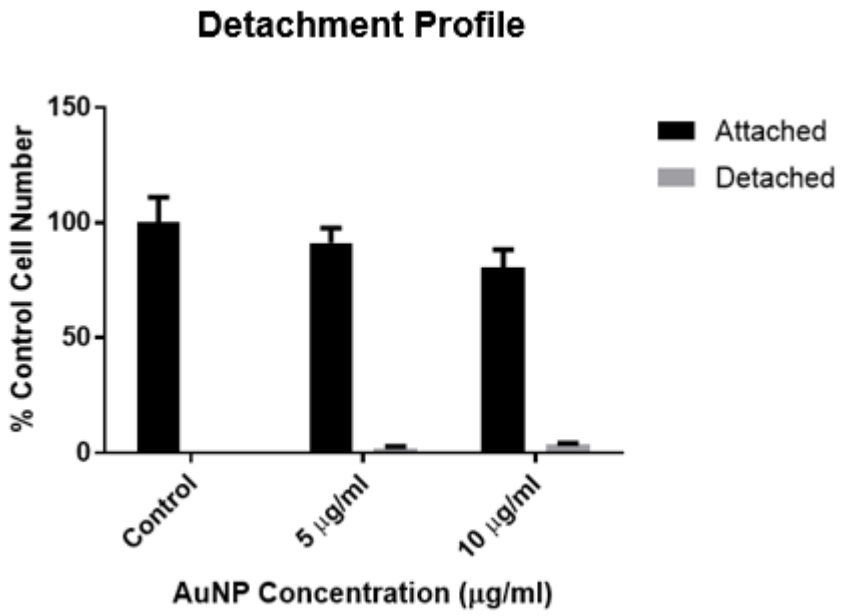

Figure 5.4: Detachment profile of HSC cells to establish experimental protocol for the Tali cytometry assay. Cells were exposed to 0, 5 and 10 μg/ml AuNPs for 3h and trypsinized (attached) cells at 48h. Floating cells (detached) were also calculated by Tali for the total cell number. n=1 pilot experiment, with 3 technical replicates per condition. Data were plotted as mean±SEM.

5.2.2 Time-course of cell death events after AuNP exposure

It was crucial to establish a time-course of cell death events along with the type of cell death occurred after AuNP exposure. The time-points tested were 3, 24, 48 and 72h after an acute 3h exposure of 10 μg/ml AuNPs on HSC cells. To determine the type of cell death, assays to measure caspase activation and inhibition, ROS generation and mitochondrial membrane depolarization were performed. These allowed to distinguish between necrosis and intrinsic or extrinsic pathways of apoptosis. Also, cell cycle arrest was examined as a possible factor contributing to cell death or inhibition of proliferation.

5.2.2.1 Apoptotic vs necrotic mechanism of cell death

The fluorescent dyes PI and Annexin V are widely used to test cell viability and discriminate between necrotic or apoptotic pathways based on differences in plasma membrane integrity and phosphatidylserine membrane asymmetry. PI is a nuclear stain that enters the cell depending on the membrane permeability. This dye will not stain live or early apoptotic cells that have an intact plasma membrane. Instead, necrotic and late apoptotic cells allow PI entry due to a decreased plasma and nuclear membrane integrity, displaying a red fluorescence in the nucleus (Vermes et al., 2000, Darzynkiewicz et al., 1992). Annexin V on the other hand, binds to phosphatidylserine. Normally, phosphatidylserine is found in the inner leaflet of the plasma membrane, but it gets externalised during apoptosis. As a consequence, when added to the outside of cells, Annexin V will only label apoptotic cells (Vermes et al., 1995).

HSC cells were exposed to 10 μg/ml AuNPs for 3h. Staurosporine was used as a positive control for inducing apoptosis at 1 μM (Thuret et al., 2003). The percentage of cells positive for staining with PI and Annexin V was quantified. There was a trend for the percentage of PI positive cells to increase from ~15% to 30% between 24h and 48h for the AuNP treated sample. The percentage remained at that level until the end of the time-course at 72h (Figure 5.5A). A trend for an increase in the percentage of AnnexinV positive cells was noticed, beginning from 48h and only reaching ~ 12-15% (Figure 5.5B). However, neither of these increases were statistically significant compared with the controls. In contrast, staurosporine produced large and significant increases in the percentage of PI and AnnexinV positive cells within 24h, compared with the control.

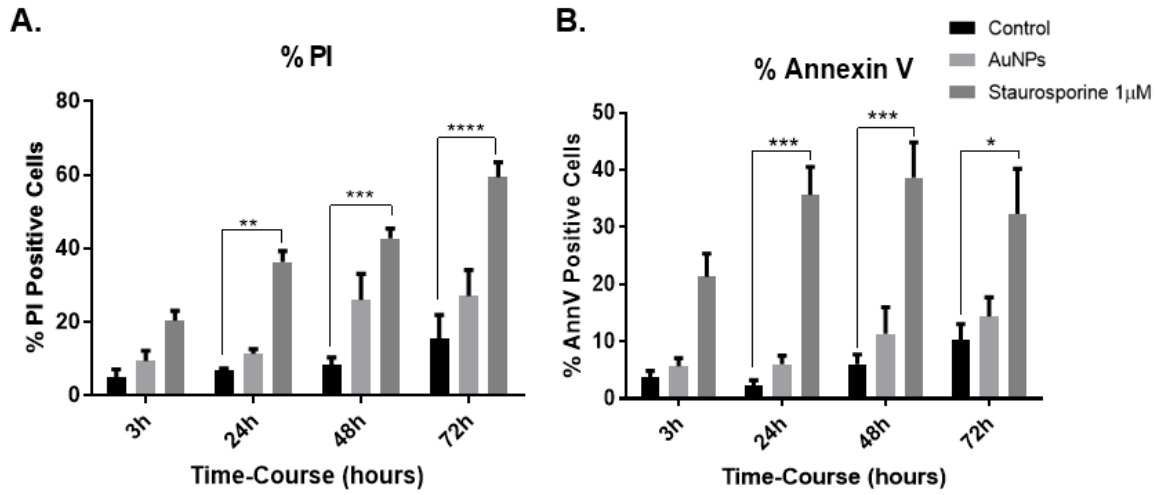

Figure 5.5: **PI and Annexin V staining in HSC cells to determine the type of cell death caused by AuNPs after an acute 3h exposure of 10 µg/ml AuNPs throughout a 72h time-course.** Results were quantified via Tali machine using **A.** PI and **B.** Annexin V fluorescent dyes. Staurosporine was used as a positive control for the induction of apoptosis. n=3 independent experiments. Data were plotted as mean±SEM. One-way ANOVA, Tukey's multiple comparison test, ****P<0.0001, *** P<0.001, ** P<0.01.

5.2.2.2 Caspases inhibition and activation

Extrinsic and intrinsic apoptotic pathways utilise different caspases. One way of distinguishing between the two pathways is the selective inhibition of certain caspases, or to measure their activation. In this case, various caspases were inhibited to determine if this inhibition prevented cell death. In parallel experiments, the activation of three caspases was assessed using specific fluorescent probes. Caspase 8 was selected because it is apical in the extrinsic pathway and caspase 9 because it is apical in the intrinsic pathway. Caspase 3/7 was selected since it is the executioner caspase at the end of both caspase cascades that commits to apoptotic cell death (Roos et al., 2016). The same protocol was followed for every assay. A time-course of 3, 24, 48 and 72h was investigated for caspase 3/7 activation after an acute 3h exposure of 10 µg/ml

AuNPs to HSC cells. This concentration was validated for its toxic potential by clonogenic assays.

A slight but non-significant increase of around 10% in caspase 3/7 positive cells was noted between the 3h and 24h time-point, followed by a steady level response throughout the time-course (Figure 5.6). Staurosporine as a positive control significantly increased the caspase 3/7 activity at all time-points.

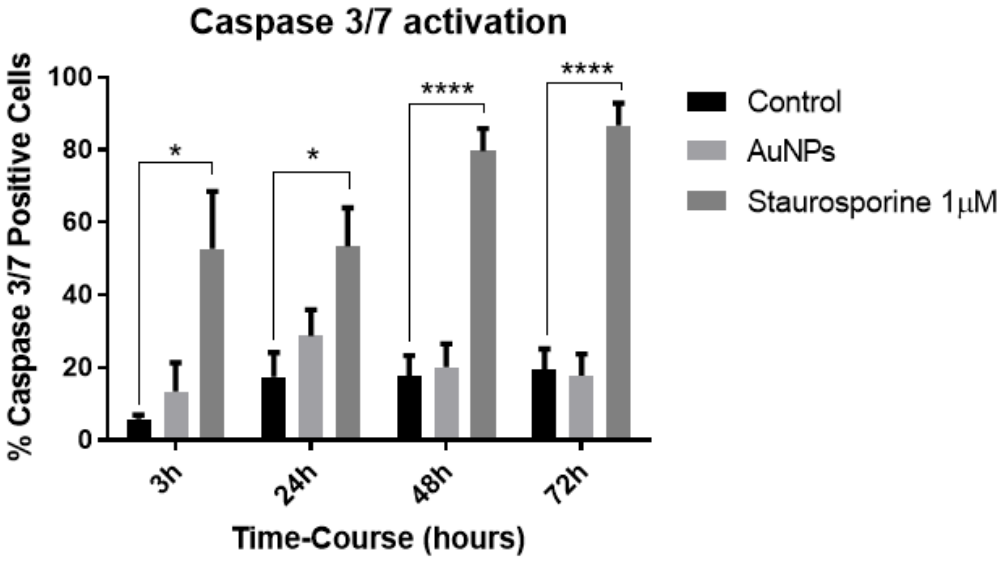

Figure 5.6: **Determination of caspase 3/7 positive cells after an acute 3h exposure of 10 µg/ml AuNPs on HSC cells throughout a 72h time-course.** Results were quantified via Tali machine using CellEvent caspase 3/7 fluorescent dye. Staurosporine was used as a positive control for the induction of apoptosis. n=3 independent experiments. Data were plotted as mean±SEM. One-Way ANOVA, Tukey's multiple comparison test, ****P<0.0001, *P< 0.05.

Caspase 8 and 9 activation assays could not be made to work reliably (Appendix Figure 9.17). For all caspases, inhibition assays were performed and are shown below. Co-incubation of cells with both caspase 3/7 inhibitor and 5 µg/ml AuNPs (the value represents the IC50 value of this batch of AuNPs) resulted in rescue of HSC cells from AuNP induced cell death as shown by clonogenic assays (Figure 5.7A). Such observation validates the above data of

Annexin V and caspase 3/7 activation, that apoptosis was involved in the cell death mechanism caused by this type of particles.

To discriminate between the extrinsic and intrinsic apoptotic pathway, cells were co-incubated with either caspase 8 or caspase 9 inhibitors along with 5 µg/ml AuNPs. Caspase 8 inhibition prevented AuNP toxicity, whereas caspase 9 inhibition had no significant effect on the prevention of AuNP induced cell death (Figure 5.7B&C). Addition of the caspase inhibitors reduced cell viability by ~30 %. Antimycin A (AMA) and Apo2L were used as positive controls and induced cell death similar to that seen by the AuNPs. The cell death caused by the positive controls was prevented by all three caspase inhibitors tested, showing that they prevented activation of the respective apoptotic pathways. Inhibition of caspase 8 and caspases 3/7 stopped the AuNP-induced cell death and brought it back to the level observed after addition of the inhibitors alone. Contrary, caspase 9 inhibition had no effect on the AuNP-induced cell death. These results indicate that AuNPs possibly activated the extrinsic apoptotic pathway.

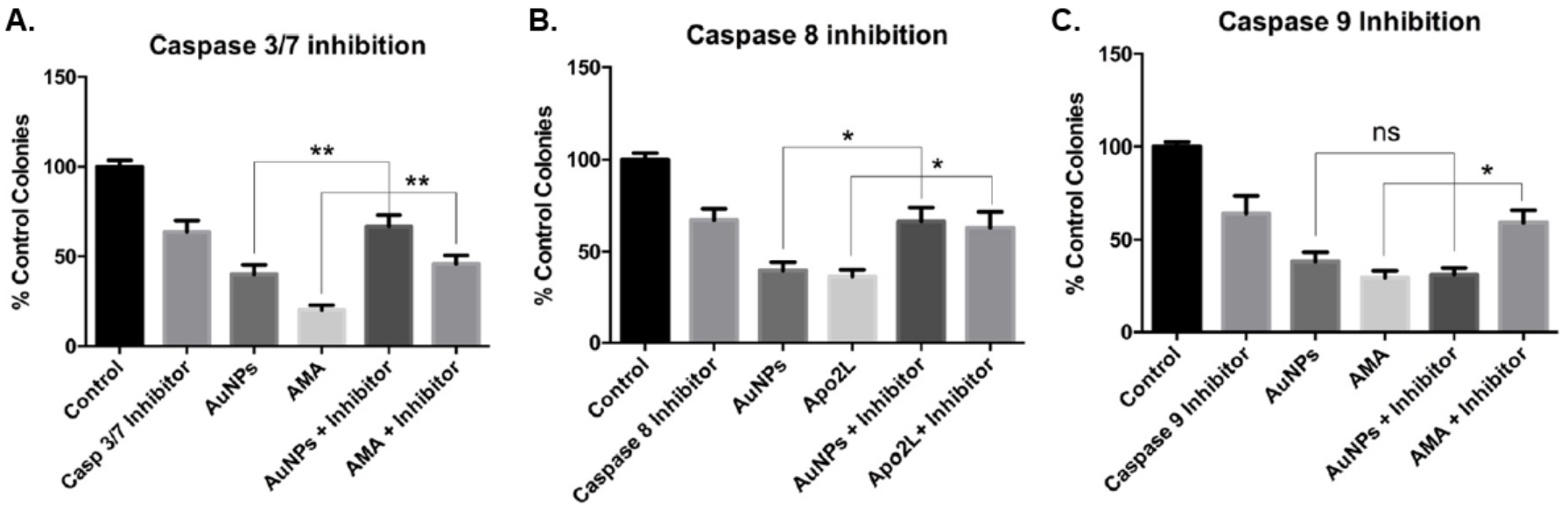

Figure 5.7: **Caspase inhibition effect on HSC cells after an acute 3h exposure of 5 µg/ml (IC50 value) AuNPs, as obtained by clonogenic assays. A.** Caspase 3/7 inhibition, **B.** Caspase 8 inhibition, **C.** Caspase 9 inhibition. Data were expressed as % control colonies and plotted as mean±SEM. Positive controls included AMA and Apo2L. n=3 independent experiments with technical triplicates per condition. One-Way ANOVA, *P< 0.05, **P<0.01.

5.2.2.3 ROS Production

To detect whether ROS generation correlated with AuNP-induced cell death, a ROS responsive fluorescent dye (ROS Brite) was used and the fluorescence was quantified by Tali. ROS Brite selectively reacts with superoxide and hydroxyl radical (www.aatbio.com). HSC cells were incubated at 10 µg/ml AuNPs for 3h and intracellular ROS generation was quantified by ROS Brite at the time-points previously used to characterise the AuNP-induced cell death mechanisms. AuNPs did not cause a significant ROS production at any time point, whilst the positive control TBHP increased ROS production after 48h and 72h (Figure 5.8)

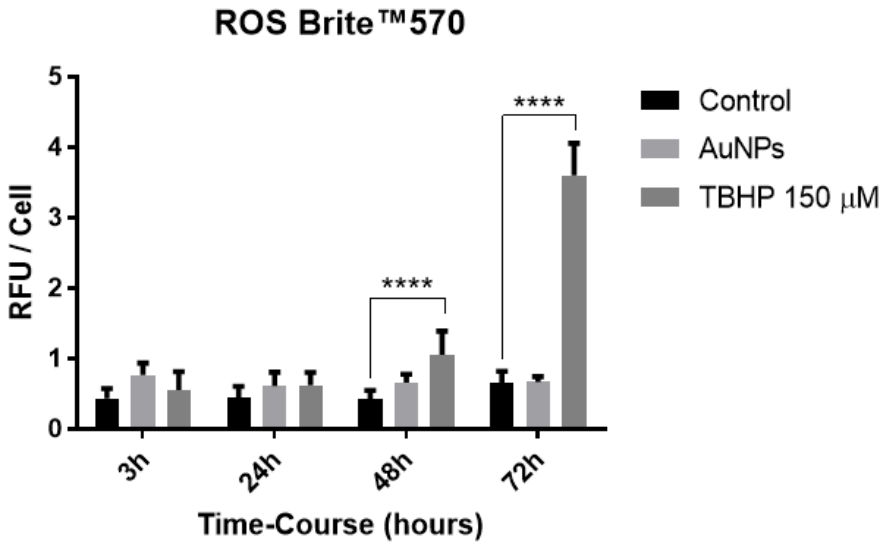

Figure 5.8: Determination of ROS production after an acute 3h exposure of 10 µg/ml AuNPs on HSC cells throughout a 72h time-course. Data were expressed as RFU/Cell and quantified by Tali using ROS Brite. TBHP was used as a positive control for ROS generation. n=3 independent experiments, Data were plotted as mean±SEM. One-Way ANOVA, Tukey's multiple comparison test, ****P<0.0001.

5.2.2.4 Mitochondrial membrane potential changes

JC-10 was used as a fluorescent dye to evaluate the changes of the mitochondrial membrane potential in HSC cells after an acute 3h exposure of AuNPs. In intact mitochondria with normal membrane potential, JC-10 concentrates in the mitochondrial matrix forming red fluorescent aggregates. In necrotic or apoptotic cells, or after a collapse of the mitochondrial membrane potential, the dye diffuses out of mitochondria, changes to a monomeric form and has green cytoplasmic fluorescence. Staurosporine and FCCP were used as positive controls to induce apoptotic cell death and membrane depolarization, respectively.

The change of mitochondrial membrane potential was measured as the ratio between red aggregated and green monomeric forms of JC-10 after AuNP exposure for a 48h time-course. Increasing ratios indicate mitochondrial membrane depolarization. Addition of FCCP caused a depolarisation of the mitochondria and a collapse of the mitochondrial membrane potential indicating that the assay was functional. Activating apoptosis with staurosporine increased the ratio of the JC-10 signal after 24h and 48h, whilst AuNP addition only caused changes after 48h (Figure 5.9) showing that changes to mitochondria and the collapse of the mitochondrial membrane potential occurred at a late stage in the cell death mechanism.

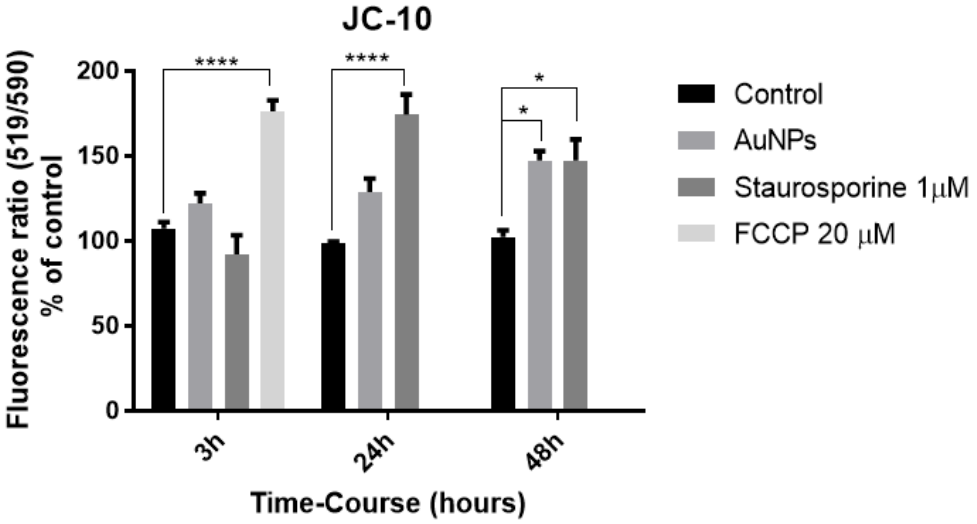

Figure 5.9: **Determination of mitochondrial membrane potential changes occurred after an acute 3h exposure of 10 µg/ml AuNPs on HSC cells throughout a 48h time-course.** Data were expressed as fluorescence ratio between aggregate (Em=515 nm) and monomeric forms (Em=590 nm) of the JC-10 dye and were quantified by Tali. Staurosporine and FCCP were used as positive controls for apoptosis and membrane depolarization, respectively. n=3 independent experiments, data were plotted as mean=±SEM. One-Way ANOVA, Tukey's multiple comparison test, ****P<0.0001, *P<0.05.

5.2.3 Cell cycle

Following a 3h exposure of 10 µg/ml AuNPs to HSC cells, the percentage of cells at G_0/G_1, S and G_2/M cell cycle phases were determined by Tali either immediately or after 24h. Nocodazole was used as a positive control at a concentration of 50 nM to cause cell cycle arrest at G_2/M phase. No significant differences were noted with the AuNP treated sample, neither with 3h or 24h exposure on HSC cells (Figure 5.10A&B). In contrast, nocodazole caused a G_2/M cell cycle arrest as expected after 24h.

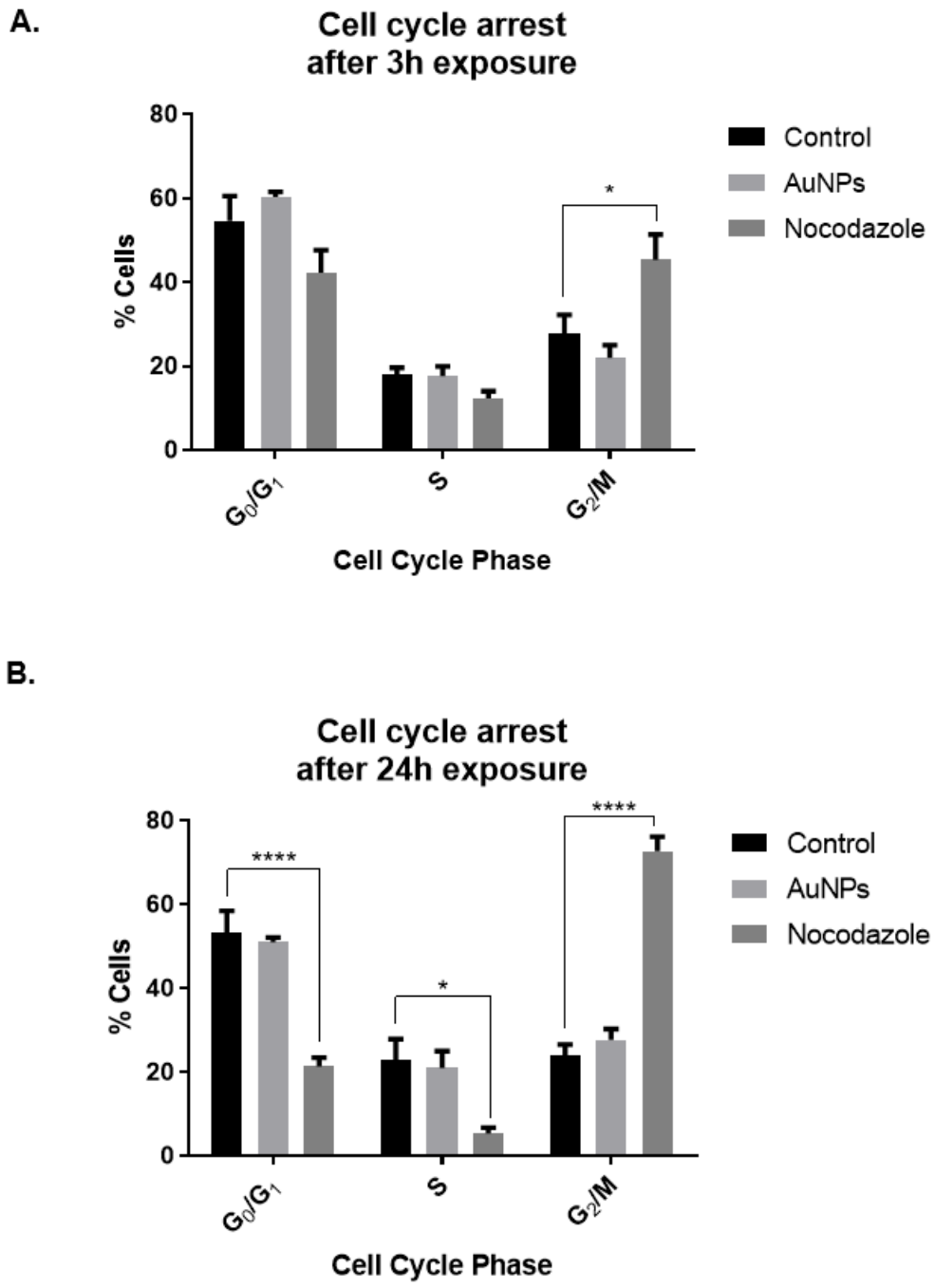

Figure 5.10: Investigation into possible cell cycle arrest caused after an acute A. 3h or B. 24h exposure of 10 µg/ml AuNPs on HSC cells. Data were expressed as % cells at G_0/G_1, S and G_2/M cell cycle phases as quantified by Tali. Nocodazole was used as a positive control for G2/M cell cycle arrest. n=3 independent experiments, Data were plotted as mean=±SEM. One-Way ANOVA, Tukey's multiple comparison test, ****P<0.0001, *P<0.05.

5.2.4 The role of cell density in AuNP-induced cell death

From all the above assays it was evident that the positive controls were working. However, it was noted that only rarely significant differences were observed between the AuNP treated sample and the control, even though the AuNPs were applied at twice the IC50 value estimated from the clonogenic assays. The only difference between the cytometry assays and the clonogenic assays was the cell density. Clonogenic assays were conducted on cells grown at a very low confluency, because otherwise cells would not grow in colonies. Contrary to this approach, the Tali machine requires higher cell density numbers for cell sorting, which is typically achieved by using a higher seeding density.

The observation of differences between the two assays presented in chapter 3 (toxicity assays based on the clonogenic method, with 10 μg/ml of AuNPs to be 2x the IC50 value) and this chapter (same AuNP concentration to trigger a trend of cell death as quantified by Tali) led to a series of experiments testing the localization of the particles. These experiments were based on using cells that were seeded in a similar high density to the ones used in the above experiments and a repetition of the experiments using cells plated at the same density but using higher AuNP concentrations. Firstly, silver staining assay was conducted for visualization of the AuNPs on HSC cells after their acute 3h exposure in a range of cell densities (Figure 5.11). In high cell densities the cells grew not in an isolated manner, but instead occurred as several clusters of cells. AuNPs accumulated on the outermost cells of such clusters, with very poor staining of cells deeper within the cluster. This implies that only cells at the edges received a toxic dose of AuNPs.

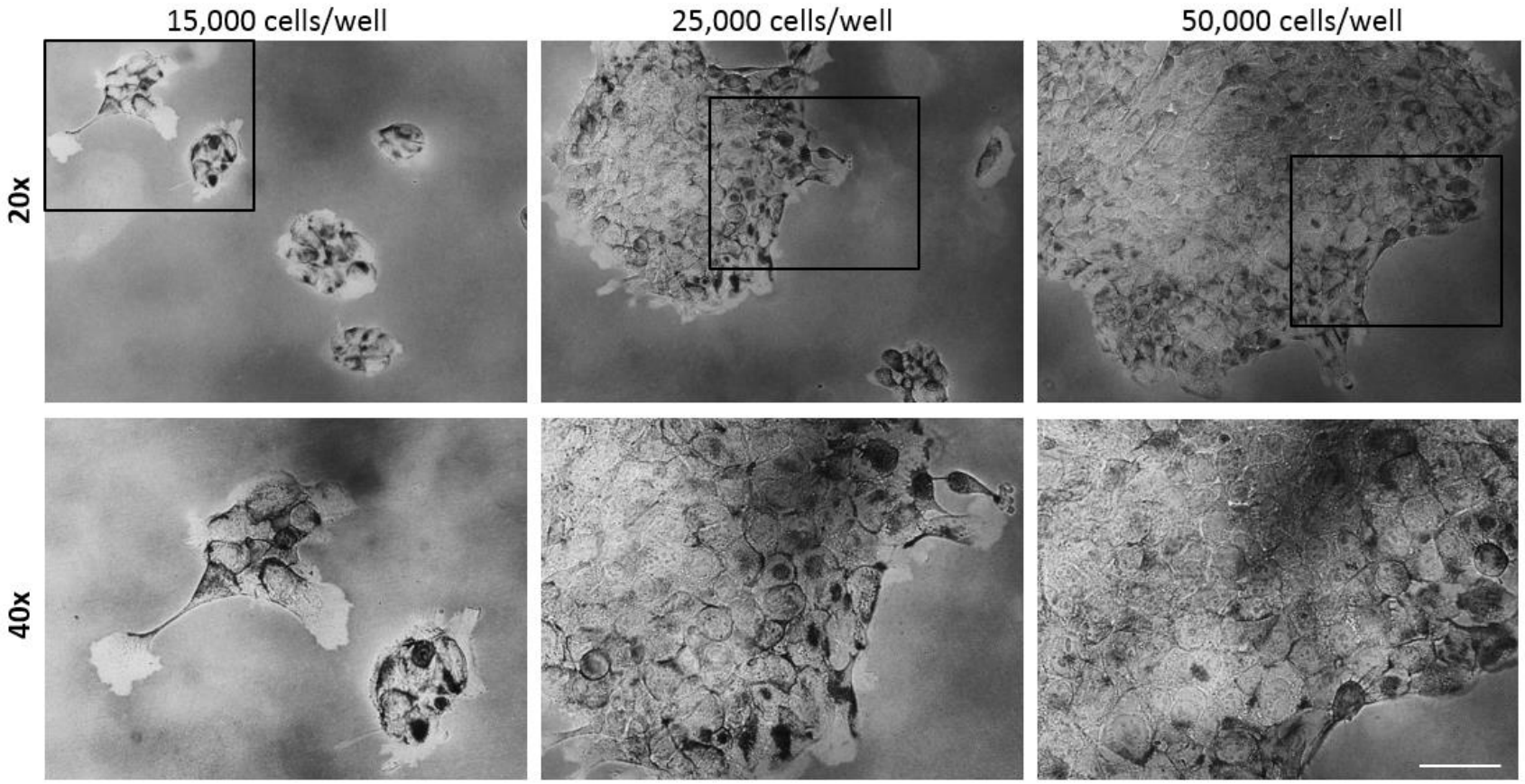

Figure 5.11: Silver staining of HSC cells after an acute 3h exposure of 10 µg/ml AuNPs as visualized under light microscopy at both 20x and 40x objective. 3 different cell densities were tested, 15,000, 25, 000 and 50,000 cells/well. Scale bar=500 µm.

Since the cell density was identified to play an important role as to how AuNPs interact with the cell surface, the total cell count after AuNP exposure was obtained using a CyQUANT cell proliferation assay. Data were presented as fluorescence intensity/seeding density quantified by using the microplate reader at Ex480/Em520 nm. Three different seeding densities were examined, 1,000, 2,000 and 4,000 cells/well in a 12-well plate, illustrating that AuNPs only reduced the cell proliferation significantly at the lowest seeding density (Figure 5.12).

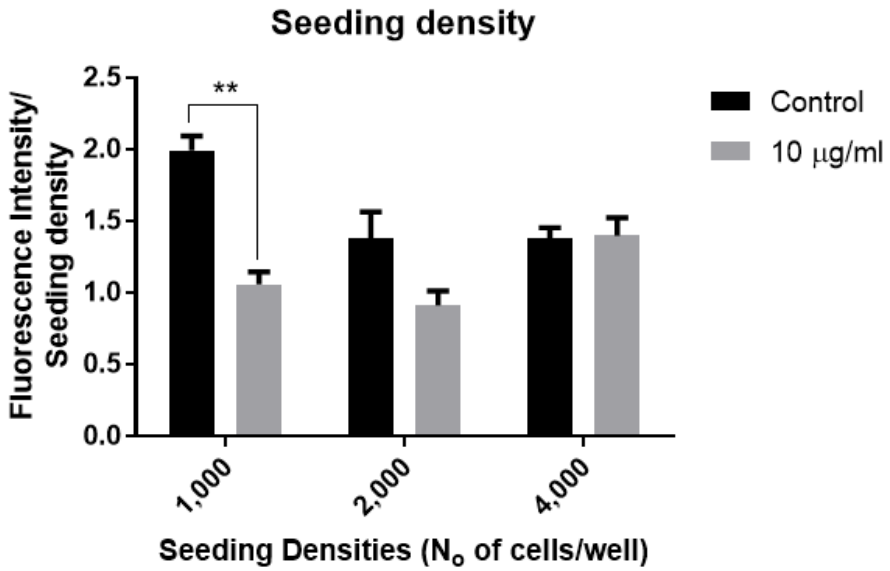

Figure 5.12: Cell proliferation of HSC cells after an acute 3h exposure of 10 μg/ml AuNP in a range of cell densities. Data were expressed as fluorescence intensity/seeding density as obtained by microplate reader at Ex480/Em520 nm and the CyQUANT cell proliferation assay. n=3 independent experiments, Data were plotted as mean=±SEM. Unpaired two-tailed t-test, **P<0.01.

These experiments highlighted a correlation between the cell density and the toxic effects of AuNPs, making it necessary to evaluate a series of AuNP concentrations in order to identify which is the concentration that triggers cell death in the higher cell densities required for cytometry assays. However, time restrictions of the project did not allow such experiments to be performed. Future directions include the identification of this AuNP concentration and repetition of all the assays presented above for a clearer illustration of the mechanism of cell death.

5.3 Discussion

This chapter focussed on investigating the mechanism of cell death caused by the 50:50 αGal:PEGamine AuNPs. A series of time-course experiments was conducted from 3h to 72h after an acute 3h exposure of AuNPs to HSC cells. The assays distinguished between necrosis and apoptosis, and between the extrinsic or intrinsic apoptotic pathway, quantified ROS production, mitochondrial membrane depolarization and phases of the cell cycle. These assays were chosen due to a literature search highlighting them as significant after exposure of metal nanomaterials to different types of cells. Within this thesis, the 50:50 αGal:Pegamine AuNPs generally produced non-significant trends in the assays presented above.

Different physico-chemical parameters such as the size and the shape of the particles, will produce a distinctive cellular response, therefore the data of this thesis based on the 50:50 αGal:PEGamine AuNPs cannot be directly compared with any other AuNPs used in the literature due to the possibility of the particles having dissimilar properties. It has to be mentioned that in this study, no significant effects were observed in most of the assays. This observation could be attributed to not necessarily a failure of the assays, due to the positive controls used working, but more likely to the mechanism of death triggered by these AuNPs, which was not tested for. However, cell density could also be responsible for the failure to observe cell death. In conclusion, either the AuNPs did not cause cell death by the tested mechanisms, or the cell density or timing used in the assays caused the toxicity of the particles to be different from that seen in other chapters.

In general, AuNPs appeared to induce both apoptosis and necrosis as shown by the PI/AnnexinV assay. A late cell death event was noted between 24h and 48h after an acute 3h exposure of AuNPs to HSC cells. It is not clear whether apoptosis or necrosis was initiated. Most studies propose apoptosis as the main mechanism of cell death caused by AuNPs. Necrosis has also been reported. For example, necrosis was induced by ROS production in hBMSC cells after exposure to AuNPs (Fan et al., 2011). Both necrosis and apoptosis was also observed in a study based on CTAB-capped AuNPs in A431 skin cancer cells (Nirmala et al., 2017). A table summarizing the properties of the AuNPs (size or surface) along with the cell type tested and the mechanism of cell death observed is presented below (Table 5.1).

Table 5.1: Comparison between the different published studies on AuNPs and the type of cell death observed.

AuNPs Properties		**Cell Type**		**Cell Death**			**Ref.**
Size	**Surface**	**Normal**	**Cancer**	**Apoptosis**	**Necrosis**	**Auto-phagy**	
1 nm	BSA		HepG-2	+	+	N/A	Dong et al., 2015
1.5 nm	TMAT (positive charge), MES (negative charge)	HaCaT		+	-	N/A	Schaeublin et al., 2011
2.3 nm	L/D-glutathione		MGC-803	+(d-glutathione > L-glutathione)	-	N/A	Zhang et al., 2015
2.7 nm	2-mercapto-1-methylimidazole		SH-SY5Y	+	N/A	N/A	Imperatore et al., 2015
1–10 nm	sodium polyacrylate (negative charge)	freshly isolated human		+	N/A	N/A	Duocher et al., 2017

		neutrophils					
4 nm, 100 nm	PEG	liver tissue of BALB/c mice		+(4 nm ~ 100 nm)	N/A	N/A	Cho et al., 2009
25.1 nm	CTAB		MCF-7	+	+	N/A	Bhamidipati et al., 2017
37 nm	N/A		A549	+	-		Ramalingam et al., 2016
20 nm	morin	PBMCs, HBL-100 cells		-	-	N/A	Kondath et al., 2014

The triggering of the apoptotic pathway by the AuNPs was confirmed by caspase 3/7 activation (Figure 5.6) and inhibition data (Figure 5.7). These data showed that a similar late response of HSC cells to AuNPs, with caspase 3/7 being affected between 3h and 24h after an acute 3h AuNP exposure. In the attempt to distinguish between extrinsic and intrinsic apoptotic pathway, inhibitors of both caspase 8 and 9 indicated possible involvement of extrinsic pathway as inhibition of caspase 8 led to rescue of cell death, but inhibition of caspase 9 did not. ROS was not elevated throughout the time-course of interest (Figure 5.8) consistent with the activation of extrinsic apoptosis, since ROS generation is usually associated with intrinsic apoptosis. Mitochondrial membrane depolarization was evident after 48h (Figure 5.9) but no cell cycle arrest was observed (Figure 5.10).

It has been shown before that the main mechanism by which AuNPs elicit apoptosis is via intrinsic apoptotic pathway, including ER and mitochondria related pathways. ROS production has also been linked to mitochondria related apoptosis. For instance, platinum coated AuNPs and gold mesoporous silica NPs

induced mitochondria related intrinsic apoptosis via ROS production in MCF-7 cells (Ahamed et al., 2016, Liu et al., 2015). Another study confirmed the mitochondria related apoptosis with citrate-coated AuNPs to elicit cytochrome c release and Bax translocation in HL7702 human liver cells (Gao et al., 2011). Most studies measure the activation of caspase 3/7, and thus not distinguish between extrinsic and intrinsic apoptosis. The activation of extrinsic apoptosis has not yet reported with AuNPs. Previously, only one study reported cleavage of caspase 8 in HaCaT cells after exposure to titanium dioxide nanoparticles for 6h, without apoptosis induction (Wright et al., 2017). Results presented in this thesis showed that inhibition of the extrinsic apoptotic pathway reduced the AuNP toxicity, which could be one of the first examples of the triggering of this pathway by AuNPs. Association of such observation with increased filopodia binding as depicted in the previous chapter should be made with caution.

In the case of the experiments performed in this thesis, no ROS changes could be measured. However, the mitochondrial membrane potential was altered 48h after an acute AuNP exposure. Specifically, mitochondrial membrane depolarization has been linked to the initiation of apoptosis and cytochrome c release. Although, release of cytochrome c is responsible for initiation of apoptosis in a caspase dependent manner, a study showed that such process is not necessarily the inevitable one (Ward et al., 2000). Mitochondrial membrane depolarization could just indicate a disturbance in the cellular ion homeostasis and depending on the level of depolarization it can lead to apoptosis in accordance with increased ROS production and ATP loss (Bossy-Wetzel et al., 1998). Therefore, it is assumed that since ROS was not elevated after exposure to the 50:50 AuNPs but membrane depolarization was evident, probably the level

of membrane potential alteration was not high enough to trigger the intrinsic apoptotic pathway.

Recent published research demonstrated the association of AuNPs with cell cycle arrest without the induction of necrosis or apoptosis. Ramalingan and colleagues indicated that biogenic AuNPs induced cell cycle arrest via oxidative stress and mitochondrial membrane alterations in A549 lung cancer cells (Ramalingan et al., 2016). In this study, no cell cycle arrest was observed with the 50:50 AuNPs neither with the 3h acute nor with the longer 24h exposure.

5.3.1 Limitations of the experimental design

5.3.1.1 Choice of time-points/time-course

As described in the chapter introduction, cell death is a highly complex process, which is characterized by a range of biochemically and morphologically distinct pathways. Many of the markers used to characterise e.g. apoptosis only show a transient, rather than a sustained increase. For instance, in Jurkat cells, caspase 8 activity peaks after around 3 hours, whereas caspase 3/7 peaks after around 7 hours (Sandquist et al., 2006). Consequently, cell death events and their timings are highly dependent on the cell type, apoptosis-inducing agent, exposure time and its concentration. Also, the same population of cells can undergo apoptosis at different time-points due to differences in the cell cycle phases of individual cells.

It is therefore possible that the markers chosen to characterise the type of cell death mechanisms in this study were the right ones, but the fact that very few changes were measured could be due to the wrong time points being chosen (for the chosen concentration of AuNPs). Therefore, the choice of the time-points

might represent a limitation of the experimental design. For future studies, it is crucial to initially determine the time-points at which the activity of interest peaks at the chosen AuNP concentration. Careful interpretation of the data is of great significance, as the absence of a change or a low signal could be misinterpreted as no apoptosis or necrosis induction occurring, rather than a time-point being missed.

5.3.1.2 Cell line

Also, the range of cell death assays presented in this chapter have been only examined on HSC cells, as this was the main cell line of the focus of this thesis. Depending on the cell line and cell type, some cell death events may be underestimated due to the cell line not expressing a protein or a receptor required for the induction of e.g. extrinsic apoptosis. For instance, MCF-7 cells lack a functional caspase 3 product thus assays detecting caspase 3/7 activity using DEVD substrate, will produce no signal (Kroemer et al., 2005).

5.3.1.3 AuNP concentration and exposure time

As mentioned above, the concentration and exposure time of the cell death-inducing agents, in this case, the AuNPs, can influence the type of stimulus produced and the mechanism of cell death. A less intense stimulus is triggered with low drug concentrations and shorter exposure times. With a longer exposure time, a compound's IC50 value decreases, meaning that it has higher toxicity (Riss and Moravec, 2004). For instance, applying high concentrations of tamoxifen on HepG2 cells, generated a caspase 3 activation within 1-2 hours, as opposed to lower concentrations of tamoxifen which triggered a caspase 3 response only after 24 hours (Sandquist et al., 2006). The values of 10 μg/ml AuNP and 3h acute exposure time were chosen based on the toxicity assays

performed in clonogenic assays (chapter 3), representing double the estimated IC50 values derived from it.

5.3.1.4 Cell culture conditions and cell density

The discrepancy in the large extent of cell death observed in the clonogenic assays performed in chapter 3 and the low amount of cell death noted in this chapter caused to consider what parameters differed between the experiments. The most obvious one was that for the experiments presented in this chapter, the cells were cultured at a higher density compared to the clonogenic assays. A high cell number of HSC cells appeared to deliver a protective effect towards the toxic AuNPs, leading to a decreased signal observed in all the assays. The role of cell density in the toxicity of nanoparticles has also been shown by previous studies (Elias et al., 2013). A study of different concentrations of tamoxifen on different densities of HepG2 cells showed that drug potency increased with lower cell densities (Riss and Moravec, 2004).

In conclusion, a possible extrinsic apoptotic mechanism was noted with the 50:50 AuNPs. No ROS production or cell cycle arrest was noted. Mitochondrial membrane depolarization was evident 48h after the acute exposure. Data need to be interpreted with caution to avoid leading to false conclusions. The choice of assays presented above intended to deliver a broad overview of the possible basic processes involved during a cell death event. If time allowed, a different approach would have been adopted for the experimental design without assuming that the IC50 value obtained by clonogenic assays will translate in a similar way to another experimental set up, this of the cytometry. However, an important aspect was raised in this chapter when performing toxicity assays, this of the cell density role in AuNP toxicity.

Chapter 6: Evaluation of AuNP Toxicity in a Range of Cancer and Normal Cell Lines

6.1 Introduction

Different tumour types are characterized by genetic and epigenetic variations depending on their tissue origin leading to differences in clinical outcomes. These variations render the cancer mechanism of action difficult to understand (Vargo-Gogola and Rosen, 2007). To enhance this understanding, various experimental models have been developed. These models include primary tumours (Burdall et al., 2003), genetically engineered mice (Vargo-Gogola and Rosen, 2007), xenografts (Leonetti et al., 2006), paraffin embedded samples, primary cell and 3D cultures (Lacroix and Leclercq, 2004) and cancer cell lines (Staveren et al., 2009).

Various types of cell lines are used in *in vitro* experiments as representative models of a cancer or a normal cell due to their ease of handling and molecular characterization, overcoming the limitations that exist with other models. Some of these limitations are the ethical approval of animal use, manipulation and characterization analysis (Staveren et al., 2009, Engel et al., 1978). In this chapter, the toxicity of different cancer cell lines and associated normal cells after an acute 3h exposure of the AuNPs will be presented.

6.1.1 Cancer cell lines as an experimental model in cancer therapy

Cancer cell lines are extensively studied for the effectiveness and the development of anti-cancer drugs (Yamori, 2003, Gazdar et al., 2010) or for identification of the phenotypic properties and biology of cancer such as migration capacity and proliferation rates (Kim et al., 2004). Other studies have shown the

use of cancer cell lines for the investigation of cellular pathways and genetic alterations or for screening of a possible biomarker for diagnostic purposes (Ferreira et al., 2013).

6.1.1.1 Advantages and disadvantages of cell lines in cancer research

Many advantages are associated with the use of cell lines in cancer research. They are easily genetically modified using siRNA, demethylation agents or expression vectors (Leone et al., 2003, Kawasaki et al., 2004). The main advantage is the creation of a well-characterized “library” of cells that can be used by different laboratories for results to be easily comparable. Also, if any contamination occurs during the experimental procedure, there is a possibility of substitution and maintenance of reproducible results if following the same experimental set up. The most important disadvantage that exist with their use is the genomic instability noted between the original tumour and the representative cell line (Anglard et al., 1992).

During continuous cell cultures, a phenotypic and genotypic drift might be possible if the correct conditions are not maintained (Vargo-Gogola and Rosen, 2007). Also, some cell lines might have been cross-contaminated and mycoplasma infections are recurrent. Lastly, the microenvironment of a cell culture differs from the original tumour which lead to a greater heterogeneity and morphological/molecular changes (Bright et al., 1997). Some of these disadvantages can be overcome by the use of other experimental model systems as discussed above. However, the use of cancer cell lines represents the most valuable tool as a first approach for a drug screening and effectiveness, which is the main focus of this chapter.

Despite the essential value of the use of cell lines in cancer studies, controversial research exists about their relevance as representative models of an original tumour (Lacroix and Leclercq, 2004, Wistuba et al., 1998). On one hand, there is an agreement that there is a genomic similarity of cancer cell lines with the original tumour they derived from (Fang et al., 2009). During the first cell culture passages, cancer cell lines retain the same molecular and morphological features as the primary tumour (Wistuba et al., 1998). Angiogenesis induction differs between the cell line and the tumour as stromal tissues presence is required. A study by Tomlinson et al., presented early evidence of the similarity argument. They reported that a breast cancer cell line shares a range of features with the original tumour, such as the same allelic loss and *BRCA1* mutation (Tomlinson et al., 1998). On the other hand, many reports have shown that cancer cell lines undergo extensive oncogene mutations, chromosomal rearrangements, gene amplification and allelic loss (Kao et al., 2009, Gazdar et al., 2010). As a result, prolonged period of cell culturing, leads to phenotypic and molecular alterations and cellular pathways modifications (Ferreira et al., 2013).

6.1.1.2 Comparison between cancer and normal cell lines in cytotoxicity drug testing

The use of cell lines allows for cytotoxicity evaluation of specific drug candidates, understanding of a drug's mechanism of action and signalling pathways activation, biomarker identification, dose responses and screening of sensitivity/resistance profile for different cell types. Comparability between different tests even months apart can be achieved by using batches of cells stored at the same passage. The outcome is cell line dependent as some cell types are more sensitive or resistant than the others (Ferreira et al., 2013) (Table 6.1). For instance, 60 nm cationic polystyrene nanosphere particles were toxic to

macrophages, whereas the same particles were less toxic to hepatoma and human microvascular endothelial cells (Xia et al., 2008).

Table 6.1: Comparison between the different published studies of AuNPs on cancer versus normal cell lines.

Size (nm)	Shape	Coating	Exposure	Time	Toxicity	Cell line	Ref.
Cancer cell lines							
1.4	Spherical cluster	Ph2PC6H4SO3H	< 0.4 mM	24h	IC50 0.24 µM IC50 0.30 µM	MV3, BLM	Tsoli et al., 2005
4, 12, 18	Spheres	CTAB, citrate, cysteine, glucose, biotin	0.001-0.25 µM	72h	MTT assay, CTAB-NPs 18 nm not toxic up to 25 µM	K562 human leukemia	Connor et al., 2005
50, 20	Rods	CTAB, PEG, anti-HER2	0.06 nM	24h	ICP-MS, AuNPs/cell (8,000 for CTAB, 3,000 for PEG, 4,400 for anti-HER2) non toxic	SK-BR-3	Cho et al., 2014
35.9 ± 6.7	Spheres	Cetuximab antibody	100 nM	-	AuNPs not toxic for cama-1, cell death for Panc-1 (IC50 ~ 100 nM) and via a necrosis pathway	Panc-1 Cama-1	Glazer et al., 2010
3.7	Spheres	PEG	0.08-100 µM	6-72h	Low toxicity (70% viability after 72h of up to 10 µM AuNPs exposure)	HeLa	Gu et al., 2009

33	Spheres	CTAB and citrate	0-120 nM	48h	No toxicity for this cell line	HepG2	Patra et al., 2007
40x18	Rods	CTAB	1 nM	6h	Slight toxicity at 150 μM in serum free media (20.8 % cell death)	HeLa	Hauck et al., 2007
Normal cell lines							
33	Spheres	CTAB and citrate	0-120 nM	48h	No toxicity observed for BHK21 up to 120 nM	BHK21	Patra et al., 2007
1.5	Spheres	MEEE, TMAT	0-100 μg/ml 25 μg/ml	6-24h	LD50 < 10 μg/ml for TMAT and LD50 = 25 μg/ml for MEEE	HaCaT	Schaeublin et al., 2011
15	Spheres	-	51 – 561 ng/cm2	4-24 h	No induction of oxidative stress or inflammatory response	MDM, MDCC	Brandenberger et al., 2010
13, 45	Spheres	-	Up to 180 μg/ml	3 to 6 days	75% and 100% cell death by apoptosis pathway after 45 nm AuNPs exposure at 25 μg/ml for 3 days and from 20 μg/ml for 6 days.	CF-31 primary dermal human fibroblast	Mironava et al., 2010

Normal cells undergo apoptosis, a programmed cell death for the removal of senescent or damaged cells and for tissue remodelling. Also, they divide by signals sent from adjacent cells and communicate via gap junctions in their cell

membranes with neighbouring cells (Bhowmick et al., 2004). Cancer cells on the other hand, are resistant to apoptotic signals, they divide uncontrollably and have lost gap junctions. Moreover, normal cells can repair any DNA damage as opposed to cancer cells which allow mutations to accumulate often accompanied by chromosomal alterations such as gene amplifications, deletions, translocations (Lowe et al., 2004).

Cellular senescence is a feature of normal cells indicating that there is a limit in the number of cell divisions any cell type can undergo (Collado et al., 2010). Cancer cells indefinitely divide. During cell division, telomerase enables telomere replication, which in normal cells shortens after every cell cycle (Evan and Littlewood, 1998). Cancer cells constitutively express telomerase, maintaining the length of telomeres.

In the next section of this chapter, the cytotoxicity of the 50:50 αGal:PEGamine AuNPs is presented in a range of cancer and normal cell lines.

6.2 Results

The cytotoxicity of the 50:50 αGal:PEGamine AuNPs was evaluated in a range of cancer and corresponding normal cell lines. As discussed in chapter 3, clonogenic assays were used to determine the cytotoxic potential of the AuNPs in HSC and HaCaT cell lines. However, the same assay could not be used for other cell types as they do not have the ability to grow in colonies needed for a clonogenic assay. Therefore, an assay similar to the clonogenic assay was conducted for the range of cell lines tested, which was the CyQUANT cell proliferation assay. Both assays measure the proliferative capability of cells after an acute 3h exposure to AuNPs.

CyQUANT is an assay that accurately measures the proliferation rate of a cell population based on cellular DNA content and can be used as an indicator of cytotoxicity. It is a highly sensitive, accurate and fast way of analysing the number of cultured cells in a microplate set up as it can detect as few as 10-50 cells remaining on the plate (Jones et al., 2001). This assay is independent of the metabolic state of cells, generating steady fluorescent signal across a range of cell types and conditions (Jones et al., 2001). The results presented below from CyQUANT assays were a result of a time-course and do not represent an end-point toxicity. An end-point of day 6 is also presented and compared between the cell types tested to mimic the time-point at which the clonogenic assays were performed. The time-course provided complimentary information into the timing of cell death and allowed to distinguish between a cytostatic or cytotoxic potential of the AuNPs. A comparison between the control and the highest concentration AuNP for all cell lines is also depicted in a bar chart towards the end of this section.

In the CyQUANT assays, fluorescence intensity was measured which relates to the amount of DNA remaining in the well after exposure to AuNPs. To translate this value into cell number measurements, a standard curve relating the fluorescence intensity to the actual cell number was plotted. The standard curve was only conducted for HSC cells and is presented below (Figure 6.1). Within this study it was attempted to directly correlate the cell proliferation and amounts of DNA between the cell lines. The cells were seeded at different confluences and allowed to attach to the plates for a minimum of 6h before fixation by freezing as required by the assay protocol. This should not have allowed sufficient time for the cells to divide, but either loss of non-attached cells, or cell division could affect the accuracy of the results. Therefore, it was concluded that an accurate estimate of the cell number based on measurements of fluorescence intensity was not possible and the data will be presented as changes in the fluorescence normalised to the number of seeded cells.

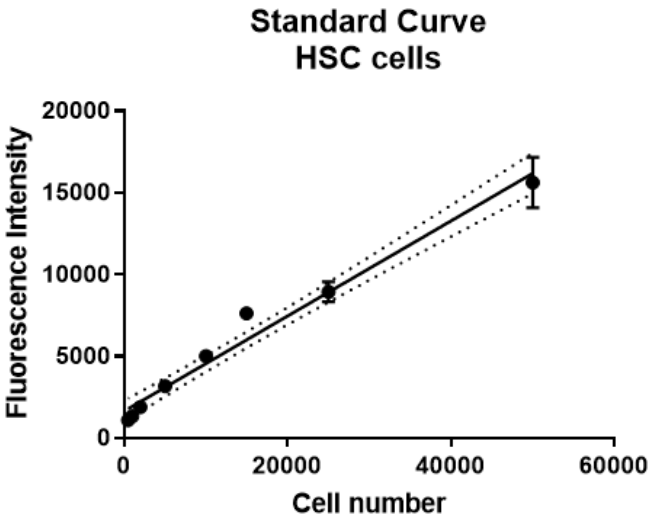

Figure 6.1: Standard curve to correlate the number of HSC cells with the fluorescence measured in the CyQUANT assay. Data were obtained on the day of seeding and were expressed as mean±SEM, n=1 with 3 replicates. Dotted lines represent 95% CI.

A list of all the cell lines and their origin investigated in this chapter are presented in chapter 2 (Table 2.2). The tissue types examined include skin (HSC/HaCaT), breast (MCF-7/HMEC), kidney (A498/HEK-293), brain (U-373/hA), cervical (HeLa) and colorectal (Caco-2). Their choice was based on the fact that they represent cells from possible target organs for AuNPs toxicity. The focus of this analysis was to test a range of cancer and corresponding normal cell lines *in vitro* from different tissue types throughout the body in order to determine the cytotoxic potential of the AuNPs. Therefore, the above cell lines were considered a good *in vitro* model for a general screening of the AuNPs toxicity. Also, the availability and easy access to these cell types as they were taken from The Open University bank of cells was an advantage.

CyQUANT assays were performed every day for a time-course of 6 days. The concentrations of the AuNPs used were 0, 5 and 10 μg/ml. These concentrations were chosen according to the maximum concentration used in clonogenic assays in chapter 3, which resulted in < 5 colonies left after an acute 3h exposure of the 50:50 αGal:PEGamine AuNPs.

6.2.1 HSC/HaCaT skin cancer and human keratinocyte cell lines

Regarding the skin cancer HSC and normal keratinocyte cell lines, a selective toxicity was noted throughout the time-course of the assay. Specifically, in HSC cells AuNPs at 10 μg/ml were toxic from day 1 (Figure 6.2A) and fluorescence intensity remained at a baseline level, as opposed to the normal growth observed for HaCaT cells for the same concentration (Figure 6.2B).

6.2.2 MCF-7/HMEC

For the breast cancer MCF-7 and mammary epithelial HMEC non-cancerous cells, the results were similar with regard to the different concentrations of AuNPs. Compared to untreated controls, the highest AuNPs concentration increased the toxicity ~2 fold for both the MCF-7 and HMEC cells. The pattern of fluorescence intensity for the MCF-7 throughout the days was inconsistent. For the HMEC cell line, an increase in fluorescence was noted throughout the time-course (Figure 6.2C&D).

6.2.3 A498/HEK-293

The kidney cancer and normal cell lines, A498 and HEK-293 appeared to be less affected by the AuNPs in terms of their fluorescence and cell number. For the A498 cell line, a pattern of exponential growth and increase in fluorescence was noted, with both 5 and 10 µg/ml AuNPs concentration to have a slight effect from day 2, leading to a decrease in fluorescence intensity without causing a stationary result, but allowing cells to proliferate (Figure 6.2E). Data for HEK-293 showed an increase in fluorescence intensity with 10 µg/ml AuNPs concentration, plateauing from day 5 to day 6 (Figure 6.2F).

6.2.4 U-373/hA astrocytes

For the U-373 and primary astrocytes hA cell lines, the toxic potential of the AuNPs was not evident. Both cell lines were not affected by the AuNPs, with no change in fluorescence to be observed for U-373 from day 1 to day 2 for both 5 and 10 µg/ml AuNPs concentration as opposed to the control cells (Figure 6.2G). hA astrocytes growth appeared to be much slower as compared to any other cell line (Figure 6.2H).

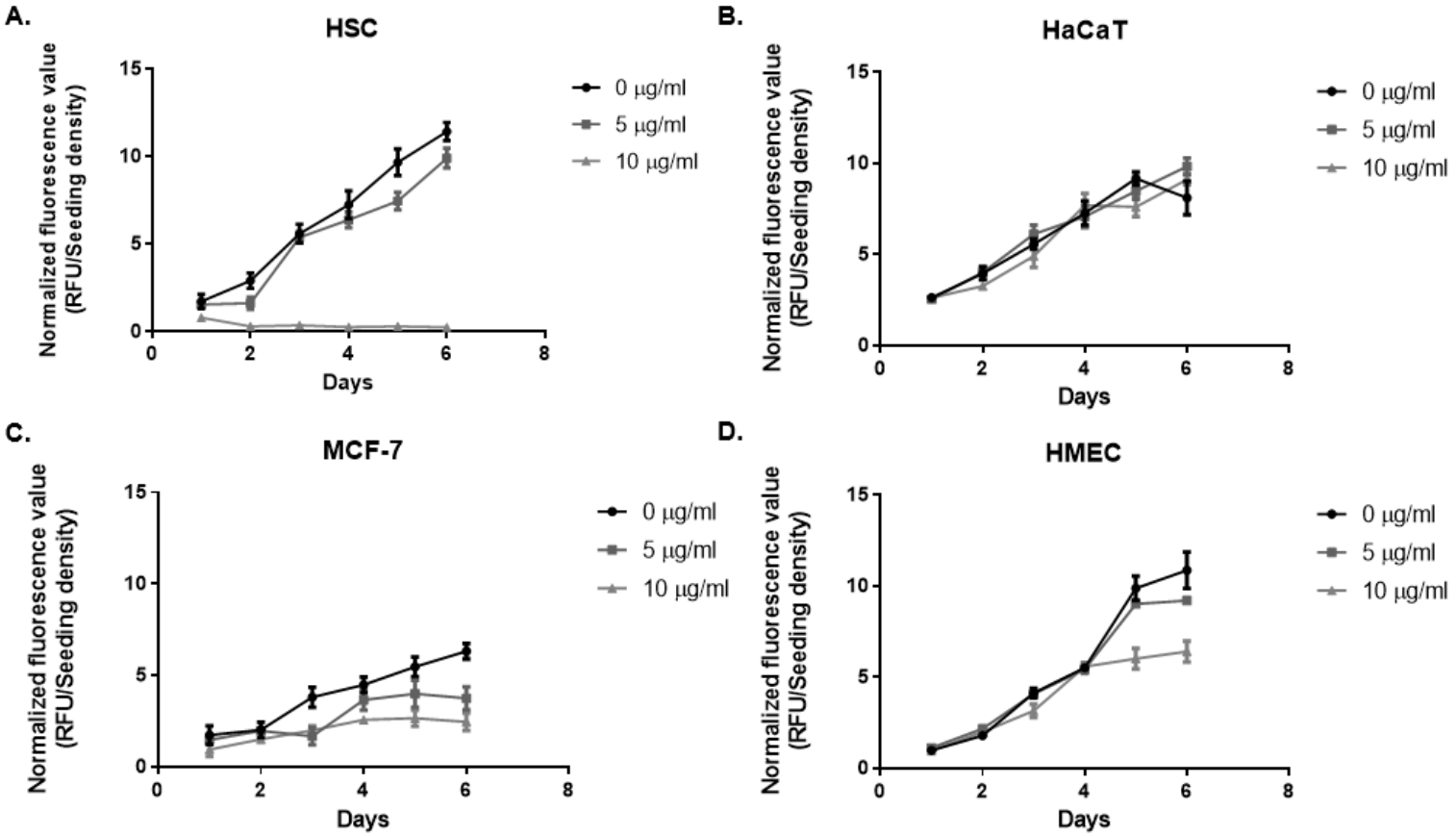
A.
HSC
Normalized fluorescence value (RFU/Seeding density)
Days
0 μg/ml
5 μg/ml
10 μg/ml
B.
HaCaT
C.
MCF-7
D.
HMEC

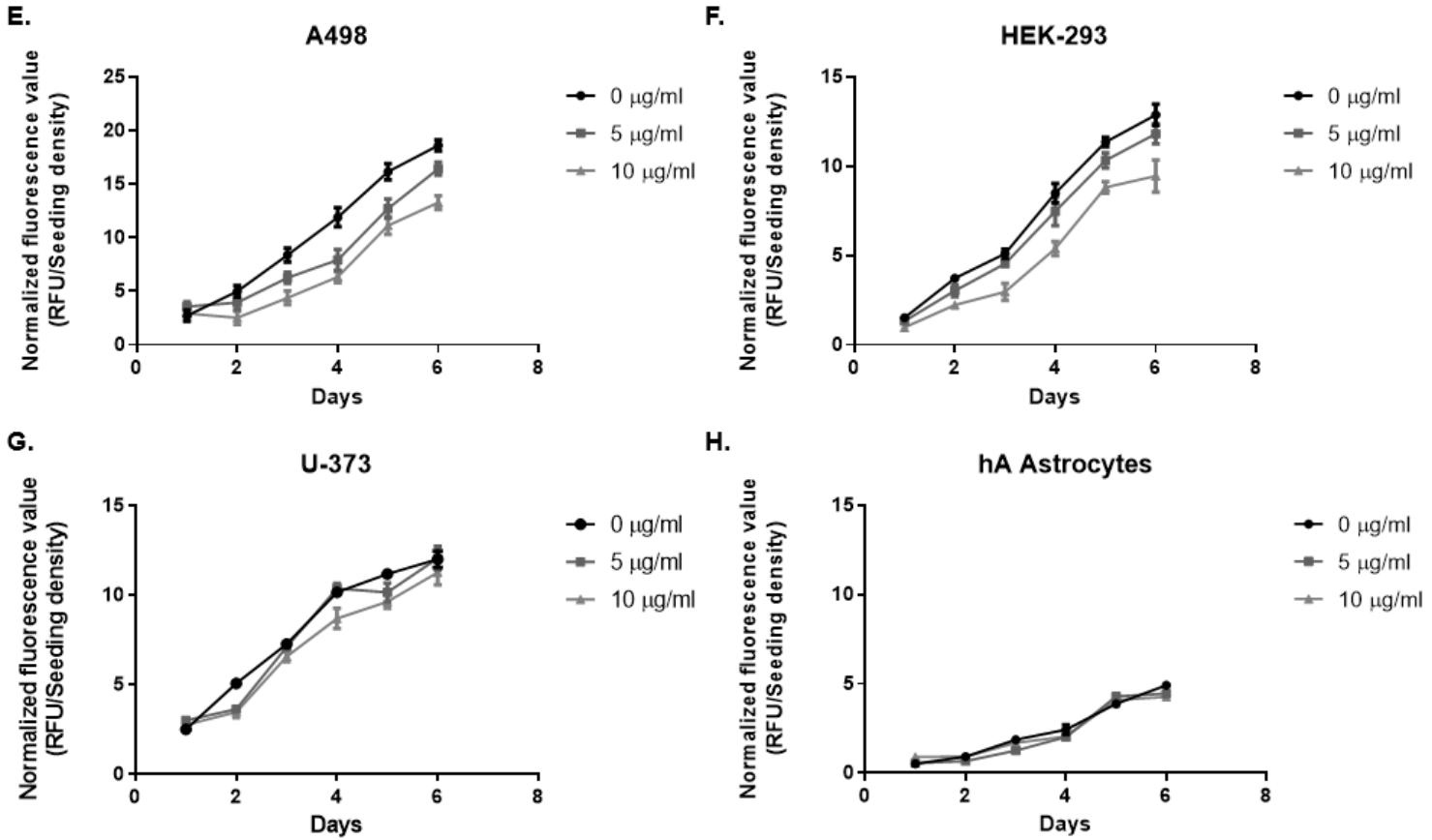

Figure 6.2: Cell proliferation assays throughout a 6 day time-course on a range of cancerous and normal cell lines after an acute 3h exposure of 50:50 αGal:PEGamine AuNPs at 0, 5, and 10 µg/ml. The cell lines tested included **A.** HSC, **B.** HaCaT, **C.** MCF-7, **D.** HMEC, **E.** A498, **F.** HEK-293, **G.** U-373 and **H.** hA astrocytes. The fluorescence measured for each well was normalized to the corresponding seeding density and the calculated factor was plotted as a measure of the relative number of cells. Data were plotted as mean±SEM from 3 independent experiments, with n=3 per condition.

6.2.5 Caco-2 and HeLa

Two additional types of cancer cell lines were also examined. Caco-2 and HeLa do not represent a pair of cancer and corresponding normal cell lines tested but were evaluated for the potential toxicity of AuNPs. They both showed a similar response to AuNPs. Data for the Caco-2 cell line indicated that this type of cell line was not affected by the AuNPs exposure and there was an increase of fluorescence intensity observed throughout the time-course (Figure 6.3A). On the other hand, data for HeLa cells, showed a slight inconsistent decrease in fluorescence between day 3 and day 5, with cells to recover any toxic potential of the highest concentration AuNPs (Figure 6.3B).

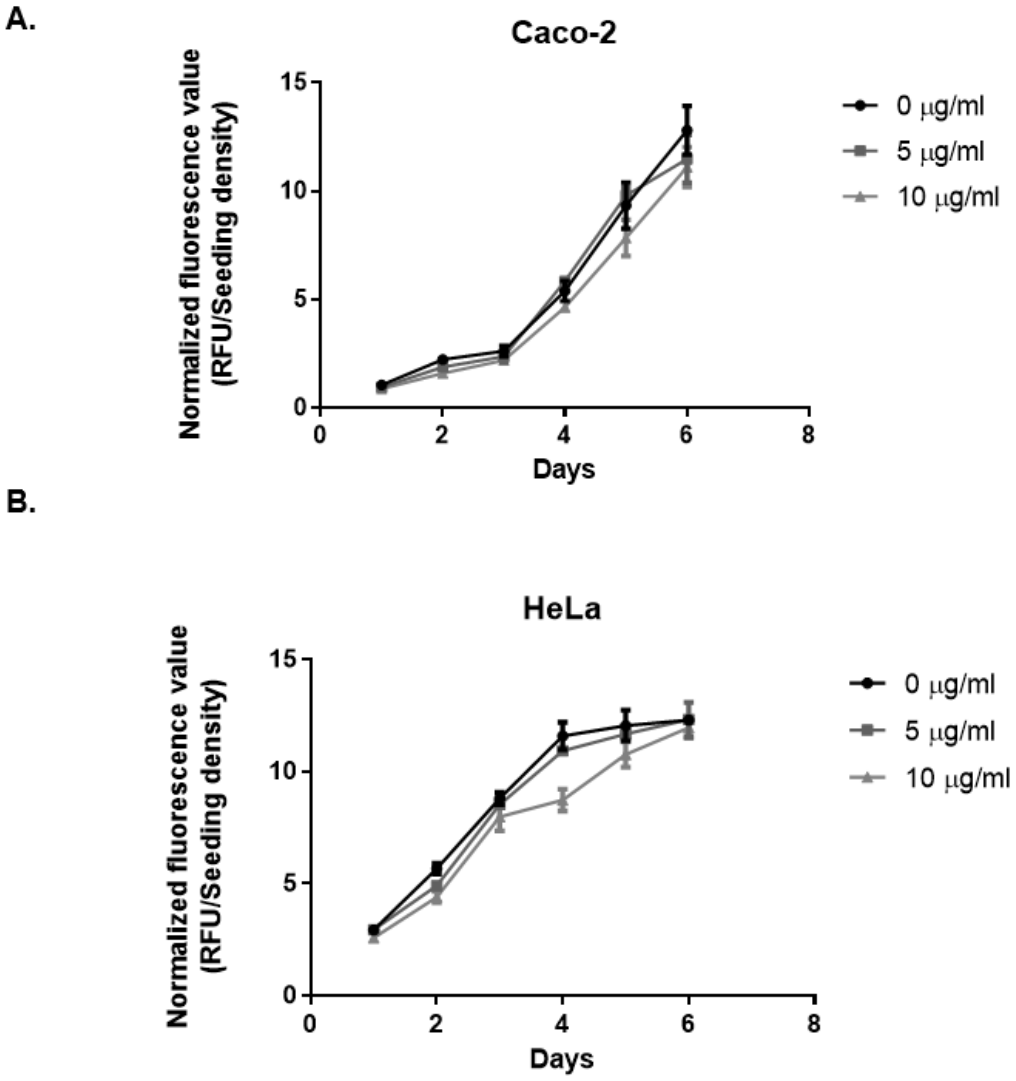

Figure 6.3: CyQUANT cell proliferation assay throughout a 6-day time-course on A. Caco-2 and B. HeLa cells after an acute 3h exposure of 50:50 αGal:PEGamine AuNPs at 0, 5, and 10 μg/ml. The fluorescence measured for each well was normalized to the corresponding seeding density and the calculated factor was plotted as a measure of the relative number of cells. Data were plotted as mean ±SEM from 3 independent experiments, with n=3 per condition.

A comparison of the toxicity caused by the highest concentration of AuNPs on day 6, a time-point similar to the endpoint of the clonogenic assays presented in Chapter 3, is shown below (Figure 6.4). This allows a comparison of the significance of the cytotoxic potential of AuNPs long term after an acute 3h exposure as performed in this chapter using the CyQUANT assay. These data depicted that 6 days after an acute 3h AuNP exposure, the different cell types were differently affected by 10 μg/ml AuNPs. Specifically, HSC, MCF-7, HMEC, A-498 and HEK-293 cells showed a lack of proliferation ability caused by AuNPs exposure, whilst the rest of the cell lines tested were not affected.

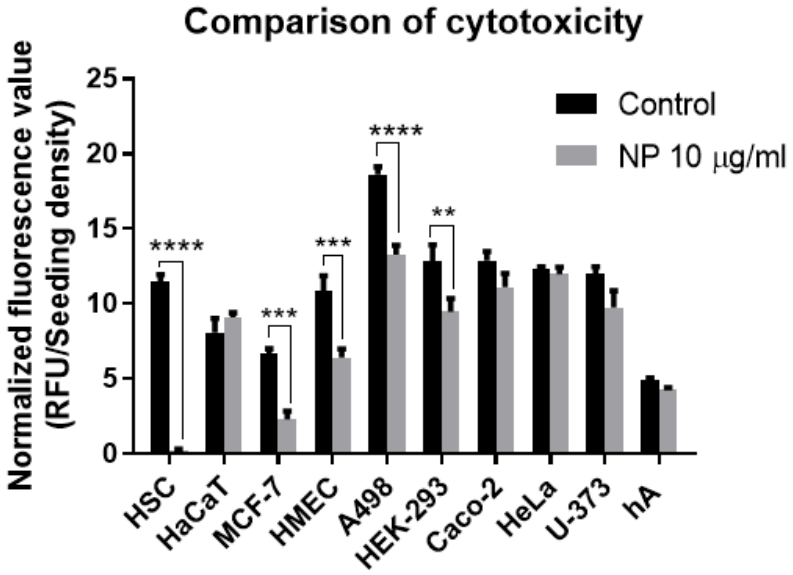

Figure 6.4: Comparison of cytotoxicity of AuNPs after an acute 3h exposure to 0 and 10 μg/ml at day 6 of a time-course for CyQUANT cell proliferation assay. Results were plotted as fluorescence intensity/seeding density and as mean±SEM from 3 independent experiments, with n=3 per condition. Two-way Anova, Sidak's multiple test, **** P<0.0001, ***P<0.001, **P<0.01

6.3 Discussion

A variety of cancer and normal cell lines were investigated for the toxic potential of 50:50 αGal:PEGamine AuNPs at 0, 5 and 10 µg/ml. These concentrations were chosen from previous assessments on cytotoxicity of these particles. CyQUANT cell proliferation assays showed that AuNPs were toxic for some of the cell lines whereas others remained unaffected. In summary, proliferation of HSC, MCF-7, HMEC, A498 and HEK-293 cells (Figure 6.4) was affected at the highest concentration of 10 µg/ml AuNPs, whereas HaCaT, Caco-2, HeLa, U-373 and hA cells did not show any significant decrease in their normalized fluorescence intensity value throughout the 6 day time-course after an acute 3h AuNP exposure.

The results obtained for the different cell lines were expressed as normalized fluorescence intensity/seeding density. Cells were seeded at different densities at day 0 of the experiment because of their different proliferation rates. Cell proliferation refers to the increase of cell number over time and is a result of a balance between cell divisions and cell death (Cooper, 2000). Cancer cells have increased proliferation rates (Tubiana, 1989). Therefore, the goal was to achieve ~80% confluency on day 6 at the end of the time-course and cell densities for each cell type were adjusted accordingly. Plotting the fluorescence intensity without converting it to cell number for each time-point in the time-course is acceptable according to other studies and literature searches. Specifically, effects on cell proliferation have been used as a measure to evaluate the cytotoxic potential of compounds. A number of fluorescence based assays have been widely used in order to determine the cell proliferation capacity of cells. These assays are based on the DNA content of cells, their metabolic activity or

cell division (Cooper, 2000, Salic and Mitchison, 2008, Duellman et al., 2015, Mosman et al., 1983).

On the other hand, many studies have examined the cytotoxic potential of nanoparticles by the use of techniques such as MTT or alamarBlue reagent which measures the reductive ability of cells (Berridge and Tan, 1993). Cell cycle distribution studies have also been utilized mainly for detecting alterations in growth patterns of cells (Kurowaka et al., 2008). Advantages and disadvantages of each method are not the focus of this section, thus it is not discussed in more detail. However, as a concluding remark CyQUANT was chosen based on literature searches as the most robust, sensitive and fast to perform method. Also, its protocol has minimal interference with any other substance and experimental design required straight-forward characterization of reagents concentrations and incubations times (Jones et al., 2001).

Another point that needs to be mentioned is that the fluorescence intensity level measured in control cells, not treated with AuNPs, varied between the cell lines. Such effect could be attributed to firstly, different cell types having different amounts of DNA and secondly, it could be dependent on their stage of cell cycle. Cells at G_0/G_1 phase have one set of paired chromosomes/cell, in the S phase the amount of DNA varies due to DNA synthesis and in the G_2/M phase there are two sets of paired chromosomes prior to cell division (Cooper, 2000). Depending on the phase of cell cycle, different amount of DNA was measured in the samples. Therefore, comparisons within the cell type being investigated were presented for the control and treated with AuNPs sample, without comparing differences between cell lines.

6.3.1 AuNPs toxicity in a range of normal and cancer cell lines

As presented above, a cell type dependent toxicity was observed with some of the cell lines to be affected and some others not. Such effect is in agreement with other studies that showed the same pattern (Sohaebuddin et al., 2010). Most of the research on this area is published for silica nanoparticles and not for AuNPs *in vitro*. A previous study suggested that differences in cytotoxicity of silica nanoparticles between cell lines could be due to the differences in their metabolic and proliferation rates (Chang et al., 2007). Another study that discussed the cytotoxic effects of 15, 60 and 200 nm silica nanoparticles on A549, HaCaT, THP-1 and NRK-52E proposed that toxicity is both cell and nanoparticle size dependent (Hsiao et al., 2014). They depicted that HaCaT cells were tolerant due to lower uptake of NPs (Hsiao et al., 2014).

Other studies such as this of Nabeshi et al., has correlated NP uptake with toxicity (Nabeshi et al., 2010). As shown in chapter 3, HaCaT cells were also not affected in this study, confirming the data from published research showing that epithelial cells or tumour cells are less sensitive to phagocytic or fibroblast cells for silica nanoparticles (Lanone et al., 2009). No selective toxicity pattern was observed in any cell line other than HSC and HaCaT cells and in a smaller degree, MCF-7and HMEC. A discussion of the possible features that could play a role in the sensitivity and resistance of the cell lines is attempted below.

As previous studies have shown and are cited above, the amount of Au inside the cells could play a role in their toxicity. However, it was evident in chapter 4 that amount of Au did not correlate with toxicity. Instead the amount of AuNPs sticking to the cell surface via filopodia was. Due to time limitations, the actual amount of Au inside the cells was not counted in each cell line. However,

data presented for HSC cells, showed that the number of filopodia and the AuNPs sticking to them play an important role in the toxicity of these AuNPs. Not a lot of research has investigated the filopodia density in different cell types. In cancer cell lines, increased filopodia protrusions have been observed (Jacquemet et al., 2017). FiloQuant is an automated tool utilized to obtain information on filopodia dynamics, length and density (Jacquemet et al., 2017). It is the only example found for an assay that measures filopodia dynamics and density. When being applied to a range of cell types, an increased filopodia density was shown in MCF-10 breast cancer cells (Jacquemet et al., 2017). In order to assess the validity of the theory, that filopodia density could be correlated to toxicity in vitro, FiloQuant analysis should be applied to the range of cell lines tested followed by TEM counts of AuNPs in cells.

Another theory that could explain why different cells appeared to be more or less sensitive to the AuNPs toxicity could be the localization and the type of internalization/uptake mechanism of the AuNPs and the mechanism of cell death that was triggered. For example, silica nanoparticles have been tested for their cytotoxic potential in HUVEC and HeLa cells, showing differential responses to the cell types examined and attributing this effect to potential differences in their uptake and localization (Blechinger et al., 2013). Also, the function of each cell type and the properties of the nanoparticles interacting with their cell surface could be of vital significance to how toxic these particles are.

Lastly, there is another cell structure apart from filopodia that is important for the contact of particles with the cell membrane, this of glycocalyx. The glycocalyx is a structure of glycolipids and glycoproteins on the outside of the cell membrane, which contributes to cell communication, recognition and adhesion (Reitsma, 2007). The thickness of the glycocalyx is dependent on the cell type

(Tarbel and Cancel, 2016). Specifically, cancer cells are found to have thicker and more robust glycocalyx than normal cell types (Tarbel and Cancel, 2016). This structure could be of great importance for the interaction of AuNPs with the cell membrane or the internalization of the particles into the cells and could thus explain any differential toxicity observed between the cell lines.

To conclude, a range of cell lines have been tested for the AuNPs toxicity. In general, the heterogeneity of each cell line is a complex topic and multiple factors can be responsible for the variation in the toxicity of AuNPs observed between the cell lines. An important issue has to be mentioned with regard to the cell lines being taken from The Open University's liquid nitrogen bank. The significance of any cell line characterization prior to experiments is vital in order to avoid data misinterpretation. Such significance is noted by Horbach and Hallfman, who illustrated that misidentification of cell types has led to approximately 32,755 published articles to contain data from mislabelled or cross-contaminated cell lines (Horbach and Hallfman, 2017).

Lastly, the cytotoxic potential of the 50:50 αGal:PEGamine AuNPs was investigated in a range of cell lines but it can be concluded that depending on the cell type, these particles can be used either as a toxic agent at a concentration of around 10 μg/ml or as a drug delivery agent below that concentration to ensure no toxic potential of the drug carrier for specific cell types.

Chapter 7: Conclusions and Future Directions

Despite important breakthroughs in cancer biology throughout the years, cancer remains a challenge and a leading cause of death worldwide. The importance of nanomedicine and utilizing formulations at the nano-scale level which selectively cause toxicity on cancer cells without affecting the normal cell lines, was highlighted by Patra et al., which described how AuNPs induced selective responses between a human carcinoma lung cell line, a baby hamster kidney cell line and a human hepatocellular liver carcinoma (Patra et al., 2007).

The work presented in this thesis has contributed to the field of nanomedicine by a) identifying key parameters during the synthesis of AuNPs that play a significant role in their toxicity, such this of their synthesis time and ligand density, b) flagging an issue of batch variability and how it should be addressed to avoid any data misinterpretation, c) demonstrating the uptake of AuNPs by skin cancer cells and their preference to bind to filopodia, d) providing an insight into the mechanism of cell death caused by AuNPs and e) increasing the understanding that toxicity of nanomaterials is cell type dependent.

In chapter 3, the cytotoxicity of 2 nm αGal:PEGamine AuNPs was presented. Firstly, a batch variability issue was identified regarding the differential toxicities of the AuNPs on HSC and HaCaT cells, based on their IC50 values as obtained by clonogenic assays. A series of experiments were designed in a way to unravel the factor responsible for the variability detected. By eliminating and narrowing down factors, a novel feature was identified that played a significant role in the toxicity of these AuNPs, this of their synthesis time (Figure 3.11).

In chapter 4, the focus was on three AuNPs, with synthesis times of 1h, 2h and 5h. Full physicochemical analysis was conducted, with the only difference

noted between them to be the ligand density surrounding the Au core. Increasing synthesis time led to a less dense ligand packed particle. Uptake by HSC cells was also examined and a remarkable adhesion of the AuNPs to filopodia was discovered under TEM (Figure 4.14). Gromnicova et al., showed that the same αGal:PEGamine AuNPs were internalized via an active transport mechanism, thus further studies into the uptake of these nanoparticles involving chemical inhibitors did not follow (Gromnicova et al., 2016).

In chapter 5, an attempt to distinguish between the apoptotic and necrotic cell death mechanisms was presented. Cytotoxicity of the AuNPs was prevented by co-incubation with a caspase 8 inhibitor, but with not a caspase 9 inhibitor, suggesting a possible extrinsic apoptotic mechanism of cell death (Figure 5.7). The role of cell density was evaluated, indicating that the toxicity of the AuNPs was affected by this factor (Figure 5.11).

In chapter 6, the cytotoxicity of the 50:50 αGal:PEGamine AuNPs was tested in a range of cancer and normal cell lines. Data presented in this part of the thesis illustrated that depending on the cell type, these particles can either be used as a toxic agent at a concentration of around 10 μg/ml or as a drug delivery agent below that concentration to ensure no toxic potential of the drug carrier.

Limitations of this study were analysed and discussed throughout the various chapters. The main limitations can be summarized into the following statements:

- Batch variability consisted a major challenge at the beginning of the project. This thesis led to identification of the parameters producing such variability. Full physicochemical characterization and control of the AuNPs synthesis process can minimize batch to batch variations.

Also, moving production of the AuNPs to continuous flow processing could ensure consistent manufacturing of the particles.

- The reason of the choice of experimental assays and design was analysed in appropriate parts throughout the thesis. However, limitations might exist regarding types of assays used, incubation times, seeding densities and choice of time-courses, especially for unravelling the mechanism of cell death.
- Characterization of cell lines presented on chapter 6 and cellular maturation test was out of the scope of this study, but the importance of it was highlighted by Horbach and Halffman due to the significant amount of published data based on misidentified cell types (Horbach and Halffman, 2017).

Future directions include the identification of the AuNP concentration appropriate for the cell death assays and repetition of the experiments presented in chapter 5 for a clearer illustration of the mechanism of cell death. Also, a better insight into the role of filopodia and the cell type needs to be gained. Lastly, evaluation of whether AuNPs can either be utilized as drug delivery agents or toxic agents at a specific concentration, dependent on cell type, needs to be confirmed.

References

Abdelbary M. A. Elhissi, Waqar Ahmed, Israr Ul Hassan, Vinod. R. Dhanak, and Antony D'Emanuele (2012) Carbon Nanotubes in Cancer Therapy and Drug Delivery, Journal of Drug Delivery,10:827-837

Ahamed, M. Akhtar, M.J. Khan, M.A.M. Alhadlaq, H.A. Alrokayan, S.A. (2016) Cytotoxic response of platinum-coated gold nanorods in human breast cancer cells at very low exposure levels. Environ. Toxicol. 31:1344–1356.

Albanese, A., Tang, P.S. & Chan, W.C.W., (2012) The Effect of Nanoparticle Size, Shape, and Surface Chemistry on Biological Systems. Annual Review of Biomedical Engineering, 14(1):1–16.

Alexis F, Basto P, Levy-Nissenbaum E, et al. (2008) HER-2-targeted nanoparticle-affibody bioconjugates for cancer therapy. Chem Med Chem. 3(12):1839–1843.

Alkilany AM, Murphy. (2010) Toxicity and cellular uptake of gold nanoparticles: what we have learned so far? J Nanopart Res .12:2313–2333

Alkilany AM, Nagaria PK, Hexel CR, Shaw TJ, Murphy CJ, Wyatt MD. (2009) Cellular uptake and cytotoxicity of gold nanorods: molecular origin of cytotoxicity and surface effects. Small. 5:701–708.

Anglard P, Trahan E, Liu S, Latif F, Merino MJ, Lerman MI, Zbar B, Linehan WM. (1992) Molecular and cellular characterization of human renal cell carcinoma cell lines. Cancer research 52(2): 348-356.

Ansar, S.M. et al., (2011) Determination of the Binding Affinity, Packing, and Conformation of Thiolate and Thione Ligands on Gold Nanoparticles. The Journal of Physical Chemistry C, 115(3): 653–660.

Arjonen A, Kaukonen R, Ivaska J. (2011) Filopodia and adhesion in cancer cell motility. Cell Adh. Migr. [Internet]. 5(5): 421–30. Available from: http://www.ncbi.nlm.nih.gov/pubmed/21975551.

Auffan M, Bottero JY, Chaneac C, Rose J. (2010) Inorganic manufactured nanoparticles: how their physicochemical properties influence their

biological effects in aqueous environments. Nanomedicine (Lond). 5:999–1007.

Bae, Y. et al. (2005) Preparation and biological characterization of polymeric micelle drug carriers with intracellular pH-triggered drug release property: tumor permeability, controlled subcellular drug distribution, and enhanced in vivo antitumor efficacy. Bioconjug. Chem. 16: 122–130

Bagwe RP, Hilliard LR, Tan WH. (2006) Surface modification of silica nanoparticles to reduce aggregation and nonspecific binding. Langmuir. 22:4357–4362.

Barani, H. & Montazer, M. (2008) A Review on Applications of Liposomes in Textile Processing. Journal of Liposome Research, 18(3):249-262

Bar-Ilan O, Albrecht RM, Fako VE, and Furgeson DY. (2009) Toxicity Assessments of Multisized Gold and Silver Nanoparticles in Zebrafish Embryos. Small. 5(16): 1897–1910

Beddoes CM, Case CP, Briscoe WH. (2015) Understanding nanoparticle cellular entry: A physicochemical perspective. Adv Colloid Interface Sci. 218: 48–68.

Berridge MV, Tan AS. (1993) Characterization of the cellular reduction of 3-(4,5-dimethylthiazol-2-yl)-2,5-diphenyltetrazolium bromide (MTT): subcellular localization, substrate dependence, and involvement of mitochondrial electron transport in MTT reduction. Arch Biochem Biophys. 303(2):474–82

Bertrand, N., Bouvet. C., Moreau, P., Leroux, J. (2010) Transmembrane pH-Gradient Liposomes to Treat Cardiovascular Drug Intoxication. ACS Nano. 4(12): 7552–8

Bhamidipati, M.; Fabris, L. (2017) Multiparametric assessment of gold nanoparticle cytotoxicity in cancerous and healthy cells: The role of size, shape, and surface chemistry. Bioconjug. Chem. 28: 449–460.

Bharali, D.J. et al. (2009) Nanoparticles and cancer therapy: a concise review with emphasis on dendrimers. Int. J. Nanomed. 4: 1–7

Bhattacharya, R.; Mukherjee, P. (2008) Biological properties of naked metal nanoparticles. Adv. Drug. Delivery Rev., 60:1289–1306.

Bhowmick, N.A., Neilson, E.G., and Moses, H.L. (2004) Stromal fibroblasts in cancer initiation and progression. Nature. 432: 332–337

Blackadar CB. (2016) Historical review of the causes of cancer. World Journal of Clinical Oncology. 7(1):54-86

Blechinger, Julia, Bauer, Alexander T., Torrano, Adriano A., Gorzelanny, Christian,Bräuchle, Christoph, Schneider, Stefan W. (2013) Uptake Kinetics and Nanotoxicity of Silica Nanoparticles Are Cell Type Dependent Small, 9(23): 3970-3980

Bossy-Wetzel E, Green DR. (2000) Detection of apoptosis by Annexin V labeling. Methods Enzymol 322:15–18

Bossy-Wetzel, E., Newmeyer, D. D. and Green, D. R. (1998) Mitochondrial cytochrome c release in apoptosis occurs upstream of DEVD-specific caspase activation and independently of mitochondrial transmembrane depolarization EMBO J. 17(1): 37–49

Boukamp P., Petrussevska R. T., Breitkreutz D., Hornung J., Markham A., Fusenig N. E. (1988) Normal keratinization in a spontaneously immortalized aneuploid human keratinocyte cell line. The Journal of Cell Biology. 106(3):761–771

Brandenberger C, Rothen-Rutishauser B, Mühlfeld B, Schmid O, Ferron A, et al. (2010) Effects and uptake of gold nanoparticles deposited at the air–liquid interface of a human epithelial airway model. Toxicology and applied pharmacology 242: 56-65

Bright RK, Vocke CD, Emmert-Buck MR, Duray PH, Solomon D, Fetsch P, Rhim JS, Linehan WM, Topalian SL. (1997) Generation and genetic characterization of immortal human prostate epithelial cell lines derived from primary cancer specimens. Cancer research 57(5): 995-1002

Brust, M. et al., (1994) Synthesis of thiol-derivatised gold nanoparticles in a two-phase Liquid–Liquid system. J. Chem. Soc., Chem. Commun., 0(7): 801–802

Burdall SE, Hanby AM, Lansdown MR, Speirs V. (2003) Breast cancer cell lines: friend or foe? Breast cancer research: BCR 5(2): 89-95.

Butterworth KT, Coulter JA, Jain S, Forker J, McMahon SJ, Schettino G, et al. (2010) Evaluation of cytotoxicity and radiation enhancement using 1.9 nm gold particles: potential application for cancer therapy. Nanotechnology 21: 295101.

C. Wright, A. K. V Iyer, L. Wang, N. Wu, J. S. Yakisich, Y. Rojanasakul and N. Azad (2017) Effects of titanium dioxide nanoparticles on human keratinocytes. Drug Chem. Toxicol. 40, 90–100

Candeloro, P. et al., (2011) Nanoparticle microinjection and Raman spectroscopy as tools for nanotoxicology studies. The Analyst, 136(21): 4402. Available at: http://xlink.rsc.org/?DOI=c1an15313g [Accessed April 20, 2018].

Cedervall T, Lynch I, Lindman S, åBerggrd T, Thulin E, et al. (2007) Understanding the nanoparticleprotein corona using methods to quantify exchange rates and affinities of proteins for nanoparticles. Proceedings of the National Academy of Sciences 104: 2050–2055

Cevc, G (1993). Rational design of new product candidates: the next generation of highly deformable bilayer vesicles for noninvasive, targeted therapy. Journal of Controlled Release. 160 (2): 135–146

Chang, Ke Liang B. Chang, Deng-Fwu Hwang, and Zwe-Ling Kong (2007) In Vitro Cytotoxicitiy of Silica Nanoparticles at High Concentrations Strongly Depends on the Metabolic Activity Type of the Cell Line Environ. Sci. Technol. 41(6): 2064–2068

Chauhan A, Zubair S, Tufail S, Sherwani A, Sajid M, Raman SC, Azam A, Owais M. (2011) Fungusmediated biological synthesis of gold nanoparticles: potential in detection of liver cancer. 6: 2305 – 2319

Chen X-J, Zhang X-Q, Liu Q, Zhang J, Zhou G. (2018) Nanotechnology: a promising method for oral cancer detection and diagnosis. Journal of Nanobiotechnology. 16:52

Cherukuri P, Glazer ES, Curley SA. (2010) Targeted hyperthermia using metal nanoparticles. Adv Drug Deliv Rev. 62(3):339–345

Chidambaram M, Manavalan R, Kathiresan K. (2011) Nanotherapeutics to overcome conventional cancer chemotherapy limitations. J Pharm Pharm Sci. 14(1):67–77

Chithrani BD, Ghazani AA, Chan WCW. (2006) Determining the size and shape dependence of gold nanoparticle uptake into mammalian cells. Nano Lett. 6: 662.

Chithrani BD, Stewart J, Allen C, Jaffray DA. (2009) Intracellular uptake, transport, and processing of nanostructures in cancer cells. Nanomedicine Nanotechnology, Biol Med. 5:118–127.

Cho, W.-S.; Kim, S.; Han, B.S.; Son, W.C.; Jeong, J. (2009) Comparison of gene expression profiles in mice liver following intravenous injection of 4 and 100 nm-sized PEG-coated gold nanoparticles. Toxicol. Lett. 191: 96–102

Cho TJ, MacCuspie RI, Gigault J, Gorham JM, Elliott JT, et al. (2014) Highly stable positively charged dendron-encapsulated gold nanoparticles. Langmuir 30: 3883-3893

Choi YE, Kwak JW, Park JW. (2010) Nanotechnology for early cancer detection. Sensors. 10(1):428–455.

Choi, Y. et al. (2005) Synthesis and functional evaluation of DNA-assembled polyamidoamine dendrimer clusters for cancer cell-specific targeting. Chem. Biol. 12: 35–43

Chun-Ping Jen et al. (2004) A Nonviral Transfection Approach in Vitro: The Design of a Gold Nanoparticle Vector Joint with Microelectromechanical Systems. Langmuir 20(4):1369-74

Cobley CM, Chen J, Cho EC, Wang LV, Xia Y. (2011) Gold nanostructures: a class of multifunctional materials for biomedical applications. Chem Soc Rev 40: 44–56.

Coleman SC, Stewart ZA, Day TA, Netterville JL, Burkey BB, Pietenpol JA. (2002) Analysis of cell-cycle checkpoint pathways in head and neck cancer cell lines: implications for therapeutic strategies. Archives of otolaryngology--head & neck surgery 128(2): 167-176

Collado, M. and Serrano, M. (2010) Senescence in tumours: evidence from mice and humans. Nat. Rev. Cancer. 10: 51–57

Conner, S.D. & Schmid, S.L., (2003) Regulated portals of entry into the cell. Nature, 422(6927): 37–44.

Connor, E. E.; Mwamuka, J.; Gole, A.; Murphy, C. J.; Wyatt, M. D. (2005) Gold nanoparticles are taken up by human cells but do not cause acute cytotoxicity. Small, 1: 325–327

Conrad M, et al. (2016) Regulated necrosis: disease relevance and therapeutic opportunities. Nat Rev Drug Discov. 15:348–66

Cooper GM. (2000) The Cell: A Molecular Approach. 2nd edition. Sunderland (MA): Sinauer Associates; Cell Proliferation in Development and Differentiation.

Croy SR, Kwon GS. (2016) Polymeric micelles for drug delivery. Curr Pharm Des. 12(36):4669-84.

Czabotar PE, et al. (2014) Control of apoptosis by the BCL-2 protein family: implications for physiology and therapy. Nat Rev Mol Cell Biol. 15:49–63.

Dal Canto MC, Gurney ME. (1994) Development of central nervous system pathology in a murine transgenic model of human amyotrophic lateral sclerosis. Am J Pathol 145:1271–9.

Darzynkiewicz Z, Bruno S, Del Bino G, Gorczyca W, Hotz MA, Lassota P, Traganos F. (1992) Features of apoptotic cells measured by flow cytometry. Cytometry. 13:795–808

De Jong W, Borm P. (2008) Drug delivery and nanoparticles: applications and hazards. Int J Nanomedicine 3: 133–49

De Serrano LO, Burkhart DJ. (2017) Liposomal vaccine formulations as prophylactic agents: design considerations for modern vaccines. Journal of Nanobiotechnology 15:83.

Debnath J, Baehrecke EH, Kroemer G. (2005) Does autophagy contribute to cell death? Autophagy 1:66– 74.

DeLong RK, Reynolds CM, Malcolm Y, Schaeffer A, Severs T, Wanekaya (2010) Functionalized gold nanoparticles for the binding, stabilization and delivery of therapeutic DNA, RNA, and other biological macromolecules. Nanotechnol Sci Appl 2010: 53–63.

Derjaguin, B.; Landau, L. (1993) Theory of the Stability of Strongly Charged Lyophobic Sols and of the Adhesion of Strongly Charged Particles in Solutions of Electrolytes. Prog. Surf. Sci. 43: 30–59.

Dobrovolskaia, S. E.; McNeil, M. A. (2007) Immunological properties of engineered nanoparticles. Nat. Nanotechnol., 2: 469–478.

Donaldson K, Borm PJA, Castranova V, Gulumian M. (2009) The limits of testing particle-mediated oxidative stress in vitro in predicting diverse pathologies; relevance for testing of nanoparticles. Particle and Fibre Toxicology. 6:13

Dong X, Mumper RJ. (2010) Nanomedicinal strategies to treat multidrug-resistant tumors: current progress. Nanomedicine (Lond). 5(4):597–615.

Dong, L.; Li, M.; Zhang, S.; Li, J.; Shen, G.; Tu, Y.; Zhu, J.; Tao, J. (2015) Cytotoxicity of BSA-stabilized gold nanoclusters: In vitro and in vivo study. Small 11: 2571–2581

Dubertret, B. et al., (2002) In Vivo Imaging of Quantum Dots Encapsulated in Phospholipid Micelles. Science, 298(5599): 1759–1762

Duellman SJ, Zhou W, Meisenheimer P, Vidugiris G, Cali JJ, Gautam P, Wennerberg K, Vidugiriene J. (2015) Bioluminescent, Nonlytic, Real-Time Cell Viability Assay and Use in Inhibitor Screening. Assay Drug Dev Tech.13(8):456–65.

Durocher, I.; Noël, C.; Lavastre, V.; Girard, D. (2017) Evaluation of the in vitro and in vivo proinflammatory activities of gold(+) and gold(0) nanoparticles. Inflamm. Res. 66: 981–992

Eck, W.; Nicholson, A. I.; Zentgraf, H.; Semler, W.; Bartling S. N. (2010) Anti-cd4-targeted gold nanoparticles induce specific contrast enhancement on peripheral lymphonodes in x-ray computed tomography in live mice. Nano Lett., 10: 2318–2321

Elias DR, Poloukhtine A, Popik V, Tsourkas A. (2013) Effect of ligand density, receptor density, and nanoparticle size on cell targeting. Nanomedicine 9: 194–201

Engel LW, Young NA, Tralka TS, Lippman ME, O'Brien SJ, Joyce MJ. (1978) Establishment and characterization of three new continuous cell lines derived from human breast carcinomas. Cancer research 38(10): 3352-3364

Evan, G. and Littlewood (1998) A matter of life and cell death. Science. 281: 1317–1322

Faix, J. & Rottner, K. (2006) The making of filopodia. Curr. Opin. Cell Biol. 18: 18–25

Fan, J. Li, T., Hung, W., Chen, C., Yeh, J. (2011) Cytotoxicity and differentiation effects of gold nanoparticles to human bone marrow mesenchymal stem cells. Biomed. Eng. Appl. Basis Commun. 23: 141–152

Fang Y, Elahi A, Denley RC, Rao PH, Brennan MF, Jhanwar SC. (2009) Molecular characterization of permanent cell lines from primary, metastatic and recurrent malignant peripheral nerve sheath tumors (MPNST) with underlying neurofibromatosis-1. Anticancer research 29(4): 1255-1262.

Fanord F, Fairbairn K, Kim H, Garces A, Bhethanabotla V, Gupta VK. (2011) Bisphosphonate- modified gold nanoparticles: a useful vehicle to study the treatmentNanotechnology. 22: 035102

Fassas, A. and Anagnostopoulos, A. (2005) The use of liposomal daunorubicin (DaunoXome) in acute myeloid leukemia. Leuk. Lymphoma 46: 795–802

Feinberg AP, Ohlsson R, Henikoff S. (2006) The epigenetic progenitor origin of human cancer. Nat Rev Genet. 7(1):21–33.

Fenart, L. et al. (1999) Evaluation of effect of charge and lipid coating on ability of 60-nm nanoparticles to cross an in vitro model of the blood–brain barrier. J. Pharmacol. Exp. Ther. 291: 1017–1022

Feng, Z. Vivian et al. (2015) Impacts of Gold Nanoparticle Charge and Ligand Type on Surface Binding and Toxicity to Gram-Negative and Gram-Positive Bacteria Chemical Science 6(9): 5186–5196

Ferlay J, Shin HR, Bray F, Forman D, Mathers C, Parkin DM. (2010) Estimates of worldwide burden of cancer in 2008: GLOBOCAN 2008. Int J Cancer. 127(12):2893–2917

Ferrari, M. (2005) Cancer nanotechnology: opportunities and challenges. Nat. Rev. Cancer 5: 161–171

Ferreira, Filomena Adega and Raquel Chaves (2013) The Importance of Cancer Cell Lines as in vitro Models in Cancer Methylome Analysis and Anticancer Drugs Testing, Oncogenomics and Cancer Proteomics Cesar Lopez-Camarillo, Book of Oncogenomics and Cancer Proteomics - Novel Approaches in Biomarkers Discovery and Therapeutic Targets in Cancer, Available at: https://www.intechopen.com/books/oncogenomics-and-cancer-proteomics-novel-approaches-in-biomarkers-discovery-and-therapeutic-targets-in-cancer/the-importance-of-cancer-cell-lines-as-in-vitro-models-in-cancer-methylome-analysis-and-anticancer-drugs [Accessed 25 February, 2019]

Formigli L, Papucci L, Tani A, Schiavone N, Tempestini A, Orlandini GE, Capaccioli S, Orlandini SZ. (2000) Aponecrosis: morphological and biochemical exploration of a syncretic process of cell death sharing apoptosis and necrosis. J Cell Physiol 182:41–9

Fratoddi, I., Venditti, I., Cametti, C., & Russo, M. V. (2015). How toxic are gold nanoparticles? The state-of-the-art. Nano Research 8(6): 1771–1799

Fuchs Y, et al. (2015) Live to die another way: modes of programmed cell death and the signals emanating from dying cells. Nat Rev Mol Cell Biol. 16:329–44.

Galluzzi L, et al. (2016) Caspases connect cell-death signaling to organismal homeostasis. Immunity. 44:221–31

Galluzzi L, et al. (2012) Molecular definitions of cell death subroutines: recommendations of the Nomenclature Committee on Cell Death 2012. Cell Death Differ. 19:107–20

Galluzzi L, et al. (2016) Regulated cell death and adaptive stress responses. Cell Mol Life Sci. 73:2405–10

Galluzzi L., Vitale L. et al. (2018) Molecular mechanisms of cell death: recommendations of the Nomenclature Committee on Cell Death 2018 Cell Death & Differentiation 25:486–541

Gao, W.; Xu, K.; Ji, L.; Tang, B. (2011) Effect of gold nanoparticles on glutathione depletion-induced hydrogen peroxide generation and apoptosis in HL7702 cells. Toxicol. Lett. 205: 86–95

Gao, X. et al. (2005) In vivo molecular and cellular imaging with quantum dots. Curr. Opin. Biotechnol. 16: 63–72

Gazdar AF, Girard L, Lockwood WW, Lam WL, Minna JD. (2010) Lung cancer cell lines as tools for biomedical discovery and research. Journal of the National Cancer Institute 102(17): 1310-1321

Ghosh, P.; Han, G.; De, M.; Kim, C. K.; Rotello, V. M. (2008) Gold nanoparticles in delivery applications. Adv. Drug. Delivery Rev., 60: 1307–1315

Gibbs DD, Pyle L, Allen M, et al. (2002) A phase I dose-finding study of a combination of pegylated liposomal doxorubicin (Doxil), carboplatin and paclitaxel in ovarian cancer. Br J Cancer 86: 1379–84

Giljohann DA, Seferos DS, Patel PC, Millstone JE, Rosi NL, Mirkin CA. (2007) Oligonucleotide loading determines cellular uptake of DNA-modified gold nanoparticles. Nano Lett. 7: 3818–3821

Glazer ES, Massey KL, Zhu C, Curley SA (2010) Pancreatic carcinoma cells are susceptible to noninvasive radio frequency fields after treatment with targeted gold nanoparticles. Surgery 148: 319-324

Goodman CM, Mccusker CD, Yilmaz T, Rotello VM. (2004) Toxicity of Gold Nanoparticles Functionalized with Cationic and Anionic Side Chains. Bioconjugate Chem. 15: 897-900

Gozuacik D, Kimchi A. (2004) Autophagy as a cell death and tumor suppressor mechanism. Oncogene 23:2891–906

Grass, R. N.; Limbach, L. K.; Athanassiou, E. K.; Stark, W. J. (2010) Exposure of aerosols and nanoparticle dispersions to in vitro cell cultures: a review on the dose relevance of size,mass, surface and concentration. J. Aerosol Sci., 41: 1123–1142

Gromnicova, R. et al., (2016) Transport of Gold Nanoparticles by Vascular Endothelium from Different Human Tissues V. P. Shastri, ed. PLOS ONE, 11(8): e0161610

Gu F, Zhang L, Teply BA et al. (2008) Precise engineering of targeted nanoparticles by using self-assembled biointegrated block copolymers. Proc. Natl Acad. Sci. USA 105: 2586–2591

Gu YJ, Chen J, Lin CC, Lam YW, Cheng SH, et al. (2009) Nuclear penetration of surface functionalized gold nanoparticles. Toxicology and applied pharmacology 237: 196-204

Guillermo, F. et al., (2014) Aggregation behaviour of gold nanoparticles in saline aqueous media. Journal of Nanoparticle Research 16:2376:1-11

Gulson B, Wong H. (2016) Stable isotopic tracing – a way forward for nanotechnology. Environ Health Perspect. 114:1486–1488

Gupton, S. L. & Gertler, F. B. (2007) Filopodia: the fingers that do the walking. Sci STKE. 21(400):5

Hainfeld J, Slatkin D, Smilowitz H. (2004) The use of gold nanoparticles to enhance radiotherapy in mice. Phys Med Biol 49: 309–15

Hall S. (1997) Archaeological Chemistry By A. Mark Pollard and Carl Heron (University of Bradford). Royal Society of Chemistry Journal of the American Chemical Society119 (16): 3849-3850

Hanahan, D. and Folkman (1996) Patterns and emerging mechanisms of the angiogenic switch during tumorigenesis. J. Cell. 86: 353–364

Harush-Frenkel, O. et al., (2007) Targeting of nanoparticles to the clathrin-mediated endocytic pathway. Biochemical and Biophysical Research Communications, 353(1): 26–32

Hauck T.S, Ghazani A.A, Chan W.C. (2007) Assessing the Effect of Surface Chemistry on Gold Nanorod Uptake, Toxicity, and Gene Expression in Mammalian Cells. Small, 4: 153-159

Hébert E, Debouttière P, Lepage M, Sanche L, Hunting D. (2010) Preferential tumour accumulation of gold nanoparticles, visualised by magnetic

resonance imaging: Radiosensitisation studies in vivo and in vitro. Int J Radiat Biol 86: 692–700

Hillaireau, H.; Couvreur, P. (2009) Nanocarriers' entry into the cell: relevance to drug delivery. Cell. Mol. Life Sci., 66: 2873-2896

Hiroshi Kurokawa, Toshifumi Morimura, Aki Hanyu, Hiroshi Hama, Hatsuki Osawa, Saori Kashiwagi, Kiyoko Fukami, Takaki Miyata, Hiroyuki Miyoshi, Takeshi Imamura, Masaharu Ogawa, Hisao Masai, Atsushi Miyawaki (2008) Visualizing spatiotemporal dynamics of multicellular cell-cycle progression. Cell. 132(3): 487–498.

Hitomi J, Christofferson DE, Ng A, Yao J, Degterev A, Xavier RJ, Yuan J. (2008) Identification of a molecular signaling network that regulates a cellular necrotic cell death pathway. Cell. 135(7):1311-23

Hofmann WK, de Vos S, Tsukasaki K, Wachsman W, Pinkus GS, Said JW, Koeffler HP. (2001) Altered apoptosis pathways in mantle cell lymphoma detected by oligonucleotide microarray. Blood 98:787–94.

Hondow, N., Brydson, R. & Brown, A. (2014) The use of transmission electron microscopy in the quantification of nanoparticle dose. Journal of Physics: Conference Series, 522(1): 12055

Horbach SP, Halffman W (2017) The ghosts of HeLa: How cell line misidentification contaminates the scientific literature. PLoS ONE 12(10): e0186281.

Hsiao I, Gramatke AM, Joksimovic R, Sokolowski M, Gradzielski M, et al. (2014) Size and Cell Type Dependent Uptake of Silica Nanoparticles. J Nanomed Nanotechnol 5:248

Huang X, Jain P, El-Sayed I, El-Sayed M. (2008) Plasmonic photothermal therapy (PPTT) using gold nanoparticles. Lasers Med Sci 2008; 23: 217–28.

Ichihara, K. et al., (2013) Encapsulation-Induced Remarkable Stability of a Hydrogen-Bonded Heterocapsule. Chemistry - A European Journal, 19(11): 3685–3692

Immordino, M.L. et al. (2006) Stealth liposomes: reviewof the basic science, rationale, and clinical applications, existing and potential. Int. J. Nanomed. 1: 297–315

Imperatore, R.; Carotenuto, G.; Di Grazia, M.A.; Ferrandino, I.; Palomba, L.; Mariotti, R.; Vitale, E.; De Nicola, S.; Longo, A.; et al. (2015) Imidazole-stabilized gold nanoparticles induce neuronal apoptosis: An in vitro and in vivo study. J. Biomed. Mater. Res. A 103: 1436–1446

Irma Colombo, Enrico Sangiovanni, Roberta Maggio, et al. (2017) HaCaT Cells as a Reliable In Vitro Differentiation Model to Dissect the Inflammatory/Repair Response of Human Keratinocytes Mediators of Inflammation Volume 2017, Article ID 7435621, 12 pages

Iversen, T.-G.; Skotland, T.; Sandvig, K. (2011) Endocytosis and intracellular transport of nanoparticles: Present knowledge and need for future studies. Nano Today, 6: 176-185

Jacquemet G, Hamidi H, Ivaska J. (2015) Filopodia in cell adhesion, 3D migration and cancer cell invasion. Curr. Opin. Cell Biol. 36: 23–31

Jacquemet G, Ilkka Paatero, Alexandre F. Carisey, Artur Padzik, Jordan S. Orange, Hellyeh Hamidi, Johanna Ivaska (2017) FiloQuant reveals increased filopodia density during breast cancer progression J Cell Biol jcb.201704045

Jaffee EM, Dang CV, Agus DB, et al. (2017) Future cancer research priorities in the USA: a Lancet Oncology Commission. The Lancet Oncology. 18:11

James ND, Coker RJ, Tomlinson D, et al. (1994) Liposomal doxorubicin (Doxil): An effective new treatment for Kaposi's sarcoma in AIDS. Clin Oncol (R Coll Radiol) 6:294–6

Jepson MA, Clark MA. (1998) Studying M cells and their role in infection. Trends Microbiol. 6:359–365

Jokerst, J. V et al., (2011) Nanoparticle PEGylation for imaging and therapy. Nanomedicine, 6(4): 715–728

Jones LJ1, Gray M, Yue ST, Haugland RP, Singer VL. (2001) Sensitive determination of cell number using the CyQUANT cell proliferation assay. J Immunol Methods. 254(1-2):85-98

Julien O, et al. (2016) Quantitative MS-based enzymology of caspases reveals distinct protein substrate specificities, hierarchies, and cellular roles. Proc Natl Acad Sci U S A 113:E2001–10

Kafshgari, M., Harding, F. & Voelcker, N., (2015) Insights into Cellular Uptake of Nanoparticles. Current Drug Delivery, 12(1): 63–77

Kao J, Salari K, Bocanegra M, Choi YL, Girard L, Gandhi J, Kwei KA, Hernandez-Boussard T, Wang P, Gazdar AF et al. (2009) Molecular profiling of breast cancer cell lines defines relevant tumor models and provides a resource for cancer gene discovery. PloS one 4(7): e6146

Kawasaki H, Taira K. (2004) Induction of DNA methylation and gene silencing by short interfering RNAs in human cells. Nature 431(7005): 211-217

Khan JA, Pillai B, Das TK, Singh Y, Maiti S. Molecu- lar (2007) Effects of Uptake of Gold Nanoparticles in HeLa Cells . ChemBioChem. 8: 1237

Kievit, F.M. et al., (2011) Cancer Nanotheranostics: Improving Imaging and Therapy by Targeted Delivery Across Biological Barriers. Available at www.advmat.de www.MaterialsViews.com [Accessed at 20 April, 2018]

Kim C, Ghosh P, Rotello V. (2009) Multimodal drug delivery using gold nanoparticles. Nanoscale 1: 61–7

Kim H, et al. (2006) Hierarchical regulation of mitochondrion dependent apoptosis by BCL-2 subfamilies. Nat Cell Biol. 8:1348–58

Kim JB, Stein R, O'Hare MJ (2004) Three-dimensional in vitro tissue culture models of breast cancer – a review. Breast Cancer Res Treat 85(3):281-91

Kim, J., Piao, Y. & Hyeon, T. (2009) Multifunctional nanostructured materials for multimodal imaging, and simultaneous imaging and therapy. Chemical Society reviews, 38(2): 372–90

Kimling J, Maier M, Okenve B, Kotaidis V, Ballot H, and Plech A. (2006) Turkevich Method for Gold Nanoparticle Synthesis Revisited. J. Phys. Chem. B. 110 (32): 15700–15707

Klumpp C., K. Kostarelos, M. Prato, and A. Bianco (2006) Functionalized carbon nanotubes as emerging nanovectors for the delivery of therapeutics Biochimica et Biophysica Acta, vol. 1758(3): 404–412

Kondath, S.; Raghavan, B.S.; Anantanarayanan, R.; Rajaram, R. (2014) Synthesis and characterisation of morin reduced gold nanoparticles and its cytotoxicity in MCF-7 cells. Chem.-Biol. Interact. 224: 78–88

Kressel M, Groscurth P. (1994) Distinction of apoptotic and necrotic cell death by in situ labelling of fragmented DNA. Cell Tissue Res 278:549–56

Kreuter, J. et al. (2003) Direct evidence that polysorbate-80-coated poly(butylcyanoacrylate) nanoparticles deliver drugs to the CNS via specific mechanisms requiring prior binding of drug to the nanoparticles. Pharm. Res. 20: 409–416

Kroemer G, et al. (2009) Classification of cell death: recommendations of the Nomenclature Committee on Cell Death Cell Death Differ. 16: 3–11

Kromer et al. (2005) Classification of cell death Cell death differ 12: 1463-7

Kumar S, Harrison N, Richards-Kortum R, Sokolov K. (2007) Plasmonic nanosensors for imaging intracellular biomarkers in live cells. Nano Lett 7: 1338–43

Lacroix M, Leclercq G. (2004) Relevance of breast cancer cell lines as models for breast tumours: an update. Breast cancer research and treatment 83(3): 249-289

Lanone S, Rogerieux F, Geys J, Dupont A, Maillot-Marechal E, et al. (2009) Comparative toxicity of 24 manufactured nanoparticles in human alveolar epithelial and macrophage cell lines. Part FibreToxicol 6: 14

Lasagna-Reeves C, Gonzalez-Romero D, Barria MA, Olmedo I, Clos A, Ramanujam VMS, Urayama A, Vergara L, Kogan MJ, Soto C. (2010) Bioaccumulation and toxicity of gold nanoparticles after repeated administration in mice. Biochem Biophys Res Commun. 393:649–655

Lee S, Chon H, Lee M, Choo J, Shin S, Lee Y, et al. (2009) Surface-enhanced Raman scattering imaging of HER2 cancer markers overexpressed in single MCF7 cells using antibody conjugated hollow gold nanospheres. Biosens Bioelectron 24: 2260–3

Lee, J.-S. et al. (2010) “Magnet-in-the-Semiconductor” FePt−PbS and FePt−PbSe Nanostructures: Magnetic Properties, Charge Transport, and Magnetoresistance. Journal of the American Chemical Society, 132(18): 6382–6391

Leone G, Voso MT, Teofili L, Lubbert M. (2003) Inhibitors of DNA methylation in the treatment of hematological malignancies and MDS. Clin Immunol 109(1): 89-102

Leonetti C, Scarsella M, Zupi G, Zoli W, Amadori D, Medri L, Fabbri F, Rosetti M, Ulivi P, Cecconetto L et al. (2006) Efficacy of a nitric oxide-releasing nonsteroidal anti-inflammatory drug and cytotoxic drugs in human colon cancer cell lines in vitro and xenografts. Molecular cancer therapeutics 5(4): 919-926

Lewinski N, Colvin V, Drezek R. (2010) Cytotoxicity of nanoparticles. Small. 4:26–49.

Li P, et al. (1997) Cytochrome c and dATP-dependent formation of Apaf-1/caspase-9 complex initiates an apoptotic protease cascade. Cell. 91:479–89

Libutti SK, Paciotti GF, Byrnes AA, Alexander HR Jr, Gannon WE, Walker M, et al. (2010) Phase I and pharmacokinetic studies of CYT-6091, a novel PEGylated colloidal gold-rhTNF nanomedicine. Clin Cancer Res 16: 6139–49

Ling, D. et al., (2014) Multifunctional Tumor pH-Sensitive Self-Assembled Nanoparticles for Bimodal Imaging and Treatment of Resistant Heterogeneous Tumors. Journal of the American Chemical Society, 136(15): 5647–5655

Ling, D., Hackett, M. J., & Hyeon, T. (2014). Surface ligands in synthesis, modification, assembly and biomedical applications of nanoparticles. Nano Today, 9(4): 457–477

Liu C, Li BQ, Mi CC. (2009) Fast transient thermal analysis of gold nanoparticles in tissue-like medium. IEEE Trans Nanobioscience 8: 271–80

Liu H, Doane TL, Cheng Y, et al. (2015) Control of Surface Ligand Density on PEGylated Gold Nanoparticles for Optimized Cancer Cell Uptake. Part. Part. Syst. Charact. [Internet]. 32(2): 197–204

Liu, G. et al., (2003) Nanoparticles of Compacted DNA Transfect Postmitotic Cells. Journal of Biological Chemistry, 278(35): 32578–32586

Liu, G.; Li, Q.; Ni, W.; Zhang, N.; Zheng, X.; Wang, Y.; Shao, D.; Tai, G. (2015) Cytotoxicity of various types of gold-mesoporous silica nanoparticles in human breast cancer cells. Int. J. Nanomed. 10: 6075–6087

Louzada S, Adega F, Chaves R. (2012) Defining the sister rat mammary tumor cell lines HH-16 cl.2/1 and HH-16.cl.4 as an in vitro cell model for Erbb2. PloS one 7(1): e29923

Love, J.C. et al., (2005) Self-Assembled Monolayers of Thiolates on Metals as a Form of Nanotechnology. Chemical Reviews, 105(4): 1103–1170

Low A, Bansal V. (2010) A visual tutorial on the synthesis of gold nanoparticles. Biomed Imaging Interv J. 6(1):e9

Lowe, S.W., Cepero, E., and Evan, G (2004) Intrinsic tumour suppression. Nature. 432: 307–315

Lund, T., Callaghan, M. F., Williams, P., Turmaine, M., Bachmann, C., Rademacher, T., Bayford, R. (2011) The influence of ligand organization on the rate of uptake of gold nanoparticles by colorectal cancer cells. Biomaterials, 32: 9776–9784

Madani SY, Naderi N, Dissanayake O, Tan A, Seifalian AM. (2011) A new era of cancer treatment: carbon nanotubes as drug delivery tools. Int J Nanomedicine. 6:2963–2979

Maeda, H. et al. (2000) Tumor vascular permeability and the EPR effect in macromolecular therapeutics: a review. J. Control. Release 65: 271–284

Maiorano, G.; Sabella, S.; Sorce, B.; Brunetti, V.; Malvindi, M. A.; Cingolani, R.; Pompa, P. P. (2010) Effects of Cell Culture Media on the Dynamic

Formation of Protein Nanoparticle Complexes and Influence on the Cellular Response. ACS Nano 4: 7481–7491

Mallavarapu, A. & Mitchison, T. (1999) Regulated actin cytoskeleton assembly at filopodium tips controls their extension and retraction. J. Cell Biol. 146: 1097–1106

Marquis, B. J.; Love, S. A.; Brown, K. L.; Haynes, C. L. (2009) Analytical methods to assess nanoparticle toxicity. Analyst 134: 425–439

Martin MN, Basham JI, Chando P, Eah SK. (2010) Charged gold nanoparticles in non-polar solvents: 10-min synthesis and 2D self-assembly Langmuir. 26 (10): 7410

Matsumura Y, Maeda H. (1986) A new concept for macromolecular therapeutics in cancer chemotherapy: mechanism of tumoritropic accumulation of proteins and the antitumor agent smancs Cancer Res. 46(12 Pt 1):6387-92

Maurice Tubiana (1989) Tumor Cell Proliferation Kinetics and Tumor Growth Rate, Acta Oncologica, 28(1): 113-121

May, R.; Machesky, L. (2001) Phagocytosis and the actin cytoskeleton. J. Cell Sci., 114: 1061-1077

McCarthy, J. & Weislender, R., (2008) Multifunctional magnetic nanoparticles for targeted imaging and therapy Advanced Drug Delivery Reviews, 60(11): 1241–1251

McMahon, H.; Boucrot, E. (2011) Molecular mechanism and physiological functions of clathrin-mediated endocytosis. Nat. Rev. Mol. Cell Biol., 12: 517-533

Menjoge, A.R. et al. (2010) Dendrimer-based drug and imaging conjugates: design considerations for nanomedical applications. Drug Discov. Today 15: 171–185

Micallef L., Belaubre F., Pinon A., et al. (2009) Effects of extracellular calcium on the growth-differentiation switch in immortalized keratinocyte HaCaT cells compared with normal human keratinocytes. Experimental Dermatology. 18(2):143–151

Mironava T, Hadijargyrou M, Simon M, Jurukovski V, Rafailovich MH (2010) Gold nanoparticles cellular toxicity and recovery: effect of size, concentration and exposure time. Nanotoxicology 4(1):120-37

Misra R., Sarbari Acharya and Sanjeeb K. Sahoo (2010) Cancer nanotechnology: application of nanotechnology in cancer therapy Drug Discovery Today 15: 843-849

Misra, R. and Sahoo, S.K. (2010) Intracellular trafficking of nuclear localization signal conjugated nanoparticles for cancer therapy. Eur. J. of Pharm. Sci. 39: 152–163

Mohanty, C. and Sahoo, S.K. (2010) The in vitro stability and in vivo pharmacokinetics of curcumin prepared as an aqueous nanoparticulate formulation. Biomaterials 31: 6597–6611

Monopoli M, Walczyk D, Campbell A, Elia G, Lynch I, et al. (2011) Physical-chemical aspects of protein corona: Relevance to in vitro and in vivo biological impacts of nanoparticles. Journal of the American Chemical Society 133: 2525–2534

Monteiro-Riviere NA, Inman AO, Oldenburg SJ. (2010) Interactions of aluminum nanoparticles with human epidermal keratinocytes. J Appl Toxicol. 30:276–285

Mora, R. et al., (1999) Caveolin-2 localizes to the golgi complex but redistributes to plasma membrane, caveolae, and rafts when co-expressed with caveolin-1. The Journal of biological chemistry, 274(36): 25708–17

Mosmann T. (1983) Rapid colorimetric assay for cellular growth and survival: Application to proliferation and cytotoxicity assays. J. Immunol. Meth. 65:55–63

Moss OR, Wong VA. (2006) When nanoparticles get in the way: impact of projected area on in vivo and in vitro macrophage function. Inhal Toxicol. 18:711–716

Muller, R; Keck, C (2004) Challenges and solutions for the delivery of biotech drugs – a review of drug nanocrystal technology and lipid nanoparticles. Journal of Biotechnology. 113 (1–3): 151–170

Muñoz, A.; Costa, M. (2012) Elucidating the mechanisms of nickel compound uptake: A review of particulate and nano-nickel endocytosis and toxicity. Toxicol. Appl. Pharmacol., 260: 1-16

Nabeshi H, Yoshikawa T, Matsuyama K,Nakazato Y, Arimori A, et al. (2010) Size-dependent cytotoxic effects of amorphous silica nanoparticles on Langerhans cells. Pharmazie 65: 199-201

Nakamura Y., Ai Mochida, Peter L. Choyke, and Hisataka Kobayashi (2016) Nanodrug Delivery: Is the Enhanced Permeability and Retention Effect Sufficient for Curing Cancer? Bioconjugate Chem. 27(10): 2225-2238

Nan A, Bai X, Son SJ, Lee SB, Ghandehari H. (2008) Cellular uptake and cytotoxicity of silica nanotubes. Nano Lett. 8:2150–2154

Nebbioso A, Tambaro FP, Dell'Aversana C, Altucci L. (2018) Cancer epigenetics: Moving forward. Greally JM, ed. PLoS Genetics. 14(6):e1007362

Nel A, Xia T, Mädler L, Li N. (2006) Toxic potential of nanomaterials at nanolevel. Science. 311:622–674

Nie, S. et al. (2007) Nanotechnology applications in cancer. Annu. Rev. Biomed. Eng. 9: 257–288

Nirmala, J.G.; Akila, S.; Narendhirakannan, R.T.; Chatterjee, S. (2017) Polyphenols stabilized gold nanoparticles induce cytotoxicity and apoptotic cell death in A431 skin cancer cell lines. Adv. Powder Technol. 28:1170–1184

Oberdörster G, Maynard A, Donaldson K, et al. (2005) Principles for characterizing the potential human health effects from exposure to nanomaterials: elements of a screening strategy. Part Fibre Toxicol. 2:1–35

Ohta Y, Suzuki N, Nakamura S, Hartwig JH, Stossel TP (1999) The small GTPase RalA targets filamin to induce filopodia". Proc. Natl. Acad. Sci. U.S.A. 96 (5): 2122–8

Olie RA, et al. (1998) Apparent caspase independence of programmed cell death in Dictyostelium. Curr Biol.8:955–58

Organisation for Economic Co-operation and Development (OECD). (2016) Physical-Chemical Properties of Nanomaterials: Evaluation of Methods Applied in the OECD-WPMN Testing Programme; OECD Environment, Health and Safety Publications Series on the Safety of Manufactured Nanomaterials ENV/JM/MONO(2016)7;OECD: Paris, France

Otsuki Y, Li Z, Shibata MA. (2003) Apoptotic detection methods–from morphology to gene. Prog Histochem Cytochem 38:275

Pan Y, Leifert A, Ruau D et al (2009) Gold nanoparticles of diameter 1.4 nm trigger necrosis by oxidative stress and mitochondrial damage. Small 5(18):2067–2076

Pan, Y.; Neuss, S.; Leifert, A.; Wen, F.; Simon, U.; Schmid, G.; Brandau, W.; Jahnen-Dechent, W. (2007) Size-dependent cytotoxicity of gold nanoparticles. Small 3: 1941–1949

Park JW. (2002) Liposome-based drug delivery in breast cancer treatment. Breast Cancer Res. 4(3):95-9

Park K. (2012) Polysaccharide-based near-infrared fluorescence nanoprobes for cancer diagnosis. Quantitative Imaging in Medicine and Surgery. 2(2):106-113

Pasparakis M, et al. (2015) Necroptosis and its role in inflammation. Nature. 517:311–20

Patra CR, Bhattacharya R, Mukhopadhyay D, Muk- herjee P. (2010) Fabrication of gold nanoparticles for targeted therapy in pancreatic cancer. Advanced Drug Delivery Reviews. 62: 346–361

Patra HK, Banerjee S, Chaudhuri U, Lahiri P, Dasgupta AK (2007) Cell selective response to gold nanoparticles. Nano- medicine 3:111–119

Pelkmans, L. & Helenius, A., (2002) Endocytosis via caveolae. Traffic (Copenhagen, Denmark), 3(5): 311–20

Peng, G.; Tisch, U.; Adams, O.; Hakim, M.; Shehada, N.; Broza, Y. Y.; Billan, S.; Abdah-Bortnyad, R.; Kuten, R.; Haick, H. (2009) Diagnosing lung cancer in exhaled breath using gold nanoparticles. Nat. Nanotechnol. 4: 669–673

Perrault SD, Chan WCW. (2009) Synthesis and Surface Modification of Highly Monodispersed, Spherical Gold Nanoparticles of 50-200 nm J. Am. Chem. Soc. 131 (47): 17042

Pinaud, F. et al. (2006) Advances in fluorescence imaging with quantum dot bioprobes. Biomaterials 27: 1679–1687

Podila, R. et al., (2012) Effects of surface functional groups on the formation of nanoparticle-protein corona. Applied Physics Letters, 101(26): 263701

Portney, N.G. and Ozkan, M. (2006) Nano-oncology: drug delivery, imaging, and sensing. Anal. Bioanal. Chem. 384: 620–630

Puri A, Kramer-Marek G, Campbell-Massa R, et al. (2008) HER2-specific affibody-conjugated thermosensitive liposomes (Affisomes) for improved delivery of anticancer agents. J Liposome Res. 18(4):293–307

Qiu, Y.; Liu, Y.; Wang, L. M.; Xu, L. G.; Bai, R.; Ji, Y. L.; Wu, X. C.; Zhao, Y. L.; Li, Y. F.; Chen, C. Y. (2010) Surface Chemistry and Aspect Ratio Mediated Cellular Uptake of Au Nanorods. Biomaterials 31: 7606–7619

Qureshi S. R., Y. P. Sahni, S. K. Singh, M.A. Bhat, A.A. Dar, S.A. Quadri (2011) Nanotechnology based drug delivery systems Journal of Pharmaceutical Research and Opinion 1(6): 161 – 165

Ramalingam, V.; Revathidevi, S.; Shanmuganayagam, T.S.; Muthulakshmi, L.; Rajaram, R. (2016) Biogenic gold nanoparticles induce cell cycle arrest through oxidative stress and sensitize mitochondrial membranes in A549 lung cancer cells. RSC Adv. 6: 20598–20608.

Rasmussen, K.; Rauscher, H.; Mech, A.; Riego Sintes, J.; Gilliland, D.; González, M.; Kearns, P.; Moss, K.; Visser, M.; Groenewold, M.; et al. (2018) Physico-chemical properties of manufactured nanomaterials—Characterisation and relevant methods. An outlook based on the OECD Testing Programme. Regul. Toxicol. Pharmacol. RTP 92: 8–28

Rausch, K.; Reuter, A.; Fischer, K.; Schmidt, M. (2010) Evaluation of Nanoparticle Aggregation in Human Blood Serum. Biomacromolecules 11, 2836–2839

Reitsma, Sietze. (2007) The endothelial glycocalyx: composition, functions, and visualization." European Journal of Physiology. 454(3): 345-359

Renault S, Baudrimont M, Mesmer-DudonsN, Gon- zalez P, Mornet S, Brisson A. (2008) Impacts of gold nanoparticle exposure on two freshwater species: a phytoplanktonic alga (Scenedesmus subspicatus) and a benthic bivalve (Corbicula fluminea). Gold Bulletin 41(2): 116-126

Riedl SJ, et al. (2007) The apoptosome: signalling platform of cell death. Nat Rev Mol Cell Biol. 8:405–13

Riss T. Richard A. Moravec (2004) Use of Multiple Assay Endpoints to Investigate the Effects of Incubation Time, Dose of Toxin, and Plating Density in Cell-Based Cytotoxicity Assays ASSAY and Drug Development Technologies 2(1): 3123-228

Roebben, G.; Rasmussen, K.; Kestens, V.; Linsinger, T.P.J.; Rauscher, H.; Emons, H.; Stamm, H. (2013) Reference materials and representative test materials: The nanotechnology case. J. Nanopart. Res.15

Roos WP, et al. (2016) DNA damage and the balance between survival and death in cancer biology. Nat Rev Cancer. 16:20–33

Rosenblum D, Joshi N, Tao W, Karp JM, Peer D. (2018) Progress and challenges towards targeted delivery of cancer therapeutics. Nature Communications. 9:1410

Roth J. (1996) The silver anniversary of gold: 25 years of the colloidal gold marker system for immunocytochemistry and histochemistry. Histochem Cell Biol 106: 1–8

Rothberg, K.G. et al., (1992) Caveolin, a protein component of caveolae membrane coats. Cell, 68(4): 673–82

Rothen-Rutishauser BM, Kiama SG, Gehr P. (2005) A three-dimensional cellular model of the human respiratory tract to study the interaction with particles. Am J Respir Cell Mol Biol. 32:281– 289

Sagnella, S.; Drummond, C. (2012) Drug Delivery: A Nanomedicine Approach. Australian Biochemist. The Australian Society for Biochemistry and Molecular Biology. 43: 5–8

Sahay, G.; Alakhova, D.; Kabanov, A. (2010) Endocytosis of nanomedicines. J. Control. Release, 145: 182-95

Sahoo, S.K. and Labhasetwar, V. (2003) Nanotech approaches to drug delivery and imaging. Drug Discov. Today 8: 1112–1120

Sajanlal PR, Sreeprasad TS, Samal AK, Pradeep T. (2011) Anisotropic nanomaterials: structure, growth, assembly, and functions. Nano Rev. 2: 3402

Salic, A., & Mitchison, T. J. (2008). A chemical method for fast and sensitive detection of DNA synthesis in vivo. Proceedings of the National Academy of Sciences of the United States of America, 105(7): 2415–2420

Sardar R, Funston AM, Mulvaney P, Murray RW. (2009) Gold Nanoparticles: Past, Present, and Future. Langmuir. 25(24): 13840–13851

Sasahira T, Kirita T. (2018) Hallmarks of Cancer-Related Newly Prognostic Factors of Oral Squamous Cell Carcinoma. International Journal of Molecular Sciences. 19(8):2413

Schaeublin, N.M.; Braydich-Stolle, L.K.; Schrand, A.M.; Miller, J.M.; Hutchison, J.; Schlager, J.J.; Hussain, S.M. (2011) Surface charge of gold nanoparticles mediates mechanism of toxicity. Nanoscale 3: 410–420

Schmid, O.; Moller,W.; Semmler-Behnke,M.; Ferron,G. A.; Karg,E.; Lipka, J.; Schulz, H.; Kreyling, W. G.; Stoeger, T. (2009) Dosimetry and toxicology of inhaled ultrafine particles (review). Biomarkers 14: 67–73

Schubertová V, Martinez-Veracoechea FJ, Vácha R. (2015) Influence of ligand distribution on uptake efficiency. Soft Matter 11(14): 2726–2730

Schwartz LM, Smith SW, Jones ME, Osborne BA. (1993) Do all programmed cell deaths occur via apoptosis? Proc Natl Acad Sci USA 90:980–4

Scita, G., Confalonieri, S., Lappalainen, P. & Suetsugu, S. (2008) IRSp53: crossing the road of membrane and actin dynamics in the formation of membrane protrusions. Trends Cell Biol. 18: 52–60

Scorrano L, Ashiya M, Buttle K, Weiler S, Oakes SA, Mannella CA, Korsmeyer SJ. (2002) A distinct pathway remodels mitochondrial cristae and mobilizes cytochrome c during apoptosis. Dev Cell 2:55– 67

Sekino, Y., Kojima, N. & Shirao, T. (2007) Role of actin cytoskeleton in dendritic spine morphogenesis. Neurochem. Int. 51: 92–104

Sengupta, S. et al. (2005) Temporal targeting of tumour cells and neovasculature with a nanoscale delivery system. Nature 436: 568–572

Shang, L., Nienhaus, K. & Nienhaus, G., (2014) Engineered nanoparticles interacting with cells: size matters. Journal of Nanobiotechnology, 12(1): 5

Shukla R, Bansal V, Chaudhary M, Basu A, Bhonde RR, Sastry M (2005) Biocompatibility of gold nanoparticles and their endocytotic fate inside the cellular compartment: a microscopic overview. Langmuir 21:10644–10654

Sigal, Y. J., Quintero, O. A., Cheney, R. E. & Morris, A. J. (2007) Cdc42 and ARP2/3-independent regulation of filopodia by an integral membrane lipid-phosphatase-related protein. J. Cell Sci. 120: 340–352

Sikora K. (2002) The impact of future technology on cancer care. Clin Med. 2(6):560–568

Singh OP, Nehru RM. (2008) Nanotechnology and cancer treatment. Asian J Exp Sci. 22(2):6

Singh P, Pandit S, Mokkapati VRSS, Garg A, Ravikumar V, Mijakovic I. (2018) Gold Nanoparticles in Diagnostics and Therapeutics for Human Cancer. International Journal of Molecular Sciences. 19(7):1979

Sinha R, Kim GJ, Nie S, Shin DM. (2006) Nanotechnology in cancer therapeutics: bioconjugated nanoparticles for drug delivery. Mol Cancer Ther. 5(8):1909–1917

Smith, A. et al., (2008) Bioconjugated quantum dots for in vivo molecular and cellular imaging. Advanced Drug Delivery Reviews, 60(11): 1226–1240

Soenen, S. J.; De Cuyper, M. (2009) Assessing cytotoxicity of (iron-oxide based) nanoparticles: An overwiew of different methods exemplified with cationic magnetoliposomes. Contrast Media Mol. Imaging 4: 207–219

Soenen, S. J.; Rivera-Gil, P.; Montenegro, J-M.; Parak, W. J.; De Smedt, S. C.; Braeckmans, K. (2011) Cellular toxicity of inorganic nanoparticles: Common aspects and guidelines for improved nanotoxicity evaluation. Nano Today, 6: 446–465

Sohaebuddin SK1, Thevenot PT, Baker D, Eaton JW, Tang L. Part Fibre (2010) Nanomaterial cytotoxicity is composition, size, and cell type dependent. Toxicol. 21: 7:22

Soo Choi, H. et al., (2007) Renal clearance of quantum dots. Nature Biotechnology, 25(10): 1165–1170

Sperling R, Rivera Gil P, Zhang F, Zanella M, Parak W. (2008) Biological applications of gold nanoparticles. Chem Soc Rev 37: 1896–908

Staveren WC, Solis DY, Hebrant A, Detours V, Dumont JE, Maenhaut C. (2009) Human cancer cell lines: Experimental models for cancer cells in situ? For cancer stem cells? Biochimica et biophysica acta 1795(2): 92-103

Steketee, M. B. & Tosney, K. W. (2002) Three functionally distinct adhesions in filopodia: shaft adhesions control lamellar extension. J. Neurosci. 22: 8071–8083

Stockert J. C, Alfonso Blázquez-Castro (2017) Fluorescence Microscopy in Life Sciences. Bentham Science Publishers.

Sundquist T., Moravec R. Nles A. et al. (2006) Timing your apoptosis assays Cell notes 16: 18-21

Sung, J. H.; Ji, J. H.; Park, J. D.; Song, M. Y.; Song, K. S.; Ryu, H. R.; Yoon, J. U.; Jeon, K. S.; Jeong, J.; Han, B. S.; Chung, Y. H.; Chang, H. K.; Lee, J. H.; Kim, D. W.; Kelman, B. J.; Yu, I. J. (2011) Acute inhalation toxicity of silver nanoparticles.Part. Fibre Toxicol. 8: 16-18

Svenson, S. and Tomalia, D.A. (2005) Dendrimers in biomedical applications–reflections on the field. Adv. Drug Deliv. Rev. 57: 2106–2129

Tarbell J, Cancel L. (2016) The glycocalyx and its significance in human medicine. J Intern Med. 280(1):97-113

Teeguarden JG, Hinderliter PM, Orr G, Thrall BD, Pounds JG. (2007) Particokinetics in vitro: dosimetry considerations for in vitro nanoparticle toxicity assessments. Toxicol Sci. 95:300–312

Thomas S, Popov VL, Walker DH (2010) Exit Mechanisms of the Intracellular Bacterium Ehrlichia PLoS ONE 5(12): e15775

Thuret G, Chiquet C, Herrag S, et al. (2003) Mechanisms of staurosporine induced apoptosis in a human corneal endothelial cell line. The British Journal of Ophthalmology. 87(3):346-352

Tian Xia, Michael Kovochich, Monty Liong, Jeffrey I. Zink, and Andre E. Nel (2008) Cationic Polystyrene Nanosphere Toxicity Depends on Cell-Specific Endocytic and Mitochondrial Injury Pathways ACS Nano 2(1): 85-96

Timbrell,J. A. (1998) Biomarkers in toxicology. Toxicology, 129: 1–12

Tomlinson GE, Chen TT, Stastny VA, Virmani AK, Spillman MA, Tonk V, Blum JL, Schneider NR, Wistuba, II, Shay JW et al. (1998) Characterization of a breast cancer cell line derived from a germ-line BRCA1 mutation carrier. Cancer research 58(15) 3237- 3242

Torchilin, V (2006). Multifunctional nanocarriers. Advanced Drug Delivery Reviews. 58 (14): 1532–55

Torchilin, V. (2008) Antibody-modified liposomes for cancer chemotherapy. Expert Opin. Drug Deliv. 5: 1003–1025

Torchilin, V.P. et al. (2003) Immunomicelles: targeted pharmaceutical carriers for poorly soluble drugs. Proc. Natl. Acad. Sci. U. S. A. 100: 6039–6044

Tran, N.; Webster, T. J. (2013) Understanding magnetic nanoparticle osteoblast receptor-mediated endocytosis using experiments and modeling. Nanotechnology, 24: 185102

Tsien RY (1998) The green fluorescent protein. Annu Rev Biochem 67: 509–44

Tsoli M, Kuhn H, Brandau W, Esche H, Schmid G. (2005) Cellular Uptake and Toxicity of Au55 Clusters. Small. 1(8-9): 841–844

Turmaine M, Raza A, Mahal A, Mangiarini L, Bates GP, Davies SW. (2000) Nonapoptotic neurodegeneration in a transgenic mouse model of Huntington's disease. Proc Natl Acad Sci USA 97:8093–7

Vallat L, Magdelenat H, Merle-Beral H, Masdehors P, Potocki de Montalk G, Davi F, Kruhoffer M, Sabatier L, Orntoft TF, Delic J. (2003) The resistance of B-CLL cells to DNA damage-induced apoptosis defined by DNA microarrays. Blood 101:4598–606

Van Doren EAF, Temmerman PRHD, Francisco AD, Mast J. (2011) Determination of the volume specific surface area by using transmission electron tomography for characterization and definition of nanomaterials. Jour- nal of Nanobiiotechnology. 9:17

Vargo-Gogola T, Rosen JM. (2007) Modelling breast cancer: one size does not fit all. Nature reviews Cancer 7(9): 659-672

Vasioukhin, V., Bauer, C., Yin, M. & Fuchs, E. (2000) Directed actin polymerization is the driving force for epithelial cell–cell adhesion. Cell 100: 209–219

Verma, A. et al., (2008) Surface-structure-regulated cell-membrane penetration by monolayer-protected nanoparticles. Nature Materials, 7(7): 588–595

Vermes I, Haanen C, Reutelingsperger C. (2000) Flow cytometry of apoptotic cell death. J Immunol Methods. 243:167–190

Vermes I, Haanen C, Steffens-Nakken H, Reutelingsperger C. (1995) A novel assay for apoptosis. Flow cytometric detection of phosphatidylserine expression on early apoptotic cells using fluorescein labeled Annexin V. J Immunol Methods 184: 39–51

Villiers CL, Freitas H, Couderc R, Villiers MB, Marche PN (2009) Analysis of the toxicity of gold nanoparticles on the immune system: effect on dendritic cell functions. J Nanopart Res 12:55–60

Vinodgopal K, Neppolian B, Lightcap IV, Grieser F, Ashokkumar M, Kamat PV. (2010) Sonolytic Design of Graphene−Au Nanocomposites. Simultaneous and Sequential Reduction of Graphene Oxide and Au(III) J. Phys. Chem. Lett., 1(13): 1987–1993

Wang, W. et al., (2012) Autonomous Motion of Metallic Microrods Propelled by Ultrasound. ACS Nano, 6(7): 6122–6132

Wang, X. et al. (2008) Application of nanotechnology in cancer therapy and imaging. CA Cancer J. Clin. 58: 97–110

Ward, M. W., Rego, A. C., Frenguelli, B. G. and Nicholls, D. G. (2000) Mitochondrial membrane potential and glutamate excitotoxicity in cultured cerebellar granule cells. J. Neurosci. 20: 7208 -7219

Weinlich R, et al. (2017) Necroptosis in development, inflammation and disease. Nat Rev Mol Cell Biol. 18:127–36

Weissleder, R. et al., (2005) Cell-specific targeting of nanoparticles by multivalent attachment of small molecules. Nature Biotechnology, 23(11): 1418–1423

White MK, Cinti C. (2004) A morphologic approach to detect apoptosis based on electron microscopy. Methods Mol Biol 285:105–11

William J. Ray, Jr. and Joseph M. Puvathingal (1985) A simple procedure for removing contaminating aldehydes and peroxides from aqueous solutions of polyethylene glycols and of nonionic detergents that are based on the polyoxyethylene linkage. Analytical Biochemistry, 146(2): 307-312

Wistuba, II, Behrens C, Milchgrub S, Syed S, Ahmadian M, Virmani AK, Kurvari V, Cunningham TH, Ashfaq R, Minna JD et al. (1998) Comparison of features of human breast cancer cell lines and their corresponding tumors. Clinical cancer research: an official journal of the American Association for Cancer Research 4(12): 2931-2938

Wu, Z. & Jin, R., (2010) On the Ligand’s Role in the Fluorescence of Gold Nanoclusters. Nano Letters, 10(7): 2568–2573

Wyllie AH. (1980) Glucocorticoid-induced thymocyte apoptosis is associated with endogenous endonuclease activation. Nature 284: 555–6

Xiao, F. et al., (2011) On the role of low-energy electrons in the radiosensitization of DNA by gold nanoparticles. Nanotechnology, 22(46): 465101

Yamori T. (2003) Panel of human cancer cell lines provides valuable database for drug discovery and bioinformatics. Cancer Chemother Pharmacol 52(Suppl 1):S74-9

Yang Q, Jones SW, Parker CL, Zamboni WC, Bear JE, Lai SK. (2014) Evading Immune Cell Uptake and Clearance Requires PEG Grafting at Densities Substantially Exceeding the Minimum for Brush Conformation. Mol. Pharm. 11(4): 1250–1258

Yang ST, Liu Y, Wang YW, Cao A (2013) Biosafety and bioapplication of nanomaterials by designing proteinnanoparticle interactions. Small, 27: 1635-53

Yang W., P. et al. (2015) Zwitterionic gel encapsulation promotes protein stability, enhances pharmacokinetics, and reduces immunogenicity. Proceedings of the National Academy of Sciences of the United States of America, 112(39): 12046–51

Yin, Y. & Alivisatos, A.P. (2005) Colloidal nanocrystal synthesis and the organic–inorganic interface. Nature, 437(7059): 664–670

You, C.-C., Agasti, S.S. & Rotello, V.M., (2008) Isomeric Control of Protein Recognition with Amino Acid- and Dipeptide-Functionalized Gold Nanoparticles. Chemistry - A European Journal, 14(1): 143–150

You, C.-C., Arvizo, R.R. & Rotello, V.M., (2006) Regulation of a-chymotrypsin activity on the surface of substrate-functionalized gold nanoparticles Issue 4: 294 - 301

Yu, T.; Greish, K.; McGill, L.D.; Ray, A.; Ghandehari, H. (2012) Influence of geometry, porosity, and surface characteristics of silica nanoparticles on acute toxicity: Their vasculature effect and tolerance threshold. ACS Nano 6: 2289–2301

Yu, W.W. et al., (2007) Forming Biocompatible and Nonaggregated Nanocrystals in Water Using Amphiphilic Polymers. Journal of the American Chemical Society, 129(10): 2871–2879

Yuan J., Najafov, Ayaz et al. (2016) Necroptosis and Cancer, Trends Cancer. 3(4): 294-301

Yum K, Wang N, Yu MF. (2010) Nanoneedle: A multifunctional tool for biological studies in living cells. Nanoscale. 2: 363-372

Zhang G, Yang Z, Lu W, Zhang R, Huang Q, Tian M, et al. (2009) Influence of anchoring ligands and particle size on the colloidal stability and in vivo biodistribution of polyethylene glycol-coated gold nanoparticles in tumor-xenografted mice. Biomaterials 30: 1928–36

Zhang J, Campbell RE, Ting AY, Tsien RY. (2002) Creating new fluorescent probes for cell biology. Nat Rev Mol Cell Biol 3:906–18

Zhang, C.; Zhou, Z.; Zhi, X.; Ma, Y.; Wang, K.; Wang, Y.; Zhang, Y.; Fu, H.; Jin, W.; Pan, F.; et al. (2015) Insights into the distinguishing stress-induced cytotoxicity of chiral gold nanoclusters and the relationship with GSTP1. Theranostics 5: 134–149

Zhang, L.W. & Monteiro-Riviere, N.A., (2009) Mechanisms of Quantum Dot Nanoparticle Cellular Uptake. Toxicological Sciences, 110(1): 138–155

Zhang, X. D.; Guo, M. L.; Wu, H. Y.; Sun, Y. M.; Ding, Y. Q.; Feng, X.; Zhang, L. A. (2009) Irradiation stability and cytotoxicity of gold nanoparticles for radiotherapy. Int. J. Nanomedicine, 4: 165–173

Zhao, F. et al., (2011) Cellular Uptake, Intracellular Trafficking, and Cytotoxicity of Nanomaterials. Small, 7(10): 1322–1337

Zhao, Y. et al., (2009) Small-molecule-directed nanoparticle assembly towards stimuli-responsive nanocomposites. Nature Materials, 8(12): 979–985

Zhu, M., Perrett, S. & Nie, G., (2013) Understanding the Particokinetics of Engineered Nanomaterials for Safe and Effective Therapeutic Applications Small. 9(9-10): 1619-34

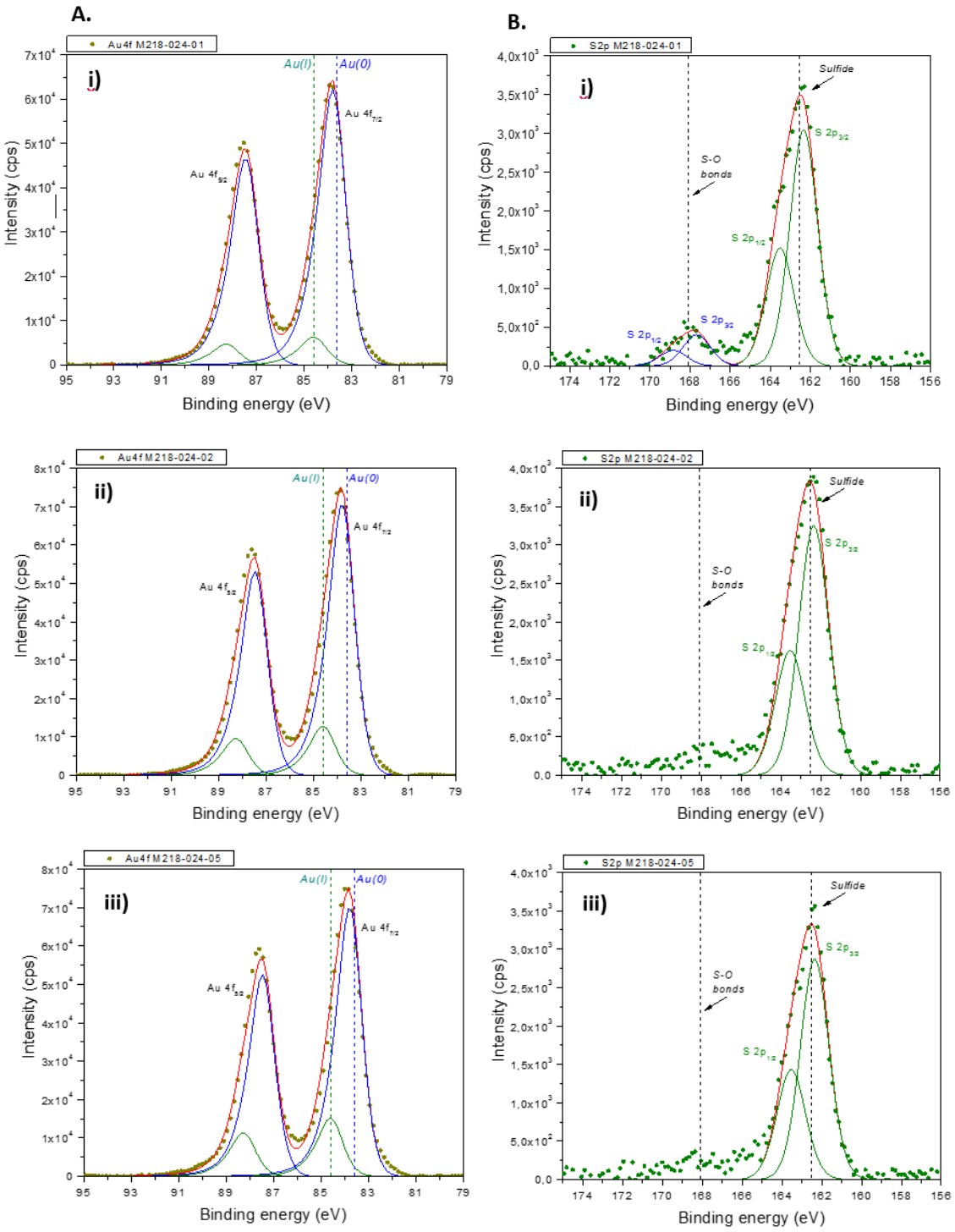

Figure 9.1: High resolution XPS spectra of A. Au 4f and B. S2p peaks. i) 1h synthesis, **ii)** 2h, **iii)** 5h synthesis AuNPs. The expected positions for the Au(I) and Au(0) states are at around 84.6 eV and 83.6 eV for the Au 4f7/2 peak. The expected position for the sulfide S 2p3/2 peak is at around 162.7 eV and S-O bonds at around 168.0 eV. Calculated S:Au ratios: 1h=0.054, 2h=0.048, 5h= 0.047.

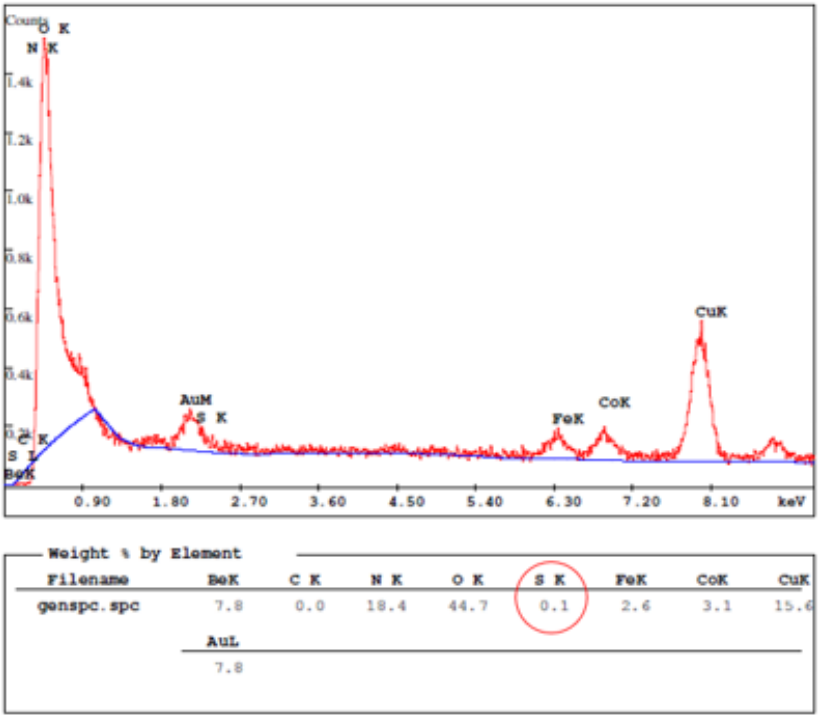

Figure 9.2: **EDX spectra of 1h AuNP.** % Wt element was analysed to obtain S:Au ratio for the determination of lihand density surrounding the Au core. S value was at baseline level.

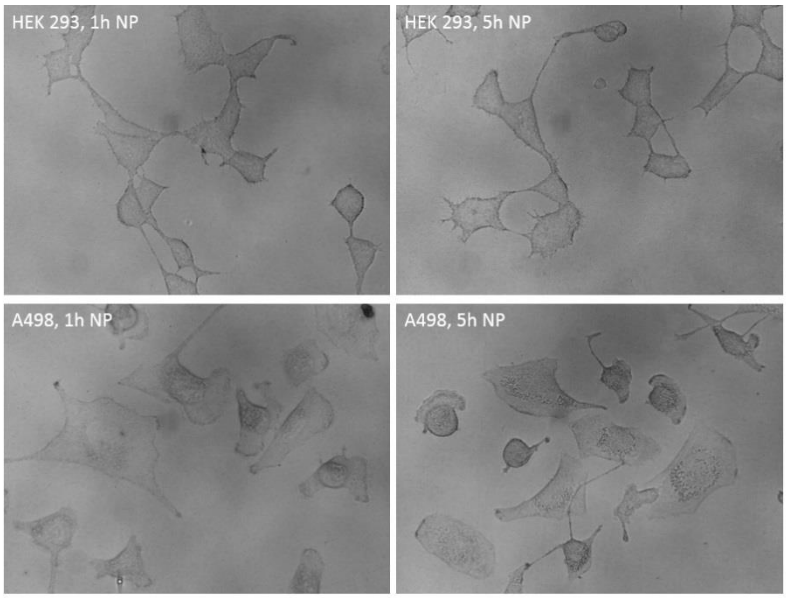

Figure 9.3: **Silver staining of 1h and 5h synthesis time AuNPs after an acute 3h exposure at 4^0C degrees on HEK-293 and A498 cells.** Pictures are taken under a light microscope at 40x objectives and only silver staining channel is shown. Scale bar=500nm.

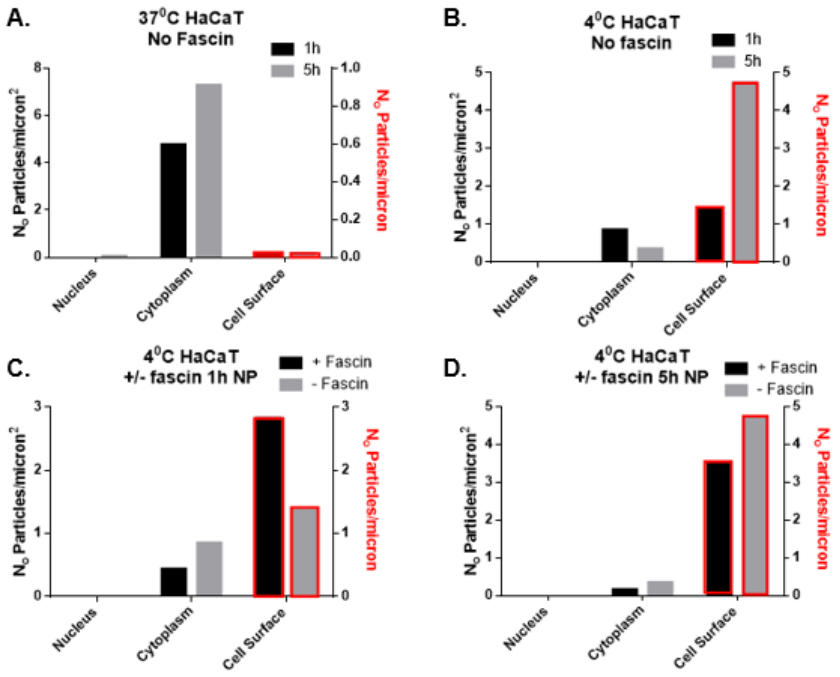

Figure 9.4: Quantification based on TEM images of silver enhanced 1h and 5h synthesis time AuNPs after an acute 3h exposure of 10 µg/ml on HaCaT cells. A. At 37⁰C, **B.** at 4⁰C, **C.** with +/- fascin for 1h AuNPs and **D.** +/- fascin for the 5h AuNPs. Quantitation of AuNP counts was conducted per micron^2 for nucleus and cytoplasm (left axis) and AuNP counts per micron for cell surface (right axis, bars with red border). n=1 with two technical replicates per condition.

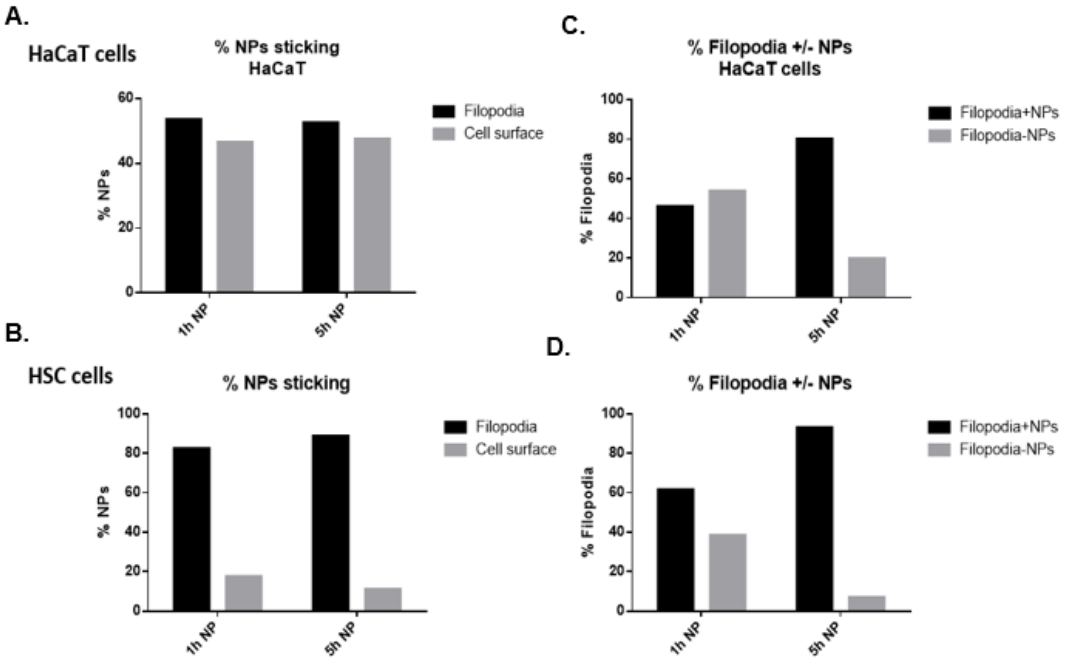

Figure 9.5: Representation of the percentage AuNPs of 1h and 5h synthesis times sticking to filopodia or cell surface for A. HaCaT cells, **B.** HSC cells, **C.** % filopodia decorated with AuNPs on HaCaT cells and D. % filopodia decorated with AuNPs on HSC cells. n=1 with two technical replicates per condition.

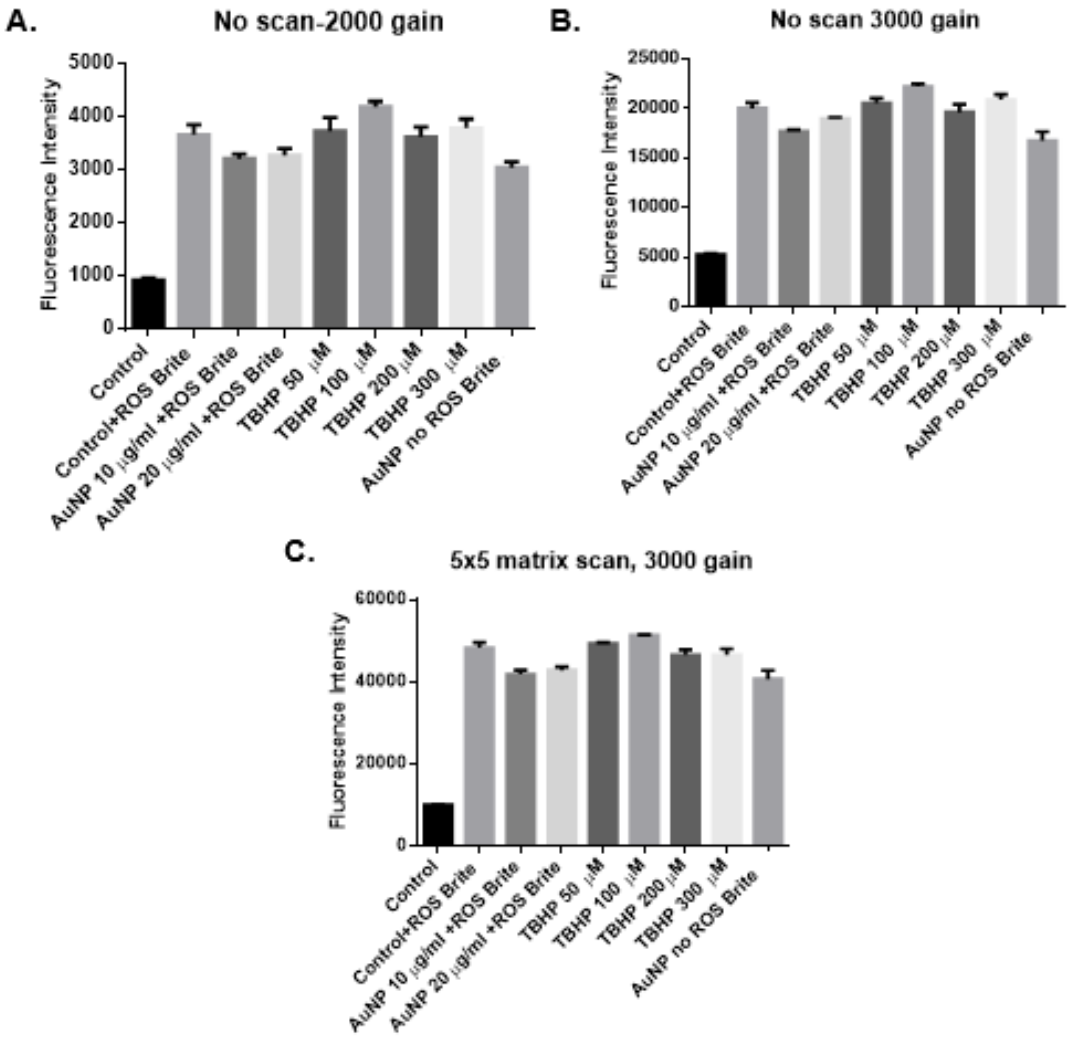

Figure 9.6: **Fluorescence intensity measurements of ROS Brite on HSC cells for the investigation of ROS generation after an acute 3h exposure of AuNPs at 10 µg/ml and 20 µg/ml.** TBHP was used as a positive control and various concentrations. The measurements were obtained by FluoStar fluorescence microplate reader at Ex556/Em 566 nm. n=1.

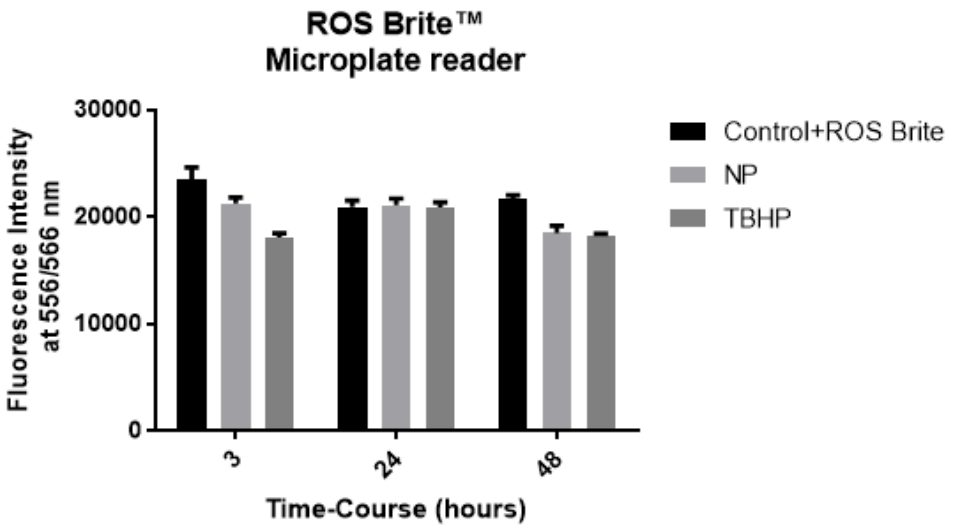

Figure 9.7: **Fluorescence intensity measurements of ROS Brite on HSC cells after an acute 3h exposure of AuNPs at 10 µg/ml.** The measurements were obtained by FluoStar fluorescent microplate reader at 556/566 nm at specific time-points of 3, 24 and 48h, throughout a time-course after AuNP exposure. TBHP was used as a positive control for ROS production. n=1 pilot experiment, with 3 replicates per condition, Error bars=±SEM.

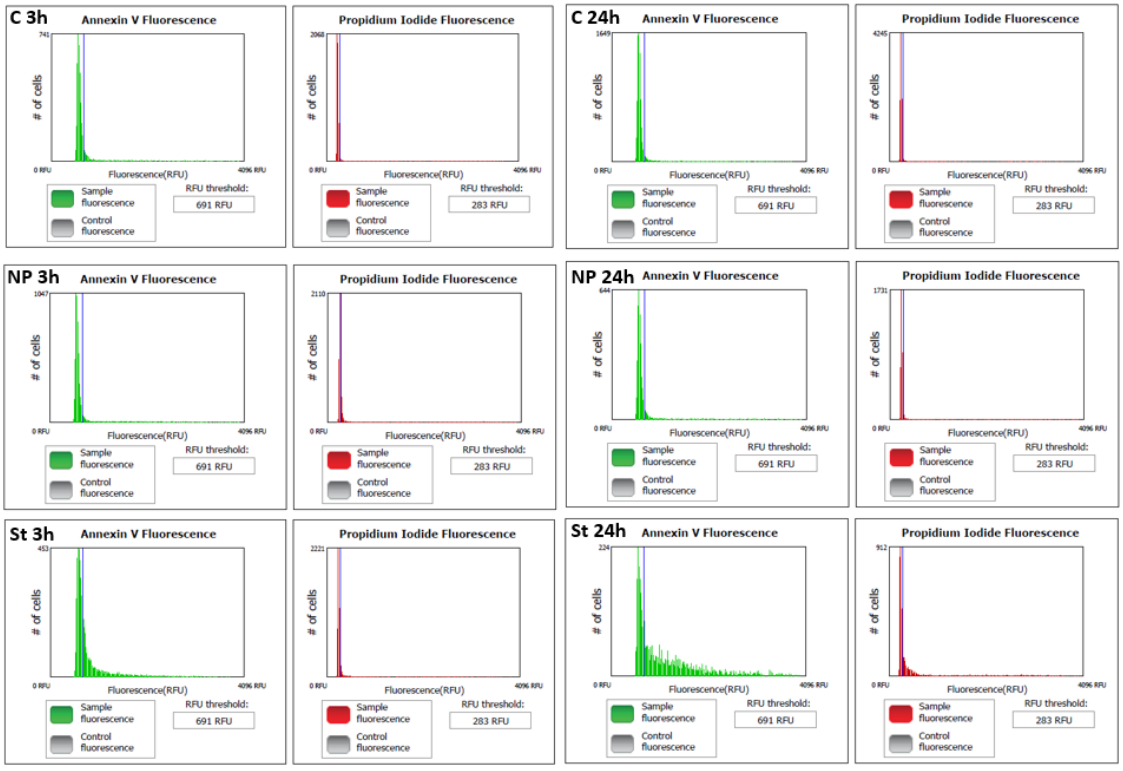

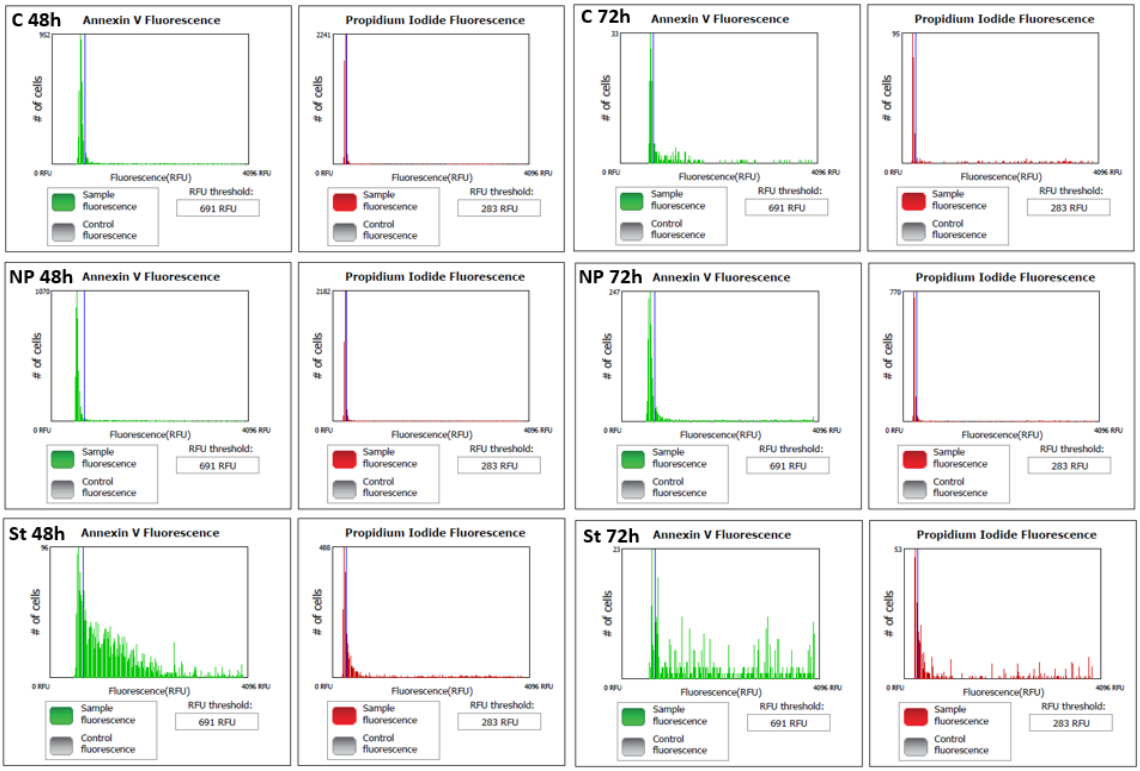

Figure 9.8: **Spectra of PI/AnnV fluorescence as generated by Tali after an acute 3h exposure of AuNPs on HSC cells.** A time-course of 72h was followed and included 3h, 24, 48 and 72h time-points. Staurosporine (St) was used as a positive control.

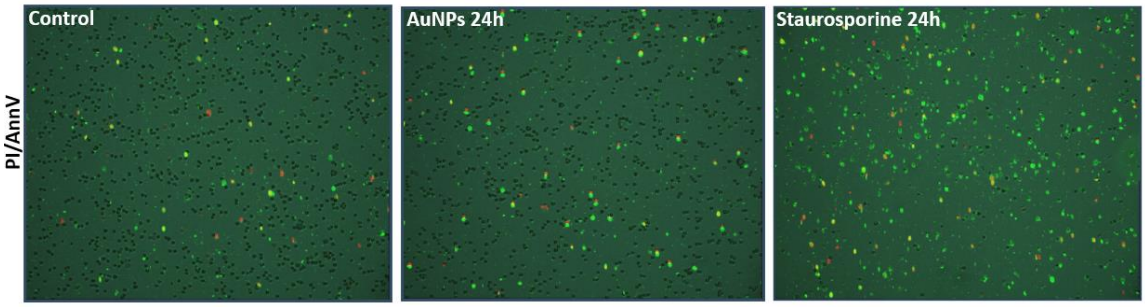

Figure 9.9: **Images of composite channels of PI/AnnV signals as obtained by Tali after an acute 3h exposure of AuNPs on HSC cells.** Staurosporine was used as a positive control. Images were taken at 24h time-point after the acute exposure.

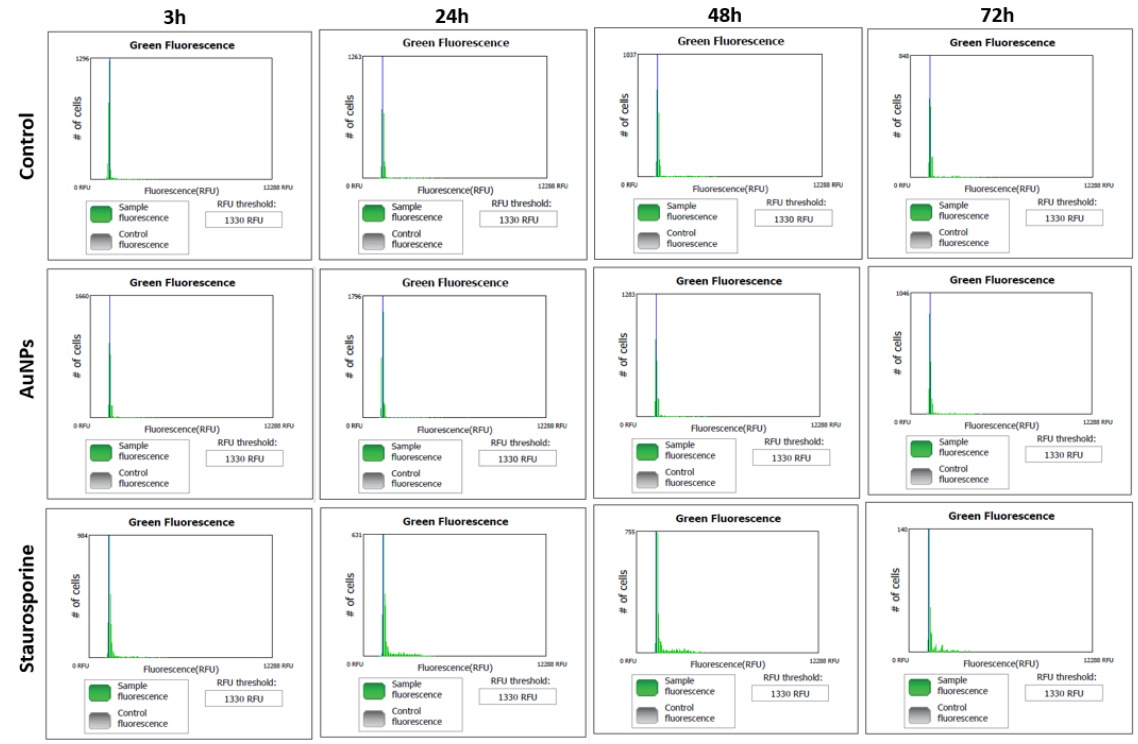

Figure 9.10: **Spectra of Caspase 3/7 fluorescence as generated by Tali after an acute 3h exposure of AuNPs on HSC cells.** A time-course of 72h was followed and included 3h, 24, 48 and 72h time-points. Staurosporine (St) was used as a positive control.

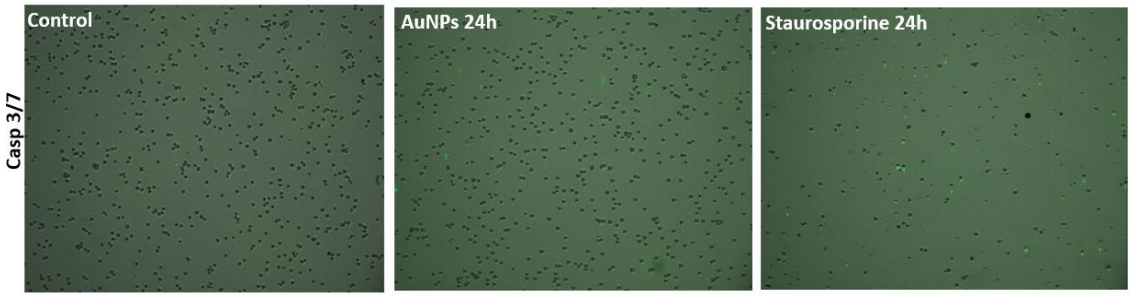

Figure 9.11: Images of composite channels of Caspase 3/7 signals as obtained by Tali after an acute 3h exposure of AuNPs on HSC cells. Staurosporine was used as a positive control. Images were taken at 24h time-point after the acute exposure.

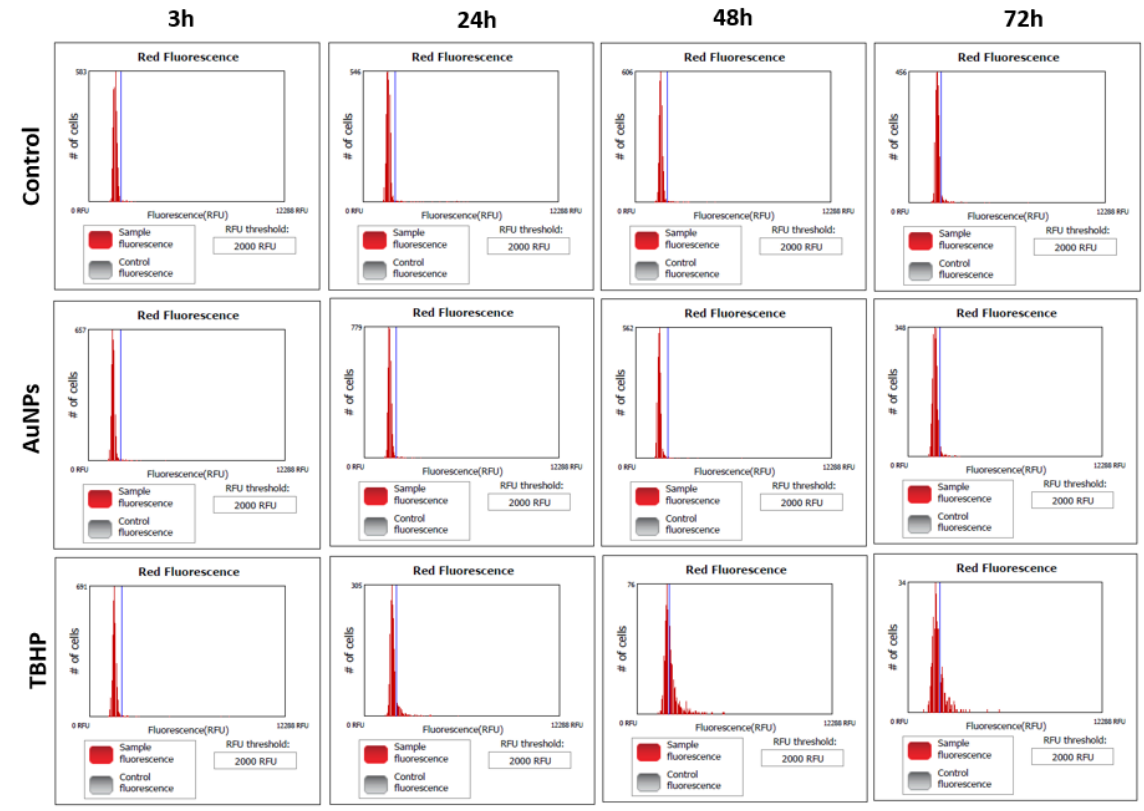

Figure 9.12: Spectra of ROS Brite fluorescence as generated by Tali after an acute 3h exposure of AuNPs on HSC cells. A time-course of 72h was followed and included 3h, 24, 48 and 72h time-points. TBHP was used as a positive control.

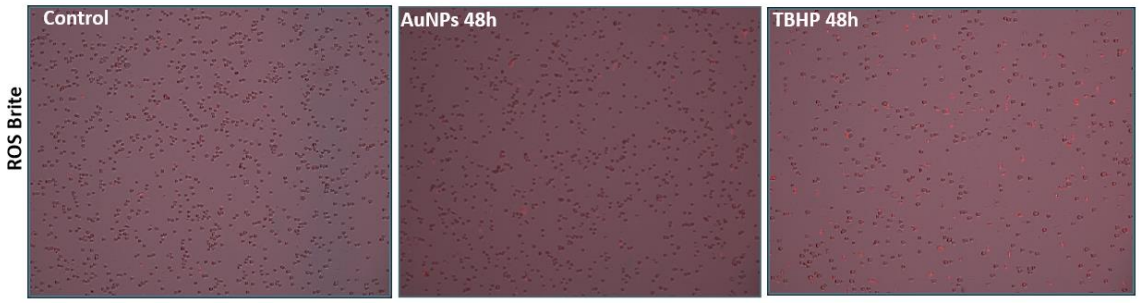

Figure 9.13: Images of composite channels of ROS Brite signals as obtained by Tali after an acute 3h exposure of AuNPs on HSC cells. TBHP was used as a positive control. Images were taken at 48h time-point after the acute exposure.

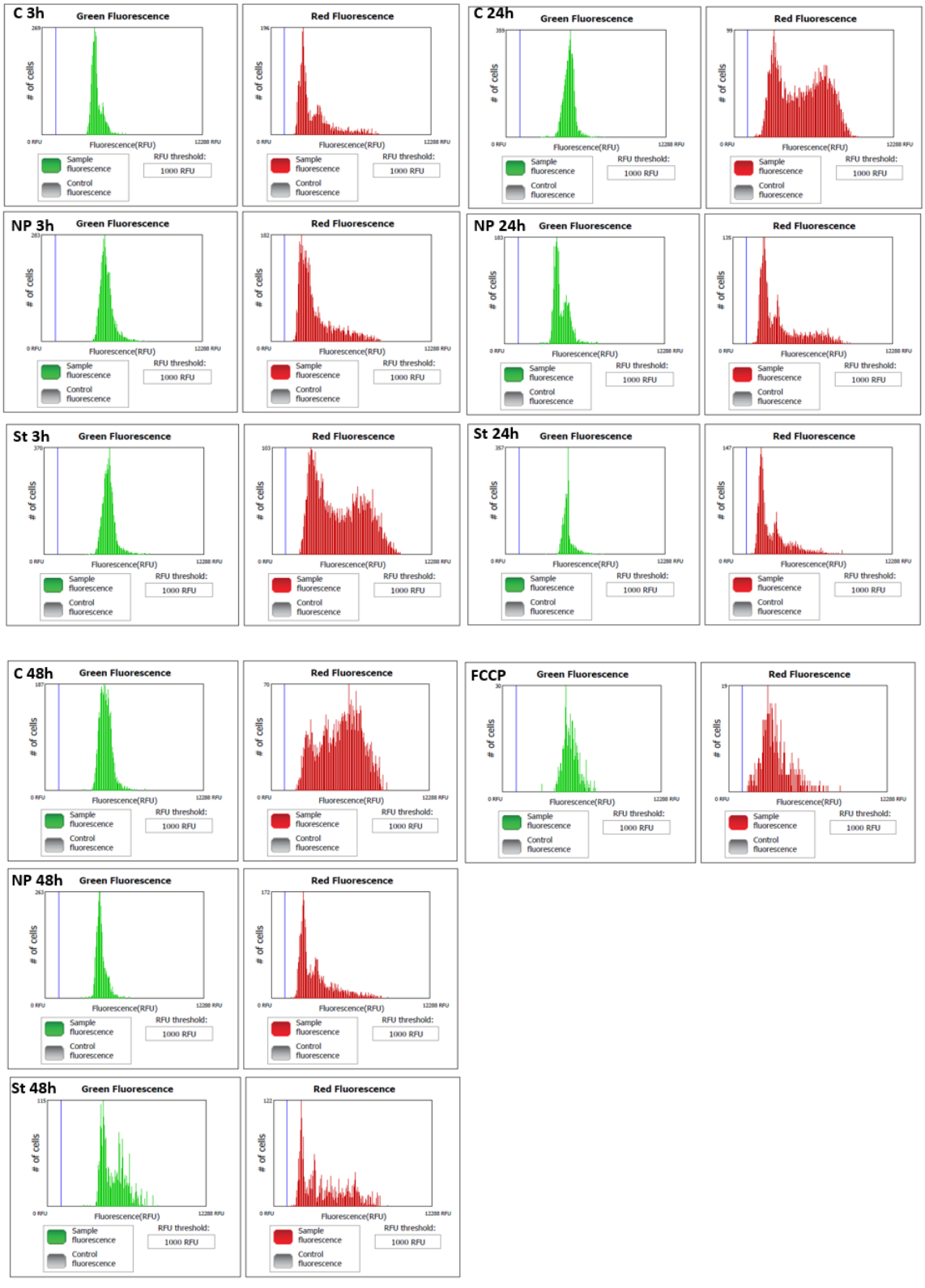

Figure 9.14: Spectra of JC-10 fluorescence as generated by Tali after an acute 3h exposure of AuNPs on HSC cells. A time-course of 72h was followed and included 3h, 24, 48 and 72h time-points. Staurosporine (St) was used as a positive control.

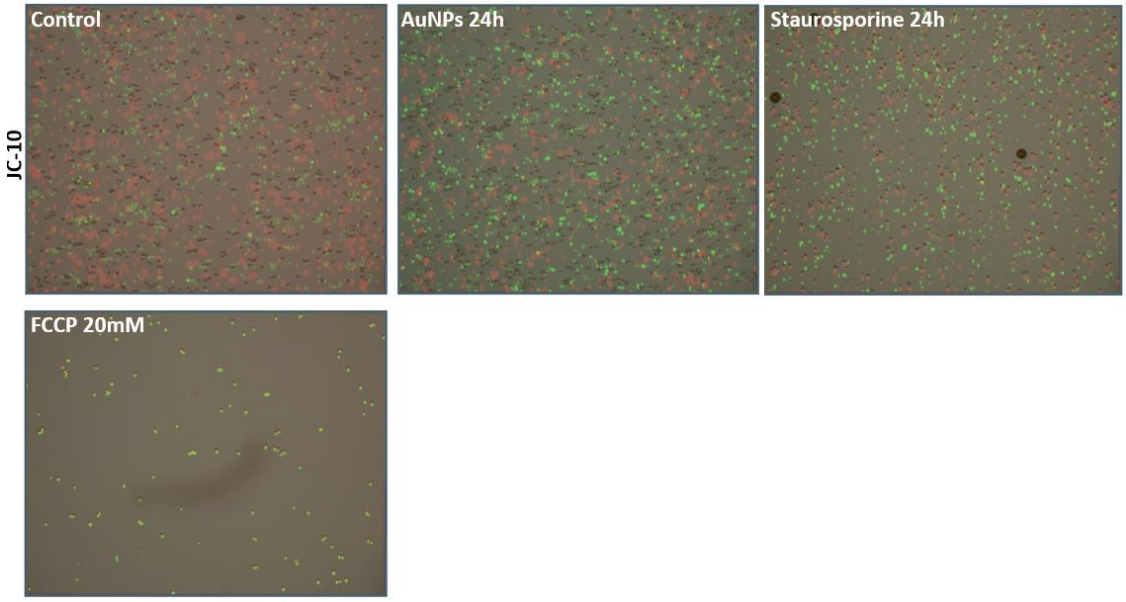

Figure 9.15: Images of composite channels of JC-10 signals as obtained by Tali after an acute 3h exposure of AuNPs on HSC cells. FCCP was used as a positive control for membrane depolarization. Images were taken at 24h time-point after the acute exposure.

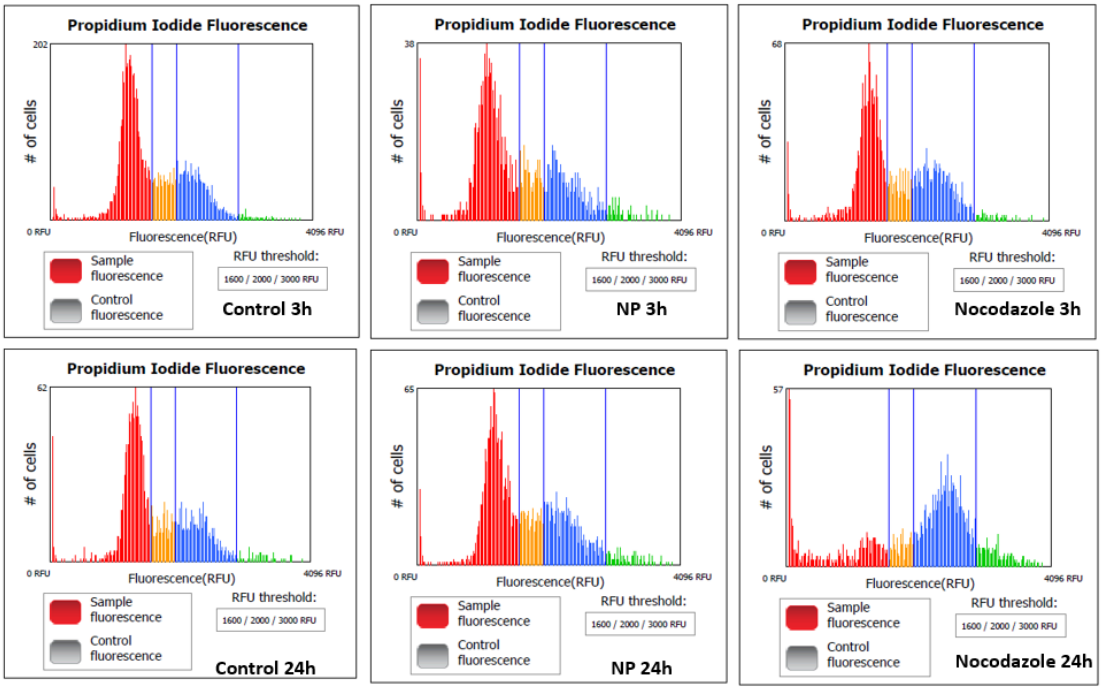

Figure 9.16: Spectra of cell cycle fluorescence as generated by Tali after an acute 3h exposure of AuNPs on HSC cells. A time-course of 72h was followed and included 3h, 24, 48 and 72h time-points. Nocodazole was used as a positive control.

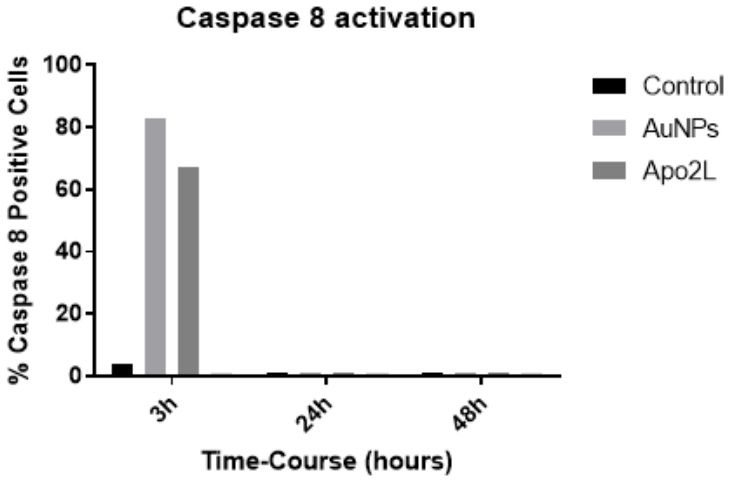

Figure 9.17: Determination of caspase 8 activation on HSC cells after an acute 3h exposure of AuNPs at 10 µg/ml. Results were quantified via Tali. Apo2L was used as a positive control for the activation of caspase 8. A time-course of 3h, 24h and 48h was conducted. n=1